DOE/BC/14126-11

(DE89000768)

FOSSIL ENERGY

# PRESSURE TRANSIENT ANALYSIS FOR COMPOSITE SYSTEMS

## SUPRI TR 68

By

Anil Kumar Ambastha

October 1989

Performed Under Contract No. FG19-87BC14126

Stanford University Petroleum Research Institute

Stanford, California

Bartlesville Project Office
U. S. DEPARTMENT OF ENERGY
Bartlesville, Oklahoma

DOE/BC/14126-11

Distribution Category UC-122

# PRESSURE TRANSIENT ANALYSIS FOR COMPOSITE SYSTEMS

SUPRI TR 68

By

Anil Kumar Ambastha

October 1989

Work Performed Under Contract No. FG19-87BC14126

Prepared for

U. S. Department of Energy

Assistant Secretary for Fossil Energy

Thomas B. Reid, Project Manager

Bartlesville Project Office

P. O. Box 1398

Bartlesville, OK 74005

Prepared by

Stanford University Petroleum Research Institute

Stanford, CA 94305-4042

# TABLE OF CONTENTS

# LIST OF TABLES

# LIST OF FIGURES

## ACKNOWLEDGEMENTS

Financial support was provided by the Stanford University Petroleum Research Institute (SUPRI) under DOE contracts DE-AC0381SF11564 and DE-F619-87BC14126 and by the SUPRI Industrial Advisory Committee.

# ABSTRACT

A composite reservoir model is used to analyze well-tests from a variety of enhanced oil recovery projects, geothermal reservoirs, and acidization projects. A composite reservoir is made up of two or more regions. Each region has its own rock and fluid properties. Transient pressure behavior of a well in a two-region composite reservoir has been considered extensively in the literature, and several methods have been proposed to estimate front (or discontinuity) radius, or swept volume. This study considers transient pressure derivative behavior of a well in a two-region composite reservoir to establish the applicability and the limitations of different methods to estimate front radius or swept volume. A finite-radius well with wellbore storage and skin is assumed to produce (or inject) at a constant rate. Three outer boundary conditions are considered: infinite, closed, and constant-pressure. A study of drawdown and buildup responses has resulted in a set of correlating parameters for the pressure derivative responses, and new design and interpretation relations for well-tests in composite reservoirs. Guidelines have been presented for the applicability of different methods to estimate front radius. Producing time effects on buildup responses show that analyzing a well-test after short producing (or injection) time may be difficult.

Dynamic phenomena, such as phase changes and multi-phase flow effects in a region near the front, can cause a sharp pressure drop at the front. Such a sharp pressure drop is modeled as a thin skin at the front in this study. An analytical solution for the transient pressure behavior of a well in a two-region composite reservoir with a skin at the front is obtained using the Laplace transformation. A thin skin at the front can explain a short duration pseudosteady state even for small mobility and storativity contrasts. The effects of a skin at the front are similar to the effects of storativity ratio. Thus, neglecting a thin skin at the front can cause large errors in parameter estimation using a type-curve matching method.

Pressure derivative behavior of a well in a homogeneous, or a three-region composite reservoir is also discussed. Several well tests from composite reservoirs are analyzed to establish the applicability and the limitations of the deviation time method to estimate front radius.

# 1. INTRODUCTION

A composite reservoir is made up of two or more regions. Each region has its own rock and fluid properties. A composite system can occur naturally or may be artificially created. Aquifers with two different permeabilities forming two regions, oil and water regions or gas and oil regions with different properties in a reservoir are examples of naturally occurring two-region composite systems. Secondary or tertiary recovery projects, like water flooding, polymer flood, gas injection, in-situ combustion, steam drive, and $CO_2$ miscible flooding artificially create conditions wherein the reservoir can be viewed as consisting of two regions with different rock and/or fluid properties. A stimulation program, such as acidizing, can result in a permeability discontinuity. *Wattenbarger* and *Ramey* (1970) treated a finite thickness skin region as a composite system.

In a gas condensate or a geothermal reservoir, pressure reduction near the well causes changes in relative permeabilities as the fluid changes phase, and in the case of water, significant changes in compressibility (*Horne et al.*, 1980; *Grant* and *Sorey*, 1979). *Horne et al.* (1980) state that the appearance of a flashing front in a water region or the start of condensation in a steam region may result in a sharp discontinuity in reservoir properties. Vaporization/condensation at a sharp discontinuity may also resemble an apparent skin effect at the discontinuity. *Mangold et al.* (1981) studied the effects of a thermal discontinuity on well test analysis in geothermal reservoirs. They stated that the presence of different temperature regions in non-isothermal reservoirs may resemble permeability boundaries during well testing. *Benson* and *Bodvarsson* (1986) state that falloff data from geothermal reservoirs can be analyzed with a composite reservoir model. Thus, many well-test scenarios in geothermal and hydrocarbon reservoirs may be modeled by a composite reservoir.

This study considers transient pressure derivative behavior of a well in a two-region, composite reservoir with an infinitesimally thin skin at the discontinuity. The effects of a thin skin at the discontinuity on the transient pressure and pressure derivative behavior of a well in a composite reservoir is considered important because a thin skin at the discontinuity may be a practical approach to model the following physical situations:

1. Vaporization at the discontinuity while injecting cold water in a hot geothermal reservoir,
2. Condensation at the steam front such as in steam injection projects,
3. Cases where a transition region is apparent. For in-situ combustion cases, *Onyekonwu* (1985) observed a transition region. Pressure profiles presented in Figs. 6.8 and 6.11 of *Onyekonwu* (1985) suggest that the system may be modeled as a two-region reservoir with a thin skin at the discontinuity, and
4. Simulated $CO_2$ flooding results show that about 60% of the overall pressure drop occurs in a small region around the discontinuity (*Tang* and *Ambastha*, 1988). Such pressure drops at a discontinuity may be approximately modeled as a thin skin at the discontinuity.

The mathematical model developed in this study is discussed in Chapter 4. Chapter 2 presents the literature survey. Chapter 3 presents the problem statement and the objectives of this study.

Since a homogeneous reservoir is a special case of a composite reservoir, transient pressure derivative behavior of a well in a homogeneous reservoir is discussed in Chapter 5. Chapter 5 presents drawdown and buildup pressure derivative type-curves for a well producing at a constant rate from the center of a finite, circular reservoir. The outer boundary may be closed, or at a constant pressure. Design relations are developed for the time to the beginning and the end of infinite-acting radial flow. Producing time effects on buildup responses are also discussed.

Chapter 6 presents transient pressure derivative behavior of a well in a two-region, radial, infinite or finite composite reservoir. Both drawdown and buildup pressure derivative responses are discussed in Chapter 6. Design and interpretation equations developed in Chapter 6 should help estimate the test duration required to observe a particular feature in well test data and thus, establish the applicability of an interpretation method to determine front radius or swept volume.

A number of well tests reported in the literature exhibiting composite reservoir behavior have been analyzed in Chapter 7 to establish the applicability and the limitations of different methods to estimate a discontinuity (or front) radius or swept volume. Chapter 8 presents a discussion of results. Finally, Chapter 9 presents conclusions and recommendations for future research.

# 2. LITERATURE

Figure 2.1 shows a schematic diagram of a two-region, radial composite reservoir. The inner and outer regions of a composite reservoir have different, but uniform rock and fluid properties, and are separated by a discontinuity. The distance $R$ is the front (or discontinuity) radius, which is an important parameter sought from well tests in composite reservoirs. Strictly speaking, fronts in many composite reservoir configurations, such as thermal recovery and $CO_2$ flooding, are usually not cylindrical due to gravity and viscous fingering effects. Thus, the front (or discontinuity) radius exists only in some average sense. It is perhaps better to speak of the volume of the inner region, especially when pseudosteady data are available (*Ramey*, 1987).

In 1958, *Hazebroek et al.* analyzed pressure falloff data from water injection wells assuming water and oil bank properties to be different. *Hurst* (1960) and *Mortada* (1960) considered interference between oil fields sharing a common aquifer by two regions of different properties. *Hopkinson et al.* (1960) presented a late time approximation for the pressure drop in the inner region. *Adams et al.* (1968) analyzed pressure buildup tests in a fractured dolomite reservoir using the *Hurst* (1960) solution.

*Loucks* and *Guerrero* (1961), and *Jones* (1962) published solutions for radial composite reservoirs using Laplace transformation. *Rowan* and *Clegg* (1962) presented approximate solutions for radial composite reservoirs. *Bixel et al.* (1963), and *Bixel* and *van Poollen* (1967) considered the effects of linear and radial discontinuities in composite reservoirs on pressure buildup and drawdown behaviors. *Bixel* and *van Poollen* (1967) recommended a semi-log type-curve matching method to determine the distance to the discontinuity. *Barua* and *Horne* (1987) used automated type-curve matching with success to analyze thermal recovery well test data. *Larkin* (1963) presented solutions to the diffusion equation for a line source located anywhere in a region bounded by a circular discontinuity using a Green's function presented by *Jaeger* (1944).

*Van Poollen* (1964) used the concept of drainage radius, and related the drainage radius (or the front radius in an in-situ combustion project) to a deviation time from the semi-log straight line corresponding to the inner region mobility. Later, *van Poollen* (1965) used pressure falloff data from in-situ combustion projects to locate the burning front radius using the deviation time method. *Kazemi* (1966) and *Merrill et al.* (1974) also discuss the deviation time method. *Kazemi et al.* (1972) discuss the problems in the interpretation of pressure falloff tests in reservoirs with and without fluid banks.

*Carter* (1966) presented the pressure transient behavior of a closed, radial composite reservoir with the well producing at a constant rate. He noted that a pseudosteady state period, yielding a straight line on a Cartesian graph of pressure vs. time, developed after the end of the semi-log line corresponding to the inner region mobility, but that the volume calculated from the Cartesian slope would be greater than the inner region volume. *Closmann* and *Ratliff* (1967) presented a solution for a well producing at a constant pressure from a closed, radial composite reservoir. *Turki* (1986) presented solutions in Laplace space for a well producing at a constant pressure from a radial, infinite or finite composite reservoir.

*Wattenbarger* and *Ramey* (1970) modeled a finite-thickness skin region as a composite reservoir. They obtained pressure transient behavior for such systems using

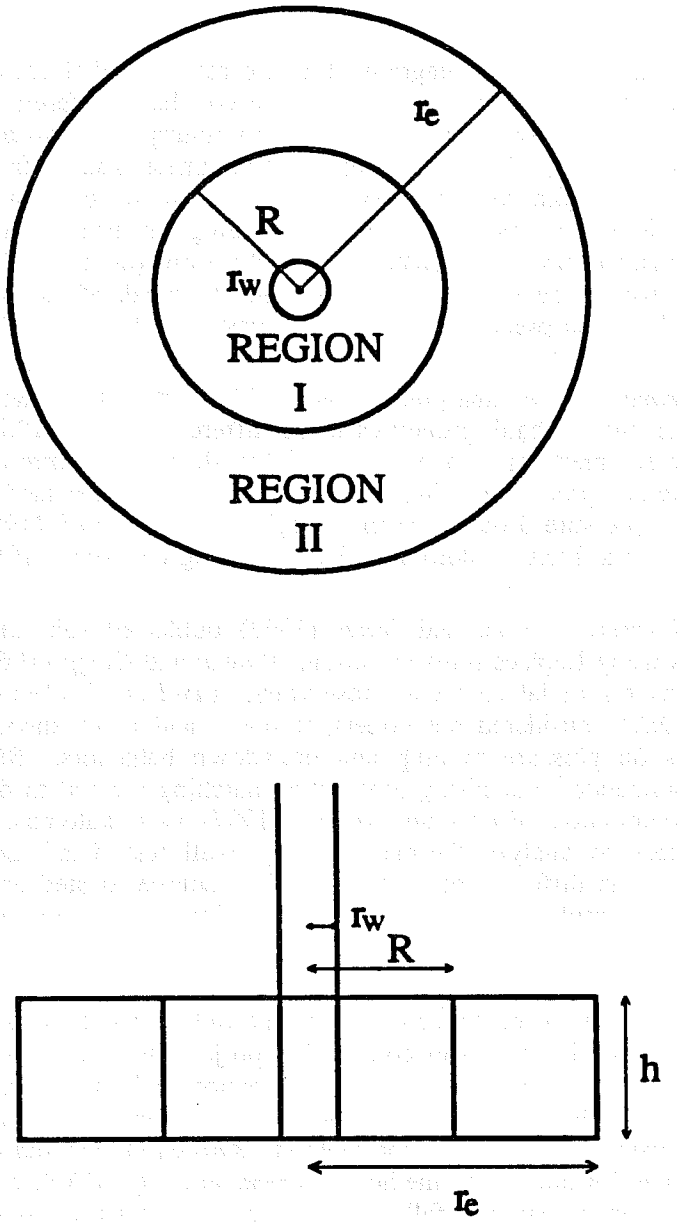


Figure 2.1: Two-region, radial composite reservoir.

finite-difference techniques. Their solutions correspond to a range of mobility ratio between 0.1 and 3.6. Mobility ratio, $M$, for a two-region composite reservoir is:

$$M = \frac{(k/\mu)_1}{(k/\mu)_2} \quad . \tag{2.1}$$

*Odeh* (1969) observed that pressure data measured at a shut-in well in a composite reservoir may exhibit a semi-log straight line corresponding to the inner region mobility, and then a transition followed by a second semi-log straight line corresponding to the outer region mobility. He presented an equation relating the dimensionless discontinuity radius, $R_D$, with the dimensionless intersection time, $t_{DX}$, for equal storativity in both regions as:

$$R_D^2 = \frac{2.25\ t_{DX}}{M^{M\ /\ (M\ -\ 1)}} \ , \tag{2.2}$$

where:

$$R_D = \frac{R}{r_w} \ , \text{ and} \tag{2.3}$$

$$t_{DX} = \frac{0.000264\ k_1\ t_X}{(\phi\mu c_t)_1\ r_w^2} \quad . \tag{2.4}$$

*Ramey* (1970) presented a more general relation between $R_D$ and $t_{DX}$ as:

$$R_D^2 = \frac{2.2458\ t_{DX}}{\eta^{M\ /\ (M\ -\ 1)}} \ , \tag{2.5}$$

where the diffusivity ratio, $\eta$, is:

$$\eta = \frac{(k/\phi c_t \mu)_1}{(k/\phi c_t \mu)_2} \quad . \tag{2.6}$$

*Merrill et al.* (1974) presented a graphical correlation for the dimensionless intersection time using a numerical simulator. *Brown* (1985) also discusses the *Merrill et al.* correlation. The intersection time method depends on the observation of two semi-log straight lines in pressure data. *Sosa et al.* (1981) studied the effects of relative permeability and mobility ratio on simulated pressure falloff behavior in water injection wells. *Sosa et al.* (1981) used the deviation time and the intersection time methods to analyze simulated falloff tests.

*Eggenschwiler et al.* (1979) developed a pseudosteady state method to estimate inner swept volume for composite reservoirs with large storativity and mobility contrasts between the two regions, such as in in-situ combustion and steam injection

projects. They presented an analytical solution in Laplace space for the transient pressure behavior of a well producing at a constant rate from a two-region, radial infinite composite reservoir. *Horne et al.* (1980) extended the *Eggenschwiler et al.* solution to finite composite reservoirs. *Eggenschwiler et al.* observed that for large mobility and storativity contrasts between the two regions:

1. The initial wellbore storage effect dies quickly, and a semi-log straight line corresponding to the inner region mobility develops almost immediately on shut-in,
2. The first semi-log straight line corresponding to the inner region mobility is followed by a pseudosteady Cartesian straight line characteristic of the inner swept volume. The slope, $m_c$, of the Cartesian line may be used to calculate the inner swept volume, $V_s$, through a relation expressed in field units as:

$$m_c = \frac{5.615qB}{V_s\ c_t}\ , \text{ and} \tag{2.7}$$

3. Finally, a second semi-log straight line corresponding to the outer region mobility may appear.

The pseudosteady state method is independent of the geometry of the inner swept region, and has been applied by several investigators to field and simulated cases with apparent success. *Walsh et al.* (1981), *Messner* and *Williams* (1982a and b), *Onyekonwu et al.* (1984 and 1986), *Fassihi* (1984), *Da Prat et al.* (1985), and *Onyekonwu* (1985) have applied the pseudosteady-state method to well tests in in-situ combustion and steam injection projects. *Horne et al.* (1980) analyzed geothermal well test data using the pseudosteady state method. *MacAllister* (1987) used the pseudosteady state method to analyze well tests in $CO_2$ flooding projects. *Tang* (1982) and *Satman et al.* (1980) extended the pseudosteady state method to cases where pseudosteady state did not develop completely due to insufficient mobility and storativity contrasts between the two regions. *Teng* (1984) studied the conditions for the existence of pseudosteady state for rectangular shaped inner regions.

*Stanislav et al.* (1987) included the effects of heat losses on pressure behavior during the period of falloff testing in a radial, two-region composite reservoir. They found that under certain conditions, the net effect of heat losses on pressure behavior may be significant and may dominate the pseudosteady state period of pressure response. *Abbaszadeh-Dehghani* and *Kamal* (1987) studied pressure transient testing of water injection wells using two-region and multi-region composite reservoir models. They found that the assumption of a stationary front during falloff is generally acceptable and that a waterflooding system is better represented by a multi-region reservoir. *Abbaszadeh-Dehghani* and *Kamal* used a type-curve matching of pressure and pressure derivative data simultaneously to analyze pressure transient tests in water injection wells. *Olarewaju* and *Lee* (1987a) used type-curve matching of pressure and pressure derivative data simultaneously to analyze well tests exhibiting composite reservoir behavior due to acidizing and fracturing.

*Olarewaju* and *Lee* (1987b) presented an analytical solution in Laplace space for two-region, radial composite reservoirs produced at either a constant bottomhole pressure or a constant rate. They included a wellbore phase redistribution model suggested by *Fair* (1981) in their solution. *Olarewaju* and *Lee* (1987b) analyzed field tests exhibiting composite reservoir behavior using an automatic type-curve matching procedure.

*Onyekonwu* and *Horne* (1983) studied pressure transient behavior in reservoirs with spherically discontinuous properties. *Satman* (1981) presented an analytical study of transient flow in multilayered, radial, and infinitely large composite reservoirs with fluid banks. Using the analytical solution for multilayered, composite reservoirs (*Satman*, 1981), *Satman* and *Oskay* (1985) studied the effects of a tilted front on well test analysis in radial composite reservoirs. *Obut* (1983), and *Obut* and *Ertekin* (1984) presented a composite reservoir solution for an elliptical flow geometry. They assumed that the swept volume in the presence of an infinite-conductivity vertical fracture at the injection well can be idealized as an elliptical region. *Stanislav et al.* (1986) reported a similar study.

*Satman* (1985) presented an analytical study of interference in single-layer, radial, and infinitely large composite reservoirs. *Hatzignatiou et al.* (1987) presented an analytical study of interference in multi-layered, radial, and infinitely large composite reservoirs with crossflow between layers.

*Onyekonwu* (1985), and *Barua* and *Horne* (1985) presented analytical solutions for three-region, radially infinite, composite reservoirs. Thus, the transient pressure behavior of composite reservoirs has been considered extensively. However, when a straight line is sought on a pressure vs. a function of time graph, we seek a constant slope. Thus, pressure derivatives can be used to identify this condition.

A pressure derivative graph can enhance a pressure signal, and may be more sensitive to disturbances in reservoir conditions (*Bourdet et al.*, 1983a and b, and 1984). Also, times of specific flow events from pressure derivative analysis can often be different from those from pressure analysis (*Aarstad*, 1987). *Larsen* (1983) stated that it is not appropriate to test the accuracy of design equations based on pressure derivatives with those based on pressure responses. However, such a comparison may show the need for improvements in well test design and interpretation. Appendix A shows the differences in the time to the beginning of infinite-acting radial flow for a line-source and a finite-radius well from pressure and the pressure derivative analysis. *Vongvuthipornchai* and *Raghavan* (1988) discuss several design relations for the end of the storage-dominated period, and for the start of infinite-acting radial flow for a well in an infinite reservoir. They concluded that for analysis techniques based on semi-log methods, a criterion based on the pressure derivative response is the appropriate criterion for determining the time at which the semi-log straight line begins. Design relations based on the pressure derivative responses also ensure that the slope is correct within a specified tolerance.

Because of enhancement of detail on a pressure derivative graph, improved type-curve matching may be possible using a pressure derivative type-curve. To use pressure derivatives, design equations and type-curves based on pressure derivatives for the system under consideration are necessary. *Brown* (1985) investigated drawdown pressure derivative behavior of two-region, radial, and infinitely-large composite reservoirs. He limited his study to mobility ratios of the order of 0.4 to 2.0, and storativity ratios of the order of 0.3 to 3.0. Such mobility and storativity ratios are typical of cases with finite-thickness skin regions around the wellbore. Storativity ratio, $F_S$, for a two-region composite reservoir is:

$$F_S = \frac{(\phi c_t)_1}{(\phi c_t)_2} = \frac{M}{\eta} \quad . \tag{2.8}$$

In summary, different methods have been proposed to estimate a front (or discontinuity) radius from pressure-time data. These methods are:

1. Deviation Time Method,
2. Intersection Time Method,
3. Type-curve Matching Method, and
4. Pseudosteady State Method.

The deviation time method uses the time at the end of the semi-log pressure-time line corresponding to the inner region mobility to calculate a front (or discontinuity) radius, based on a theoretical dimensionless deviation time. The deviation time method was proposed by *van Poollen* (1964 and 1965). The intersection time method uses the intersection time of two semi-log lines corresponding to the mobilities of the inner and outer regions to calculate a front radius, using a theoretical dimensionless intersection time. The intersection time method was proposed by *Odeh* (1969), *Ramey* (1970), and *Merrill et al.* (1974). A semi-log type-curve matching method was proposed by *Bixel* and *van Poollen* (1967). *Eggenschwiler et al.* (1979) proposed a pseudosteady state method for large mobility and storativity contrast situations. However, design relations based on pressure derivative analysis of composite reservoirs have not appeared in the literature. Accurate design relations should help establish the applicability of the interpretation methods to determine front radius or swept volume. A detailed study of drawdown and buildup pressure derivative behavior for two-region, radial composite reservoirs has not appeared in the literature to our knowledge. The effects of a thin skin at the discontinuity on the transient response of a well in a two-region, composite reservoir also does not appear to have been considered previously in the literature.

# 3. PROBLEM STATEMENT

As discussed in Chapter 2, transient pressure behavior of composite reservoirs has been considered extensively. However, transient pressure derivative behavior of composite reservoirs has attracted little attention. Therefore, this study investigates drawdown and buildup pressure derivative behavior of two-region, radial composite reservoirs. The objectives of this study are:

1. To develop an analytical solution, similar to the *Eggenschwiler et al.* (1979) solution, for two-region, radial composite reservoirs with an infinitesimally thin skin at the discontinuity,
2. To develop design and interpretation relations based on pressure derivative behavior for well tests in either homogeneous or composite reservoirs,
3. To develop new pressure derivative type-curves for type-curve matching analysis of well tests in either homogeneous or composite reservoirs, and
4. To analyze well tests reported in the literature exhibiting composite reservoir behavior to establish the applicability and the limitations of different methods to estimate a discontinuity (or front) radius, or swept volume.

# 4. MATHEMATICAL MODEL FOR A TWO-REGION COMPOSITE RESERVOIR WITH A SKIN AT THE DISCONTINUITY

*Eggenschwiler et al.* (1979) presented an analytical solution in Laplace space for a well with storage and skin, and producing at a constant rate from a two-region, radial, and infinitely large composite reservoir. *Horne et al.* (1980) extended the *Eggenschwiler et al.* solution to finite composite reservoirs with a closed or a constant-pressure outer boundary, but with no wellbore storage or skin.

In this section, a mathematical model for a two-region, radial composite reservoir with wellbore storage and skin at the active (injection or production) well, and an infinitesimally thin skin at the discontinuity is presented. The surface production or injection rate at the active well is assumed constant. The outer boundary may be infinite, closed or at a constant pressure. Other assumptions include:

1. The formation is horizontal, of uniform thickness, and homogeneous on each side of the discontinuity,
2. The front (or discontinuity) is of infinitesimal thickness in the radial direction, and can be considered stationary throughout the test period,
3. Flow is laminar and radial,
4. Single phase flow of a fluid with slight, but constant compressibility occurs in each region,
5. Gravity and capillarity effects are negligible,

## 4.1 MATHEMATICAL DEVELOPMENT

The governing equations and boundary conditions in dimensionless form for a radial, two-region composite reservoir are:

**Governing equations:**

$$\frac{1}{r_D}\frac{\partial}{\partial r_D}\left[r_D\frac{\partial p_{D1}}{\partial r_D}\right]=\frac{\partial p_{D1}}{\partial t_D} \qquad \text{for} \quad 1 \le r_D \le R_D \text{ , and} \tag{4.1}$$

$$\frac{1}{r_D}\frac{\partial}{\partial r_D}\left[r_D\frac{\partial p_{D2}}{\partial r_D}\right]=\eta\frac{\partial p_{D2}}{\partial t_D} \qquad \text{for} \qquad R_D \le r_D \le r_{eD} \text{ (or} < \infty \text{ )} \tag{4.2}$$

**Inner boundary conditions:**

$$C_D\frac{dp_{wD}}{dt_D}-\left[\frac{\partial p_{D1}}{\partial r_D}\right]_{r_D=1}=1 \text{ , and} \tag{4.3}$$

$$p_{wD}=p_{D1}-s\left[\frac{\partial p_{D1}}{\partial r_D}\right]_{r_D=1}. \tag{4.4}$$

**Conditions at the discontinuity:**

$$\frac{\partial p_{D2}}{\partial r_D} = M \frac{\partial p_{D1}}{\partial r_D} \quad \text{for} \quad r_D = R_D \quad \text{and} \quad t_D > 0 \text{ , and} \tag{4.5}$$

$$r_D \frac{\partial p_{D1}}{\partial r_D} = -\frac{1}{s_f}\left[p_{D1} - p_{D2}\right] \quad \text{for} \quad r_D = R_D \quad \text{and} \quad t_D > 0 \text{ .} \tag{4.6}$$

**Outer boundary conditions:**

$$\text{Infinite:} \quad p_{D2}(r_D, t_D)\Big]_{r_D \to \infty} = 0 \text{ ,} \tag{4.7}$$

$$\text{Closed:} \quad \frac{\partial p_{D2}}{\partial r_D} = 0 \text{ at } r_D = r_{eD} \text{ ,} \tag{4.8}$$

$$\text{Constant–pressure:} \quad p_{D2}(r_{eD}, t_D) = 0 \text{ .} \tag{4.9}$$

**Initial conditions:**

$$p_{D1}(r_D, 0) = 0 \text{ , and} \tag{4.10}$$

$$p_{D2}(r_D, 0) = 0 \text{ .} \tag{4.11}$$

The dimensionless variables used in Eqs. (4.1) through (4.11) are:

$$p_{D1} = \frac{k_1 h}{141.2\ qB\mu_1}(p_i - p_1) \text{ ,} \tag{4.12}$$

$$p_{D2} = \frac{k_1 h}{141.2\ qB\mu_1}(p_i - p_2) \text{ ,} \tag{4.13}$$

$$p_{wD} = \frac{k_1 h}{141.2\ qB\mu_1}(p_i - p_w) \text{ ,} \tag{4.14}$$

$$\eta = \frac{\left[k\ /\ \phi\mu c_t\right]_1}{\left[k\ /\ \phi\mu c_t\right]_2} \text{ ,} \tag{4.15}$$

$$M = \frac{(k\ /\ \mu)_1}{(k\ /\ \mu)_2} \text{ ,} \tag{4.16}$$

$$r_D = \frac{r}{r_w} , \tag{4.17}$$

$$r_{eD} = \frac{r_e}{r_w} , \tag{4.18}$$

$$R_D = \frac{R}{r_w} , \tag{4.19}$$

$$t_D = \frac{0.000264\, k_1}{(\phi\mu c_t)_1} \frac{t}{r_w^2} , \tag{4.20}$$

$$C_D = \frac{5.615\, C}{2\pi\, (\phi c_t)_1 h r_w^2} , \tag{4.21}$$

$$s = \frac{k_1 h}{141.2\, qB\mu_1} \Delta p_s , \text{ and} \tag{4.22}$$

$$s_f = \frac{k_1 h}{141.2\, q_f\, B\mu_1} \Delta p_{s_f} . \tag{4.23}$$

Following the approach of *Eggenschwiler et al.* (1979), a general solution to Eqs. (4.1) and (4.2) with appropriate initial and boundary conditions was obtained using the Laplace transformation. A general solution for the dimensionless pressure drops in Laplace space for regions I and II are:

$$\bar{p}_{D1}(r_D, l) = C_1\, I_0(r_D\sqrt{l}) + C_2\, K_0(r_D\sqrt{l}) \quad \text{for } 1 \le r_D \le R_D , \tag{4.24}$$

$$\bar{p}_{D2}(r_D, l) = C_3\, I_0(r_D\sqrt{l\eta}) + C_4\, K_0(r_D\sqrt{l\eta}) \quad \text{for } R_D \le r_D \le r_{eD} \text{ (or } \infty\text{)} . \tag{4.25}$$

In Eqs. (4.24) and (4.25) and all subsequent equations, the transformed time variable is identified by the symbol, $l$. The dimensionless wellbore pressure drop in Laplace space is:

$$\bar{p}_{wD}(l) = C_1 \left[ I_0(\sqrt{l}) - s\sqrt{l}\; I_1(\sqrt{l}) \right] + C_2 \left[ K_0(\sqrt{l}) + s\sqrt{l}\; K_1(\sqrt{l}) \right] . \tag{4.26}$$

The constants $C_1$ through $C_4$ are obtained by solving the following system of equations resulting from the use of boundary conditions (Eqs. (4.3) through (4.9)) in Laplace space:

$$\text{Using Eqs. (4.3) and (4.4):} \quad \alpha_{11}\, C_1 + \alpha_{12}\, C_2 = \frac{1}{l} , \tag{4.27}$$

$$\text{Using Eq. (4.6):} \quad \alpha_{21} C_1 + \alpha_{22} C_2 + \alpha_{23} C_3 + \alpha_{24} C_4 = 0 , \tag{4.28}$$

$$\text{Using Eq. (4.5):} \quad \alpha_{31} C_1 + \alpha_{32} C_2 + \alpha_{33} C_3 + \alpha_{34} C_4 = 0 , \text{ and} \tag{4.29}$$

$$\text{Using Eq. (4.7) or (4.8) or (4.9):} \quad \alpha_{43} C_3 + \alpha_{44} C_4 = 0 , \tag{4.30}$$

The term $\alpha_{ij}$ denotes the coefficient of $C_j$ in the $i$th equation. Equation (4.27) is the first equation, and Eq. (4.30) is the fourth equation in the system of equations. The terms $\alpha_{ij}$ are:

$$\alpha_{11} = C_D \, l\left[I_0(\sqrt{l}) - s\sqrt{l} \; I_1(\sqrt{l})\right] - \sqrt{l} \; I_1(\sqrt{l}) , \tag{4.31}$$

$$\alpha_{12} = C_D \, l\left[K_0(\sqrt{l}) + s\sqrt{l} \; K_1(\sqrt{l})\right] + \sqrt{l} \; K_1(\sqrt{l}) , \tag{4.32}$$

$$\alpha_{21} = I_0(R_D \sqrt{l}) + s_f \; R_D \sqrt{l} \; I_1(R_D \sqrt{l}) , \tag{4.33}$$

$$\alpha_{22} = K_0(R_D \sqrt{l}) - s_f \; R_D \sqrt{l} \; K_1(R_D \sqrt{l}) , \tag{4.34}$$

$$\alpha_{24} = - K_0(R_D \sqrt{l\eta}) , \tag{4.35}$$

$$\alpha_{31} = M\sqrt{l} \; I_1(R_D \sqrt{l}) , \tag{4.36}$$

$$\alpha_{32} = - M\sqrt{l} \; K_1(R_D \sqrt{l}) , \text{ and} \tag{4.37}$$

$$\alpha_{34} = \sqrt{l\eta} \; K_1(R_D \sqrt{l\eta}) . \tag{4.38}$$

The remaining $\alpha$'s depend on the specified outer boundary condition and are given by:

**Infinite outer boundary:**

A bounded solution for $\bar{p}_{D2}$ ($r_D \rightarrow \infty$ , $l$) is obtained from Eq. (4.25) provided $C_3 = 0$, as $I_0$ ($r_D \sqrt{l\eta}$) $\rightarrow \infty$ as $r_D \rightarrow \infty$. Therefore, $\alpha_{23}$, $\alpha_{33}$ and $\alpha_{43}$ in Eqs. (4.28) through (4.30) are set to zero. Also, $\alpha_{44} = 0$, as $K_0$ ($r_D \sqrt{l\eta}$) in Eq. (4.25) approaches zero as $r_D \rightarrow \infty$. Thus:

$$\alpha_{23} = \alpha_{33} = \alpha_{43} = \alpha_{44} = 0 . \tag{4.39}$$

**Closed outer boundary:**

$$\alpha_{23} = -I_0(R_D\sqrt{l\eta}) , \tag{4.40}$$

$$\alpha_{33} = -\sqrt{l\eta}\, I_1(R_D\sqrt{l\eta}) , \tag{4.41}$$

$$\alpha_{43} = I_1(r_{eD}\sqrt{l\eta}) , \text{ and} \tag{4.42}$$

$$\alpha_{44} = -K_1(r_{eD}\sqrt{l\eta}) . \tag{4.43}$$

**Constant-pressure outer boundary:**

$$\alpha_{23} = -I_0(R_D\sqrt{l\eta}) , \tag{4.40}$$

$$\alpha_{33} = -\sqrt{l\eta}\, I_1(R_D\sqrt{l\eta}) , \tag{4.41}$$

$$\alpha_{43} = I_0(r_{eD}\sqrt{l\eta}) , \text{ and} \tag{4.44}$$

$$\alpha_{44} = K_0(r_{eD}\sqrt{l\eta}) . \tag{4.45}$$

This completes the solution of the transient pressure problem for a radial, two-region composite reservoir with a thin skin at the discontinuity. Transient pressure and pressure derivative responses for different cases were generated by inverting the solution numerically from Laplace space to real space using the *Stehfest* (1970) inversion algorithm.

## 4.2 VERIFICATION OF SOLUTION

The solution presented in Sec. 4.1 includes a thin skin at the discontinuity. In the absence of a thin skin at the discontinuity ($s_f = 0$), the solution presented in Sec. 4.1 is identical to the *Eggenschwiler et al.* (1979) solution for an infinitely large reservoir. The solution presented in Sec. 4.1 is identical to the *Horne et al.* (1980) solution for finite composite reservoirs if $s_f = C_D = s = 0$. *Eggenschwiler et al.* checked their solution against *Agarwal et al.* (1970), and *Wattenbarger* and *Ramey* (1970) solutions for a well in a homogeneous reservoir. For a homogeneous reservoir, the two regions have the same properties and thus, $M = \eta = 1$. For a homogeneous reservoir with $s_f = 0$, $R_D$ is arbitrary, and the subscript 1 may be dropped from the definitions of the dimensionless variables in Eqs. (4.12) through (4.22). *Tang* (1982) also discusses the *Eggenschwiler et al.* verification efforts. No further verification seems necessary.

# 5. HOMOGENEOUS RESERVOIR

This chapter presents design equations for a well producing from the center of either an infinitely large or a finite, circular, homogeneous reservoir. This chapter also presents drawdown and buildup pressure derivative type-curves for a well producing at a constant rate from the center of a finite, circular, homogeneous reservoir. Early time response (wellbore storage and skin effects) is correlated by $C_D e^{2s}$ and late time response (outer boundary effects) by $r_{eD}^2/C_D$. The outer boundary may be closed, or at a constant pressure. Producing time effects on buildup responses of a well in a finite, homogeneous reservoir are also discussed. Transient pressure or pressure derivative responses for a well in a homogeneous reservoir have been generated using the solution presented in Chapter 4.1 by setting $M = \eta = 1$, $s_f = 0$, and an arbitrary $R_D$. Several pressure derivatives used in this chapter are given as:

$$\frac{dp_{wD}}{dt_D} = L^{-1}\left[\, l\bar{p}_{wD} \,\right] \quad , \tag{5.1}$$

$$\frac{dp_{wD}}{d\,\ln t_D} = t_D \frac{dp_{wD}}{dt_D} \quad , \text{ and} \tag{5.2}$$

$$\frac{d\,\ln (p_{wD})}{d\,\ln (t_D)} = \frac{t_D}{p_{wD}} \frac{dp_{wD}}{dt_D} \quad . \tag{5.3}$$

## 5.1 INFINITELY LARGE RESERVOIR

Design equations are developed based on the drawdown pressure derivative behavior for a well with or without wellbore storage, and producing from an infinitely large, homogeneous reservoir. The well is assumed to produce at a constant rate.

As shown in Appendix A, the time to the beginning of infinite-acting radial flow with an error in slope of 2% for a well with no wellbore storage is:

$$t_D \geq 140 \, . \tag{5.4}$$

The time in Eq. (5.4), though correct, is of little practical importance because of storage and skin. However, it is much larger than the time based on a 2% error in pressure, and this emphasizes an important result of this study. Pressure and pressure derivatives may appear to indicate greatly different event times.

*Agarwal et al.* (1970) presented a log-log type-curve for the drawdown pressure behavior of a well with wellbore storage and skin, and producing at a constant rate. They used $C_D$ and $s$ as the parameters on their type-curve. *Earlougher* and *Kersch* (1974) first used $C_D e^{2s}$, but *Gringarten et al.* (1979) presented storage and skin type-curve with $C_D e^{2s}$ as it is now popularly used. This appears to be the type-curve that will be used in the future. *Bourdet et al.* (1983a) presented a drawdown pressure derivative type-curve with $C_D e^{2s}$ as the correlating parameter.

Transient pressure response for a well in an infinitely large, homogeneous reservoir exhibits the following flow regimes as time grows longer:

1. Storage-dominated period,
2. Transition period, and
3. Infinite-acting radial flow period.

During the storage-dominated period, the dimensionless wellbore pressure drop and the semilog pressure derivative are:

$$p_{wD} = t_D/C_D \quad , \text{and} \tag{5.5}$$

$$\frac{dp_{wD}}{d \ln t_D} = \frac{t_D}{C_D} \quad . \tag{5.6}$$

During the transition period, the pressure derivative response shows a maximum for $C_D e^{2s} > 1$ (Fig. A.1). At late time, wellbore storage effects cease to be important, and an infinite-acting radial flow develops. During the infinite-acting radial flow period, the dimensionless wellbore pressure drop and the semilog pressure derivative are:

$$p_{wD} = \frac{1}{2}\left[\ln (t_D) + 0.80907 + 2s\right] \quad , \text{and} \tag{5.7}$$

$$\frac{dp_{wD}}{d \ln t_D} = 1/2 \quad . \tag{5.8}$$

Design equations for the time to the end of storage-dominated period and the time to the beginning of infinite-acting radial flow are developed in Appendix B. Appendix B also reports the development of additional design equations to be presented elsewhere in this study. The dimensionless time to the end of storage-dominated period is:

$$\frac{t_D}{C_D} \approx 0.048 \log (C_D e^{2s}) - 0.03 \quad . \tag{5.9}$$

Equation (5.9) describes the time by which the slope of a log-log graph of pressure vs. time has decreased by 2% from the initial value of unity.

*Agarwal et al.* (1970) approximated the time to the end of storage-dominated period as the time at which the sandface rate is equal to 20% of the surface rate. They approximated the time to the end of storage-dominated period by:

$$\frac{t_D}{C_D} = 0.4 \qquad \text{for } s = 0, \text{ and}$$

$$= 0.2\, s \qquad \text{for } s > 0 \quad . \tag{5.10}$$

*Gringarten et al.* (1979) presented the time to the end of storage-dominated period as:

$$\frac{t_D}{C_D} = \alpha \ln\left[3\alpha C_D e^{2s}\right] \quad \text{for } C_D e^{2s} > 10^3 \quad . \tag{5.11}$$

Equation (5.11) was derived by comparing the $p_{wD}$ values from the rigorous solution for the drawdown response for a well with storage and skin, and located in an infinite homogeneous reservoir with those from Eq. (5.5). The parameter $\alpha$ is the tolerance, in fraction, defining the difference between the two solutions. *Gringarten et al.* (1979) used three values of $\alpha$: 0.01, 0.05, and 0.1.

Table 5.1 presents a comparison of the times forecast from Eqs. (5.9), (5.10), and (5.11) for selected values of $C_D e^{2s}$, $C_D$, and $s$. The results from Eq. (5.11) presented in Table 5.1 are obtained using $\alpha = 0.02$ and 0.1.

**Table 5.1 - A comparison of design relations for the time to the end of storage-dominated period**

| $C_D e^{2s}$ | $C_D$ | $s$ | $t_D/C_D$ from | | | |
|---|---|---|---|---|---|---|
| | | | This Study | Agarwal et al. | Gringarten et al. | |
| | | | Eq. (5.9) | Eq. (5.10) | Eq. (5.11) with $\alpha = 0.02$ | Eq. (5.11) with $\alpha = 0.1$ |
| $10^5$ | $10^4$ | 1.15 | 0.22 | 0.23 | 0.17 | 1.03 |
| | $10^3$ | 2.30 | | 0.46 | | |
| | $10^2$ | 3.45 | | 0.69 | | |
| | 10 | 4.61 | | 0.92 | | |
| $10^{10}$ | $10^5$ | 5.76 | 0.47 | 1.15 | 0.4 | 2.18 |
| | $10^4$ | 6.91 | | 1.38 | | |
| | $10^3$ | 8.06 | | 1.61 | | |
| | 10 | 10.36 | | 2.07 | | |
| $10^{20}$ | $10^5$ | 17.27 | 0.97 | 3.45 | 0.86 | 4.48 |
| | $10^4$ | 18.42 | | 3.68 | | |
| | $10^2$ | 20.72 | | 4.14 | | |
| | 10 | 21.87 | | 4.38 | | |

Table 5.1 shows that the results from Eq. (5.9), and Eq. (5.11) with $\alpha = 0.02$ are comparable, even though $t_D/C_D$ from Eq. (5.9) is always slightly larger than that from Eq. (5.11) with $\alpha = 0.02$. Thus, the results from the design relations based on the pressure derivative analysis [Eq. (5.9)] and the pressure analysis [Eq. (5.11) with $\alpha = 0.02$] are the same for the time to the end of storage-dominated period. *Vongvuthipornchai* and *Raghavan* (1988) also discuss this observation. Using the preceding observation, *Vongvuthipornchai* and *Raghavan* also showed that the time for the end of storage-dominated period from Eq. (5.10) should be the same as the time from Eq. (5.11) with $\alpha = 0.1$. Though the results from Eq. (5.10), and Eq. (5.11) with $\alpha = 0.1$ are not exactly the same in Table 5.1, it is apparent that for a given $C_D e^{2s}$, the results from Eq. (5.10), and Eq. (5.11) with $\alpha = 0.1$ would be approximately the same, if $s$ were large.

Appendix B shows that the time at which the semilog pressure derivative is within 2% of 0.5 is:

$$\frac{t_D}{C_D} \approx 280 + 180 \log (C_D e^{2s}) \quad , \tag{5.12}$$

and the time at which the semilog pressure derivative is within 5% of 0.5 is:

$$\frac{t_D}{C_D} \approx 30 + 110 \log (C_D e^{2s}) \quad . \tag{5.13}$$

The dimensionless time estimates from the design equations (5.12) and (5.13) are considerably larger than the dimensionless time estimates from the presently available design equations derived from an analysis of pressure responses such as $t_D/C_D > (60 + 3.5\ s)$ of *Ramey et al.* (1973), and $t_D/C_D > 50\ e^{0.14\ s}$ of *Chen* and *Brigham* (1978). Again the pressure derivative results are quite different from pressure results. The *Chen* and *Brigham* results were based on times when slopes of the pressure graphs were approximately valid.

## 5.2 FINITE RESERVOIR

Transient pressure response for a well producing from a finite reservoir of circular, square, and rectangular drainage shapes has been studied by *van Everdingen* and *Hurst* (1949); *Miller et al.* (1954); *Aziz* and *Flock* (1963); *Earlougher et al.* (1968); *Ramey* and *Cobb* (1971); *Kumar* and *Ramey* (1974); *Cobb* and *Smith* (1975); and *Chen* and *Brigham* (1978), among others. *Mishra* and *Ramey* (1987) presented a buildup derivative type-curve for a well with storage and skin, and producing from the center of a closed, circular reservoir. Their type-curve applies for large producing times such that $t_{pD} > t_{Dpss}$. This chapter presents drawdown and buildup pressure derivative type-curves for a well producing at a constant rate from the center of a finite, circular reservoir. The outer boundary may be closed, or at a constant pressure. The differences between the responses for a well in a closed, circular reservoir (fully-developed field), and a well in a circular reservoir with a constant-pressure outer boundary (active edgewater drive system, or developed five-spot fluid-injection pattern) are discussed. Design relations are developed to estimate the time period which corresponds to infinite-acting radial flow, or to a semilog straight line on a pressure vs. logarithm of time graph. Producing time effects on buildup responses are studied using the slope of a dimensionless *Agarwal* (1980) buildup graph.

### 5.2.1 Drawdown Response

Table 5.2 shows the dimensionless wellbore pressure drop and the semilog pressure derivative expressions for a well in a finite, circular reservoir during specific flow periods.

**Table 5.2 - Dimensionless wellbore drawdown pressure and derivative expressions for a well in a finite, circular homogeneous reservoir**

| Flow period | $p_{wD}$ | $p'_{wD} = dp_{wD}/d \ln t_D$ |
|---|---|---|
| Wellbore storage | $t_D/C_D$ | $t_D/C_D$ |
| Infinite-acting radial flow | $0.5\ [\ln (t_D/C_D) + C_1]$ | 0.5 |
| Pseudosteady state (No wellbore storage, and closed reservoir) | $2\pi\ t_{DA} + C_2$ | $2\pi\ t_{DA}$ |
| Steady state (Constant-pressure outer boundary ) | $\ln (r_{eD}) + s$ | 0 |

$$C_1 = \ln (C_D e^{2s}) + 0.80907 \quad \text{, and} \qquad C_2 = 0.5 \ln \left[ \frac{2.2458\ A}{C_A r_w^2} \right] + s$$

All expressions in Table 5.2 may be written as combinations of $t_D/C_D$, $C_D e^{2s}$, and $r_{eD}^2/C_D$. For example,

$$\ln (r_{eD}) + s = \frac{1}{2} \ln \left[ \frac{r_{eD}^2}{C_D} C_D e^{2s} \right] \quad \text{, and} \tag{5.14}$$

$$C_2 = \frac{1}{2} \ln \left[ \frac{2.2458\ A}{C_A r_w^2} \right] + s = \frac{1}{2} \ln \left[ \frac{2.2458\ \pi}{C_A} \frac{r_{eD}^2}{C_D} C_D e^{2s} \right] . \tag{5.15}$$

Thus, if the dimensionless drawdown pressure and the pressure derivative responses are graphed against $t_D/C_D$, the parameters $C_D e^{2s}$ and $r_{eD}^2/C_D$ may be selected as the correlating parameters. A verification of $C_D e^{2s}$ and $r_{eD}^2/C_D$ as the correlating parameters is also shown in Fig. 5.1 for both closed and constant-pressure outer boundary cases. The individual values of $C_D$, $s$, and $r_{eD}$ used to generate the pressure derivative responses are shown on Fig. 5.1.

Figure 5.2 shows the drawdown pressure derivative type-curve developed in this study. Both closed and constant-pressure outer boundary cases are shown. From Appendix B, the dimensionless times at which the semilog pressure derivative is within 2% of 0.5 are:

$$\left. \frac{t_D}{C_D} \right]_{start} \approx 280 + 180 \log (C_D e^{2s}) \quad \text{, and} \tag{5.16}$$

$$\left. \frac{t_D}{C_D} \right]_{end} \approx \frac{0.175\ r_{eD}^2}{C_D} . \tag{5.17}$$

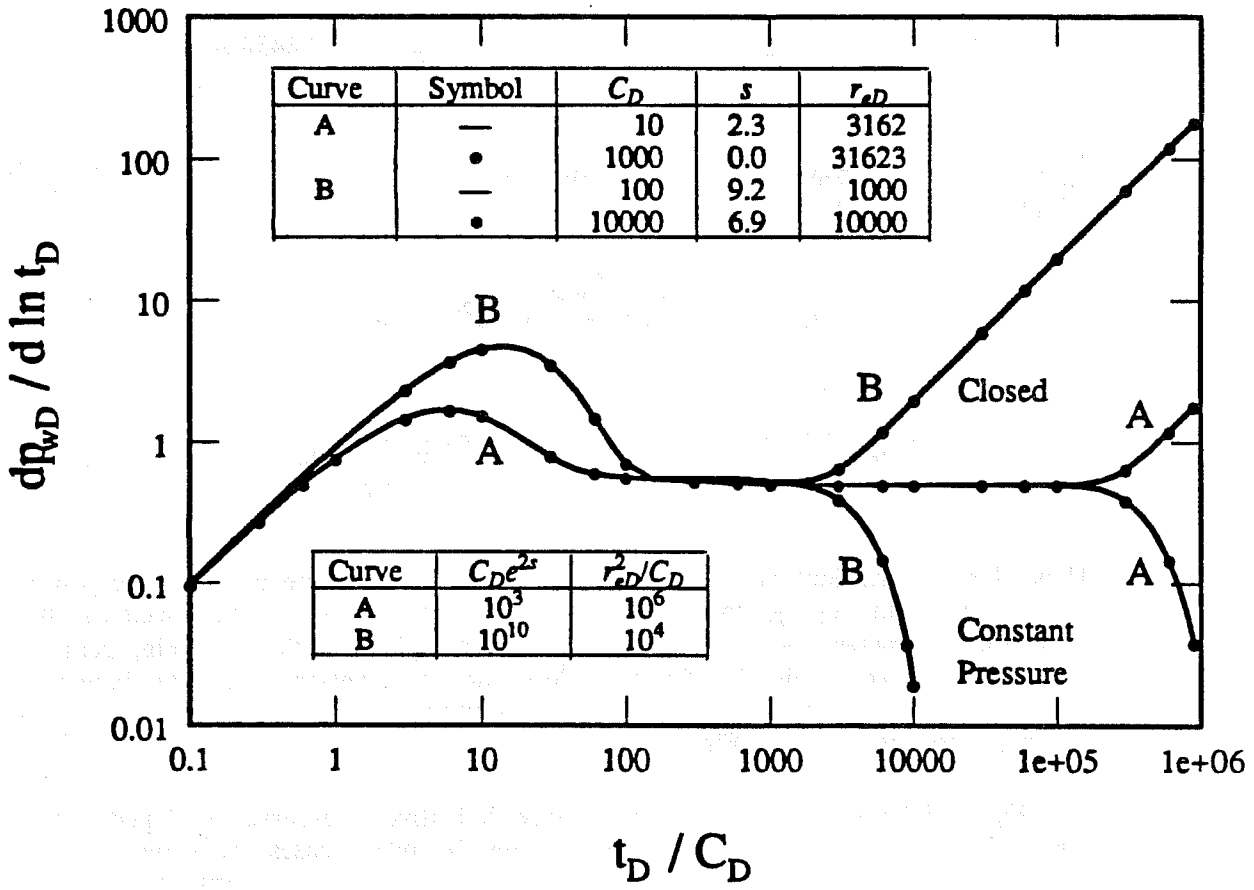


Figure 5.1: Verification of $C_De^{2s}$ and $r_{eD}^2/C_D$ as correlating parameters for drawdown responses.

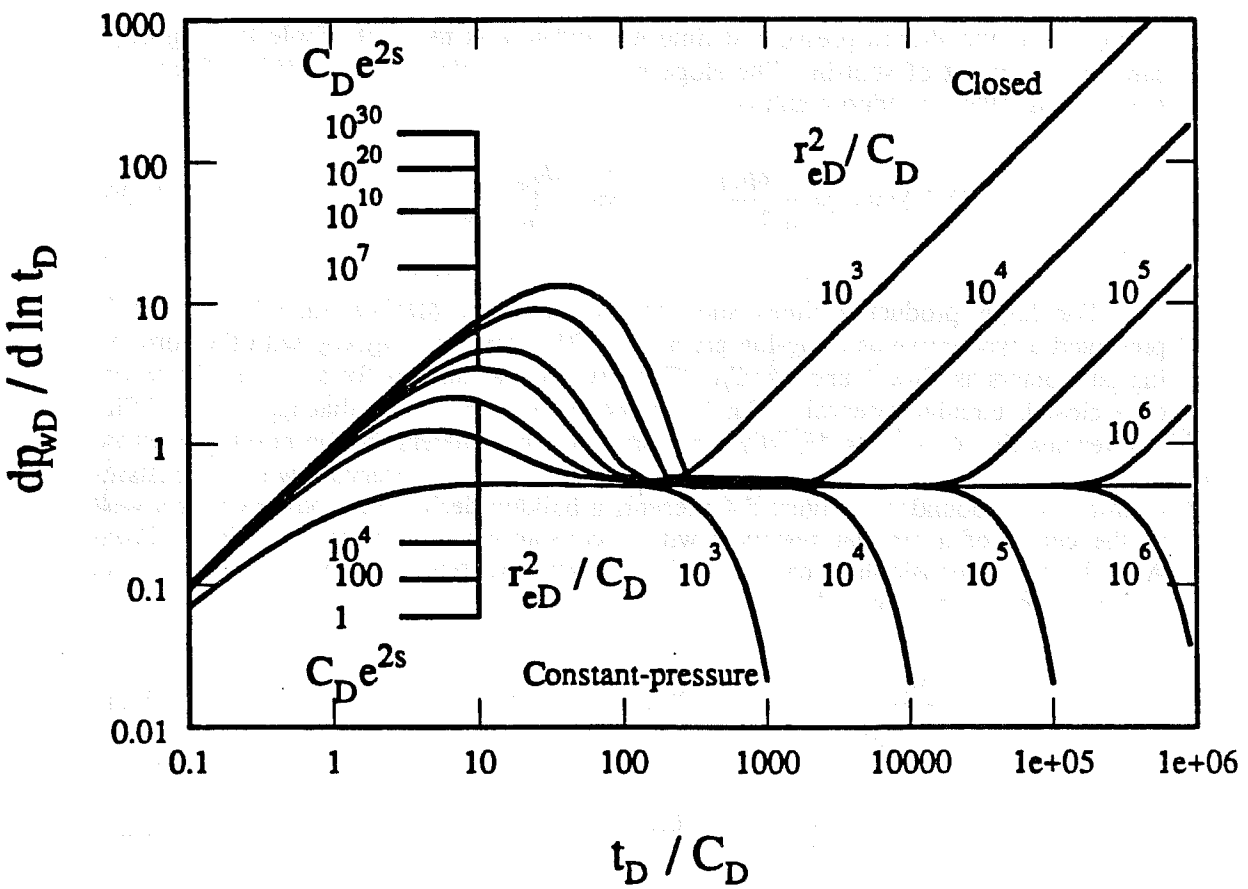


Figure 5.2: Drawdown pressure derivative type-curve.

Design Eqs. (5.16) and (5.17) apply for both closed and constant-pressure outer boundaries. Equations (5.16) and (5.17) yield a condition for the development of at least half a log cycle of semilog straight line as:

$$r_{eD}^2/C_D > 5060 + 3250 \log (C_D e^{2s}) \quad . \tag{5.18}$$

### 5.2.2 Buildup Response

The dimensionless buildup pressure is:

$$p_{wDs}\ (\Delta t_D) = \frac{kh\ (p_{ws} - p_{wf})}{141.2\ qB\mu} = p_{wD}\ (t_{pD}) + p_{wD}\ (\Delta t_D) - p_{wD}\ (t_{pD} + \Delta t_D) \quad , \tag{5.19}$$

where $p_{ws}$ is the shut-in pressure at time $\Delta t$, and $p_{wf}$ is the bottomhole flowing pressure at the instant of shut-in. The slope of a dimensionless *MDH* (*Miller, Dyes,* and *Hutchinson,* 1950) buildup graph is:

$$MDH\ Slope = \frac{dp_{wDs}}{d\ \ln (\Delta t_D)} = \Delta t_D \frac{dp_{wDs}\ (\Delta t_D)}{d\ (\Delta t_D)} \quad . \tag{5.20}$$

For large producing times such that $t_{pD} > t_{Dpss}$, *Mishra* and *Ramey* (1987) presented a type-curve as a log-log graph of *MDH* slope vs. $\Delta t_D/C_D$ with the correlating parameters as $C_D e^{2s}$ and $r_{eD}^2/C_D$. Their type-curve applies for a well in the center of a closed, circular reservoir. For large producing times such that $t_{pD} > t_{Dss}$, Fig. 5.3 verifies that $C_D e^{2s}$ and $r_{eD}^2/C_D$ are correlating parameters for the buildup pressure derivative responses of a well in the center of a circular reservoir with a constant-pressure outer boundary. Figure 5.4 presents a buildup derivative type-curve for a well in the center of a circular reservoir with a constant-pressure outer boundary. From App. B, the dimensionless times at which a semilog buildup pressure derivative is within 2% of 0.5 on Fig. 5.4 are:

$$\left.\frac{\Delta t_D}{C_D}\right]_{start} \approx 280 + 180 \log (C_D e^{2s}) \quad , \text{and} \tag{5.21}$$

$$\left.\frac{\Delta t_D}{C_D}\right]_{end} \approx \frac{0.175\ r_{eD}^2}{C_D} \quad . \tag{5.22}$$

Equations (5.21) and (5.22) yield a condition for the development of at least half a log cycle of semilog straight line, the same as Eq. (5.18).

Figure 5.5 shows buildup derivative responses for a well in a circular reservoir with two different outer boundary conditions: closed and constant-pressure. Figure 5.5 applies for $C_D e^{2s} = 1000$ and $r_{eD}^2/C_D = 10^6$. Figure 5.5 shows that for the same values of $C_D e^{2s}$ and $r_{eD}^2/C_D$, the semilog straight line is longer for a well in a circular reservoir with a constant-pressure outer boundary than for a closed outer boundary.

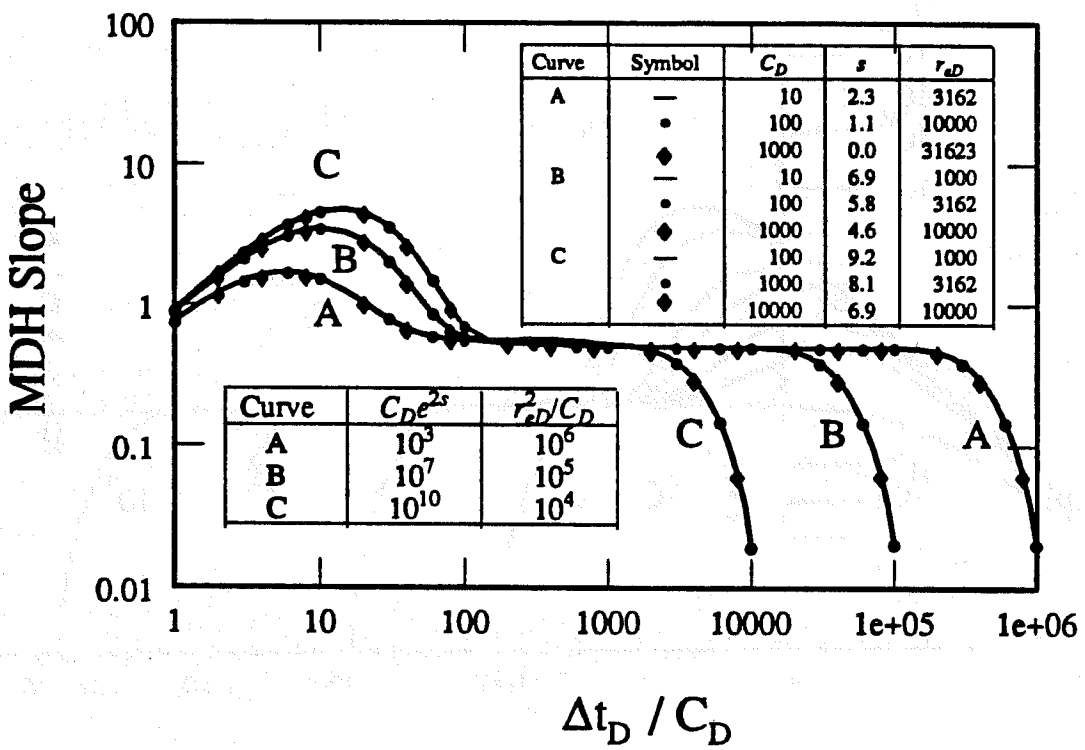


Figure 5.3: Verification of $C_De^{2s}$ and $r_{eD}^2/C_D$ as correlating parameters for buildup responses (Constant-pressure outer boundary).

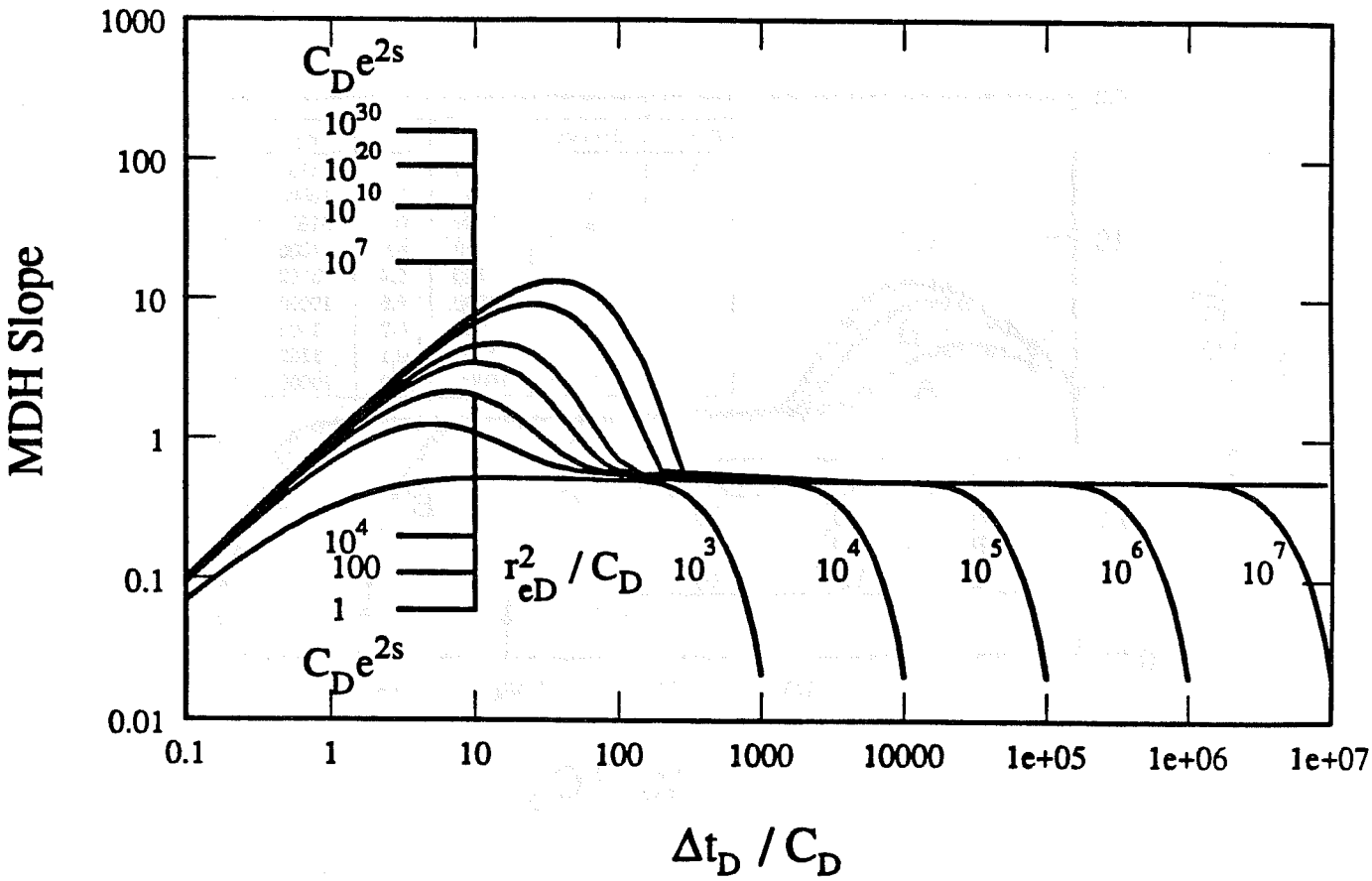


Figure 5.4: Buildup pressure derivative type-curve (Constant-pressure outer boundary).

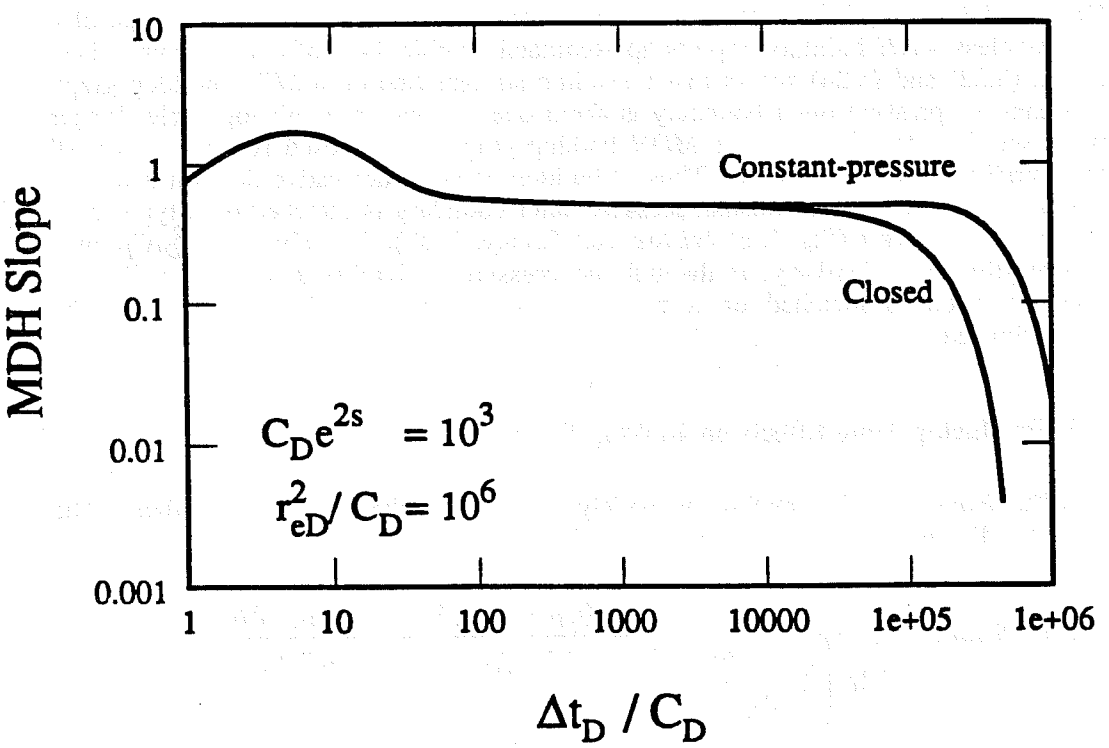


Figure 5.5: Comparison of buildup derivative responses.

From Appendix B, the dimensionless times at which the slope of a dimensionless *MDH* buildup graph for a well in a closed reservoir is within 2% of 0.5 are:

$$\left.\frac{\Delta t_D}{C_D}\right]_{start} \approx 280 + 180 \log (C_D e^{2s}) \quad , \tag{5.23}$$

$$\left.\frac{\Delta t_D}{C_D}\right]_{end} \approx \frac{0.01\, r_{eD}^2}{C_D} \quad \text{for } r_{eD}^2/C_D < 10^5 \quad \text{, and}$$

$$\approx \frac{0.005\, r_{eD}^2}{C_D} \quad \text{for } r_{eD}^2/C_D \geq 10^5 \quad . \tag{5.24}$$

Equation (5.23) is the same as Eq. (5.21). The criterion for $\left.\Delta t_D/C_D\right]_{start}$ presented by *Mishra* and *Ramey* (1987) corresponds to a dimensionless time at which the slope of a dimensionless *MDH* buildup graph is approximately within 14% of 0.5. A comparison of Eqs. (5.22) and (5.24) shows that a semilog straight line on a *MDH* buildup graph for a constant-pressure outer boundary is about one to one-and-a-half log cycles longer than a semilog straight line on a *MDH* buildup graph for a closed reservoir, with all other conditions being the same. Thus, if buildup pressure derivative data for a well in a circular reservoir with a constant-pressure outer boundary is matched on a type-curve for a closed reservoir (Fig. 2 of *Mishra* and *Ramey*, 1987), the value for $r_{eD}^2/C_D$ may be overestimated. Similarly, if the buildup pressure derivative data for a well in a closed reservoir is matched on a type-curve shown in Fig. 5.4, $r_{eD}^2/C_D$ may be underestimated.

### 5.2.3 Producing Time Effects on Buildup Response

The *Horner* (1951) method is widely used for analysis of buildup data. The slope of a dimensionless *Horner* (1951) graph is:

$$Horner\ Slope = \frac{dp_{wDs}}{d \ln\left[\dfrac{t_{pD} + \Delta t_D}{\Delta t_D}\right]} = -\frac{(t_{pD} + \Delta t_D)\Delta t_D}{t_{pD}} \cdot \frac{dp_{wDs}\ (\Delta t_D)}{d\ (\Delta t_D)} \quad . \tag{5.25}$$

*Agarwal* (1980) presented the concept of an equivalent drawdown time for analysis of buildup data using drawdown type-curves for a well in an infinite reservoir. The dimensionless equivalent drawdown time is:

$$\Delta t_{eD} = \frac{t_{pD}\ \Delta t_D}{t_{pD} + \Delta t_D} \quad . \tag{5.26}$$

*Agarwal* (1980) showed that a graph of $p_{wDs}$ vs. $\Delta t_{eD}$ correlated buildup responses for a well in an infinite reservoir with a drawdown response. The correlation was reasonable for producing times larger than the time for storage effects to become

negligible. For producing times less than the time for storage effects to become negligible, early time buildup responses did not correlate well. The slope of a dimensionless *Agarwal* (1980) buildup graph is:

$$Agarwal\ Slope = \frac{dp_{wDs}}{d\ \ln\ (\Delta t_{eD})} = \frac{(t_{pD} + \Delta t_D)\Delta t_D}{t_{pD}} \cdot \frac{dp_{wDs}\ (\Delta t_D)}{d\ (\Delta t_D)} \quad . \qquad (5.27)$$

A comparison of Eqs. (5.25) and (5.27) shows that the *Horner* slope is equal, but opposite in sign to the *Agarwal* slope. Thus, producing time effects on buildup responses may be studied by using either the *Agarwal* or the *Horner* slope.

*Aarstad* (1987) presents the *Agarwal* (1980) slope as a function of dimensionless shut-in time, $\Delta t_{DA}$, for several producing times, $t_{pDA}$, for wells without storage or skin, and located in a square or a rectangle. *Aarstad* showed that a graph of the *Agarwal* slope vs. $\Delta t_{DA}$ does not result in a single curve for all producing times, if a well is located in a square or a rectangle. Therefore, *Aarstad* used $t_{pDA}$ as a parameter to present producing time effects on buildup responses for a well in a square or a rectangle.

Figure 5.6 presents an investigation of $t_{pDA}$ as a correlating parameter for buildup behavior of a well in the center of a closed, circular reservoir. Figure 5.6 applies for $C_D e^{2s} = 10^4$ and $r_{eD}^2/C_D = 10^6$. The values of $C_D$, $s$, $t_{pD}$, and $r_{eD}$ used for various responses are shown on Fig. 5.6. From Fig. 5.6, the early time responses for $t_{pDA} \leq 10^{-5}$ do not agree with the responses for $t_{pDA} \geq 10^{-4}$. For $t_{pDA} \leq 10^{-5}$, the producing time is less than the time for storage effects to become negligible. Thus, the lack of correlation at early times is consistent with *Agarwal's* (1980) finding. At late times, the buildup responses for all producing times do not form a single curve which is consistent with the work by *Aarstad* (1987). The lack of correlation at late times is due to the finite reservoir size.

For buildup derivative data analysis, a log-log graph of $d\ (p_{ws} - p_{wf})/d\ \ln\ (\Delta t_e)$ vs. $\Delta t$ may be matched with a type-curve such as Fig. 2 of *Mishra* and *Ramey* (1987). But Fig. 5.6 shows that a type-curve matching without considering producing time effects may yield an overestimated $r_{eD}^2/C_D$ for smaller producing times.

Figure 5.7 shows an investigation of $t_{pDA}$ as a correlating parameter for the buildup behavior of a well in the center of a circular reservoir with a constant-pressure outer boundary. Figure 5.7 applies for $C_D e^{2s} = 10^4$ and $r_{eD}^2/C_D = 10^6$. The remarks for Fig. 5.6 also apply to Fig. 5.7. Thus, producing time effects may not be ignored in a type-curve matching analysis of buildup derivative data obtained from a well in a finite, circular reservoir.

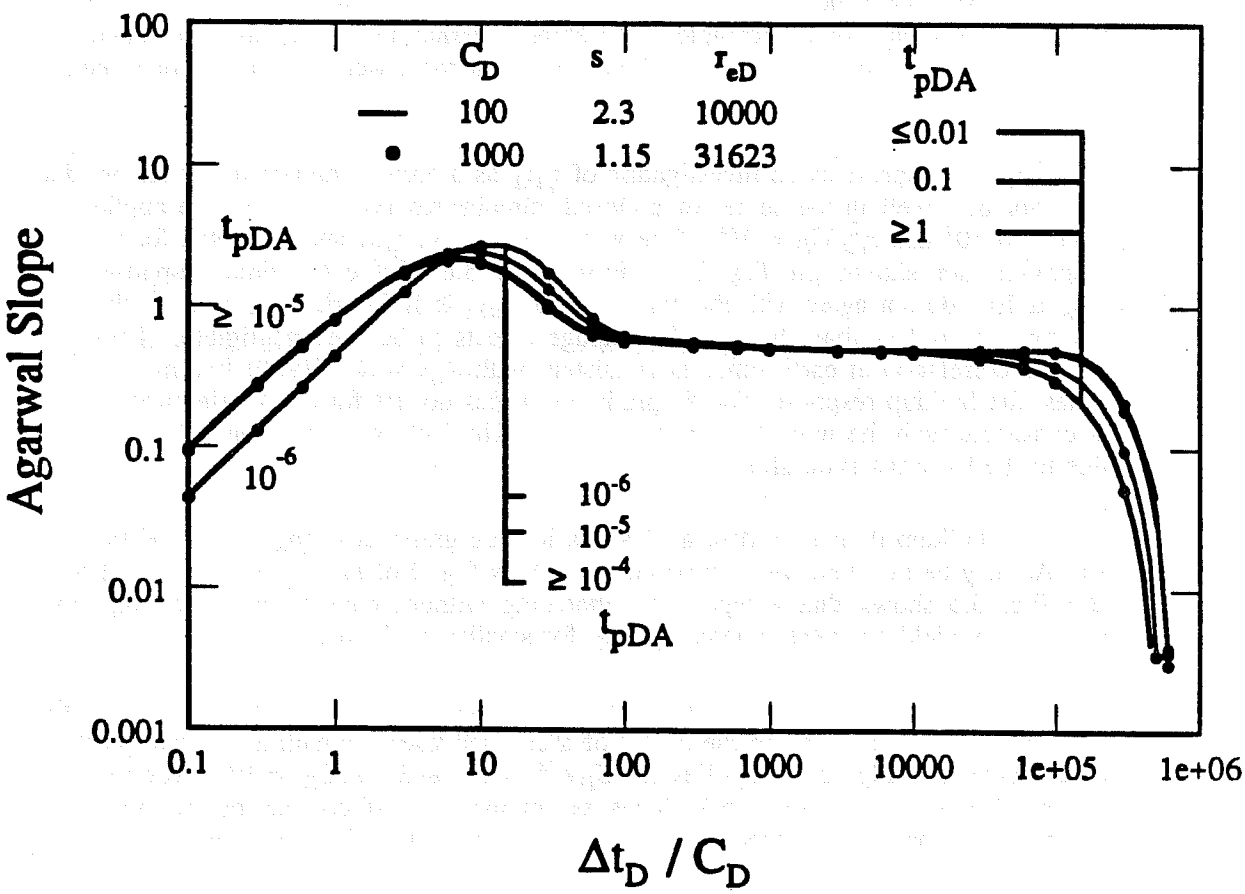


Figure 5.6: Producing time effects on buildup responses for a well in a closed reservoir ($C_De^{2s} = 10^4$, and $r_{eD}^2/C_D = 10^6$).

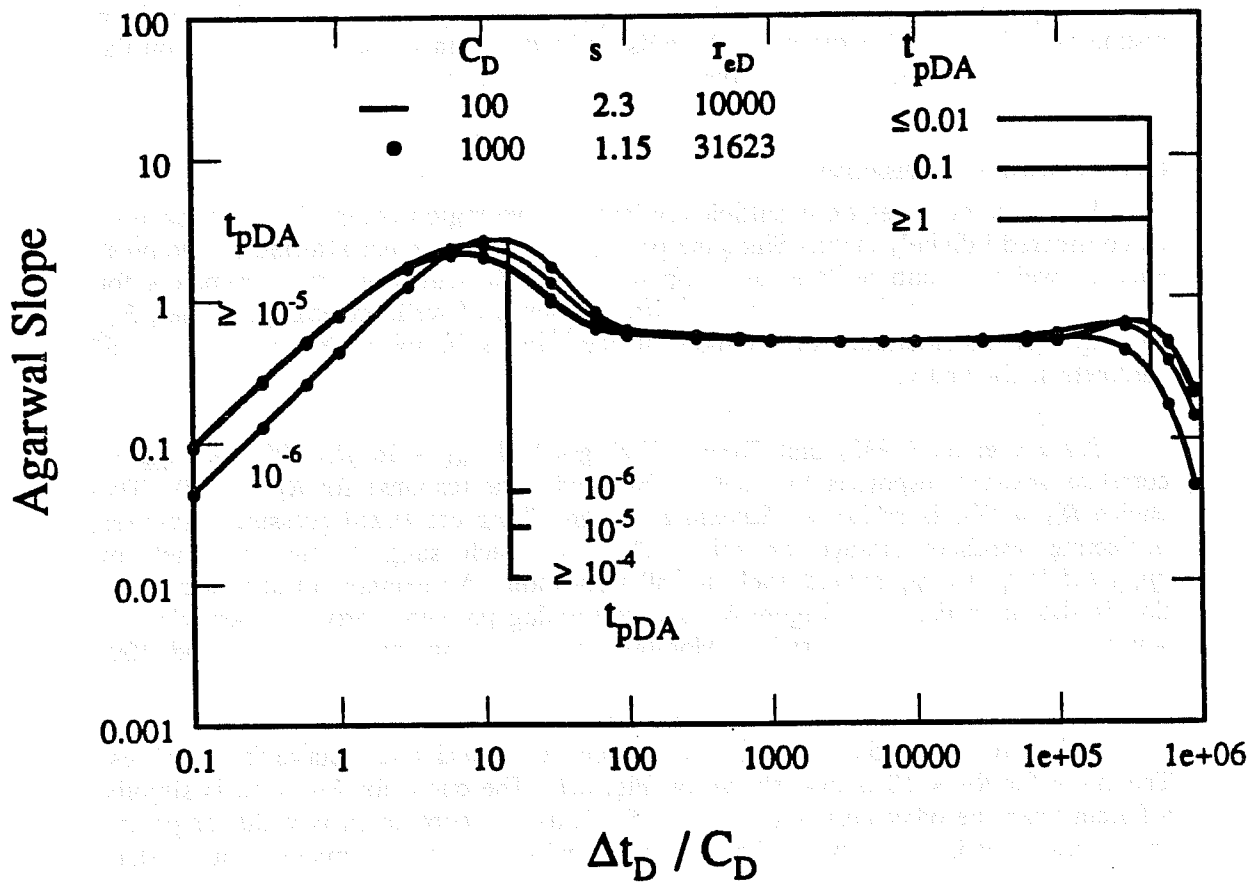


Figure 5.7: Producing time effects on buildup responses for a well in a reservoir with a constant-pressure outer boundary ($C_De^{2s} = 10^4$, and $r_{eD}^2/C_D = 10^6$).

# 6. COMPOSITE RESERVOIR

As discussed in Chapter 1, a composite reservoir represents a number of well test scenarios. Front (or discontinuity) radius, or swept volume is an important parameter sought from well tests in composite reservoirs. A brief description of the methods proposed to estimate a front (or discontinuity) radius, or swept volume appears in Chapter 2. This section considers drawdown and buildup responses for two-region composite reservoirs. Both infinitely large and finite reservoirs are considered. Implications of this study on different methods to estimate a front radius or swept volume are discussed. The effect of an infinitesimally thin skin at the discontinuity and the responses for three-region composite reservoirs are also considered.

## 6.1 TWO-REGION COMPOSITE RESERVOIR

Figure 2.1 shows a schematic diagram of a two-region, radial composite reservoir. Chapter 6.1.1 considers drawdown responses. Chapter 6.1.2 describes buildup responses. Chapter 6.1.3 discusses the effect of a thin skin at the discontinuity on the pressure derivative responses for a two-region composite reservoir.

### 6.1.1 Drawdown Response

When the outer region is sufficiently large, a two-region composite reservoir may be considered infinitely large. Since the pressure derivative is not affected by the presence of wellbore skin as long as wellbore storage is negligible, the parameters for drawdown pressure derivative responses in the absence of wellbore storage are $M$, $F_S$, and $R_D$. A consideration of wellbore storage and skin introduces two additional parameters: $C_D$ and $s$.

*Satman et al.* (1980) and *Tang* (1982) graphed $p_{wD} - \ln (R_D/500)$ vs. $t_{De}$ to correlate pressure responses for all front radii with the response for $R_D = 500$. The choice $R_D = 500$ is arbitrary. *Satman et al.* and *Tang* correlated pressure responses neglecting wellbore storage or skin. Their approach suggests that a graph of $dp_{wD} / d \ln t_D$ vs. $t_{De}$ should apply for all front radii. An example of such a correlation is shown in Fig. 6.1. Figure 6.1 shows semilog pressure derivative behavior for several dimensionless front radii. Mobility and storativity ratios are 10 and 100, respectively.

Curves for $R_D = 50$, 100 and 1000 appear to form a single curve for all times. The curve for $R_D = 10$ is also shown on Fig. 6.1. The curve for $R_D = 10$ is slightly different from the other curves for $t_{De} \leq 0.5$. Thus, the correlation is valid for practical purposes. It is likely that wellbore storage and other practical matters could affect results for $R_D < 50$ and $t_{De} < 0.5$.

Figure 6.2 shows the effect of mobility ratio on the semilog pressure derivative behavior for a fixed storativity ratio of 100 neglecting wellbore storage. The semilog pressure derivative behavior for a homogeneous reservoir ($M = 1$, $F_S = 1$) is also shown on Fig. 6.2. The first semilog straight line of slope 1/2 develops on a dimensionless graph of $p_{wD}$ vs. $\ln (t_D)$. After the end of the first semilog line, the pressure derivative rises for $M \geq 1$. During the transition period, the pressure derivative goes through a maximum above the slope of the second semilog line corresponding to the outer region mobility, if mobility, or storativity ratio, or both, are greater than unity.

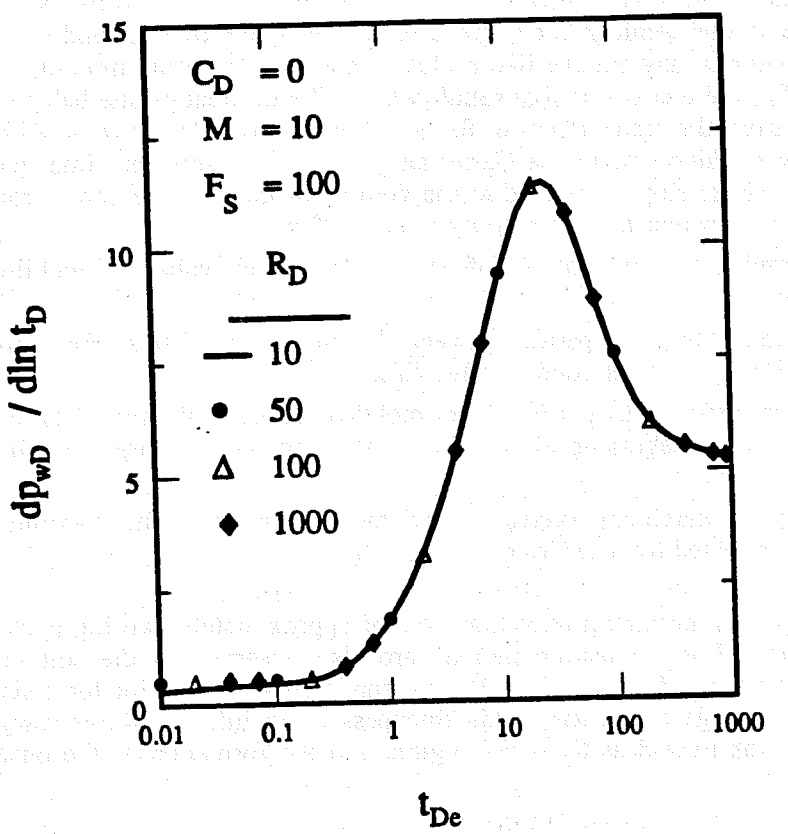


Figure 6.1: Correlation of semi-log pressure derivative for a two-region composite reservoir.

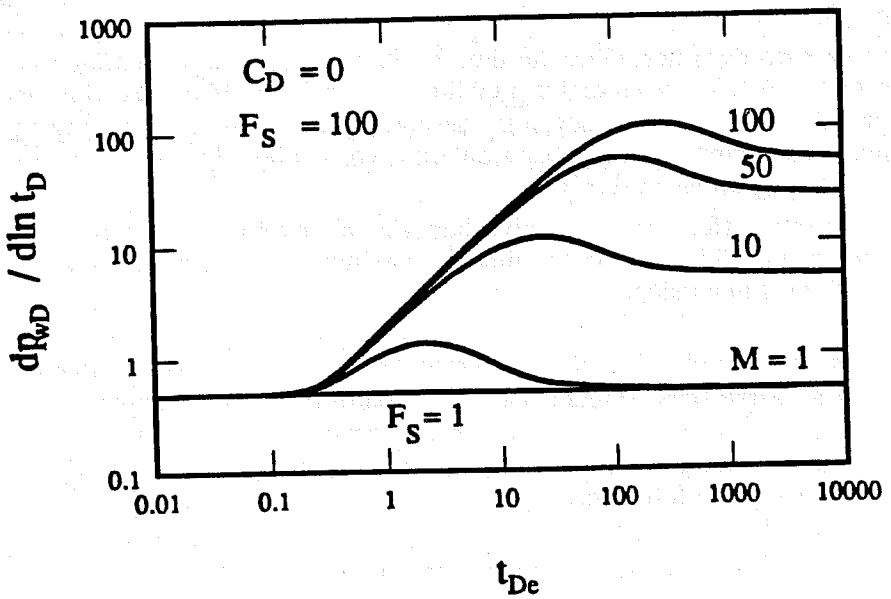


Figure 6.2: Effect of mobility ratio on semi-log pressure derivative for a two-region composite reservoir.

Even in the case of unit mobility ratio, there is a long transition between the two semilog straight lines. The second semilog line slope is $M/2$. For large mobility and storativity ratios, the inner region may behave like a closed reservoir for some time during the transition period after the end of the first semilog line. Pseudosteady state behavior of the inner region during the transition was found by *Eggenschwiler et al.* (1979). Thus, during the early transition period, a Cartesian graph of pressure vs. time may contain a straight line, whose slope is related to the volume of the inner region. From Fig. 6.2, the following is apparent for a storativity ratio of 100:

1. The first semilog line ends at $t_{De}$ of about 0.18, for all values of mobility ratio studied.
2. There is a long transition period between the end of the first semilog line and the beginning of the second semilog line.
3. The transition period is longer for larger mobility ratios. This translates to a longer time to the beginning of the second semilog line for large mobility ratios.
4. The time to the maximum derivative and the magnitude of the maximum derivative is affected by mobility ratio.

*Brown* (1985) reports a minimum transition time of approximately two log cycles for composite reservoirs. Long transition periods are also observed in the solution presented by *Wattenbarger* and *Ramey* (1970) for pressure transient behavior for a single well with wellbore storage and a finite skin thickness in an infinitely large reservoir. The skin region was treated as the inner region, and the formation as the outer region.

Figure 6.3 presents the effect of storativity ratio on semilog pressure derivative behavior for a mobility ratio of 10. For storativity ratios greater than unity, the pressure derivative rises above the value $M/2$ during the transition period, and passes through a maximum slope. Thus, a hump occurs in the pressure derivative behavior for mobility and storativity ratios larger than unity. Figure 6.3 shows the following for a mobility ratio of 10:

1. Storativity ratio does not affect the time to the end of the first semilog line corresponding to the inner region mobility, and mildly affects the time to the beginning of the second semilog line corresponding to the outer region mobility. The transition time between the two semilog lines is approximately three log cycles in duration.
2. Storativity ratio affects the derivative behavior at intermediate times. The storativity ratio mildly affects the time to maximum slope, and the magnitude of the maximum slope.

Figure 6.4 presents a graph of semilog pressure derivative vs. $t_{De}$ with mobility and storativity ratios as parameters. Figure 6.4 is a pressure derivative type-curve for composite reservoirs in the absence of wellbore storage. Analysis of Fig. 6.4 results in several empirical well test design equations for composite reservoirs. These design equations are summarized in the following.

From Fig. 6.4, the time to the end of the first semilog straight line is:

$$(t_{De})_{end} \approx 0.18 \, . \tag{6.1}$$

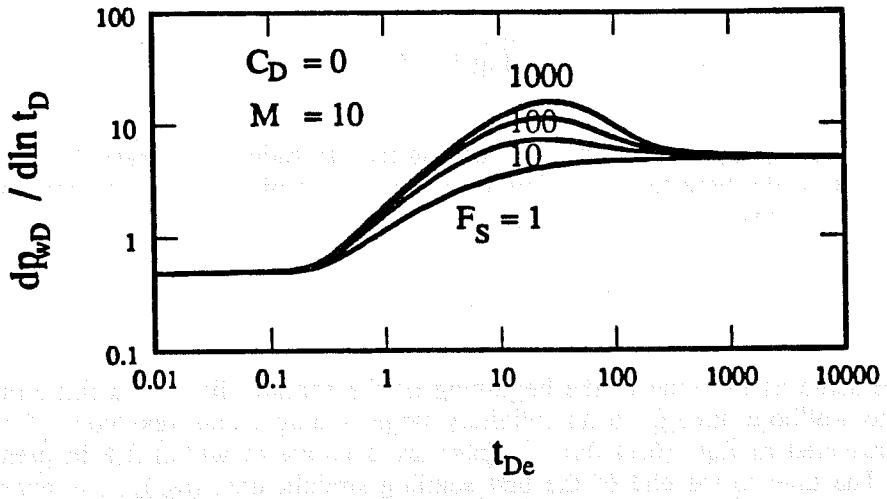


Figure 6.3: Effect of storativity ratio on semi-log pressure derivative for a two-region composite reservoir.

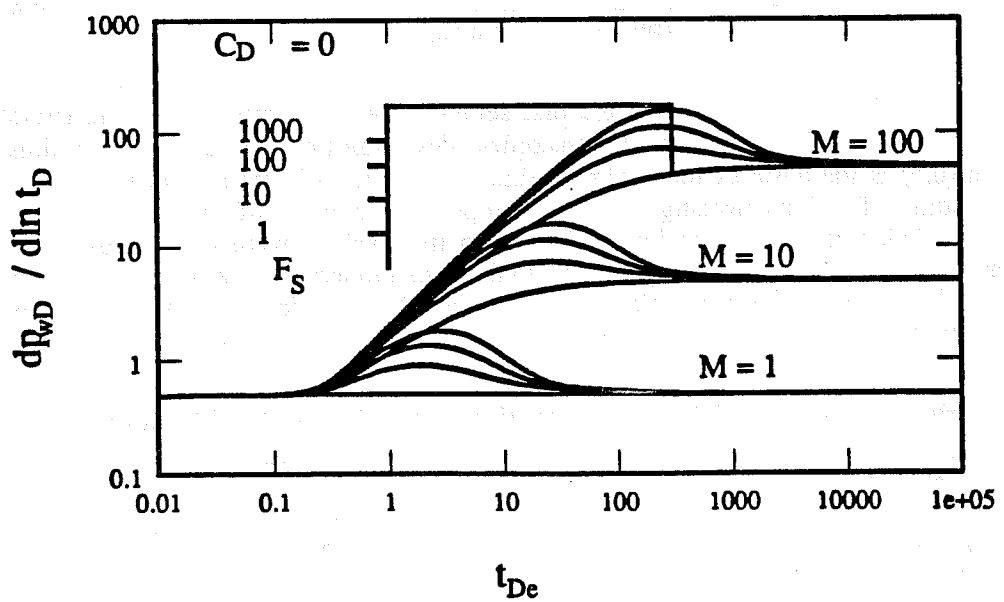


Figure 6.4: Pressure derivative type-curve for a two-region composite reservoir.

From Appendix B, the time to the maximum derivative in the transition is:

$$(t_{De})_{\max} \approx (1.8 + 0.4 \log F_S)\, M \quad , \text{ and} \tag{6.2}$$

the time of start of the second semilog line is:

$$(t_{De})_{II} \approx 90\ (1 + \log F_S)\, M \quad . \tag{6.3}$$

Equations (6.2) and (6.3) apply if mobility and storativity ratios are greater than unity. From Appendix A, the time to the beginning of the first semilog line corresponding to inner region mobility is:

$$t_D \geq 140 \quad , \tag{6.4}$$

which is the same as the time to the beginning of the semilog line for a finite-radius well with no wellbore storage in an infinitely large homogeneous reservoir. Design equations presented in Eqs. (6.1) through (6.4) are accurate to within 2% in pressure derivative. The time to the end of the first semilog straight line, $(t_{De})_{end}$, is approximately 0.21 for a 5% change from the slope of 1/2. Several investigators have developed criteria for $(t_{De})_{end}$ and $(t_{De})_{II}$ using pressure data to certain precision. In the following, we compare Eqs. (6.1) and (6.3) with other design criteria.

The time to the end of the first semilog line, also called deviation time, has been used widely to calculate front radius. The appropriate equation in field units to calculate the front radius is:

$$R = \sqrt{\frac{0.000264\ k_1}{(\phi\mu c_t)_1} \cdot \frac{t_{end}}{(t_{De})_{end}}} \quad , \tag{6.5}$$

where $t_{end}$ is the time to the end of the first semilog line on a pressure vs. log (time) graph, in hours, and $(t_{De})_{end}$ is the dimensionless deviation time based on front radius. Equation (6.5) is the basis of the deviation time method to estimate a front (or discontinuity) radius. Previous investigators have proposed a number of values for dimensionless deviation time. Dimensionless deviation time values were derived by either the drainage-radius concept, or a graphical analysis of numerical or analytical pressure responses from composite reservoirs. A summary of dimensionless deviation times, $(t_{De})_{end}$, proposed by several authors is presented in Table 6.1.

**Table 6.1 - Dimensionless deviation times presented in the literature**

| Reference | $(t_{De})_{end}$ |
|---|---|
| *Tek et al.* (1957) | 0.054 |
| *Hurst* (1960) | 0.143 |
| *Jones* (1962) | 0.063 |
| *Van Poollen* (1964) | 0.25 |
| *Merrill et al.* (1974) | 0.13 - 1.39 (Average = 0.389) |
| *Tang* (1982) | 0.4 |
| *This study* (1988) | 0.18 |

*Van Poollen* (1965) used a value for $(t_{De})_{end}$ derived on the basis of the radius of drainage concept in an earlier paper (*Van Poollen*, 1964). *Merrill et al.* (1974) derived a value for $(t_{De})_{end}$ by generating a large number of pressure falloff curves for two-zone, radial composite reservoirs using a numerical simulator. They found the dimensionless deviation time to lie between 0.13 and 1.39 by running several cases. The arithmetic average dimensionless deviation time was 0.389. They stated that the range of error using the arithmetic average value of $(t_{De})_{end} = 0.389$ would be:

$$0.58 \leq \frac{R \text{ using } (t_{De})_{end} = 0.389 \text{ in Eq. (6.5)}}{\text{Actual } R} \leq 1.89 \quad . \tag{6.6}$$

They felt that this range of error was too large, and advised against indiscriminate use of deviation time to calculate the radius of a fluid bank. *Sosa et al.* (1981) used an average dimensionless deviation time of 0.389 to analyze simulated falloff tests in water injection wells. *Sosa et al.* observed that the front radius using the deviation time method was not an accurate estimate for the radius of the water-flooded region.

*Tang* (1982) approximated $(t_{De})_{end}$ to be 0.4 by observing the pressure response from the *Eggenschwiler et al.* (1979) analytical solution. Figure 6.5 shows the semilog pressure derivative responses from the *Eggenschwiler et al.* solution for several values of mobility and storativity ratios. Figure 6.5 also includes the responses for $M < 1$ and $F_S < 1$. Figure 6.6 shows the pressure responses on a log-log graph for the same combinations of $M$ and $F_S$ as used in Fig. 6.5. The dimensionless deviation time of 0.4 on Fig. 6.6 corresponds to approximately 2% departure of the pressure response from the semilog line corresponding to the inner region mobility. However, Fig. 6.5 shows semilog pressure derivatives of 0.80 for $M = F_S = 100$, and 0.33 for $M = F_S = 0.1$ at the dimensionless time $t_{De} = 0.4$. Thus, on a derivative graph, $t_{De} = 0.4$ may correspond to approximately +60% or -34% change in slope compared to 1/2, depending on the mobility ratio. Also, though $(t_{De})_{end}$ of 0.18 and 0.4 are not dramatically different, a front radius calculated by using $(t_{De})_{end} = 0.4$ will be approximately 0.67 times a front radius calculated by using $(t_{De})_{end} = 0.18$, with all other parameters remaining the same. This is a significant difference in answers for front radius, indicating the need for accurate specification of deviation time to obtain meaningful results from the deviation time method.

Using $(t_{De})_{end} = 0.18$ in Eq. (6.5), a convenient expression in field units to calculate $R$ is:

$$R = \sqrt{\frac{k_1}{(\phi\mu c_t)_1} \frac{t_{end}}{681.8}} \quad . \tag{6.7}$$

Using $(t_{De})_{end} = 0.4$ in Eq. (6.5) yields:

$$R = \sqrt{\frac{k_1}{(\phi\mu c_t)_1} \frac{t_{end}}{1515.2}} \quad . \tag{6.8}$$

Mobility, or storativity ratio, or both should be about one order of magnitude away from unity to obtain a deviation time precisely, and thus obtain reasonable results from the use of Eq. (6.7) or (6.8). Equation (6.7) or (6.8) can be used if the assumptions of the analytical model are reasonably satisfied, and wellbore storage does not mask the first semilog line corresponding to the inner region mobility.

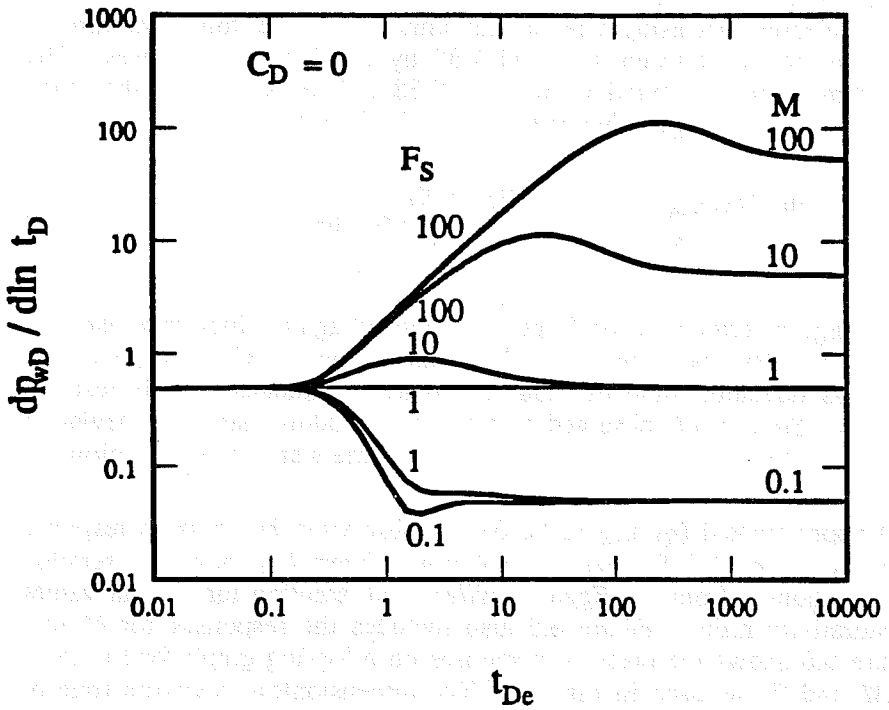


Figure 6.5: Semi-log pressure derivative for a well in a two-region composite reservoir.

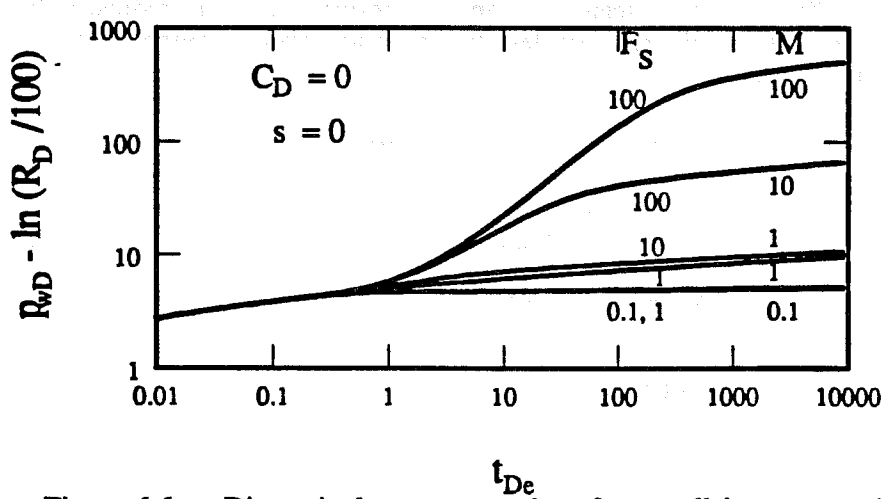


Figure 6.6: Dimensionless pressure drop for a well in a two-region composite reservoir.

As will be shown in Chapter 7, the geometry of the swept region is also a critical factor in the application of the deviation time method. If the swept inner region is not cylindrical, then the deviation time should correspond to the closest discontinuity affecting the transient response at the well. Thus, deviation time could correspond to a "minimum" front radius, and an underestimated swept volume. The swept region may not be cylindrical because of:

1. Gravity override and underride, as in case of thermal processes.
2. Viscous fingering, as in the case of unfavorable mobility ratio processes, such as $CO_2$ flooding.

The time to the beginning of the second semilog line has been of interest to many investigators. Development of a second semilog line is required for the intersection time method to determine front radius. *Odeh* (1969) investigated reservoirs with mobility ratios equal to diffusivity ratios (i.e, $F_S = 1$), that varied from 0.25 to 50 using an analytical solution. He found, by graphical methods, that the second semilog line starts at:

$$(t_{De})_{II} = 7.7\, M \quad , \qquad \text{for } F_S = 1 \, . \tag{6.9}$$

By comparing the pressure response from the *Eggenschwiler et al.* (1979) analytical solution with *Ramey's* (1970) approximate solution, *Tang* (1982) obtained:

$$(t_{De})_{II} \approx \frac{10\, M^{2 - 1/F_S}}{F_S} \quad , \qquad \text{for } M/F_S \geq 1 \, ,$$

$$\approx 0.44 + \frac{10\, M^2}{F_S} \quad , \qquad \text{for } M/F_S < 1 \, . \tag{6.10}$$

Substituting $F_S = 1$ in Eq. (6.10) for $M/F_S \geq 1$ results in:

$$(t_{De})_{II} \approx 10\, M \, . \tag{6.11}$$

Thus, Eqs. (6.9) and (6.11) produce a time to the beginning of the second semilog line in the same range, for $F_S = 1$. Equation (6.9) is accurate to within 9%, and Eq. (6.11) to within 5%. The late time dimensionless wellbore pressure-drop for a well in an infinitely large composite reservoir is:

$$p_{wD} = \frac{1}{2}\left[M \ln\left[\frac{2.2458\, t_{De}}{\eta}\right] + \ln\left[R_D{}^2\right]\right] + s \quad . \tag{6.12}$$

Although a brief derivation of Eq. (6.12) is presented in the paper by *Ramey* (1970), Eq. (6.12) is derived starting from *Ramey's* (1970) approximate solution in Appendix C. A late time drawdown solution for a well in a finite composite reservoir with a constant-pressure or a closed outer boundary is also derived in Appendix C. For a well in an infinitely large composite reservoir, the derivation in Appendix C

provides criteria for the time to the beginning of the second semilog line as:

$$(t_{De})_{II} > \frac{100\,M}{F_S} \quad , \qquad \text{for } M/F_S \geq 1 \, ,$$

$$> 100 \quad , \qquad \text{for } M/F_S \leq 1 \, . \tag{6.13}$$

Thus, Eq. (6.13) establishes a lower limit for $(t_{De})_{II}$. Any design equation presented for $(t_{De})_{II}$ must produce $(t_{De})_{II}$ larger than, or equal to those from Eq. (6.13).

Results from Eq. (6.10) were compared with those from Eq. (6.13). Results from Eq. (6.10) were poor. Equation (6.10) applies if $M$, $F_S$ and $\eta$ are all greater than unity. Equation (6.3) developed previously in this study results in a longer time than Eq. (6.10).

The difference between times computed from Eqs. (6.3) and (6.1) is the transition time to reach the second semilog line after the end of the first semilog line. Even for moderate mobility ratio cases, the transition time is so long that well tests would seldom be run long enough to observe the second semilog line. The second semilog line may also be masked by outer boundary effects. It is likely that only one semilog line will be evident in most cases. Next, a derivative type-curve matching method based on Fig. 6.4 is considered.

Wellbore storage should be small to use the type-curve presented in Fig. 6.4 for an infinitely large composite reservoir. Well test data collection to a time slightly larger than the time indicated by Eq. (6.2) is recommended, so that a bending over of the semilog pressure derivative is observed. From Appendix B, an approximate expression for the maximum semilog pressure derivative at the time $(t_{De})_{\max}$ in an infinitely large composite reservoir is:

$$\left[\frac{dp_{wD}}{dlog\ t_D}\right]_{\max} = (1.1 + \log F_S) \quad , \text{for } M = 1$$

$$= (0.7 + \log F_S)\, M \ , \text{for } M \geq 10 \, . \tag{6.14}$$

Equation (6.14) is applicable for cases where $M \geq 1$, and $F_S > 10$.

If the conditions listed are satisfied, then type-curve matching can provide values of $M$ and $F_S$. The pressure derivative match point can be used to calculate $(k/\mu)_1$ by:

$$\left[\frac{k}{\mu}\right]_1 = \frac{141.2\ q\ B}{h} \cdot \frac{(dp_{wD}\ /\ dlog\ t_D)_{Match}}{(dp_w\ /\ dlog\ t)_{Match}} \quad , \tag{6.15}$$

and the time match point yields an estimate of front radius, $R$, if the inner region properties are known. An estimate of front radius, $R$, is given by:

$$R = \sqrt{\frac{0.000264\ k_1}{(\phi\mu c_t)_1} \cdot \frac{t_{Match}}{(t_{De})_{Match}}} \quad . \tag{6.16}$$

In the following, the pseudosteady state method is considered and a correlation for the time to the end of pseudosteady state behavior is presented. Pseudosteady state behavior may be observed when $t_{DA} > 0.1$, where $t_{DA}$ is based on area, $A = \pi R^2$. *Eggenschwiler et al.* (1979) used Eq. (2.7) to relate the slope of a Cartesian straight line on a graph of pressure vs. time, and the inner zone swept volume.

During pseudosteady state, the dimensionless pressure for a well in a homogeneous reservoir is given by (*Ramey* and *Cobb*, 1971):

$$p_{wD} = 2\pi t_{DA} + \frac{1}{2}\ln\left[\frac{A}{r_w{}^2}\right] + \frac{1}{2}\ln\left[\frac{2.2458}{C_A}\right] \quad . \tag{6.17}$$

Differentiating Eq. (6.17) with respect to $t_{DA}$ results in:

$$\frac{dp_{wD}}{dt_{DA}} = 2\,\pi \quad , \tag{6.18}$$

where $t_{DA}$ is based on area, $A = \pi R^2$. The Cartesian pressure derivative during infinite-acting (semilog) radial flow for inner and outer regions, respectively, are given by:

$$\frac{dp_{wD}}{dt_{DA}} = \frac{1}{2\ t_{DA}} \quad , \text{ and} \tag{6.19}$$

$$\frac{dp_{wD}}{dt_{DA}} = \frac{M}{2\ t_{DA}} \quad . \tag{6.20}$$

Thus, based on Eqs. (6.18) through (6.20), on a log-log presentation, a Cartesian derivative would show a slope of $-1$ during infinite-acting radial flow of inner and outer regions, and would be constant at $2\,\pi$ during the pseudosteady state period. This is shown in Fig. 6.7. Dimensionless front radii of 100, 500 and 1000 are presented on Fig. 6.7. Mobility and storativity ratios are both 100 in Fig. 6.7.

Figure 6.8 presents the effect of mobility ratio on the Cartesian pressure derivative for $F_S$ of 100. Early and late time behaviors shown on Fig. 6.8 follow Eqs. (6.19) and (6.20). From Fig. 6.8, after the end of the infinite-acting radial flow corresponding to the inner region mobility, a short duration pseudosteady state period is evident, depending on the value of mobility ratio. The larger the value of mobility ratio, the longer is the duration of the pseudosteady state period.

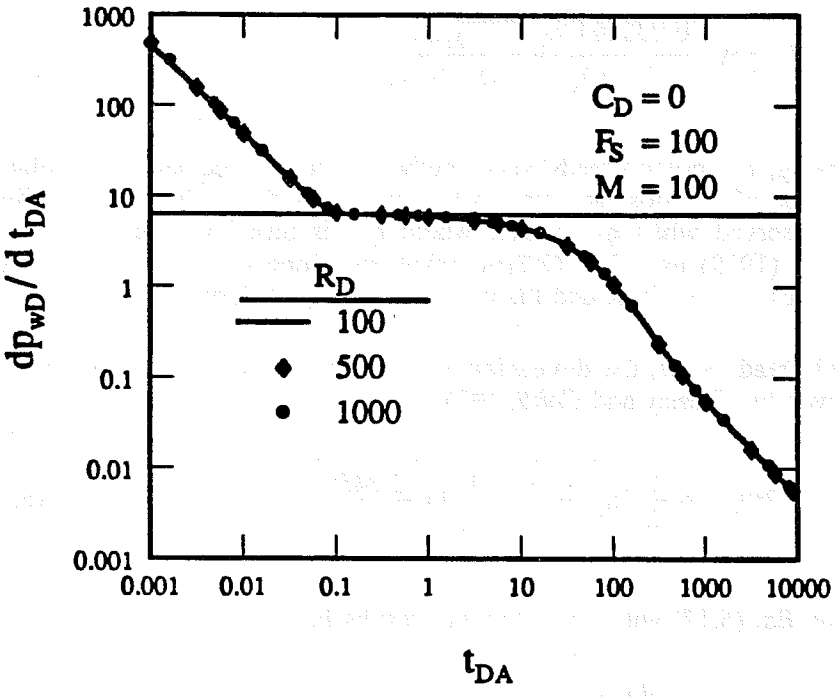


Figure 6.7: Cartesian derivative for a two-region composite reservoir.

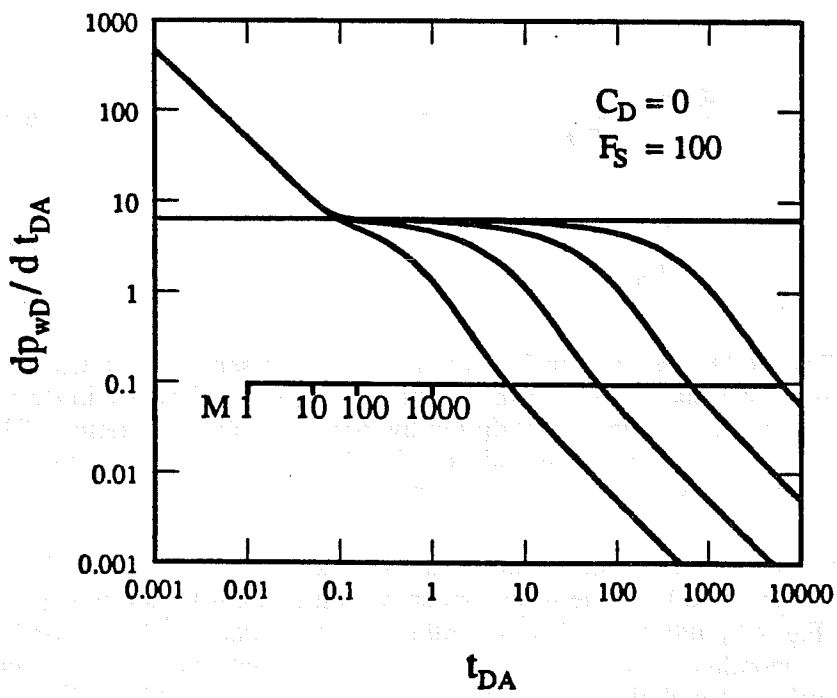


Figure 6.8: Effect of mobility ratio on Cartesian derivative for a two-region composite reservoir.

Figure 6.9 presents the effect of storativity ratio on the Cartesian pressure derivative for $M = 100$. Remarks for Fig. 6.8 also apply to Fig. 6.9. For a given mobility ratio, the pseudosteady state period increases for increasing storativity ratios. Storativity ratio also affects the Cartesian pressure derivative at intermediate times. The late time Cartesian pressure derivative is independent of the storativity ratio, and follows behavior forecast by Eq. (6.20).

Correlations for the time to the end of pseudosteady state behavior are shown on Fig. 6.10. Table 6.2 presents selected data used to develop the correlations on Fig. 6.10.

**Table 6.2 - Time to the end of pseudosteady state behavior corresponding to the inner swept volume**

| $M$ | $F_S$ | $t_{DA}$ for Cartesian slope within 2% of $2\pi$ | $t_{DA}$ for Cartesian slope within 5% of $2\pi$ |
|---|---|---|---|
| 10 | 10 | 0.108 | 0.119 |
| 20 | | 0.116 | 0.131 |
| 50 | | 0.126 | 0.157 |
| 70 | | 0.131 | 0.177 |
| 100 | | 0.136 | 0.208 |
| 200 | | 0.148 | 0.371 |
| 500 | | 0.177 | 0.811 |
| 700 | | 0.192 | 1.092 |
| 1000 | | 0.294 | 1.516 |
| 10 | 100 | 0.126 | 0.155 |
| 20 | | 0.138 | 0.207 |
| 50 | | 0.158 | 0.438 |
| 70 | | 0.173 | 0.584 |
| 100 | | 0.191 | 0.792 |
| 200 | | 0.403 | 1.483 |
| 500 | | 0.900 | 3.589 |
| 700 | | 1.207 | 4.972 |
| 1000 | | 1.672 | 7.070 |
| 10 | 1000 | 0.145 | 0.237 |
| 20 | | 0.168 | 0.422 |
| 50 | | 0.314 | 0.929 |
| 70 | | 0.435 | 1.261 |
| 100 | | 0.600 | 1.762 |
| 200 | | 1.085 | 3.444 |
| 500 | | 2.545 | 8.468 |
| 700 | | 3.541 | 11.818 |
| 1000 | | 5.012 | 16.854 |

From Fig. 6.10, the time to the end of pseudosteady state behavior is larger for larger values of mobility and storativity ratios. Using the correlation for the slope to be within 2% of $2\pi$ in Fig. 6.10, empirically, we observe that pseudosteady state behavior is likely to appear for cases with $MF_S \geq 10^4$ and $M \geq 10$, if pseudosteady state behavior is desired to last up to $t_{DA} \approx 0.2$. Correlations presented in Fig. 6.10 should be of help in choosing the correct pseudosteady Cartesian line to calculate swept volume.

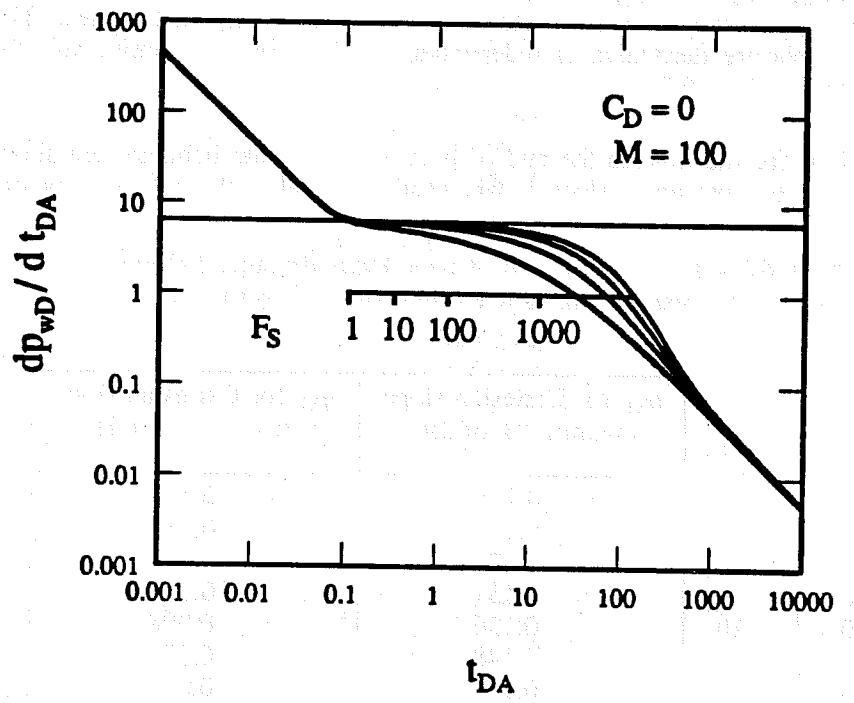


Figure 6.9: Effect of storativity ratio on Cartesian derivative for a two-region composite reservoir.

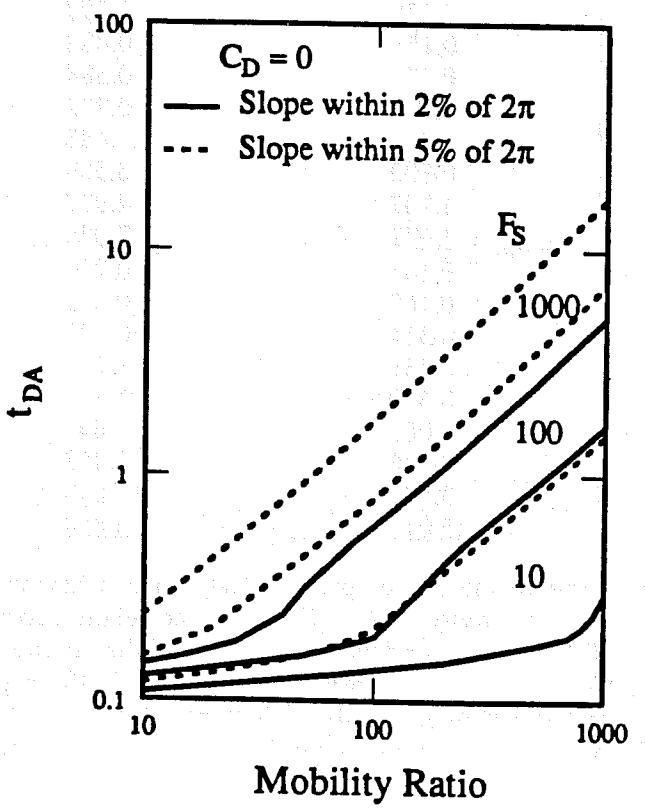


Figure 6.10: Correlation for the end of pseudosteady state for a two-region composite reservoir.

Well test analysis using any of the preceding methods discussed may fail because of:

1. Wellbore storage effects, and/or
2. Outer boundary effects.

Wellbore storage may mask the evidence of a semilog line corresponding to the inner region mobility. An empirical criterion for the time to the end of wellbore storage effects based on an analysis of pressure derivative response for a well in an infinitely large homogeneous reservoir is given by Eq. (5.9). Equation (5.9) may be used to calculate whether wellbore storage effects would decrease sufficiently approximately one-and-a-half log cycles before $(t_{De})_{end} = 0.18$. However, the limitations on the deviation time method due to wellbore storage effects may be studied directly by comparing $(t_{De})_{end}$ with the time to the beginning of the semilog line corresponding to the inner region mobility given by Eqs. (5.12) and (5.13).

Using Eq. (5.12) and $(t_{De})_{end} = 0.18$, the following relation may be obtained to observe at least one-half log cycle of a semilog line corresponding to the inner region mobility:

$$\frac{R_D^2}{C_D} \geq 17.6\ [280 + 180 \log (C_D e^{2s})] \ . \tag{6.21}$$

Another form of Eq. (6.21) is:

$$R_D \geq 4.2 \sqrt{C_D\ [280 + 180 \log (C_D e^{2s})]} \ . \tag{6.22}$$

For $C_D = 100$ and $s = 0$, Eq. (6.22) yields $R_D \geq 1062$. This result emphasizes the need to minimize wellbore storage effects in composite reservoir well tests.

Less strict criteria for $R_D^2/C_D$ and $R_D$ to observe at least one-half log cycle of the semilog line corresponding to the inner region mobility result by using Eq. (5.13) and $(t_{De})_{end} = 0.21$ as:

$$\frac{R_D^2}{C_D} \geq 15.2\ [30 + 110 \log (C_D e^{2s})] \ , \text{ and} \tag{6.23}$$

$$R_D \geq 3.9 \sqrt{C_D\ [30 + 110 \log (C_D e^{2s})]} \ . \tag{6.24}$$

For $C_D = 100$ and $s = 0$, Eq. (6.24) yields $R_D \geq 617$, again emphasizing the need to minimize wellbore storage effects in composite reservoir well tests.

A comparison of the time to the end of wellbore storage effects (Eq. (5.9)) with $t_{DA} = 0.1$ yields criteria for observing pseudosteady state data despite wellbore storage effects:

$$\frac{R_D^2}{C_D} \geq \frac{[0.048 \log (C_D e^{2s}) - 0.03]}{0.1 \pi} \quad , \text{and} \tag{6.25}$$

$$R_D \geq 1.784 \sqrt{C_D \ [0.048 \log (C_D e^{2s}) - 0.03]} \quad . \tag{6.26}$$

Even after the end of storage-dominated period, there is a transition time before the onset of pseudosteady state. The transition time between the end of storage domination and the onset of pseudosteady state is not considered in the development of Eqs. (6.25) and (6.26). The transition time between the end of wellbore storage effects and the beginning of infinite-acting radial flow corresponding to the inner region mobility is considered in the development of Eqs. (6.21) through (6.24). Thus, Eqs. (6.25) and (6.26) are less reliable criteria than Eqs. (6.21) through (6.24). In practice, $R_D^2/C_D$ or $R_D$ would have to be larger than those forecast from Eq. (6.25) or (6.26) to observe pseudosteady state behavior. Still, a comparison of the results from Eq. (6.22) or (6.24), and Eq. (6.26) is important qualitatively.

For $C_D = 100$ and $s = 0$, Eq. (6.26) yields $R_D \geq 5$. Thus, the results from Eq. (6.22) or (6.24), and Eq. (6.26) suggest that in some cases, wellbore storage effects may mask the semilog line corresponding to the inner region mobility, but pseudosteady state data may still be obtained. That is, due to wellbore storage effects, there may be cases when the inner region mobility may not be obtained, and the deviation time method may not be applicable, but the pseudosteady state method may be used to estimate a swept volume provided sufficient mobility and storativity contrasts exist between the inner and the outer region. Drawdown pressure derivative responses for a well with storage and skin, and located in the center of an infinitely large composite reservoir is considered in the following.

Five parameters, $C_D$, $s$, $R_D$, $M$, and $F_S$, describe the drawdown pressure and pressure derivative responses for a well with storage and skin, and located in an infinitely large composite reservoir. However, the pressure and the pressure derivative expressions during the wellbore storage period, the infinite-acting radial flow period corresponding to the inner region mobility, and the pseudosteady state period corresponding to the inner swept volume are similar to the corresponding expressions in Table 5.2 for a well in a finite, homogeneous reservoir. Thus, these expressions can be written as combinations of $t_D/C_D$, $C_D e^{2s}$, and $R_D^2/C_D$. Similarly, as shown in Eq. (6.27), the expression for the drawdown wellbore pressure drop during the infinite-acting radial flow period corresponding to the outer region mobility can be written as a combination of $t_D/C_D$, $C_D e^{2s}$, $R_D^2/C_D$, $M$, and $F_S$:

$$p_{wD} = \frac{1}{2}\left[M \ln\left[\frac{2.2458\ t_{De}}{\eta}\right] + \ln\left[R_D^2\right]\right] + s$$

$$= \frac{1}{2}\left[M \ln\left[\frac{2.2458\ F_S}{M} \cdot \frac{t_D}{C_D} \cdot \frac{C_D}{R_D^2}\right] + \ln\left[\frac{R_D^2}{C_D} \cdot C_D e^{2s}\right]\right] \quad . \tag{6.27}$$

Therefore, four parameters, $C_D e^{2s}$, $R_D^2/C_D$, $M$, and $F_S$, describe the drawdown response for a well with storage and skin, and located in an infinitely large composite

reservoir. Also, pressure and/or pressure derivative may be graphed as a function of either $t_D/C_D$ or $t_{De}$ because:

$$t_{De} = \frac{t_D}{R_D^2} = \frac{t_D}{C_D} \cdot \frac{C_D}{R_D^2} \quad , \tag{6.28}$$

and $R_D^2/C_D$ is one of the correlating parameters.

A grouping of three parameters, $C_D$, $s$, and $R_D$, into two parameters, $C_D e^{2s}$ and $R_D^2/C_D$, is indicated graphically in Figs. 6.11 through 6.13 for $M = 10$, and $F_S = 100$. Figure 6.11 is a graph of semilog pressure derivative as a function of $t_D/C_D$. Figure 6.12 is a graph of semilog pressure derivative as a function of $t_{De}$. Figure 6.12 also shows the response for $C_D = 0$. Figure 6.13 is a graph of Cartesian pressure derivative as a function of $t_{DA}$, where $t_{DA} = t_{De}/\pi$. Curve A on Figs. 6.11 through 6.13 is for $C_D e^{2s} = 10^{10}$ and $R_D^2/C_D = 10^4$. Curve B on Figs. 6.11 through 6.13 is for $C_D e^{2s} = 10^{10}$ and $R_D^2/C_D = 100$. The individual combinations of $C_D$, $s$, and $R_D$ used to generate curves A and B of Figs. 6.11 through 6.13 are shown below Fig. 6.11.

Figure 6.11 shows a correlation of early time wellbore storage dominated response in terms of a single parameter $C_D e^{2s}$. However, depending on the values of $C_D e^{2s}$ and $R_D^2/C_D$, infinite-acting radial flow corresponding to the inner region mobility may develop as in curve A, or may not develop as in curve B. At late time, the semilog slope is $M/2$.

Figure 6.12 shows the merger of pressure derivative responses for given values of $C_D e^{2s}$ and $R_D^2/C_D$ to the response for $C_D = 0$ after wellbore storage effects are no longer important. Thus, after discarding storage dominated data, it may be possible to use a type-curve, such as Fig. 6.4, based on zero wellbore storage to obtain $M$ and $F_S$ by type-curve matching.

Curve A in Fig. 6.13 shows the development of infinite-acting radial flow corresponding to the inner and outer region mobilities as lines of $-1$ slope on a log-log graph of Cartesian derivative vs. $t_{DA}$. A constant derivative of $2\pi$ depicts pseudosteady state flow corresponding to the inner swept volume. However, on Fig. 6.13, a constant derivative up to a $t_{DA} \approx 0.01$ for curve B shows the depletion of the wellbore fluid. Curve B of Fig. 6.13 illustrates a flattening of Cartesian pressure derivative at a value of approximately $2\pi$ for a short duration, even though no infinite-acting radial flow corresponding to the inner region mobility develops.

Figures 6.14 and 6.15 show the effect of $R_D^2/C_D$ for $M = 10$, $F_S = 100$, and $C_D e^{2s} = 10^{10}$. Figure 6.14 is a log-log graph of semilog pressure derivative vs. $t_{De}$. Figure 6.15 is a log-log graph of Cartesian pressure derivative vs. $t_{DA}$. The response for $R_D^2/C_D \geq 10^6$ on Figs. 6.14 and 6.15 is the same as the response for $C_D = 0$ or $R_D^2/C_D \rightarrow \infty$. Thus, if $R_D^2/C_D$ is large, storage effects may not be important, and well-test data may be analyzed by neglecting wellbore storage. However, if $R_D^2/C_D$ is small, the inner region may be so small that the infinite-acting radial flow corresponding to the inner region mobility, and the pseudosteady state flow corresponding to the inner swept volume may be masked by wellbore storage effects, as in Figs. 6.14 and 6.15 for $R_D^2/C_D \leq 1$. For $R_D^2/C_D \leq 1$ on Fig. 6.14, the pressure derivative responses

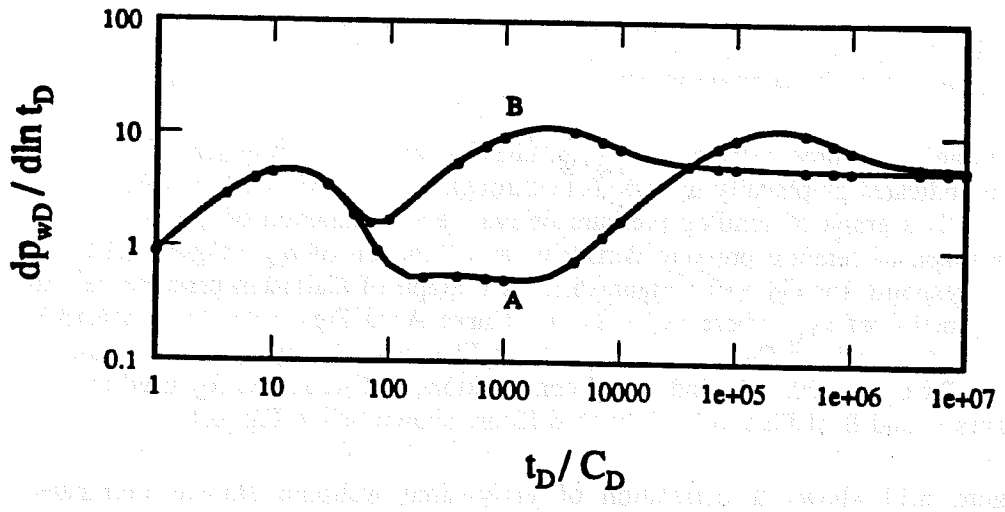


| Curve | Symbol | $C_D$ | $s$ | $R_D$ |
|---|---|---|---|---|
| A | — | 100 | 9.2 | 1000 |
| | • | 10000 | 6.9 | 10000 |
| B | — | 100 | 9.2 | 100 |
| | • | 10000 | 6.9 | 1000 |

| Curve | $C_D e^{2s}$ | $R_D^2/C_D$ |
|---|---|---|
| A | $10^{10}$ | $10^4$ |
| B | $10^{10}$ | $10^2$ |

Figure 6.11: Correlation of drawdown semi-log slope responses for a two-region composite reservoir with wellbore storage and skin ($M$ = 10, $F_S$ = 100).

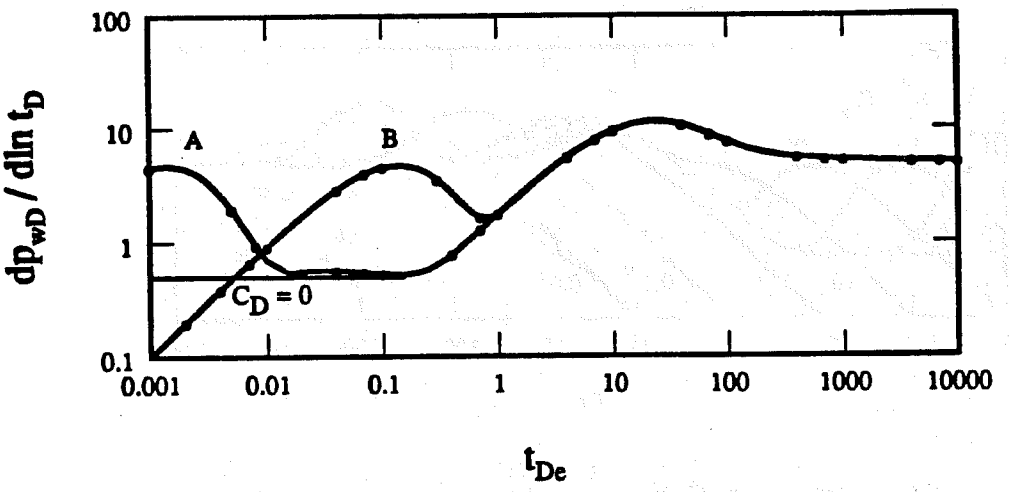


Figure 6.12: Correlation of drawdown semi-log slope responses for a two-region composite reservoir with wellbore storage and skin ($M$ = 10, $F_S$ = 100).

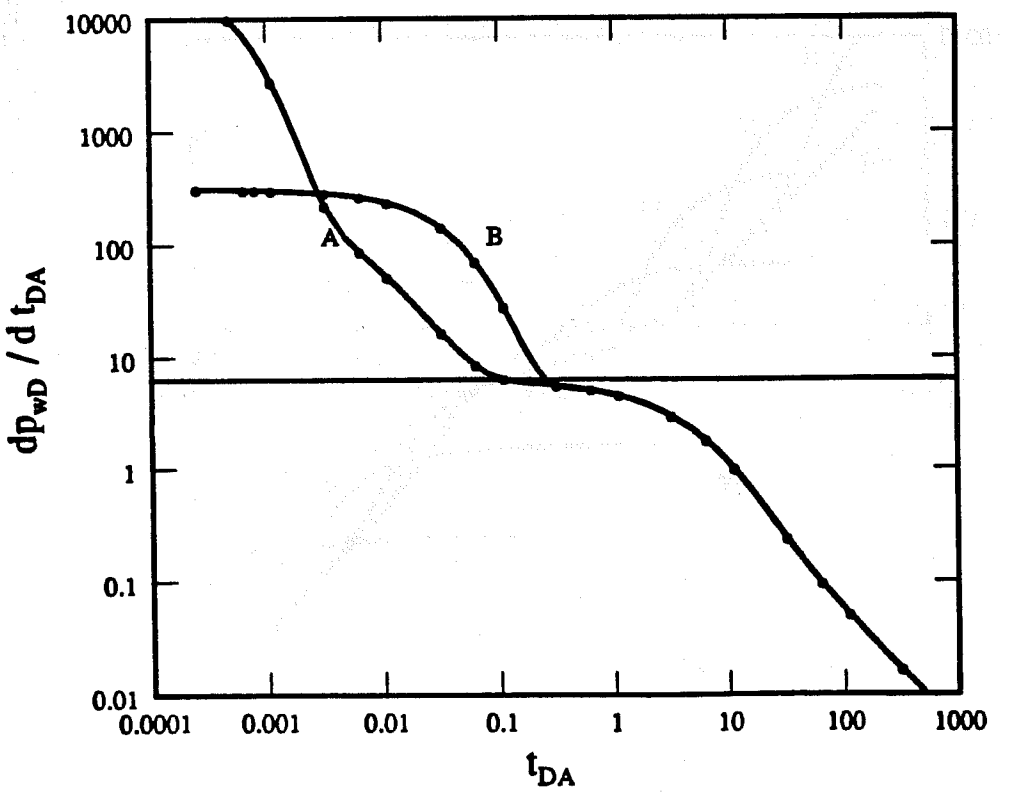


Figure 6.13: Correlation of drawdown Cartesian slope responses for a two-region composite reservoir with wellbore storage and skin ($M$ = 10, $F_S$ = 100).

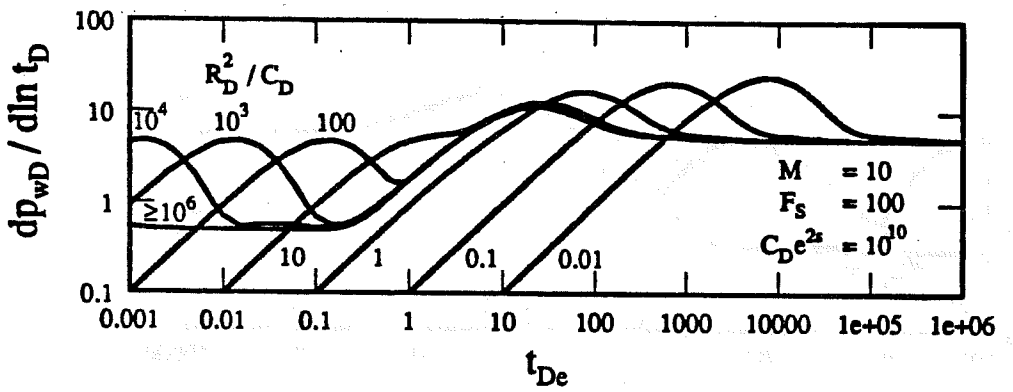


Figure 6.14: Effect of $R_D^2/C_D$ on semi-log slope response for a two-region composite reservoir with wellbore storage and skin.

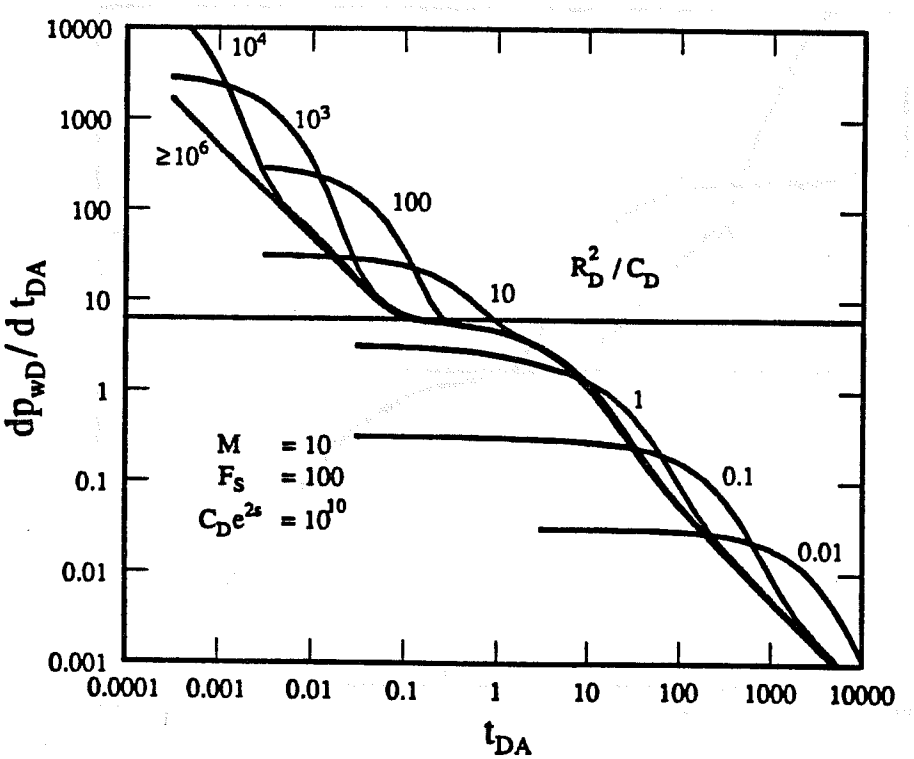


Figure 6.15: Effect of $R_D^2/C_D$ on Cartesian slope for a two-region composite reservoir with wellbore storage and skin.

show infinite-acting radial flow corresponding to the outer region mobility after a transition period following the end of wellbore storage effects.

For $C_D e^{2s} = 10^{10}$, Eq. (6.21) yields $R_D^2/C_D \geq 36608$ to observe at least one-half log cycle of the semilog line corresponding to the inner region mobility. The responses on Fig. 6.14 are consistent with the limit on $R_D^2/C_D$ from Eq. (6.21).

For $C_D e^{2s} = 10^{10}$, Eq. (6.25) yields $R_D^2/C_D \geq 1.5$ to observe pseudosteady state behavior corresponding to the inner swept volume. But Fig. 6.15 shows a flattening of Cartesian pressure derivative for a short duration at a value of approximately $2\pi$ for $R_D^2/C_D \geq 100$. Thus, Eq. (6.25) provides only an approximate lower limit for $R_D^2/C_D$ to observe pseudosteady state behavior. Also, the time to start of flattening of Cartesian pressure derivative in the presence of storage and skin effects may not correspond to $t_{DA} \approx 0.1$, as for $R_D^2/C_D = 100$ on Fig. 6.15.

Figures 6.16 and 6.17 show the effect of $C_D e^{2s}$ for $M = 10$, $F_S = 100$, and $R_D^2/C_D = 10$. Figure 6.16 is a log-log graph of semilog pressure derivative vs. $t_{De}$. Figure 6.17 is a log-log graph of Cartesian pressure derivative vs. $t_{DA}$, where $t_{DA} = t_{De}/\pi$. The response for $C_D = 0$ is also shown on both figures. Initially, a unit slope line on Fig. 6.16 and a flat Cartesian derivative on Fig. 6.17 characterize wellbore storage effects. The value of $C_D e^{2s}$ affects the time at which pressure derivative responses merge with the response for $C_D = 0$. At late time, the semilog slope is $M/2$ characterizing the infinite-acting radial flow corresponding to the outer region mobility. The parameter $R_D^2/C_D$ relates the inner swept volume with wellbore storage. For $R_D^2/C_D = 10$, the inner region is so small that wellbore storage effects mask the semilog line corresponding to the inner region mobility even for $C_D e^{2s} = 10^3$. A flattening of Cartesian pressure derivative at a value of approximately $2\pi$ is also not obvious even for $C_D e^{2s} = 10^3$. The deviation time method and the pseudosteady state method are not applicable for these values of $C_D e^{2s}$ and $R_D^2/C_D$. But thermal well test data consistently appear to exhibit either both the semilog line corresponding to the inner region mobility and the pseudosteady state data, or at least pseudosteady state data (*Ramey*, 1987). Thus, thermal well test data are characterized by a large value of $R_D^2/C_D$ and a small value of $C_D e^{2s}$.

Figures 6.18 and 6.19 present the effects of $R_D^2/C_D$, $M$, and $F_S$ on the pressure derivative responses for a fixed value of $C_D e^{2s}$. Figure 6.18 applies for $C_D e^{2s} = 1000$, and Fig. 6.19 for $C_D e^{2s} = 10^{10}$. The magnitude of $C_D e^{2s}$ may be obtained by type-curve matching the early portion of well-test data on a homogeneous reservoir type-curve, such as the *Bourdet et al.* (1983a) type-curve reproduced as Fig. A.1. Then a type-curve, such as Fig. 6.18 or 6.19, may be used to estimate $R_D^2/C_D$, $M$, and $F_S$ by type-curve matching, provided test data exists to a time larger than the time given by Eq. (6.2). Estimates for discontinuity radius or inner swept volume from the deviation time method and the pseudosteady state method may then be compared with the type-curve matching estimate for inner swept volume deduced from $R_D^2/C_D$ to place confidence in analysis.

Figure 6.20 presents the effects of $C_D e^{2s}$, $M$, and $F_S$ on the pressure derivative responses for $R_D^2/C_D = 10^4$. If $R_D$ has been obtained from the deviation time method or the pseudosteady state method, and $C_D$ has been obtained from a unit slope line on a log-log graph of pressure vs. time for the data dominated by storage effects, then the parameter $R_D^2/C_D$ is known. For a known $R_D^2/C_D$, a type-curve, such as Fig. 6.20, may be used to obtain $C_D e^{2s}$, $M$, and $F_S$ by type-curve matching, provided test data

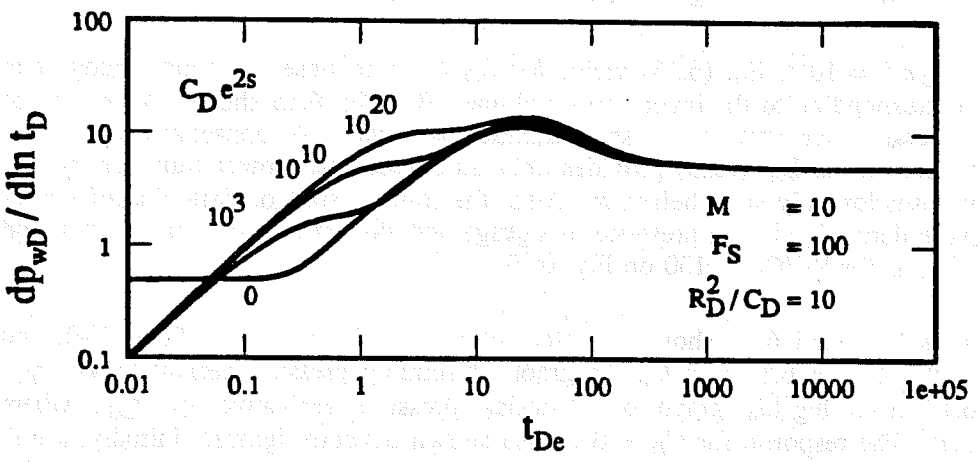


Figure 6.16: Effect of $C_De^{2s}$ on semi-log slope response for a two-region composite reservoir with wellbore storage and skin.

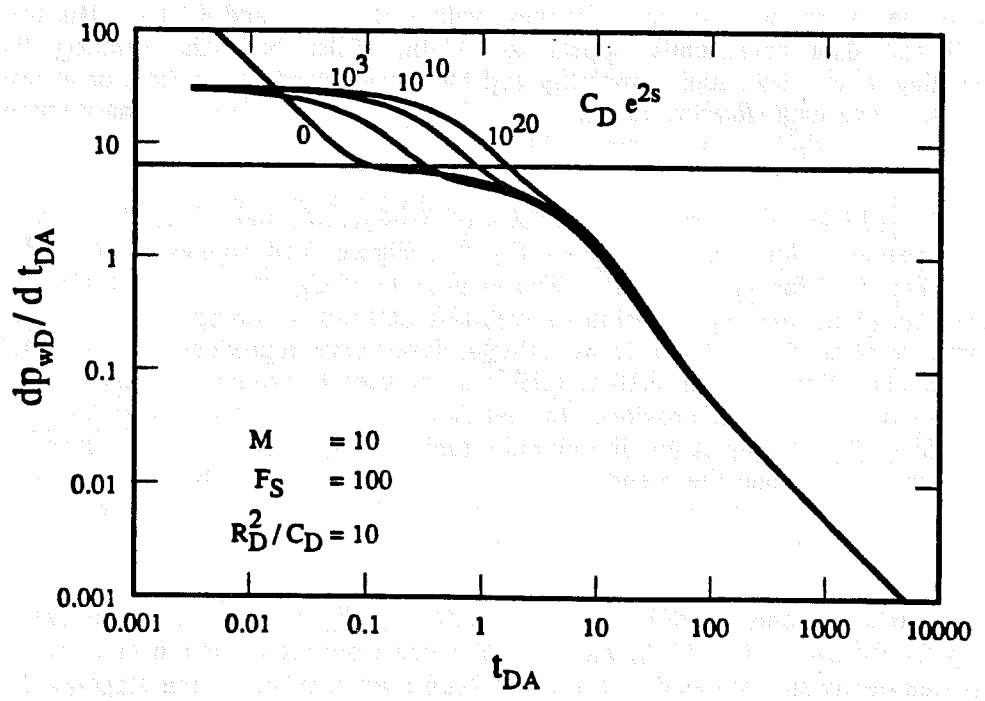


Figure 6.17: Effect of $C_De^{2s}$ on Cartesian slope for a two-region composite reservoir with wellbore storage and skin.

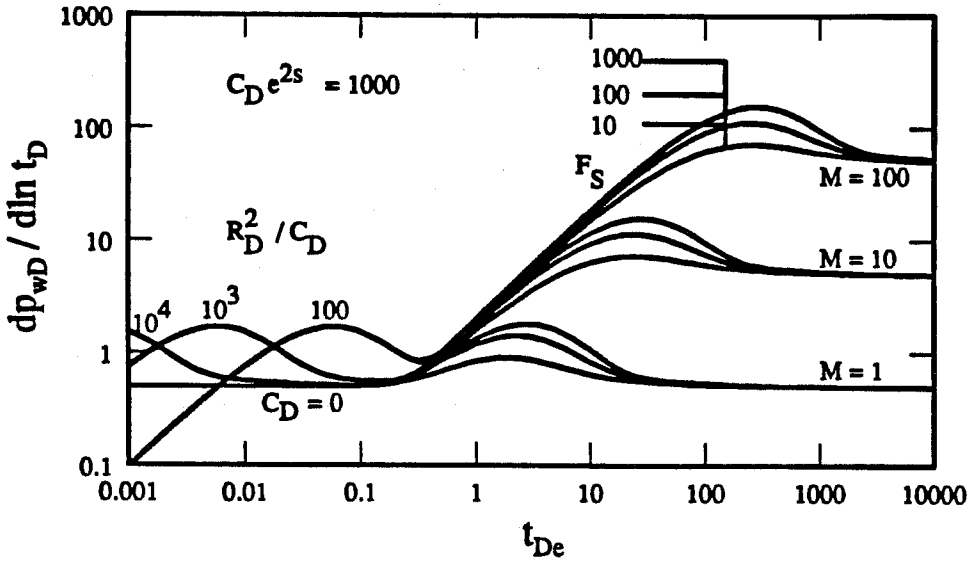


Figure 6.18: Effect of $M$, $F_S$, and $R_D^2/C_D$ on semi-log slope response for a two-region composite reservoir ($C_D e^{2s} = 10^3$).

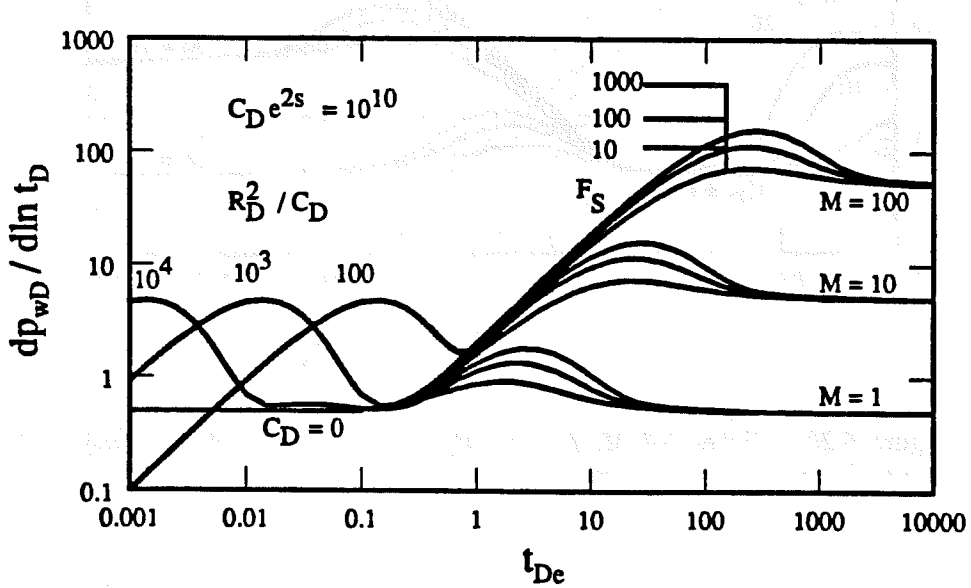


Figure 6.19: Effect of $M$, $F_S$, and $R_D^2/C_D$ on semi-log slope response for a two-region composite reservoir ($C_D e^{2s} = 10^{10}$).

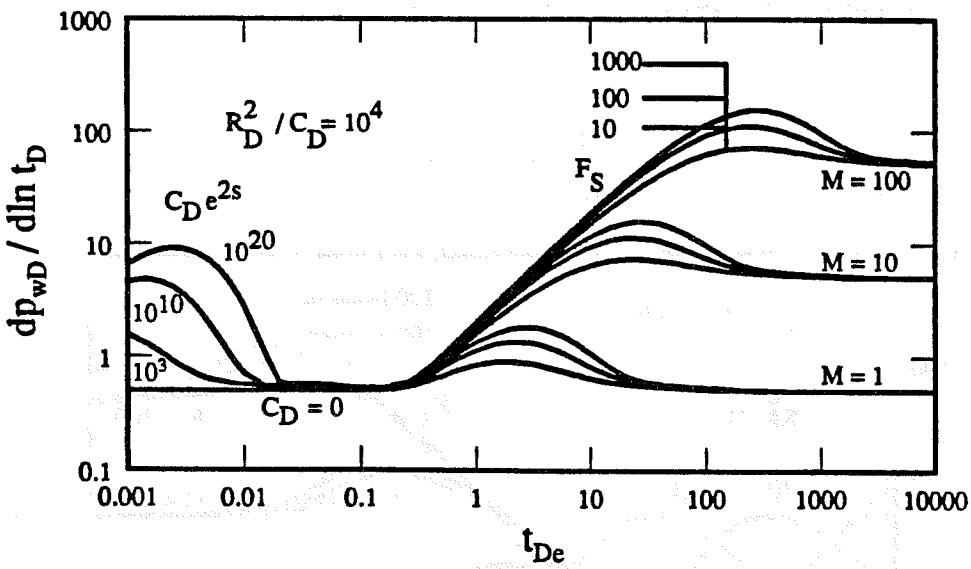


Figure 6.20: Effect of $M$, $F_S$, and $C_De^{2s}$ on semi-log slope response for a two-region composite reservoir ($R_D^2/C_D = 10^4$).

exists to a time larger than the time given by Eq. (6.2). Outer boundary effects are considered next in the absence of wellbore storage.

For finite outer boundary, Figs. 6.21 and 6.22 illustrate typical results neglecting wellbore storage effects. Figures 6.21 and 6.22 apply for $M = 10$, $F_S = 1000$, and $r_{eD} / R_D = 10$. Three cases of $R_D = 50$, 100 and 1000 are shown on both figures. The group $r_{eD} / R_D$ is a third correlating parameter for finite, composite reservoirs in addition to $M$ and $F_S$.

A reservoir approaches steady-state behavior at late times for a constant-pressure outer boundary. On a pressure derivative graph, such as Fig. 6.21, steady-state is indicated by a pressure derivative of zero. Since a large mobility and storativity contrast implies closed reservoir behavior, the semilog pressure derivative rises for some time after the end of the first semilog line corresponding to the inner region mobility on Fig. 6.21. But eventually, the outer boundary effects dominate, and the reservoir approaches steady-state after exhibiting a maximum semilog pressure derivative. As derived in Appendix C, the dimensionless wellbore pressure drop at late time for a constant-pressure outer boundary is:

$$p_{wD} = \ln (R_D) + M \ln (\frac{r_{eD}}{R_D}) + s \quad . \tag{6.29}$$

A reservoir approaches pseudosteady state behavior at late times for a closed outer boundary produced at a constant rate. Pseudosteady state is characterized by a linearly-increasing semilog pressure derivative on either a Cartesian graph or the log-log graph of Fig. 6.22. The effects of mobility and storativity contrasts, and the outer boundary are such that stabilization at a maximum derivative, and bending over of the pressure derivative is not seen in Fig. 6.22. Instead, the reservoir goes to pseudosteady state directly. As derived in Appendix C, the dimensionless wellbore pressure drop at late time for a closed outer boundary is:

$$p_{wD} = \frac{2\, t_{De}}{1 + \frac{1}{F_S}\left[\frac{r_e^2}{R^2} - 1\right]} + \chi + s \quad , \tag{6.30}$$

where:

$$\chi = \ln (R_D) - \frac{R^2}{2\, r_e^2} - \frac{\left[1 - \frac{R^2}{2\, r_e^2}\right]}{2\left[1 + \frac{1}{F_S}\left[\frac{r_e^2}{R^2} - 1\right]\right]} + \frac{M\left[1 - \frac{R^2}{r_e^2}\right]}{4\left[F_S + \frac{r_e^2}{R^2} - 1\right]}$$

$$- \frac{3\, M\left[\frac{r_e^2}{R^2} - 1\right]}{4\left[F_S + \frac{r_e^2}{R^2} - 1\right]} + \frac{M \ln (r_e/R)}{1 + \frac{R^2}{r_e^2}(F_S - 1)} \tag{6.31}$$

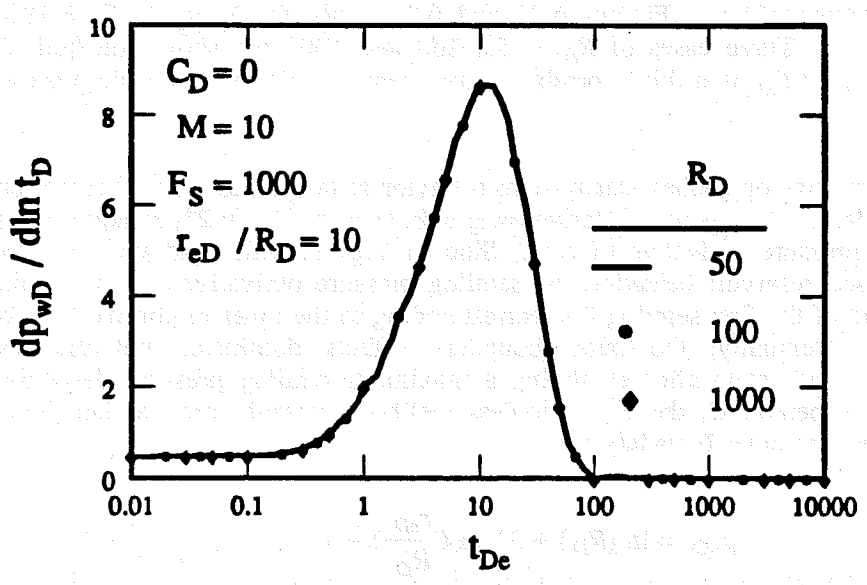


Figure 6.21: Correlation of semi-log slope for a two-region composite reservoir with a constant-pressure outer boundary.

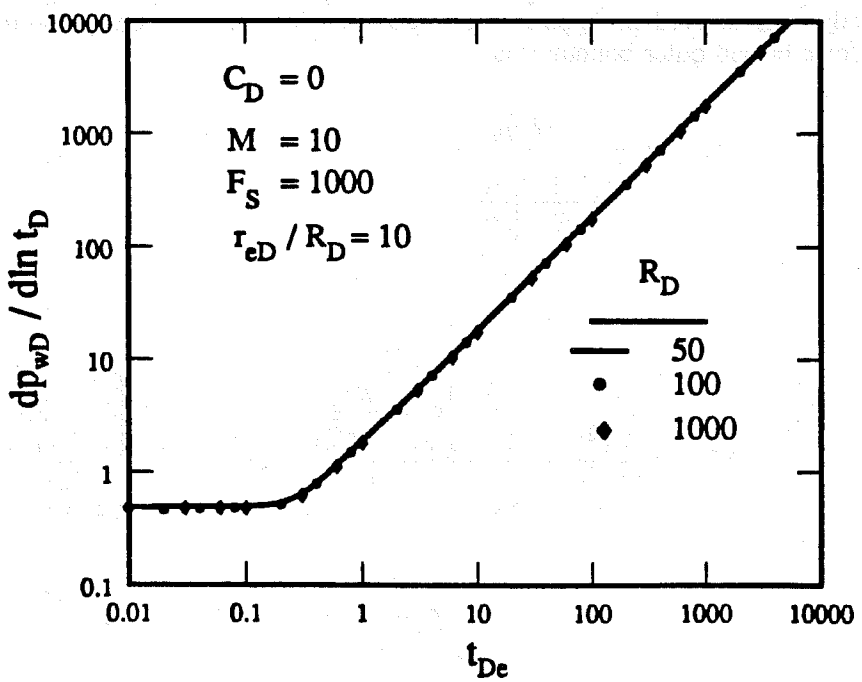


Figure 6.22: Correlation of semi-log slope for a two-region composite reservoir with a closed outer boundary.

Figures 6.23 and 6.24 show pressure derivative behavior for constant-pressure and closed outer boundaries, respectively, for several values of $r_{eD} / R_D$. Mobility and storativity ratios are 10 and 1000, respectively, for Figs. 6.23 and 6.24. Interaction of the effects of mobility and storativity contrasts, and the outer boundary determines the pressure derivative behavior at any time. Depending on the size of the outer region, a second semilog line may or may not appear. Figures 6.23 and 6.24 show that $r_{eD} / R_D$ should be greater than 1000 for the second semilog line to be evident, if $M$ = 10 and $F_S$ = 1000. Thus, even if one is willing to run a well test long enough, the second semilog line may be masked by outer boundary effects. Analysis of pressure derivative behavior for several values of $M$, $F_S$ and $r_{eD} / R_D$, for closed and constant-pressure outer boundaries, resulted in the following relation for the dimensionless time at which the pressure derivative response for a finite, composite reservoir departs from that of an infinitely large composite reservoir:

$$(t_{De})_{depart} = \frac{(r_{eD} / R_D)^2 M}{5 F_S} \quad . \tag{6.32}$$

Equation (6.32) should only be applied to cases where $M \geq 10$ and $F_S \geq 10$. Equation (6.32) is best for large values of $M$ and $F_S$ compared to unity. Equation (6.32) applies to both closed and constant-pressure outer boundaries. For the homogeneous reservoir case ($M$ = 1, $F_S$ = 1), Eq. (6.32) yields that the pressure derivative response departs from infinite-acting behavior at $t_{DA} = 0.2/\pi$. Here $t_{DA}$ is the dimensionless time based on area $A = \pi r_e^2$. A comparison of $0.2/\pi$ with 0.1 (which is $(t_{DA})_{pss}$ for a well producing at a constant rate in a closed homogeneous reservoir) indicates the results of Eq. (6.32) when $M$ and $F_S$ are close to unity.

Equation (6.32) quantifies the outer boundary effects on transient responses in composite reservoirs, and is a means to determine whether desired features will be seen on a pressure transient test. A comparison of Eq. (6.32) with Eq. (6.3) provides a limit for $r_{eD} / R_D$ to see at least one-half log cycle of second semilog line on a pressure transient test as:

$$\frac{r_{eD}}{R_D} > (10)^{1/4} \sqrt{450 \, (1 + \log F_S) \, F_S} \quad . \tag{6.33}$$

Similarly, a comparison of Eq. (6.32) with Eq. (6.2) provides a limit for $r_{eD} / R_D$ to observe a maximum semilog pressure derivative one-half log cycle before the departure of slope response from that of an infinitely large composite reservoir as:

$$\frac{r_{eD}}{R_D} > (10)^{1/4} \sqrt{(9 + 2 \log F_S) \, F_S} \quad . \tag{6.34}$$

Equations (6.33) and (6.34) show that the limiting value of $r_{eD} / R_D$ for observing a second semilog line or maximum semilog derivative is only a function of the storativity ratio. Equation (6.33) shows that for a large storativity ratio, a second semilog line will be masked because of outer boundary effects. The limit on $r_{eD} / R_D$ posed by Eq. (6.33) suggests that the intersection time method is not applicable for composite reservoir well test analysis.

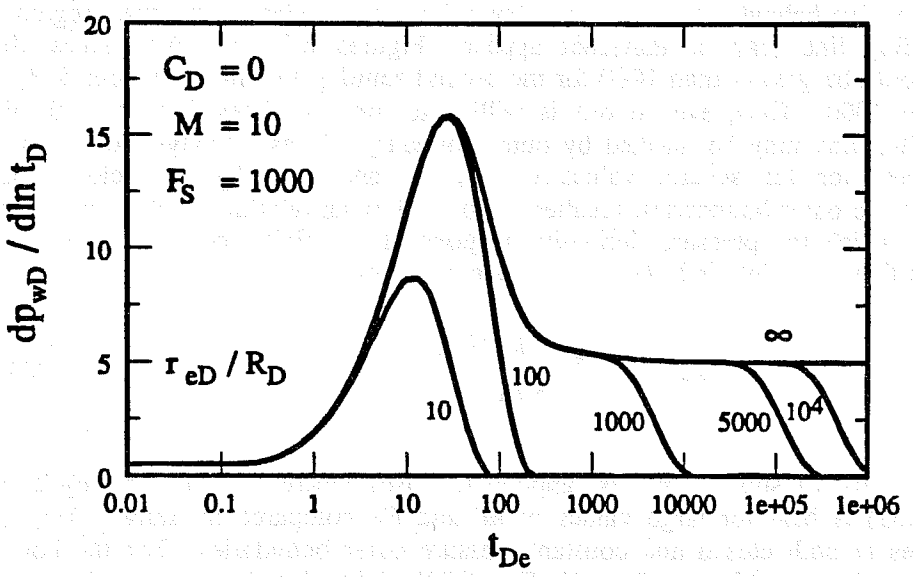


Figure 6.23: Effect of $r_{eD}/R_D$ on semi-log slope response for a two-region composite reservoir with a constant-pressure outer boundary.

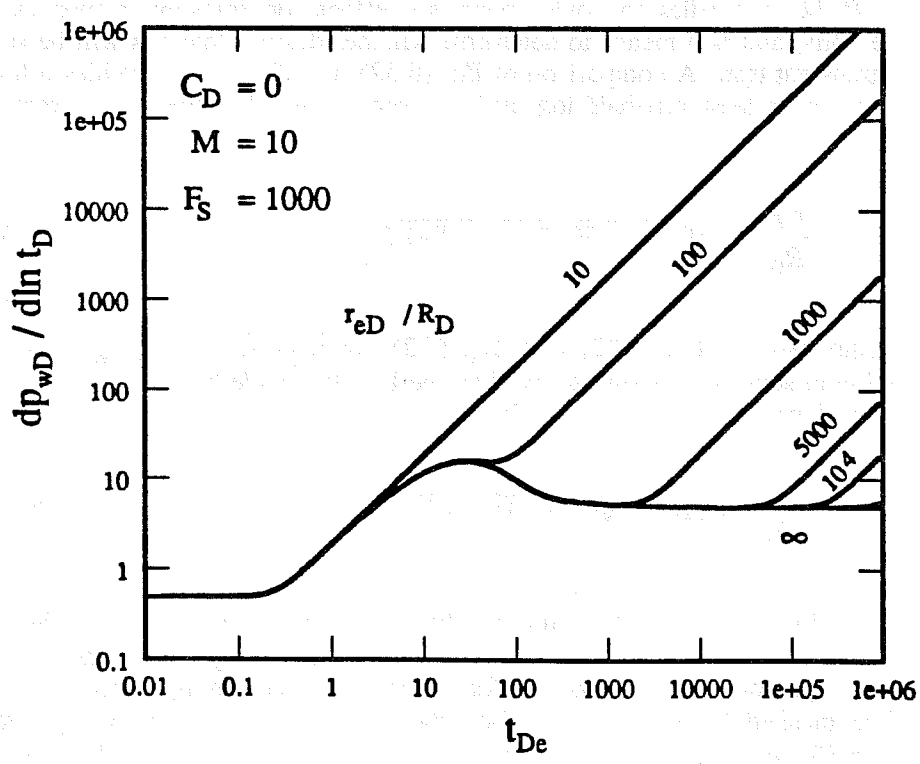


Figure 6.24: Effect of $r_{eD}/R_D$ on semi-log slope response for a two-region composite reservoir with a closed outer boundary.

There may be cases where the limit based on Eq. (6.34) is not satisfied, and therefore, a type-curve like Fig. 6.4 is not appropriate. In such cases, analysis should consider the parameter $r_{eD} / R_D$ and the outer boundary condition in addition to $M$ and $F_S$. One option is to use automated type-curve matching in these cases. However, if any of the three parameters are known with reasonable accuracy by independent means, then a type-curve can be prepared showing the effects of the other two parameters, and usual type-curve matching can be performed to estimate those parameters.

The limit on $r_{eD} / R_D$ to observe pseudosteady state behavior to a time $t_{DA} = 0.2$ results from comparing $t_{DA} = 0.2$ with Eq. (6.32). This limit is:

$$\frac{r_{eD}}{R_D} > \sqrt{\frac{\pi F_S}{M}} \quad . \tag{6.35}$$

The limit of Eq. (6.35) is more likely to be satisfied than the limits of Eq. (6.33) or (6.34), for typical values of $M$ and $F_S$ encountered in most fluid injection projects. Also, since the pseudosteady state method is independent of the geometry of the swept region, this method should yield reasonably correct swept volume and "average" front radius for irregularly swept regions.

### 6.1.2 Buildup Response

Semi-log analysis method for buildup data uses the slope of either a *Miller-Dyes-Hutchinson* (1950) graph or a *Horner* (1951) graph. A comparison of Eqs. (5.20) and (5.25) provides the relationship between the two slopes as:

$$Horner\ Slope = -\left[\frac{t_{pD} + \Delta t_D}{t_{pD}}\right] \cdot MDH\ Slope \quad . \tag{6.36}$$

*Agarwal* (1980) developed the concept of equivalent drawdown time (Eq. (5.26)) to consider producing time effects when drawdown type-curves are used to analyze pressure buildup data. *Agarwal* (1980) showed that a graph of $p_{wDs}$ (defined by Eq. (5.19)) vs. $\Delta t_{eD}$ (defined by Eq. (5.26)) correlated buildup responses from infinitely large, homogeneous or fractured reservoirs with the corresponding drawdown responses. As discussed in Chapter 5, a comparison of Eqs. (5.25) and (5.27) shows that:

$$Agarwal\ Slope = -\ Horner\ Slope \quad . \tag{6.37}$$

Thus, producing time effects on buildup responses may be studied by using either the *Agarwal* or the *Horner* slope. In this section, *Agarwal* slope has been used to illustrate the producing time effects on buildup responses from composite reservoirs.

Figure 6.25 verifies $t_{pD} / R_D^2$ as a correlating parameter for buildup responses for a well in a composite reservoir. *MDH* slope, and the negative *Horner* slope are graphed in Fig. 6.25 for $C_D = 0$, $M = 10$, $F_S = 1000$, and $t_{pD} / R_D^2 = 10$. Solid lines

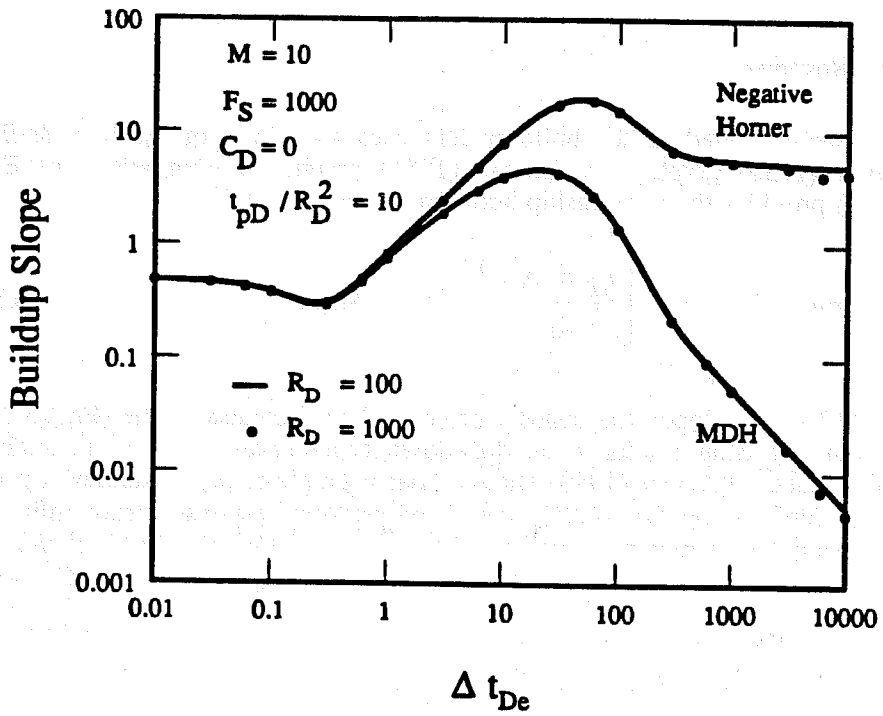


Figure 6.25: Verification of $t_{pD}/R_D^2$ as a correlating parameter for buildup response for an infinite, two-region composite reservoir.

in Fig. 6.25 are for $t_{pD} = 10^5$ and $R_D = 100$. Circles in Fig. 6.25 are for $t_{pD} = 10^7$ and $R_D = 1000$. The *MDH* and *Horner* slopes are graphed against a dimensionless shut-in time based on the discontinuity radius as:

$$\Delta t_{De} = \frac{0.000264\, k_1\, \Delta t}{(\phi\mu c_t)_1\, R^2} = \frac{\Delta t_D}{R_D^2} \quad . \tag{6.38}$$

Figure 6.25 shows that a semilog line corresponding to the inner region mobility appears in both *MDH* and *Horner* graphs. But a semilog line corresponding to the outer region mobility develops only on a *Horner* graph. The derivation in Appendix D explains this observation. Using Eqs. (D.5) and (D.6), *MDH* and *Horner* slopes at late time are:

$$MDH\ Slope = \frac{dp_{wDs}}{d\ \ln(\Delta t_D)} = \frac{M}{2} \cdot \frac{t_{pD}}{(t_{pD} + \Delta t_D)} \quad , \text{ and} \tag{6.39}$$

$$Horner\ Slope = \frac{dp_{wDs}}{d\ \ln\left[\dfrac{t_{pD} + \Delta t_D}{\Delta t_D}\right]} = -\frac{M}{2} \quad . \tag{6.40}$$

if:

$$\Delta t_{De} \geq 100\,\eta \quad , \text{for } \eta \geq 1 \quad , \text{and}$$

$$\geq 100 \quad , \text{for } \eta \leq 1 \quad . \tag{6.41}$$

Equation (6.39) shows that for $\Delta t_D >> t_{pD}$, a *MDH* slope approaches zero at late time. Equation (6.40) shows that at late time, *Horner* graph develops a semilog line of slope $-M/2$. The late time data for $R_D = 1000$ are lower than those for $R_D = 100$ because of possible instability in the *Stehfest* (1970) algorithm.

Figures 6.26 and 6.27 show the effect of $t_{pD}/R_D^2$ on *MDH* and *Agarwal* slopes for $C_D = 0$, $M = 10$, and $F_S = 1000$. Thus, for Figs. 6.26 and 6.27, $\eta = 0.01$. Figures 6.26 and 6.27 also show drawdown responses for $C_D = 0$, $M = 10$, and $F_S = 1000$. Figures 6.26 and 6.27 show that the dimensionless deviation time depends on $t_{pD}/R_D^2$. For small values of $t_{pD}/R_D^2$, deviation from the semilog line corresponding to the inner region mobility occurs earlier than $(t_{De})_{end} = 0.18$. Thus, the deviation time method may produce an inaccurate front radius estimate for small producing times. Also, for $t_{pD}/R_D^2 \leq 10$, *MDH* and *Agarwal* slopes decrease in magnitude on Figs. 6.26 and 6.27 after deviating from the slope value of 1/2. At intermediate time, the pressure derivative goes through a maximum. The value of $t_{pD}/R_D^2$ affects significantly the magnitude of maximum pressure derivative. But $t_{pD}/R_D^2$ affects mildly the time to a maximum pressure derivative. However, for $t_{pD}/R_D^2 \geq 1000$ on Figs. 6.26 and 6.27, the time and the magnitude of maximum pressure derivative are the same as those for drawdown responses. Thus, for large $t_{pD}/R_D^2$, design equations such as Eqs. (6.1), (6.2), and (6.14) are applicable. For $t_{pD}/R_D^2 \geq 1000$, *Agarwal* slope response on Fig.

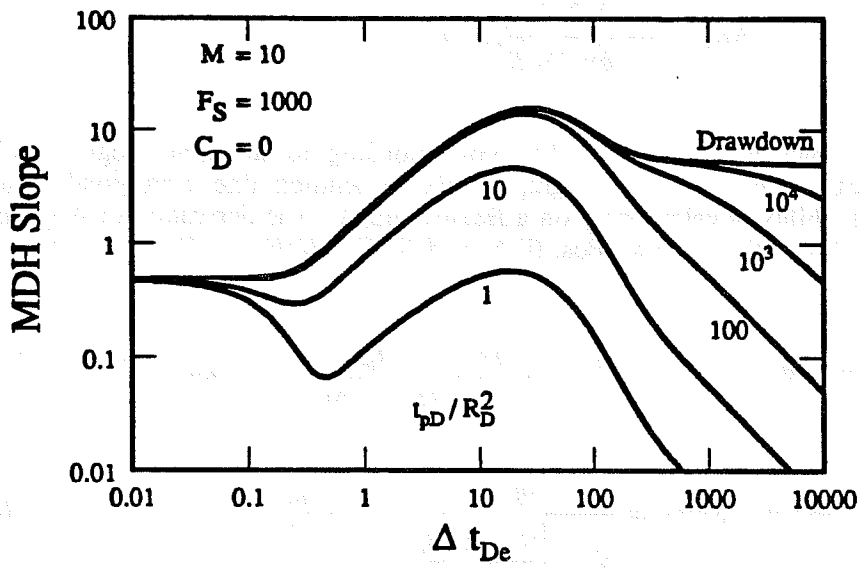


Figure 6.26: Effect of $t_{pD}/R_D^2$ on MDH slope for an infinite, two-region composite reservoir.

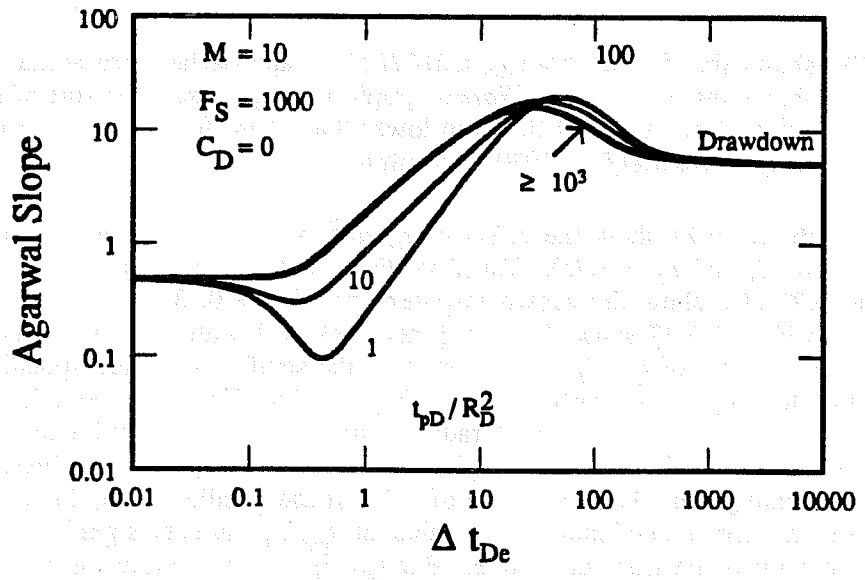


Figure 6.27: Effect of $t_{pD}/R_D^2$ on Agarwal slope for an infinite, two-region composite reservoir.

6.27 is the same as the drawdown pressure derivative response. Thus, *Agarwal* slope does not correlate responses for all $t_{pD}/R_D^2$ into a single curve. But a log-log graph of *Agarwal* slope vs. $\Delta t$ may be analyzed by a type-curve like Fig. 6.4, provided $t_{pD}/R_D^2$ is sufficiently large. For a reliable type-curve matching, $t_{pD}/R_D^2$ should be large enough for expected values of $M$ and $F_S$ that a maximum slope as forecast from Eq. (6.2) would appear in well-test data. The value of $t_{pD}/R_D^2$ required to observe a maximum slope as forecast from Eq. (6.2) depends on $M$ and $F_S$ as illustrated in Table 6.3. Table 6.3 presents the value of $t_{pD}/R_D^2$ for selected values of $M$ and $F_S$ to observe a maximum *Agarwal* slope within 5% of maximum drawdown semilog slope. Based on the data in Table 6.3, the $t_{pD}/R_D^2$ required for maximum *Agarwal* slope to be within 5% of maximum drawdown semilog slope is:

$$\log\left[\frac{t_{pD}}{R_D^2}\right] = \log(M) + \sqrt{\log(F_S)} - 1.4 \times 10^{-4} F_S \quad . \tag{6.42}$$

Figure 6.28 presents a comparison of the results from Eq. (6.42) and the data of Table 6.3. Equation (6.42) should be helpful in well test design and interpretation to estimate whether $t_{pD}/R_D^2$ is large enough that the well-test data may be type-curve matched on a drawdown type-curve such as Fig. 6.4. The value of $t_{pD}/R_D^2$ large enough for type-curve matching to be applicable implies that well-test data can also be analyzed by the deviation time method and the pseudosteady state method. For large values of $t_{pD}/R_D^2$, Fig. 6.29 illustrates the applicability of the pseudosteady state method. Figure 6.29 presents a log-log graph of Cartesian slope as a function of $\Delta t_{DA}$ for $C_D = 0$, $M = 10$, and $F_S = 1000$. A short period of constant slope of $2\pi$ develops only for $t_{pD}/R_D^2 \geq 100$ on Fig. 6.29. For $t_{pD}/R_D^2 < 100$, a flattening of a Cartesian derivative to a value other than $2\pi$ is apparent. Thus, for short producing times or small values of $t_{pD}/R_D^2$, there may be an appearance of an apparent Cartesian straight line on a graph of pressure vs. shut-in time. Analysis based on an apparent Cartesian straight line would result in an overestimated swept volume.

Figures 6.30 through 6.32 present the *MDH* slope, *Agarwal* slope, and Cartesian slope behavior for $C_D = 0$, $M = 100$, and $F_S = 10$. Thus, for Figs. 6.30 through 6.32, $\eta = 10$. Corresponding drawdown responses are also shown on Figs. 6.30 through 6.32. Remarks for Figs. 6.26, 6.27, and 6.29 also apply to Figs. 6.30 through 6.32. A decrease in *MDH* or *Agarwal* slope after the end of infinite-acting radial flow corresponding to the inner region mobility may indicate a test after short producing (injection) time. However, a decrease in semilog pressure derivative after a semilog line corresponding to the inner region mobility may also result due to:

1. A two-region composite reservoir with either $M < 1$, or $F_S < 1$, or both $M < 1$ and $F_S < 1$ as shown in Fig. 6.5 for selected cases, or
2. A three-region composite reservoir with either intermediate region mobility more than the inner region mobility, or intermediate region storativity more than the inner region storativity, or both intermediate region mobility and storativity more than the corresponding values for the inner region. The responses for a three-region reservoir discussed in Chapter 6.2 illustrate this observation.

The preceding discussion points out that well tests in composite reservoirs following a short producing (injection) time may be difficult to analyze. Also, other reservoir parameters or configurations may produce well-test data resembling a test after short

**Table 6.3 - $t_{pD}/R_D^2$ required for Agarwal maximum slope to be within 5% of drawdown maximum semi-log slope for a two-region composite reservoir**

| $M$ | $F_S$ | $t_{pD}/R_D^2$ |
|---|---|---|
| 10 | 10 | 108 |
| 20 | | 206 |
| 50 | | 595 |
| 70 | | 761 |
| 100 | | 1029 |
| 200 | | 2030 |
| 500 | | 5810 |
| 700 | | 7508 |
| 1000 | | $1.01 \times 10^4$ |
| 10 | 100 | 248 |
| 20 | | 491 |
| 50 | | 1466 |
| 70 | | 1900 |
| 100 | | 2445 |
| 200 | | 4851 |
| 500 | | $1.47 \times 10^4$ |
| 700 | | $1.90 \times 10^4$ |
| 1000 | | $2.43 \times 10^4$ |
| 10 | 1000 | 385 |
| 20 | | 766 |
| 50 | | 1927 |
| 70 | | 2541 |
| 100 | | 3843 |
| 200 | | 7631 |
| 500 | | $1.92 \times 10^4$ |
| 700 | | $2.46 \times 10^4$ |
| 1000 | | $3.83 \times 10^4$ |

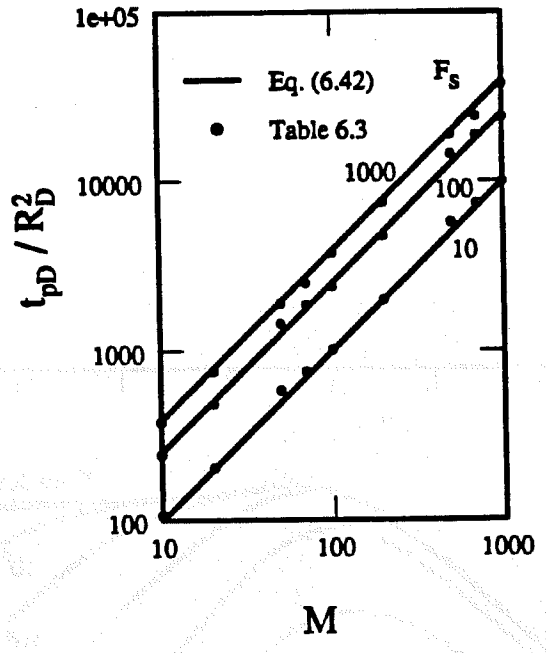


Figure 6.28: $t_{pD}/R_D^2$ required to observe maximum Agarwal slope within 5% of drawdown maximum semi-log slope for a two-region composite reservoir.

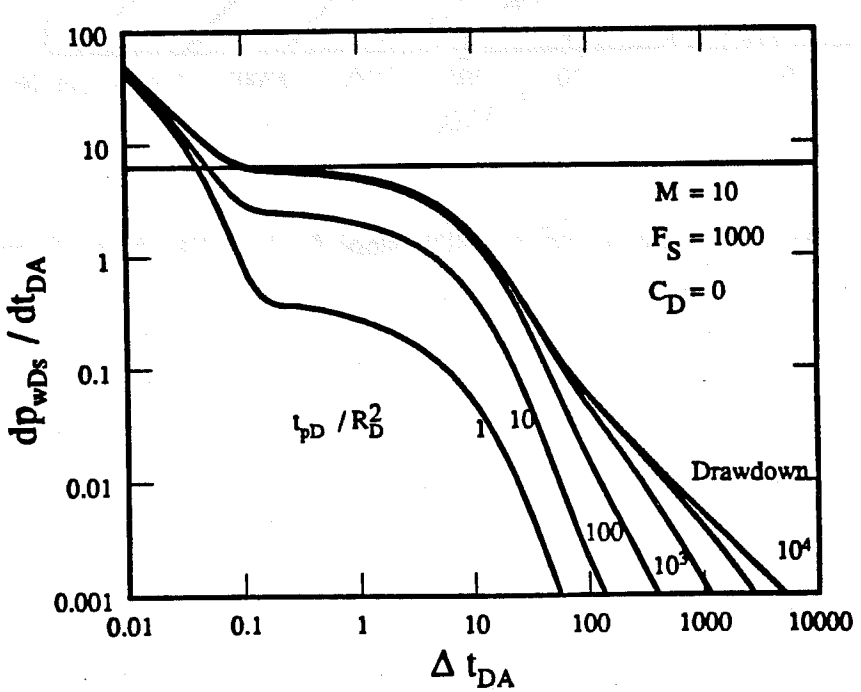


Figure 6.29: Effect of $t_{pD}/R_D^2$ on buildup Cartesian derivative for an infinite, two-region composite reservoir.

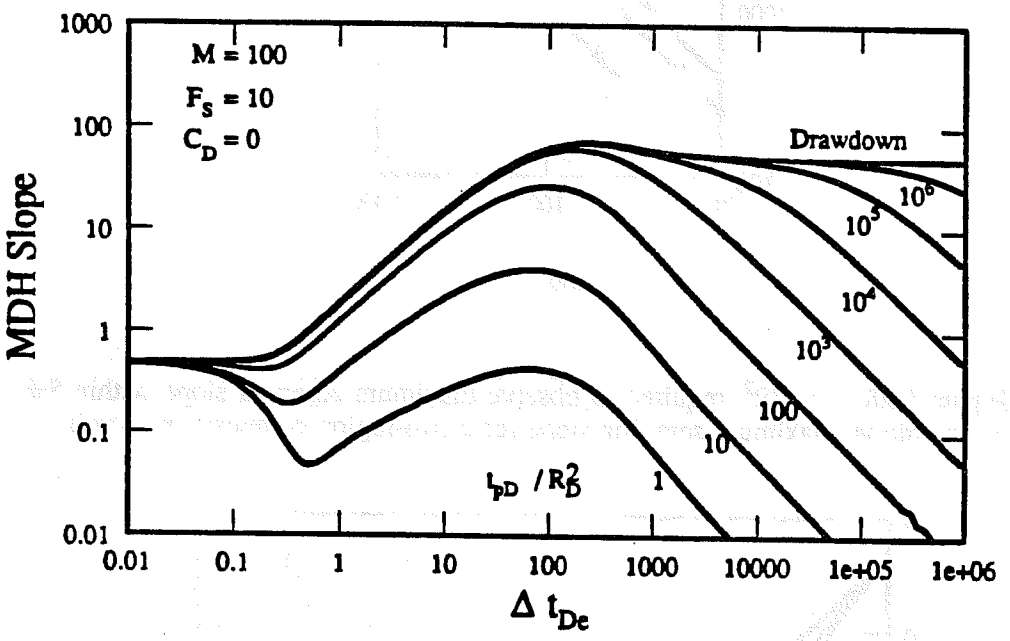


Figure 6.30: Effect of $t_{pD}/R_D^2$ on MDH slope for $M$ = 100, $F_S$ = 10, and $C_D$ = 0.

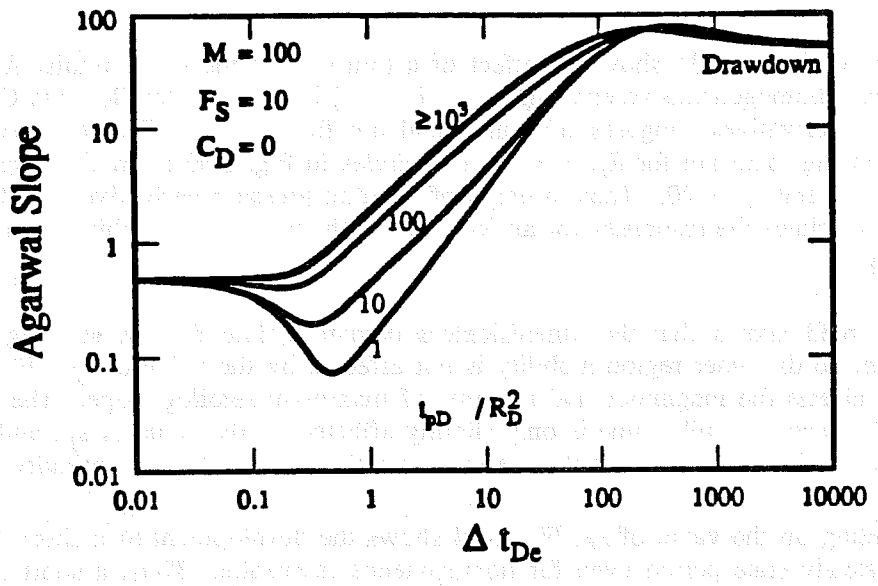


Figure 6.31: Effect of $t_{pD}/R_D^2$ on Agarwal slope for $M$ = 100, $F_S$ = 10, and $C_D$ = 0.

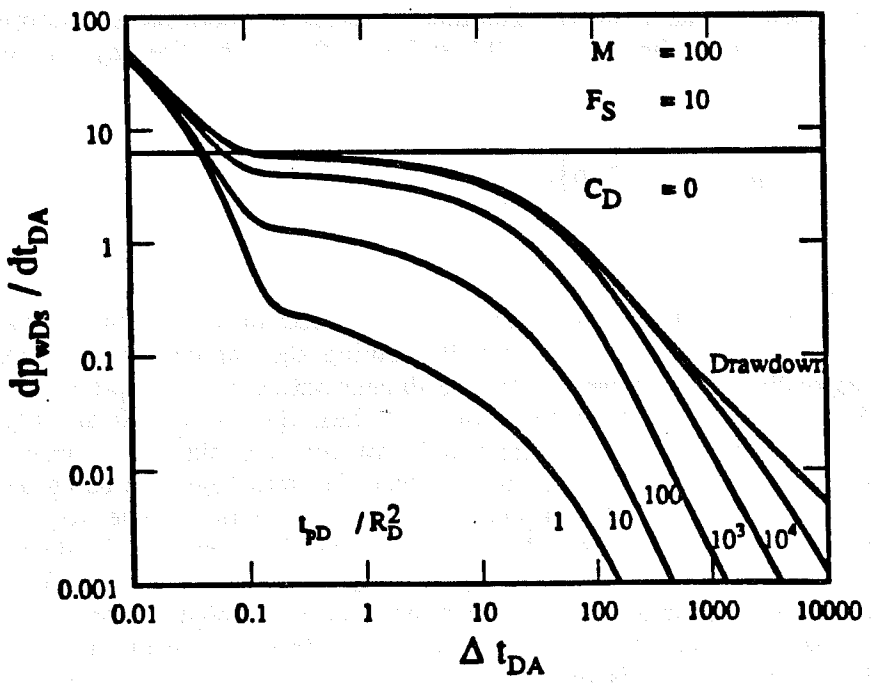


Figure 6.32: Effect of $t_{pD}/R_D^2$ on buildup Cartesian derivative for $M$ = 100, $F_S$ = 10, and $C_D$ = 0.

producing time. Therefore, an analyst has to be careful to identify a plausible reason for a particular behavior in a well test.

### 6.1.3 Effect of a Thin Skin at the Discontinuity

Figures 6.33 and 6.34 show the effect of a thin skin at the discontinuity for an infinitely large, homogeneous reservoir ($M = 1$, $F_S = 1$) in terms of semilog and Cartesian pressure derivatives. Figures 6.33 and 6.34 are for $C_D = 0$. The responses in solid lines on Fig. 6.33 are for $R_D = 100$. The circles in Fig. 6.33 show the response for $R_D = 1000$ and $s_f = 20$. Thus, a graph of semilog pressure derivative as a function of $t_{De}$ correlates the responses for all $R_D$ even in the presence of a thin skin at the discontinuity.

Figure 6.33 shows that the dimensionless deviation time from a semilog line corresponding to the inner region mobility is not affected by the value of $s_f$. But the value of $s_f$ affects the magnitude and the time of maximum semilog slope. The time to start of the second semilog line is only slightly affected by the value of $s_f$, and Eq. (6.3) approximately applies even in the presence of a thin skin at the discontinuity.

Depending on the value of $s_f$, Fig. 6.34 shows the development of a short duration pseudosteady state period even for homogeneous reservoirs. Thus, a short duration pseudosteady state period may result because of a positive value of $s_f$ even for small mobility and storativity contrasts. For a homogeneous reservoir, the *Stehfest* (1970) algorithm produced meaningless results for negative values of $s_f$.

The time interval during which the effects of $s_f$ is important is illustrated in Fig. 6.35. Figure 6.35 shows a graph of $dp_{wD}/d\ s_f$ as a function of $t_{De}$ for an infinitely large, homogeneous reservoir with $C_D = 0$. The derivative $dp_{wD}/d\ s_f$ for a given $s_f$ at any $t_{De}$ is calculated numerically. The dimensionless wellbore pressure drops from the *Stehfest* (1970) algorithm for $s_f + 0.1$ and $s_f - 0.1$ at the time $t_{De}$ are used to obtain:

$$\left.\frac{dp_{wD}}{d\ s_f}\right]_{s_f} = \frac{p_{wD}\Big]_{s_f + 0.1} - p_{wD}\Big]_{s_f - 0.1}}{0.2} \qquad (6.43)$$

The curve for $s_f = 0^+$ on Fig. 6.35 shows the effect of a vanishingly small skin at the discontinuity on $dp_{wD}/d\ s_f$. Initially, during the infinite-acting radial flow period corresponding to the inner region, the dimensionless wellbore pressure drop is given by Eq. (5.7), and is independent of $s_f$. Thus, $dp_{wD}/d\ s_f = 0$ at early time. However, after the end of infinite-acting radial flow corresponding to the inner region mobility, there is a short time period during which the inner region is being depleted. Inner region depletion corresponds to pseudosteady state flow in the inner region, and a Cartesian slope of $2\pi$ develops as in Fig. 6.34. During the pseudosteady state period, flow does not occur across the discontinuity and $dp_{wD}/d\ s_f$ remains zero. For a finite value of $s_f$, however, flow across the discontinuity occurs eventually, and $dp_{wD}/d\ s_f$ becomes non-zero. At late time, all the fluid comes from the outer region, and an infinite-acting radial flow corresponding to the outer region mobility develops. At late time, the dimensionless wellbore pressure drop for an infinitely large, homogeneous

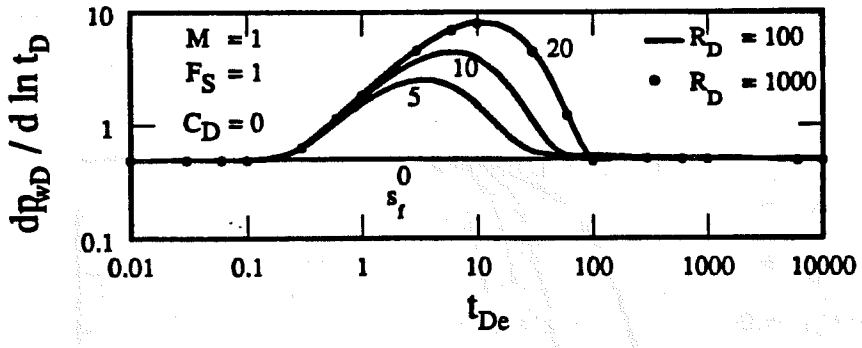


Figure 6.33: Effect of $s_f$ on semi-log slope response for $M = 1$, $F_S = 1$, and $C_D = 0$.

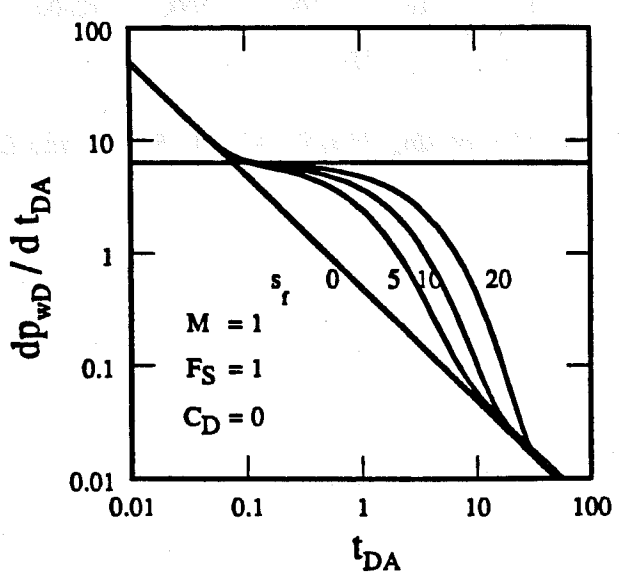


Figure 6.34: Effect of $s_f$ on Cartesian derivative for $M = 1$, $F_S = 1$, and $C_D = 0$.

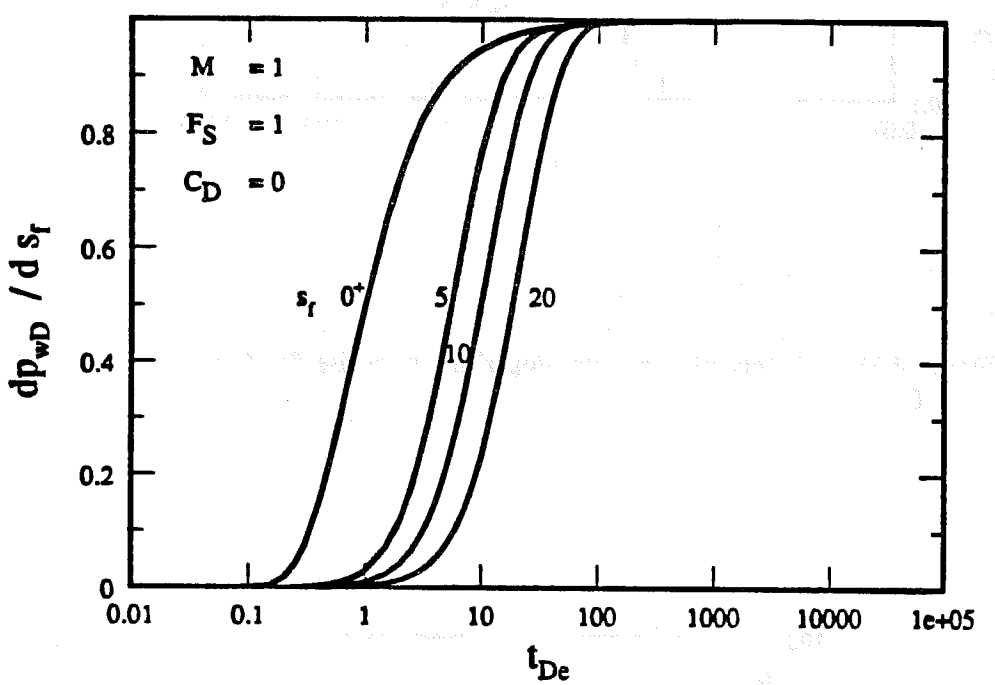


Figure 6.35: Effect of $s_f$ on $dp_{wD}/d\,s_f$ for $M = 1$, $F_S = 1$, and $C_D = 0$.

reservoir with a skin at the discontinuity is:

$$p_{wD} = \frac{1}{2}\left[\ln(t_D) + 0.80907 + 2\,s + 2\,s_f\right] \quad . \tag{6.44}$$

Equation (6.44) shows that at late time, $dp_{wD}/d\,s_f = 1$. The derivative $dp_{wD}/d\,s_f$ approaches 1 at late time on Fig. 6.35 also. Similarly, the dimensionless wellbore pressure drop at late time for an infinitely large, two-region composite reservoir with a skin at the discontinuity is:

$$p_{wD} = \frac{1}{2}\left[M\,\ln\left[\frac{2.2458\,t_{De}}{\eta}\right] + \ln(R_D^2)\right] + s + s_f \quad . \tag{6.45}$$

Equation (6.45) also shows that at late time, $dp_{wD}/d\,s_f = 1$.

Figures 6.36 and 6.37 show pressure profiles for $t_D/R_D^2 = 10$ and 1000 respectively. Figures 6.36 and 6.37 are for $M = 1$, $F_S = 1$, and $C_D = 0$. The solid lines in Figs. 6.36 and 6.37 are for $R_D = 100$. The profiles for $R_D = 1000$ and $s_f = 20$ are shown by circles in Figs. 6.36 and 6.37. Thus, the pressure profile in the reservoir at a given time for all $R_D$ is correlated to that for an arbitrary $R_D = 100$, if the dimensionless pressure drop is graphed as a function of $r_D \times (100/R_D)$. Figures 6.36 and 6.37 show that the pressure drop is significant at the discontinuity compared to the pressure drop in the swept inner region.

Figures 6.38 through 6.40 are for $M = 10$, $F_S = 100$, and $C_D = 0$. Figure 6.38 shows semilog pressure derivative behavior for several values of $s_f$. Figure 6.39 shows Cartesian pressure derivative behavior. For $M = 10$ and $F_S = 100$, the *Stehfest* (1970) algorithm produced meaningful results even for $s_f = -5$. Figure 6.38 shows that the dimensionless deviation time from a semilog line corresponding to the inner region mobility, and the time to start of second semilog line are not affected by the value of $s_f$. But a thin skin at the discontinuity affects the pressure derivative response at intermediate time. The value of $s_f$ affects the magnitude of maximum semilog pressure derivative, and the time to maximum semilog slope. Figure 6.39 shows that for a positive $s_f$, the pseudosteady state period is longer than that for $s_f = 0$. Also, for a negative $s_f$, the pseudosteady state period is shorter than that for $s_f = 0$. Figure 6.40 shows the pressure profile in the reservoir for $t_D/R_D^2 = 50$. As shown in Figs. 6.36 and 6.37, Fig. 6.40 also illustrates that the pressure drop is significant at the discontinuity compared to the pressure drop in the swept inner region.

Neglecting a thin skin at the discontinuity in type-curve matching analysis of well-test data may cause an overestimation of storativity ratio for a positive $s_f$ and an underestimation of storativity ratio for a negative $s_f$. This observation is illustrated in Fig. 6.41. Figure 6.41 shows semilog pressure derivative behavior for $M = 10$, $F_S = 100$, $C_D = 0$, and $s_f = 20$ by a solid line. The circles on Fig. 6.41 represent semilog pressure derivative behavior for $M = 10$, $F_S = 5152$, $C_D = 0$, and $s_f = 0$. The value of $F_S = 5152$ is derived using Eq. (6.14), and the maximum semilog slope, $dp_{wD}/d\,\ln t_D$, of 19.16 for the response for $s_f = 20$. The diamonds on Fig. 6.41 show the response for $M = 20$, $F_S = 32$, $C_D = 0$, and $s_f = 0$. The value of $F_S = 32$ for $M = 20$ is derived using Eq. (6.14), and the same maximum semilog slope of 19.16. The responses shown by the solid line and the circles are identical illustrating the

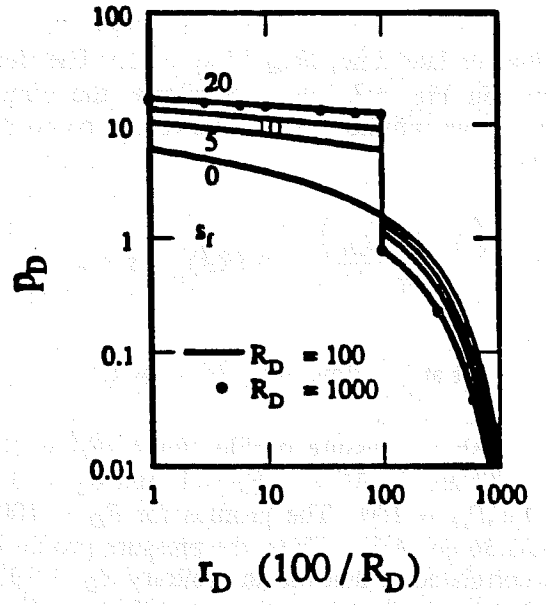


Figure 6.36: Pressure profile in the reservoir for $M = 1$, $F_S = 1$, $C_D = 0$, and $t_D/R_D^2 = 10$.

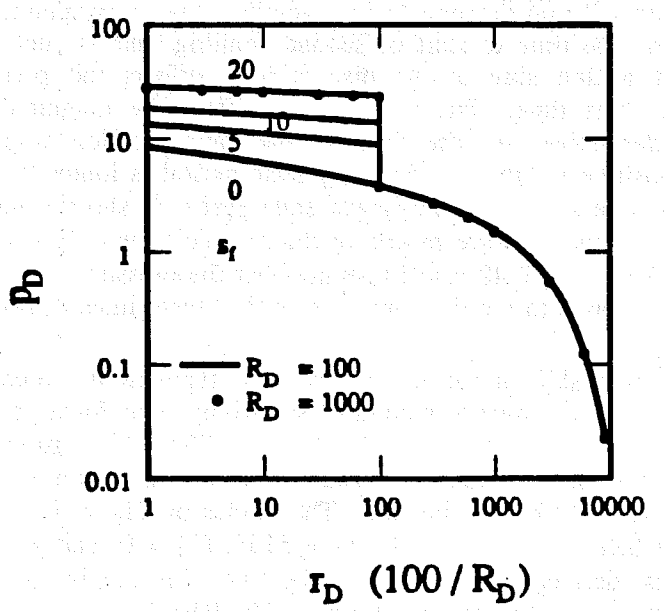


Figure 6.37: Pressure profile in the reservoir for $M = 1$, $F_S = 1$, $C_D = 0$, and $t_D/R_D^2 = 1000$.

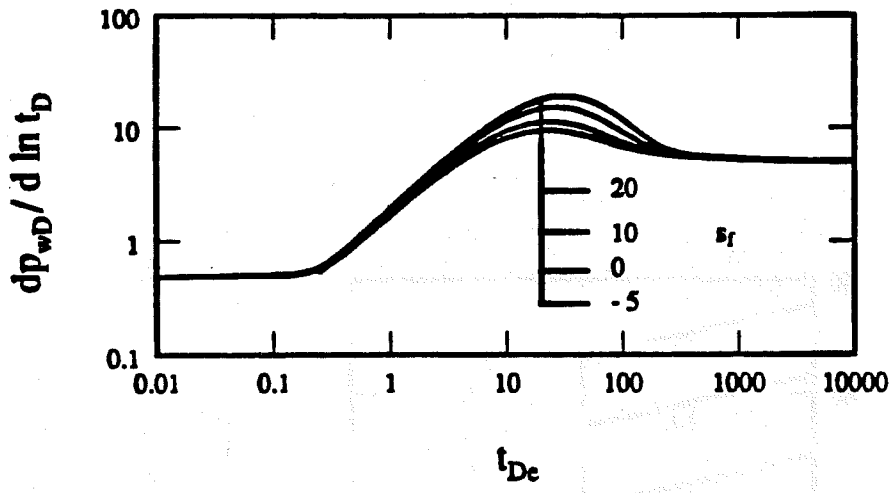


Figure 6.38: Effect of $s_f$ on semi-log slope response for $M$ = 10, $F_S$ = 100, and $C_D$ = 0.

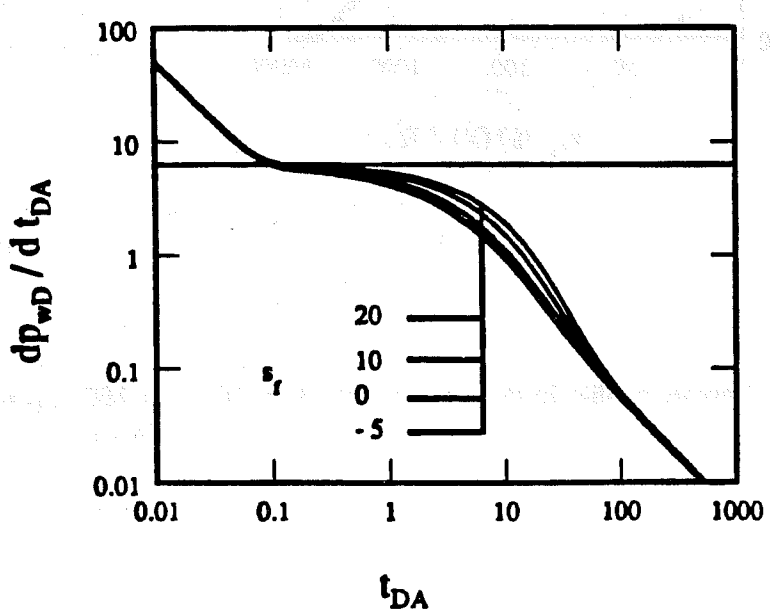


Figure 6.39: Effect of $s_f$ on Cartesian derivative for $M$ = 10, $F_S$ = 100, and $C_D$ = 0.

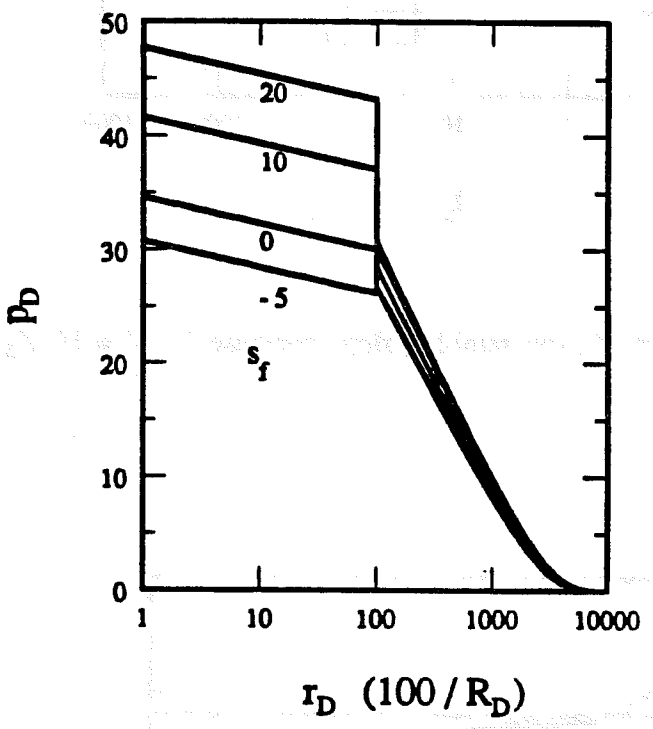


Figure 6.40: Pressure profile in the reservoir for $M$ = 10, $F_S$ = 100, $C_D$ = 0, and $t_D/R_D^2$ = 50.

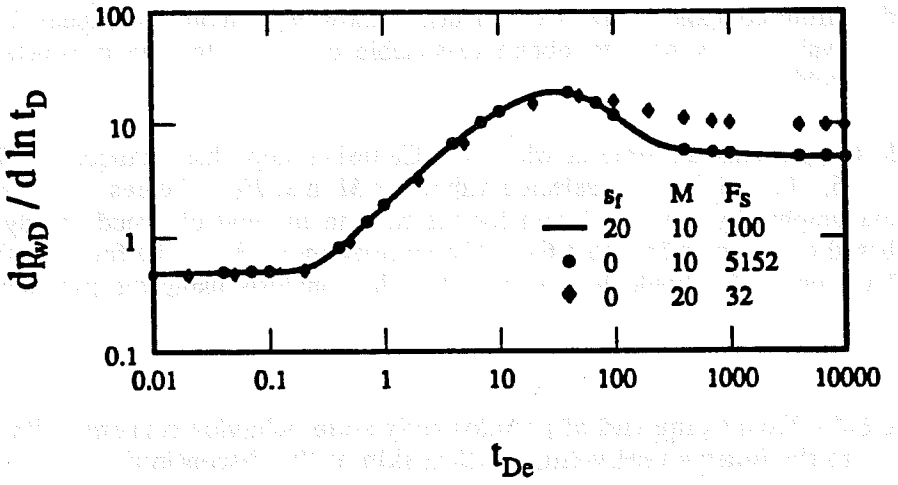


Figure 6.41: Effect of neglecting $s_f$ on type-curve matching.

possibility of obtaining a large $F_S$ from well-test data, if the effects of a positive $s_f$ are not considered. Also, if well-test data is collected up to a time slightly beyond $(t_{De})_{max}$ given by Eq. (6.2), non-unique answers for the parameters may be obtained by type-curve matching. Figure 6.41 shows that for $s_f = 0$, well-test data can be matched to obtain either $M = 10$ and $F_S = 5152$, or $M = 20$ and $F_S = 32$. *Barua* and *Horne* (1985) also discussed briefly the non-uniqueness problems in type-curve matching of well-test data from composite reservoirs. Thus, a knowledge about the expected range of parameter values may help to obtain reasonable estimates for the parameters by type-curve matching.

Table 6.4 presents the time at which the Cartesian slope has changed by 5% of $2\pi$ for $s_f = 5$, 10, and 20, and selected values of $M$ and $F_S$. Figures 6.42 through 6.44 present graphically the correlation for the time to the end of pseudosteady state behavior based on the data in Table 6.4. The correlations in Fig. 6.10 for $s_f = 0$, and Figs. 6.42 through 6.44 should help in well-test data analysis using the pseudosteady state method.

**Table 6.4 - Time to the end of pseudosteady state behavior corresponding to the inner swept volume with a skin at the discontinuity**

| $M$ | $F_S$ | $t_{DA}$ for Cartesian slope within 5% of $2\pi$ | | |
|---|---|---|---|---|
| | | $s_f = 5$ | $s_f = 10$ | $s_f = 20$ |
| 10 | 10 | 0.152 | 0.187 | 0.278 |
| 20 | | 0.164 | 0.204 | 0.305 |
| 50 | | 0.199 | 0.254 | 0.369 |
| 70 | | 0.226 | 0.289 | 0.406 |
| 100 | | 0.274 | 0.341 | 0.457 |
| 200 | | 0.437 | 0.499 | 0.614 |
| 500 | | 0.872 | 0.930 | 1.047 |
| 700 | | 1.153 | 1.213 | 1.331 |
| 1000 | | 1.576 | 1.638 | 1.759 |
| 10 | 100 | 0.193 | 0.242 | 0.346 |
| 20 | | 0.265 | 0.324 | 0.430 |
| 50 | | 0.496 | 0.552 | 0.655 |
| 70 | | 0.638 | 0.693 | 0.796 |
| 100 | | 0.847 | 0.901 | 1.006 |
| 200 | | 1.538 | 1.592 | 1.702 |
| 500 | | 3.647 | 3.703 | 3.816 |
| 700 | | 5.029 | 5.087 | 5.200 |
| 1000 | | 7.126 | 7.182 | 7.292 |
| 10 | 1000 | 0.292 | 0.345 | 0.443 |
| 20 | | 0.474 | 0.525 | 0.620 |
| 50 | | 0.978 | 1.027 | 1.123 |
| 70 | | 1.311 | 1.360 | 1.457 |
| 100 | | 1.812 | 1.861 | 1.959 |
| 200 | | 3.495 | 3.546 | 3.648 |
| 500 | | 8.518 | 8.568 | 8.669 |
| 700 | | 11.869 | 11.919 | 12.019 |
| 1000 | | 16.905 | 16.955 | 17.056 |

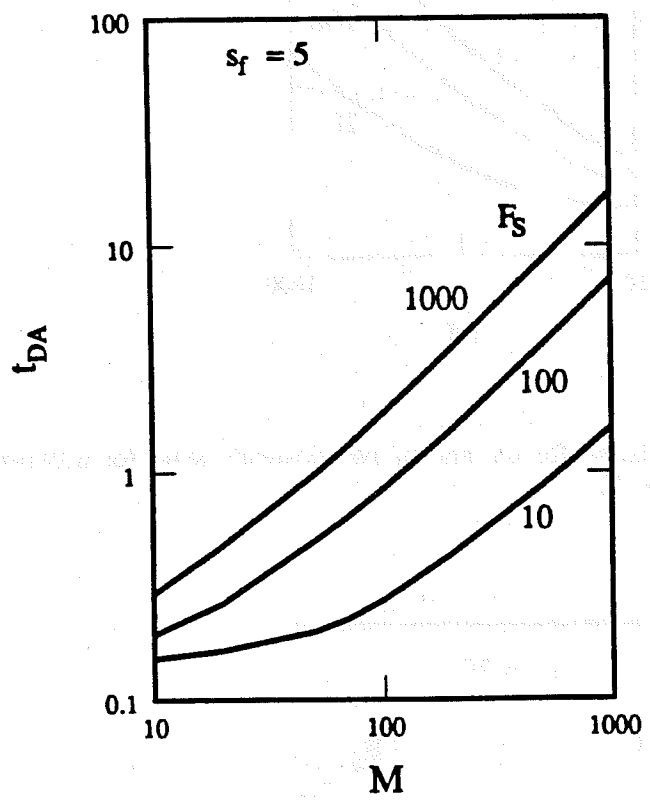


Figure 6.42: Correlation for the end of pseudosteady state for a two-region composite reservoir with $s_f = 5$.

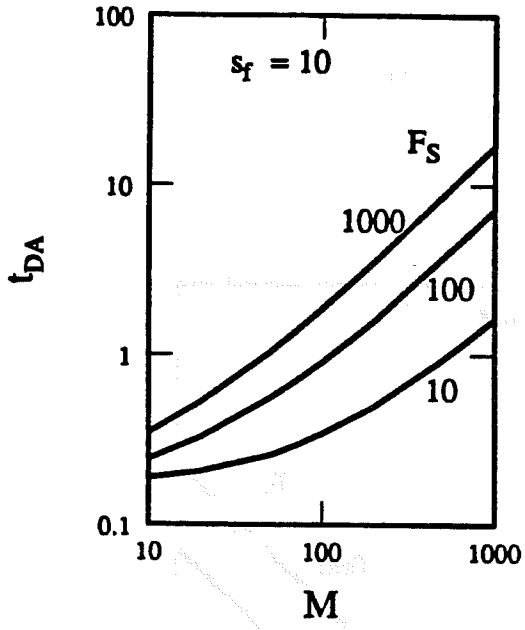


Figure 6.43: Correlation for the end of pseudosteady state for a two-region composite reservoir with $s_f = 10$.

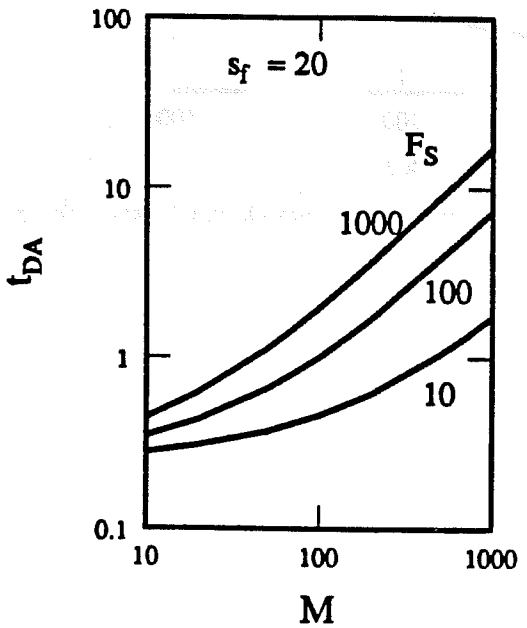


Figure 6.44: Correlation for the end of pseudosteady state for a two-region composite reservoir with $s_f = 20$.

## 6.2 THREE-REGION COMPOSITE RESERVOIR

An analytical solution in Laplace space for the transient pressure behavior of a well in a three-region composite reservoir has been presented by *Onyekonwu* (1985), and *Barua* and *Horne* (1985). To study the effects of an intermediate region on the deviation time method and the pseudosteady state method, an analytical solution for a three-region reservoir presented by *Onyekonwu* (1985) is useful. A schematic diagram of a three-region reservoir is presented in Fig. 6.45. The variables $R_1$ and $R_2$ are the inner and intermediate region radii, respectively. The parameters of an infinitely large three-region reservoir are $M_{12}$, $M_{13}$, $F_{S12}$, $F_{S13}$, $R_{D1}$, and $R_{D2}$ in the absence of wellbore storage and skin.

For a corresponding two-region reservoir,

$$M = M_{12} = M_{13} \quad , \tag{6.46}$$

$$F_S = F_{S12} = F_{S13} \quad , \text{ and} \tag{6.47}$$

$$R_D = R_{D1} \quad . \tag{6.48}$$

Should Eqs. (6.46) through (6.48) be appropriate, region 1 forms the inner region, and regions 2 and 3 form the outer region of a two-region composite reservoir.

Figure 6.46 presents a graph of semilog pressure derivative as a function of dimensionless time defined by:

$$t_{De1} = \frac{0.000264\, k_1 t}{(\phi\mu c_t)_1\, R_1^{\,2}} = \frac{t_D}{R_{D1}^2} \quad . \tag{6.49}$$

Figure 6.46 assumes $F_{S12} = F_{S13} = 1$, $M_{13} = 10$, $C_D = 0$, $R_{D1} = 100$, and $R_{D2} = 150$. The parameter of interest is $M_{12}$ on Fig. 6.46. A two-region composite reservoir solution is obtained for $M_{12} = 10$. For $R_{D1} = 100$ and $R_{D2} = 150$, the intermediate region is significant, as the intermediate region volume is 1.25 times the inner region volume. Figure 6.46 shows that the dimensionless deviation time is not affected significantly, unless $M_{12}$ is near unity. Thus, the deviation time method would result in a front radius $R_1$.

Figure 6.47 shows that the two parameters $R_{D1}$ and $R_{D2}$ can be correlated into one parameter $R_{D2}/R_{D1}$ or $R_2/R_1$. Figure 6.47 applies for $M_{12} = 10$, $M_{13} = 20$, $F_{S12} = F_{S13} = 10$, $R_2/R_1 = 1.25$, and $C_D = 0$. The responses for three different $R_{D1}$ values of 100, 500, and 1000 are shown on Fig. 6.47. Thus, the pressure transient response for a well in a three-region composite reservoir can be represented by five parameters, $M_{12}$, $M_{13}$, $F_{S12}$, $F_{S13}$, and $R_2/R_1$, in the absence of wellbore storage and skin.

Figure 6.48 shows the effect of $F_{S12}$ on the semilog pressure derivative response for $M_{12} = M_{13} = 1$, $F_{S13} = 100$, $R_2/R_1 = 1.1$, and $C_D = 0$. The responses for $F_{S12} = 1$ corresponds to a two-region reservoir with the inner region radius as $R_2$. The response for $F_{S12} = 100$ corresponds to a two-region reservoir with the inner region radius as $R_1$. The response for $F_{S12} = 1$ and 100 appear essentially identical because

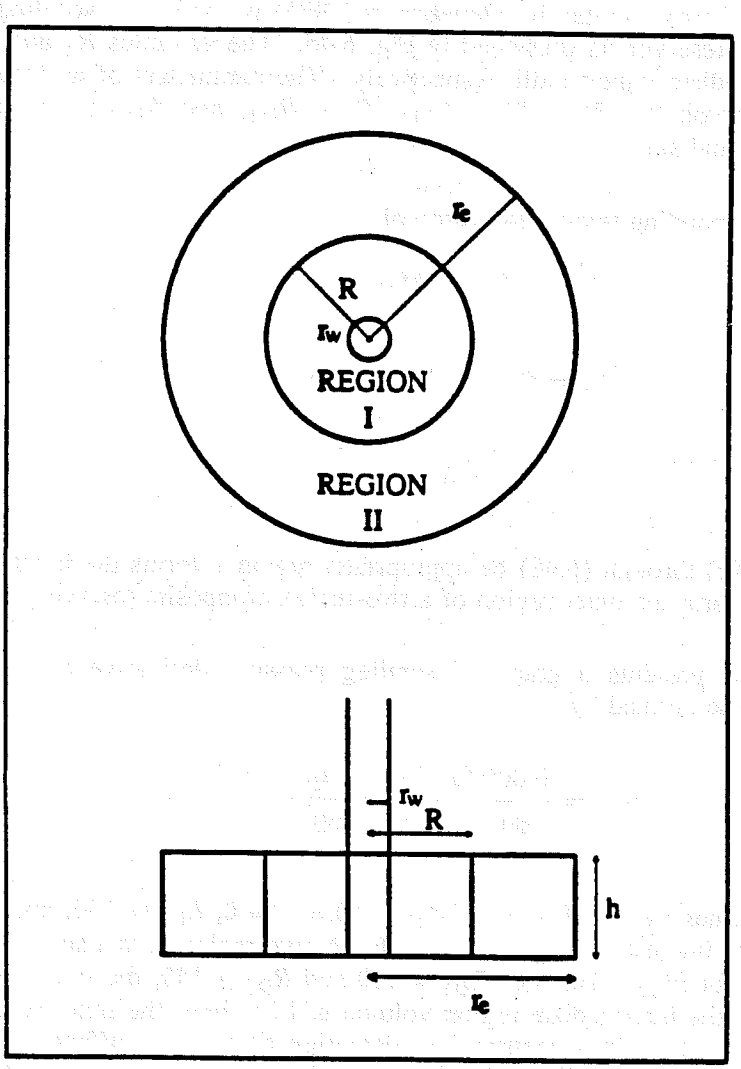


**Figure 6.45:** Three-region, radial composite reservoir.

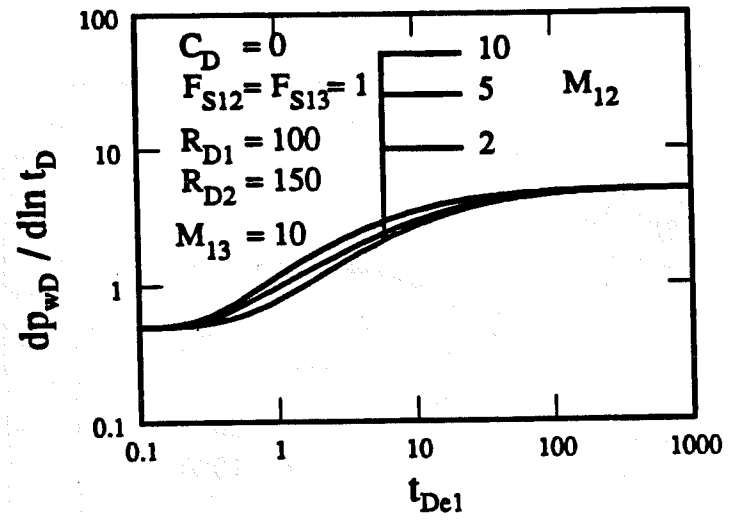


Figure 6.46: Effect of $M_{12}$ on semi-log slope response for an infinitely large, three-region composite reservoir.

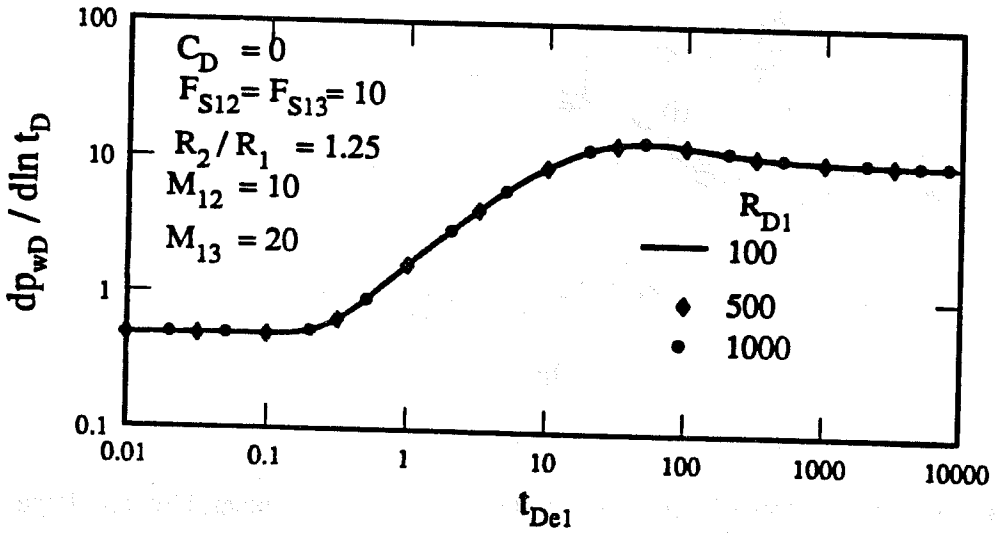


Figure 6.47: Verification of $R_2/R_1$ as a correlating parameter for drawdown responses for an infinitely large, three-region composite reservoir.

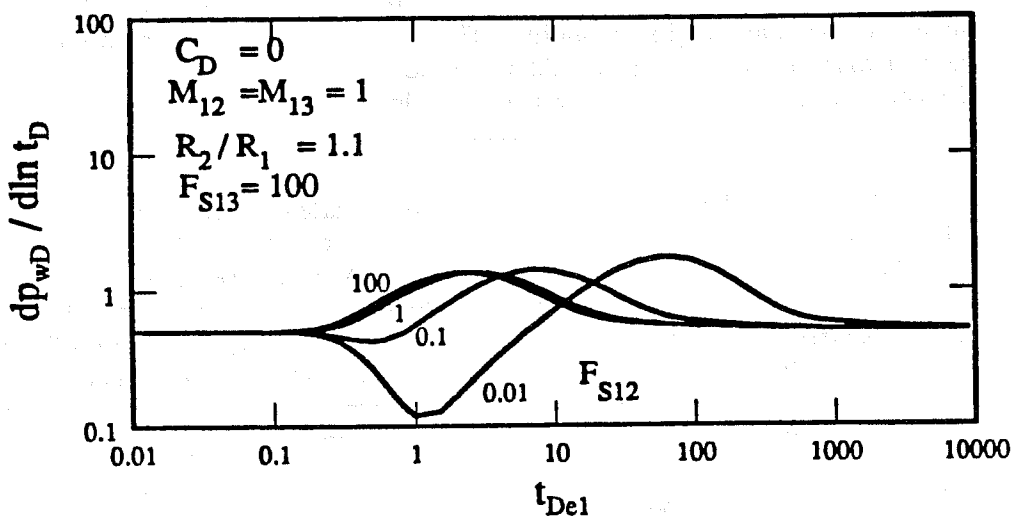


Figure 6.48: Effect of $F_{S12}$ on semi-log slope response for an infinitely large, three-region composite reservoir.

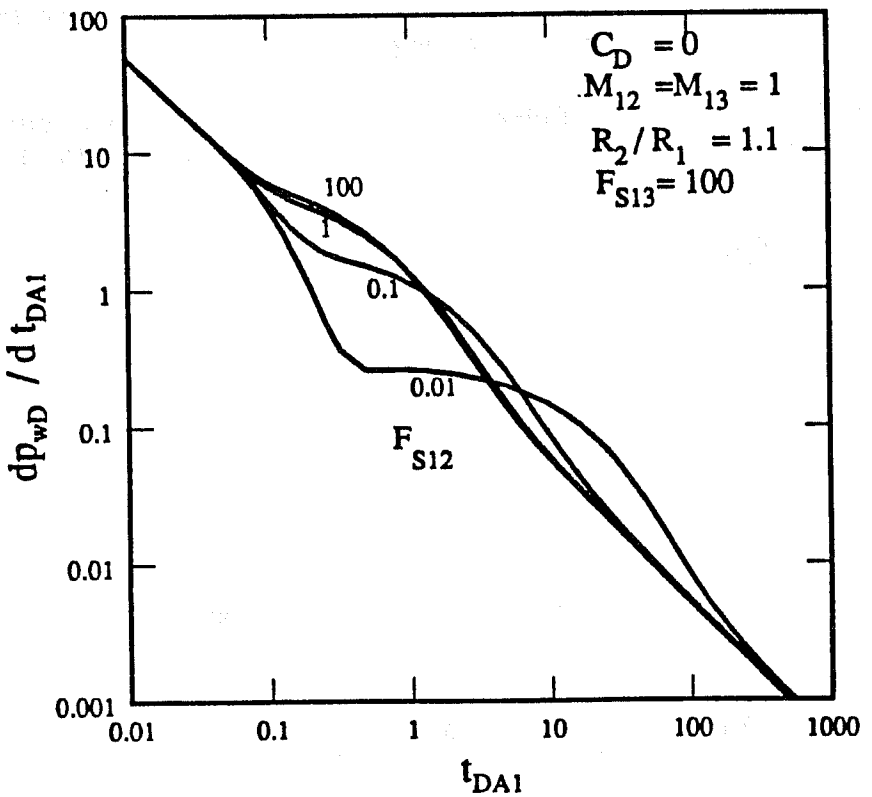


Figure 6.49: Effect of $F_{S12}$ on Cartesian slope response for an infinitely large, three-region composite reservoir.

of a small intermediate region corresponding to $R_2/R_1 = 1.1$. The responses for $F_{S12} = 0.1$ and 0.01 illustrate a decrease in semilog pressure derivative after the end of infinite-acting radial flow corresponding to the inner region mobility. The dimensionless deviation time, $(t_{De})_{end}$, is 0.18. Thus, the deviation time method would result in a front radius corresponding to $R_1$. Also, for $F_{S12} < 1$, $F_{S12}$ affects significantly the time to maximum semilog slope, and the time to start of infinite-acting radial flow corresponding to the outer region mobility. The parameter $F_{S12}$ affects mildly the magnitude of maximum semilog slope. At late time, semilog slope is $M_{13}/2$ on Fig. 6.48, and since in this case, $M_{13} = 1$, the late-time slope is the same as the early-time slope.

Figure 6.49 shows the effect of $F_{S12}$ on the Cartesian pressure derivative response for $M_{12} = M_{13} = 1$, $F_{S13} = 100$, $R_2/R_1 = 1.1$, and $C_D = 0$. Figure 6.49 shows that pseudosteady state does not develop for two-region reservoir situations of $F_{S12} = 1$ and 100 because mobility and storativity contrasts are not large enough. For $F_{S12} = 0.1$, the Cartesian pressure derivative starts to flatten at $t_{DA1}$ of about 0.3, but does not develop a constant Cartesian pressure derivative. However, for $F_{S12} = 0.01$, the Cartesian pressure derivative flattens at a value of approximately 0.264 for a period of time between $t_{DA1}$ of 0.5 and 1.1. The dimensionless time, $t_{DA1}$, is given by:

$$t_{DA1} = \frac{0.000264\, k_1 t}{(\phi\mu c_t)_1\, \pi\, R_1^2} = \frac{t_{De1}}{\pi} \tag{6.50}$$

The development of a short duration of a constant Cartesian pressure derivative may be related to the pseudosteady state corresponding to the swept volume of $R_2$. For $F_{S12} = 0.01$, and $M_{12} = M_{13} = 1$, pseudosteady state corresponding to the volume of $R_1$ does not exist because of pressure-support type behavior after the end of the semilog line corresponding to the inner region mobility.

To explore the possibility of observing a pseudosteady state period corresponding to the swept volume of $R_2$, a graph of $(dp_{wD}/dt_{DA})_{eff}$ as a function of $(t_{DA})_{eff}$ should be helpful. The expressions for effective values are:

$$\left[\frac{dp_{wD}}{dt_{DA}}\right]_{eff} = \frac{dp_{wD}}{dt_{DA1}} \cdot \frac{(\phi c_t)_{eff}\, R_2^2}{(\phi c_t)_1\, R_1^2} \quad , \text{ and} \tag{6.51}$$

$$(t_{DA})_{eff} = t_{DA1} \cdot \frac{(\phi c_t)_1\, R_1^2}{(\phi c_t)_{eff}\, R_2^2} \cdot \frac{(k/\mu)_{eff}}{(k/\mu)_1} \quad , \tag{6.52}$$

where:

$$\frac{(\phi c_t)_{eff}\, R_2^2}{(\phi c_t)_1\, R_1^2} = 1 + \frac{1}{F_{S12}} \left[(R_2/R_1)^2 - 1\right] \quad , \text{ and} \tag{6.53}$$

$$\frac{(k/\mu)_{eff}}{(k/\mu)_1} = \frac{\ln (R_{D2})}{\ln (R_{D1}) + M_{12} \ln (R_2/R_1)} \quad , \tag{6.54}$$

if the swept volume extends to $R_2$ for a three-region reservoir. Equations (6.53) and (6.54) are derived in Appendix F.

To compute $(t_{DA})_{eff}$, both $R_{D1}$ and $R_{D2}$ are needed. Figures 6.48 and 6.49 were generated for $R_{D1}$ = 100, and $R_{D1}$ = 110. Figure 6.50 presents a graph of $(dp_{wD}/dt_{DA})_{eff}$ as a function of $(t_{DA})_{eff}$. Figure 6.50 shows that pseudosteady state behavior is not observed for $F_{S12}$ = 0.1, 1, and 100. However, for $F_{S12}$ = 0.01, an effective Cartesian slope with a constant value of approximately 5.81 exists for a period of time between $(t_{DA})_{eff}$ of 0.023 and 0.05. An analysis using the effective Cartesian slope of 5.81 would result in a volume equal to $2\pi$ / 5.81 = 1.08 times the volume of $R_2$, provided correct $(\phi c_t)_{eff}$ as given by Eq. (6.53) is used for analysis. Thus, the error in estimating the volume at $R_2$ is not large. However, since an approximately constant effective Cartesian slope started at $(t_{DA})_{eff}$ of 0.023, and not at $(t_{DA})_{eff} \simeq 0.1$, only an apparent pseudosteady flow corresponding to the volume at $R_2$ developed for $F_{S12}$ = 0.01. An effective Cartesian slope of $2\pi$ starting at $(t_{DA})_{eff} \simeq 0.1$ would result in a correct volume at $R_2$. Thus, a calculation of $(t_{DA})_{eff}$ corresponding to the time of start of approximately constant effective Cartesian slope may provide an idea of whether a true, or an apparent pseudosteady state has been reached. A calculation of $(t_{DA})_{eff}$ requires evaluations of Eqs. (6.53) and (6.54). An analysis of approximately constant Cartesian slope using $(\phi c_t)_{eff}$ requires an evaluation of Eq. (6.53) only.

An evaluation of Eq. (6.53) requires estimates for $R_2/R_1$ and $F_{S12}$, provided $(\phi c_t)_1$ is known. Approximations for $R_2/R_1$ and $F_{S12}$ may be obtained by experimental or numerical simulation studies for a particular process. From a numerical simulation study of in-situ combustion falloff tests, *Onyekonwu* (1985) obtained:

$$R_2/R_1 = \sqrt{2} \quad , \text{ and} \tag{6.55}$$

$$F_{S12} = \frac{1}{1 - S_{or}} \quad , \tag{6.56}$$

where $S_{or}$ is residual oil saturation. Equations (6.55) and (6.56) result from an inspection of equations presented by *Onyekonwu* (1985) in Chapter 7.5.2. Similar numerical simulation studies should be made in the future to develop correlations for $R_2/R_1$ and $F_{S12}$ for other enhanced oil recovery processes such as steam injection and $CO_2$ flooding. To calculate $(t_{DA})_{eff}$, an estimate for $M_{12}$ is also needed, assuming that the deviation time method has been successfully used to obtain $R_1$ or $R_{D1}$. Also, $R_{D2}$ = $R_{D1} \times (R_2/R_1)$. Correlations for $M_{12}$ may be developed using experimental or numerical simulation studies.

Figures 6.51 through 6.53 show the effect of $R_2/R_1$ on semilog slope, Cartesian slope, and effective Cartesian slope response for $M_{12} = M_{13}$ = 1, $C_D$ = 0, $F_{S12}$ = 0.01, and $F_{S13}$ = 100. To calculate the effective Cartesian slope, the value for $R_{D1}$ = 100 used to generate the responses in Figs. 6.51 and 6.52 was used. Figure 6.51 shows a dimensionless deviation time of 0.18. After the end of infinite-acting radial flow corresponding to the inner region mobility, the semilog slope declines as $F_{S12}$ = 0.01. However, as the outer region effects are felt, the semilog slope starts to rise. A maximum semilog slope develops at intermediate time. At late time, the semilog slope approaches $M_{13}/2$. The parameter $R_2/R_1$ affects the time to maximum semilog slope

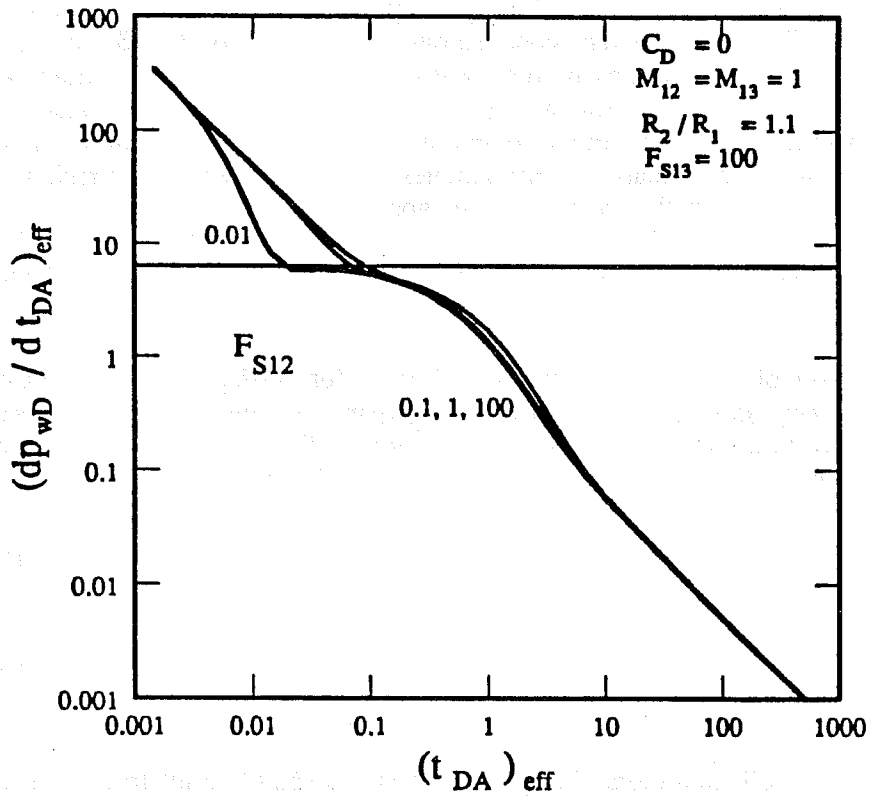


Figure 6.50: Effective Cartesian slope as a function of $(t_{DA})_{eff}$ for an infinitely large, three-region composite reservoir with $C_D = 0$, $M_{12} = M_{13} = 1$, $F_{S13} = 100$, and $R_2/R_1 = 1.1$.

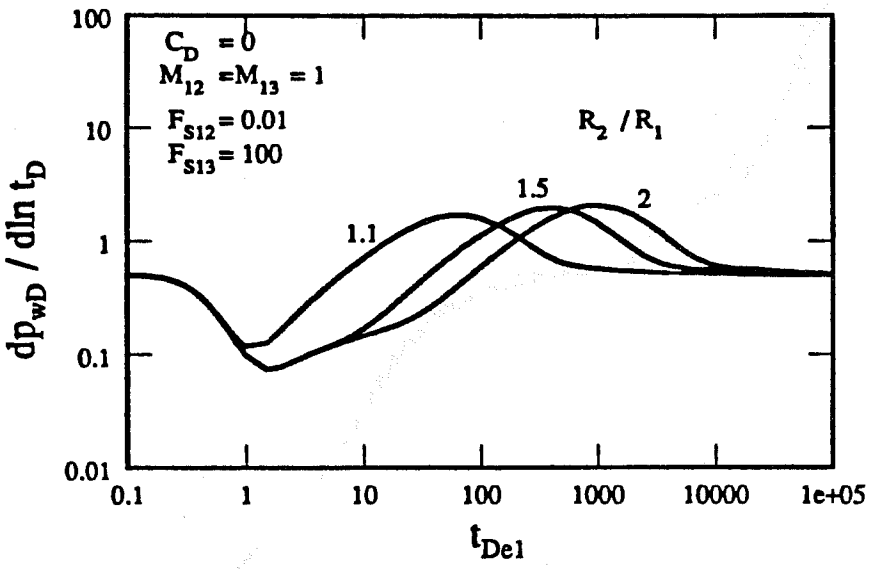


Figure 6.51: Effect of $R_2/R_1$ on semi-log slope response for an infinitely large, three-region composite reservoir.

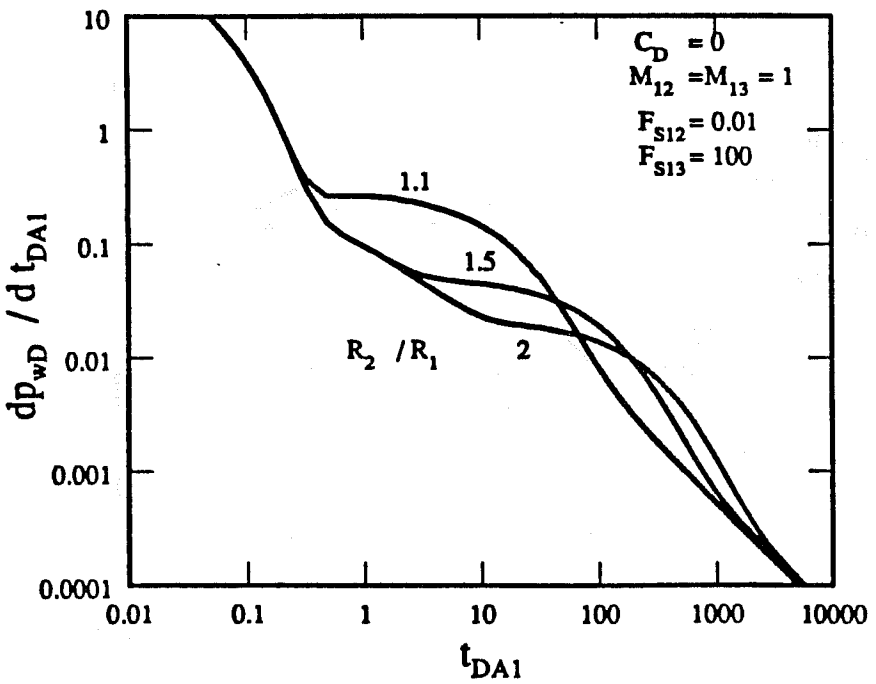


Figure 6.52: Effect of $R_2/R_1$ on Cartesian slope response for an infinitely large, three-region composite reservoir.

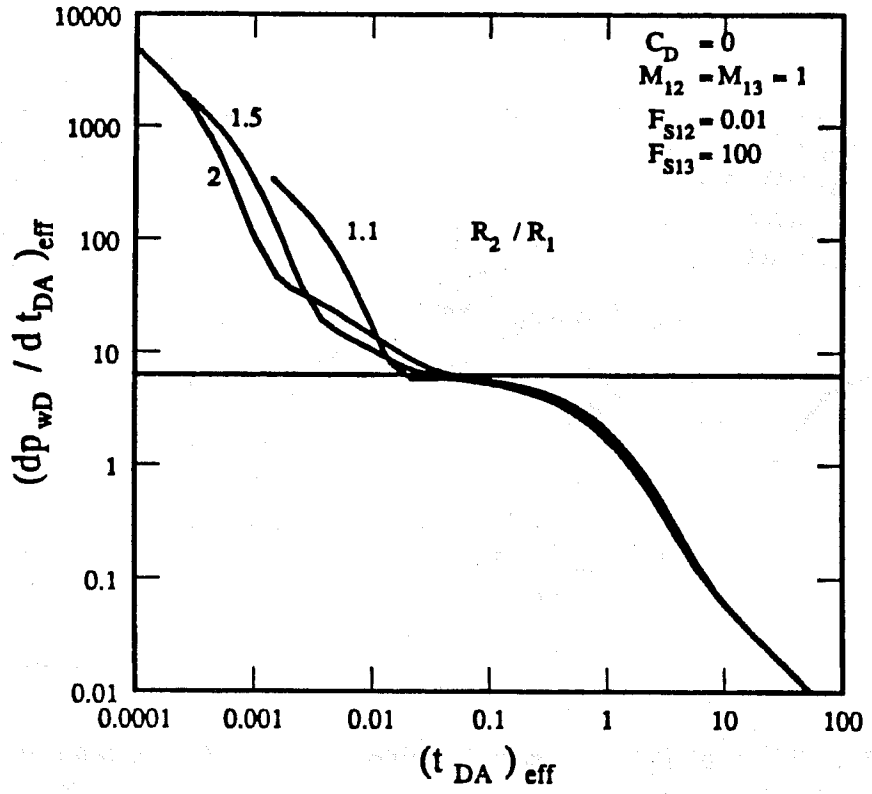


Figure 6.53: Effective Cartesian slope as a function of $(t_{DA})_{eff}$ for an infinitely large, three-region composite reservoir with $C_D = 0$, $M_{12} = M_{13} = 1$, $F_{S12} = 0.01$, and $F_{S13} = 100$.

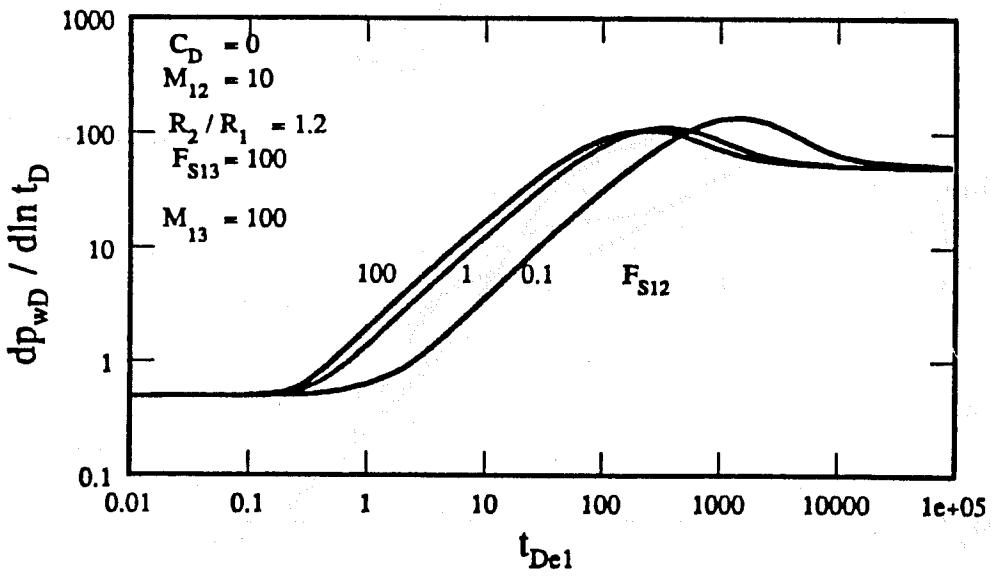


Figure 6.54: Effect of $F_{S12}$ on semi-log slope response for an infinitely large, three-region composite reservoir with $C_D = 0$, $M_{12} = 10$, $M_{13} = 100$, $F_{S13} = 100$, and $R_2/R_1 = 1.2$.

significantly, and the time to start of infinite-acting radial flow corresponding to the outer region mobility. However, the parameter $R_2/R_1$ affects the magnitude of maximum semilog slope mildly.

The response for $R_2/R_1 = 1.1$ on Fig. 6.52 is the same as the response for $F_{S12} = 0.01$ on Fig. 6.50, and has been discussed already. The responses for $R_2/R_1 = 1.5$ and 2 on Figs. 6.52 and 6.53 do not exhibit an unambiguous flattening of the Cartesian slope. But as observed from Fig. 6.53, well-test data during the time $(t_{DA})_{eff}$ between 0.02 and 0.06 may still be analyzed to obtain a slightly overestimated value for the volume at the radius $R_2$, even though a correct pseudosteady state with an effective Cartesian slope of $2\pi$ does not appear. To analyze the data using the pseudosteady state method, an estimate for $(\phi c_t)_{eff}$ is required.

Figure 6.54 shows the effect of $F_{S12}$ on the semilog pressure derivative response for $M_{12} = 10$, $M_{13} = 100$, $F_{S13} = 100$, $R_2/R_1 = 1.2$, and $C_D = 0$. For $F_{S12} = 1$ and 100, the dimensionless deviation time is 0.18, and the deviation time method would result in a front radius $R_1$. However, for $F_{S12} = 0.1$, the dimensionless deviation time is 0.35 to observe a 2% change from a semilog slope value of 1/2, and thus, Eq. (6.7) would produce an inaccurate, and probably meaningless result for the front radius. There is a time period after $t_{De1} = 0.18$ when the opposing effects of $M_{12} > 1$, and $F_{S12} < 1$ are balanced in a way to produce an apparently longer semilog line corresponding to the inner region mobility for $F_{S12} = 0.1$ on Fig. 6.54.

Figure 6.54 also shows that for $F_{S12} < 1$, $F_{S12}$ affects the time to maximum semilog slope significantly, and the time to the start of infinite-acting radial flow corresponding to the outer region mobility. The parameter $F_{S12}$ affects the magnitude of maximum semilog slope mildly. At late time, the semilog slope is $M_{13}/2$.

Figure 6.55 shows the effect of $F_{S12}$ on the Cartesian pressure derivative response for $M_{12} = 10$, $M_{13} = 100$, $F_{S13} = 100$, $R_2/R_1 = 1.2$, and $C_D = 0$. Figure 6.55 uses $R_{D1} = 100$. For $F_{S12} = 100$, a Cartesian slope of approximately $2\pi$ develops on Fig. 6.55 for $t_{DA1}$ between 0.1 and about 0.6. By $t_{DA1} = 0.6$, the Cartesian slope has changed by 5% from $2\pi$. Thus, for $F_{S12} = 100$, and $M_{12} = 10$, it appears that the pseudosteady state method using $(\phi c_t)_1$ may be used to obtain the volume of the inner region. However, based on the data in Table 6.2, the Cartesian slope changes by 5% from $2\pi$ by $t_{DA} = 0.155$ for $M = 10$, and $F_S = 100$ in a two-region composite reservoir. Thus, it is unlikely that an intermediate region with $R_2/R_1 = 1.2$, $M_{12} = 10$, and $F_{S12} = 100$ can produce a pseudosteady state period corresponding to the inner region volume lasting to $t_{DA1}$ of 0.6. Thus, the existence of a Cartesian slope of approximately constant value of $2\pi$ to $t_{DA1} = 0.6$ probably corresponds to the volume of $R_2$. Also, approximately constant Cartesian slopes for some duration for $F_{S12} = 1$ and 0.1 are also expected to correspond to pseudosteady state for the volume of $R_2$.

Figure 6.56 presents a graph of $(dp_{wD}/dt_{DA})_{eff}$ as a function of $(t_{DA})_{eff}$. Figure 6.56 shows that for $F_{S12} = 0.1$, 1, and 100, an effective Cartesian slope of approximately $2\pi$ develops at $(t_{DA})_{eff} \simeq 0.1$ representing pseudosteady state depletion of the volume of $R_2$. For $F_{S12} = 100$, and $R_2/R_1 = 1.2$, Eq. (6.53) yields:

$$\frac{(\phi c_t)_{eff}\, R_2^2}{(\phi c_t)_1\, R_1^2} = 1.0044 \quad . \tag{6.57}$$

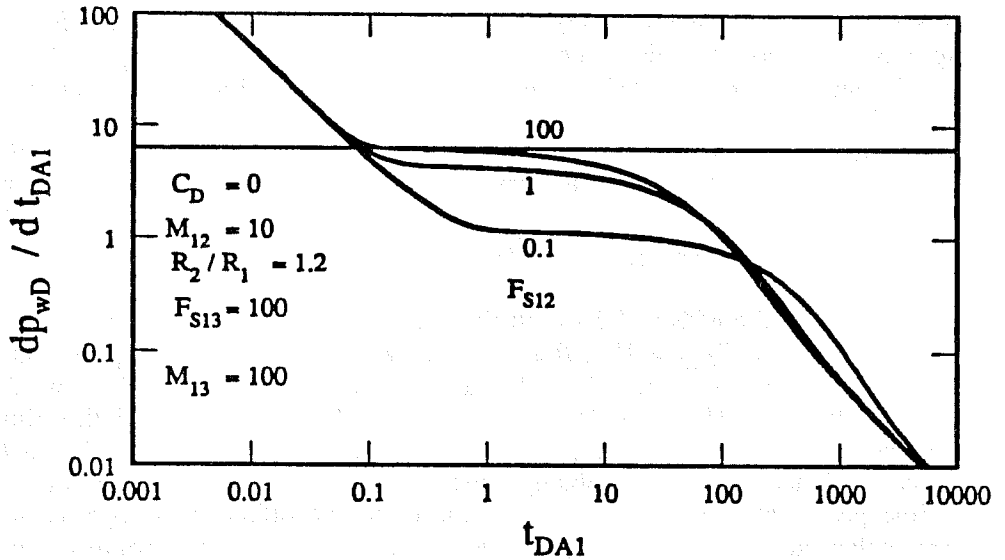


Figure 6.55: Effect of $F_{S12}$ on Cartesian slope response for an infinitely large, three-region composite reservoir with $C_D = 0$, $M_{12} = 10$, $M_{13} = 100$, $F_{S13} = 100$, and $R_2/R_1 = 1.2$.

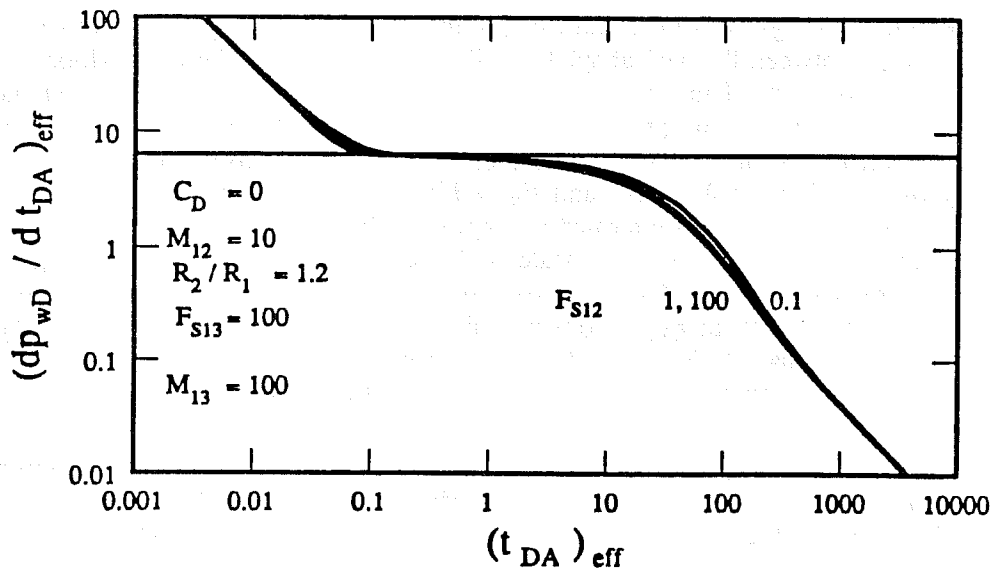


Figure 6.56: Effective Cartesian slope as a function of $(t_{DA})_{eff}$ for an infinitely large, three-region composite reservoir with $C_D = 0$, $M_{12} = 10$, $M_{13} = 100$, $F_{S13} = 100$, and $R_2/R_1 = 1.2$.

Using Eq. (6.57) in Eq. (6.51) yields:

$$\left[\frac{dp_{wD}}{dt_{DA}}\right]_{eff} = 1.0044\left[\frac{dp_{wD}}{dt_{DA1}}\right] \quad . \tag{6.58}$$

Equation (6.58) explains the development of a Cartesian slope of approximately $2\pi$ on Figs. 6.55 and 6.56 for $F_{S12} = 100$.

In summary, for a three-region reservoir, the deviation time method would result in a front radius $R_1$ if the effects of $M_{12}$ and $F_{S12}$ are not balanced in a way to produce an incorrect deviation time. The pseudosteady state method would result in a front radius $R_2$ if $(\phi c_t)_{eff}$ is used to analyze the pseudosteady data. However, at times, the development of an apparent pseudosteady state may yield an overestimated value for the volume of $R_2$. An idea about the development of an apparent pseudosteady state may be obtained by calculating $(t_{DA})_{eff}$ corresponding to the time to start of an approximately constant Cartesian slope.

# 7. ANALYSIS OF WELL TESTS

A number of well tests reported in the literature exhibiting composite reservoir behavior are analyzed in this chapter to establish the applicability and the limitations of different methods to estimate a discontinuity (or front) radius, or swept volume. Well tests considered in this chapter represent field and simulated data from in-situ combustion, steam injection, $CO_2$ flood, waterflood and acidization projects. A simulated example of an ideal composite reservoir by *Kazemi et al.* (1972) is also considered. Analysis shows the estimate of front radius to be sensitive to the real deviation time. The estimated front radius from the deviation time method may represent a lower bound for front radius, if the swept region is not cylindrical. Also, obtaining an accurate deviation time for small mobility contrasts may be difficult.

All well tests have been analyzed by the deviation time method in addition to other methods. Except for Ex. 10, deviation time has been obtained from a semilog graph of pressure vs. time, and therefore, $(t_{De})_{end} = 0.4$ (or Eq. (6.8)) is used to calculate an estimated front radius. For Ex. 10, a pressure derivative graph has been used to obtain a deviation time, and therefore $(t_{De})_{end} = 0.18$ (or Eq. (6.7)) is used to calculate an estimated front radius. The use of Eq. (6.7) or (6.8), depending on how deviation time is obtained, maintains the consistency between real data and the interpretation equation derived from the system response in dimensionless terms. Well-test data is not available in a form suitable to prepare a pressure derivative graph for any example, except Ex. 10.

## 7.1 WELL TEST EXAMPLES

Example 1 concerns a simulated in-situ combustion falloff test reported by *Onyekonwu et al.* (1984). The semilog graph of pressure vs. time is shown in Fig. 4 of *Onyekonwu et al.* They calculated $(k/\mu)_1$ of 25,001 md/cp and reported $(\phi c_t)_1$ of $3.3915 \times 10^{-4}$ per psi. The burning front in this example was at Block 14. The center of Block 14 in the simulation model was at 53.3 ft. However, a sharp drop in mobility occurred between Blocks 18 and 19 (see Table 2 of *Onyekonwu et al.*). The center of Block 18 in the simulation model was at 84.5 ft. They found that the pseudosteady state method yielded an estimate of swept volume corresponding to a radius of 84.5 ft. However, Fig. 4 of *Onyekonwu et al.* indicates a deviation time of 70 seconds yielding a front radius of 30.8 ft using Eq. (6.8). The estimated front radius of 30.8 ft does not correspond to the burning front radius.

As per *Onyekonwu et al.* (1984), a semilog line corresponding to the inner region mobility for their example should develop at a time $\geq$ 18.5 seconds, based on the criterion of $t_D \geq 25$ for the beginning of a semilog line. Thus, a modified semilog line starting from 30 seconds as shown in Fig. 7.1 may be a more accurate semilog line for this example. Figure 7.1 also shows the semilog line originally chosen by *Onyekonwu et al.* The modified semilog line has a slope of 0.16 psi/cycle yielding an estimated $(k/\mu)_1$ of 21,251 md/cp. The modified semilog line on Fig. 7.1 ends at about 250 seconds. Using a deviation time of 250 seconds in Eq. (6.8) results in an estimated front radius of 53.6 ft which is close to the burning front radius of 53.3 ft. This example shows the sensitivity of the deviation time method to the estimated real deviation time. Therefore, the selection of a proper semilog line and an accurate deviation time are crucial for the success of the deviation time method.

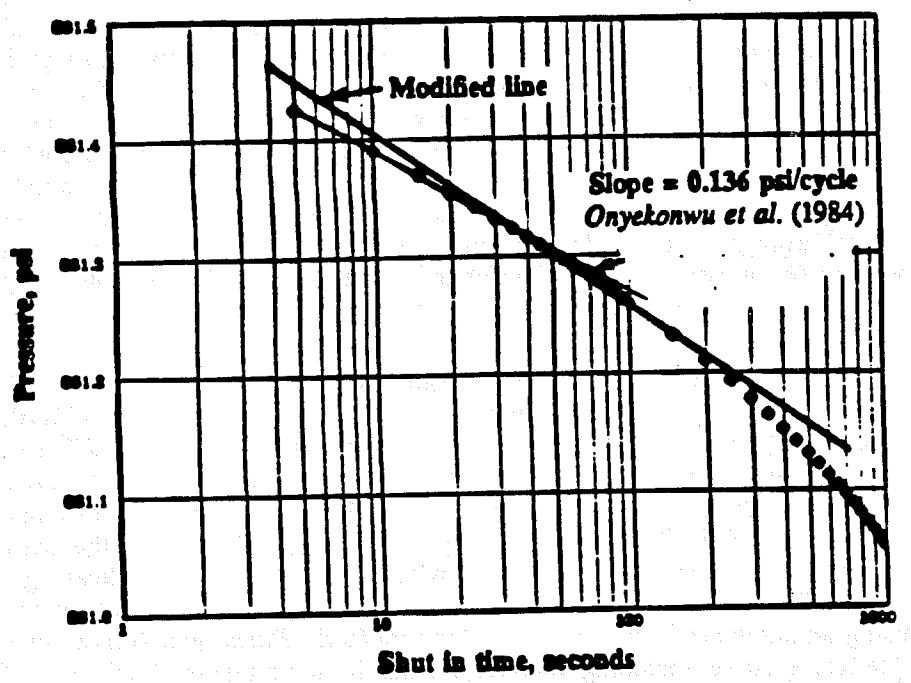


Figure 7.1: Semi-log graph for Example 1 (modified from *Onyekonwu et al.*, 1984).

Example 2 concerns a field in-situ combustion test reported by *Onyekonwu et al.* (1986). The semilog graph of pressure vs. time is shown in Fig. 12 of *Onyekonwu et al.* They calculated $(k/\mu)_1$ of 5,685.5 md/cp and $(\phi c_t)_1$ of $35.3 \times 10^{-4}$ per psi for this example. Figure 12 of *Onyekonwu et al.* shows a deviation time of 600 seconds yielding a front radius of 13.3 ft. *Onyekonwu et al.* calculated a swept pore volume of 10,300 cubic ft or a front radius of 12.8 ft from the pseudosteady state method. The estimated front radii from the deviation time method and the pseudosteady state method are quite close for this example.

Example 3 concerns a field in-situ combustion test in well B reported by *Onyekonwu* (1985). The semilog graph of pressure vs. time is shown in Fig. 9.6 of *Onyekonwu.* He calculated $(k/\mu)_1$ of 4,907.45 md/cp and reported $(\phi c_t)_1$ of $1.0262 \times 10^{-4}$ per psi. Figure 9.6 of *Onyekonwu* shows a deviation time of 0.5 hour yielding a front radius of 126 ft. *Onyekonwu* calculated a swept pore volume of 432,361.6 cubic ft or a front radius of 166 ft from the pseudosteady state method. A significant difference between the estimated front radii from the deviation time method and the pseudosteady state method indicates significant gravity override effects. If the swept region is not cylindrical, a deviation time could correspond to a "minimum" front radius (*Satman* and *Oskay*, 1985). However, the pseudosteady state method is independent of the geometry of the swept region, and the pseudosteady state method should yield an "average" front radius for any swept region shape. For this example, 126 ft appears to be an estimate of the "minimum" front radius, whereas 166 ft appears to be an estimate of the "average" front radius corresponding to the swept volume.

Example 4 concerns a field in-situ combustion test reported as Case A by *Walsh et al.* (1981). The semilog graph of pressure vs. time is shown in Fig. 5 of *Walsh et al.* They calculated $(k/\mu)_1$ of 12,647 md/cp and reported $(\phi c_t)_1$ of $119 \times 10^{-6}$ per psi. They reported the semilog line shown on Fig. 5 of their paper to last until 0.5 hour. A deviation time of 0.5 hour yields a front radius of 187 ft. *Walsh et al.* calculated a swept pore volume of 878,000 cubic ft or a front radius of 236 ft from the pseudosteady state method. A comparison of 187 ft with 236 ft suggests significant gravity override effects. But *Barua* and *Horne* (1987) obtained a front radius of 144 ft for this example, using an automated type-curve matching method. *Barua* and *Horne* state that the automated type-curve matching method results in a volumetric "average" front radius. *Barua* and *Horne* also state that *Walsh et al.* were not able to locate the correct Cartesian straight line for this example and therefore, the estimate of 236 ft is not correct. But since the estimate from the deviation time method represents the radius to the closest discontinuity affecting the pressure transient behavior, and hence a "minimum" front radius, the difference between 187 ft from the deviation time method and 144 ft from the automated type-curve matching method requires explanation. One possible explanation may lie in the sensitivity of the deviation time method to real deviation time. An examination of Fig. 5 of *Walsh et al.* suggests that a deviation time of 0.3 hours is also reasonable, which yields a front radius estimate of 144.8 ft. This estimate of 144.8 ft is in excellent agreement with the estimate of 144 ft by *Barua* and *Horne.* Thus, this example also shows the sensitivity of the deviation time method to real deviation time and therefore, the deviation time method should be used with caution. A pressure derivative graph may be useful in obtaining deviation time accurately, provided enough pressure data are recorded to prepare a smooth pressure derivative graph. Also, any error in estimating front radius results in a magnified error for the swept volume, because the swept volume is proportional to the square of the front radius.

Example 5 concerns a field in-situ combustion falloff test reported as Case B by *Walsh et al.* (1981). The semilog graph of pressure vs. time is shown in Fig. 7 of *Walsh et al.* Their Fig. 7 indicates a deviation time of 1 hour. Using $(k/\mu)_1$ of 28,839 md/cp and $(\phi c_t)_1$ of $6.258 \times 10^{-4}$ per psi reported by *Walsh et al.*, Eq. (6.8) yields an estimated front radius of 174.4 ft. Using the pseudosteady state method, *Walsh et al.* (1981) computed a swept pore volume of 2,015,000 cubic ft or a front radius of 193 ft. Using an automated type-curve matching method, *Barua* and *Horne* (1987) obtained a front radius of 173.7 ft for this example. Thus, the difference between 173.7 ft from the automated type-curve matching method and 193 ft from the pseudosteady state method may be due to the difficulty of choosing a proper Cartesian straight line for the pseudosteady state method, as both estimates should represent "average" front radius. Since a front radius of 174.4 ft from the deviation time method is close to the estimate of 173.7 ft, this example indicates minimal gravity effects.

Example 6 concerns a steam injection falloff test in Well 502 of Project A reported by *Messner* and *Williams* (1982). An analysis of the falloff test in Well 502 is presented in the Appendix of *Messner* and *Williams*. They reported $(k/\mu)_1$ of 11,200 md/cp and $(\phi c_t)_1$ of $9.408 \times 10^{-2}$ per psi. The semilog graph of pressure vs. time is shown in Fig. 5 of *Messner* and *Williams*. Their Fig. 5 indicates a deviation time of 10 hours, yielding a front radius of 28 ft from Eq. (6.8). *Messner* and *Williams* obtained a swept pore volume of 101,700 cubic ft or a front radius of 31.8 ft using the pseudosteady state method. The front radius estimate from the deviation time method compares well with the front radius estimate from the pseudosteady state method for this example.

*Sosa et al.* (1981) studied the influence of saturation gradients on pressure falloff data by considering the relative permeability characteristics of the porous medium. Simulated waterflood cases cover a range of mobility ratios from 0.5 to 2. Table 3 of *Sosa et al.* provides estimates of front radii from the deviation time method using $(t_{De})_{end} = 0.389$. The deviation time method is referred to as the "breakpoint" time method by *Sosa et al.* The estimated front radii using $(t_{De})_{end} = 0.4$ will be $\sqrt{0.389/0.4} = 0.99$ times the front radii reported in column 5 of Table 3 in *Sosa et al.* The front radii using $(t_{De})_{end} = 0.4$ also do not estimate the radius of the swept region accurately. The main reason for this is probably the difficulty of obtaining an accurate deviation time for small mobility contrasts.

Example 7 concerns a pressure transient test in a Devonian Shale well after acidization reported by *Olarewaju* and *Lee* (1987) as Ex. 2 in their paper. The well and the buildup data are provided in Table 2 of their paper. They reported $(k/\mu)_1$ of 64.53 md/cp and $(\phi c_t)_1$ of $3.6512 \times 10^{-4}$ per psi. From type-curve matching, they obtained a front radius of 3.9 ft. A semilog graph of pressure vs. time is shown in Fig. 7.2, indicating a deviation time of 0.5 hour. A semilog line on Fig. 7.2 was chosen with a slope of 9.2 psi/cycle to obtain $(k/\mu)_1$ of 64.53 md/cp. Equation (6.8) yields a front radius of 7.6 ft. Thus, the two front radii estimates are quite different. However, since the inner region mobility is 10 times larger than the outer region mobility (*Olarewaju* and *Lee*, 1987), the inner region may behave as a closed system for some time after the end of the semilog line corresponding to the inner region mobility. Figure 7.3 shows a Cartesian graph of pressure as a function of time for Ex. 7. The pseudosteady state behavior of the inner region is apparent as a Cartesian line of slope 11 psi/hour on Fig. 7.3. A Cartesian slope of 11 psi/hour results in a swept pore volume of 1,552.5 cubic ft or a front radius of 8.3 ft. The front radius estimate of 8.3 ft agrees closely with the estimated front radius of 7.6 ft using the deviation time method.

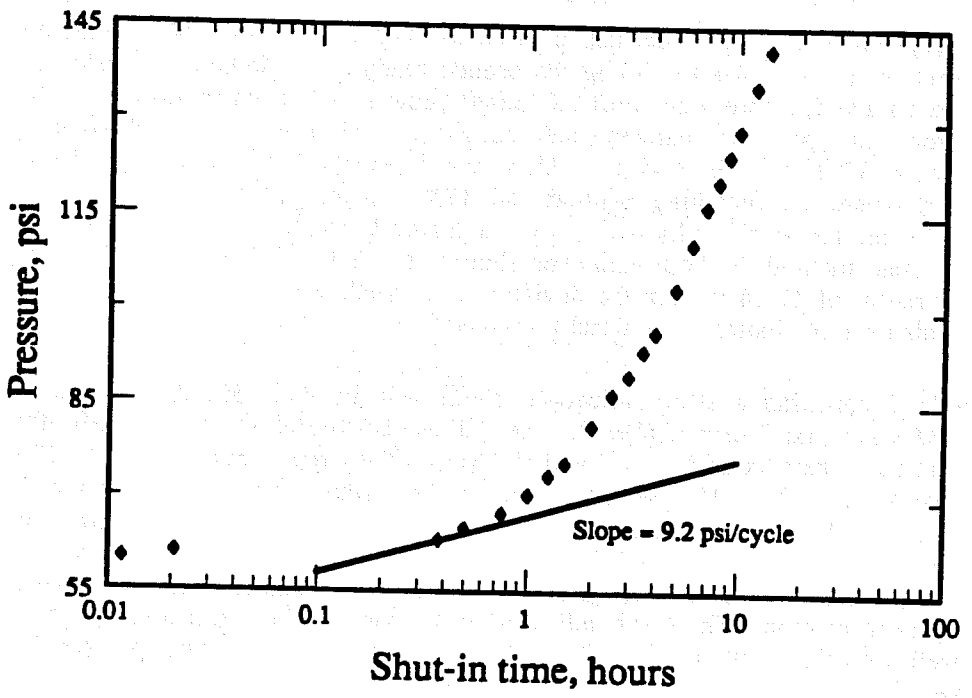


Figure 7.2: Semi-log graph for Example 7.

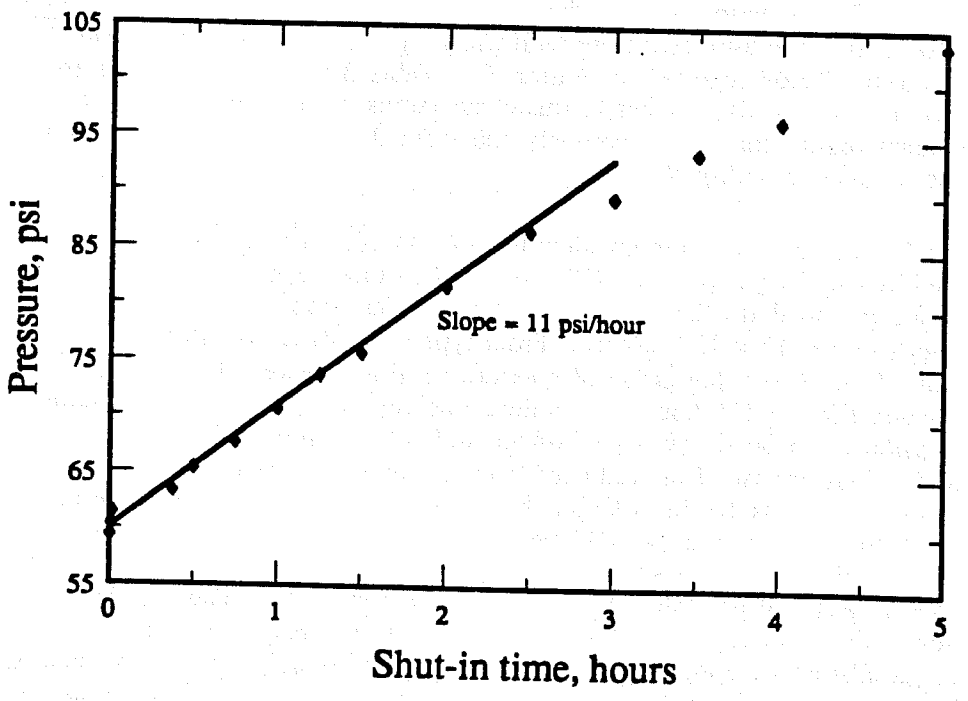


Figure 7.3: Cartesian graph for Example 7.

Example 8 concerns simulated falloff tests without wellbore storage for a liquid-filled two-region reservoir with a moving front reported by *Kazemi et al.* (1972). They reported $(k/\mu)_1$ of 100 md/cp and $(\phi c_t)_1$ of $0.895 \times 10^{-6}$ per psi. A semilog graph of pressure vs. time is shown in Fig. 2 of *Kazemi et al.* (1972), indicating a deviation time of 0.1 hour. Equation (6.8) yields a front radius of 86 ft. *Kazemi et al.* simulated a front radius of 80 ft. Thus, the front radius estimate from the deviation time method compares well with the input value of 80 ft.

Example 9 concerns a field $CO_2$ injection well test in Reservoir 1 well No. 29 reported by *MacAllister* (1987). Pressure falloff data is provided in Table 6 of his paper. He reported $(k/\mu)_1$ of 102.6 md/cp and $(\phi c_t)_1$ of $6.84 \times 10^{-6}$ per psi. Using the pseudosteady state method, he obtained a swept pore volume of 1,820,000 reservoir bbls, or a front radius of 386 ft. A deviation time of 1.5 hours (equivalent to the summation function, defined by Eq. (35) of *MacAllister* (1987), of 2.3) is obtained from Fig. 5 of *MacAllister's* paper. Equation (6.8) yields a front radius of 122 ft. Thus, the front radii estimates are quite different from the pseudosteady state method, and the deviation time method, suggesting gravity override, channeling, and/or viscous fingering effects, assuming that the pseudosteady state method was applied correctly by *MacAllister.*

Example 10 concerns a field $CO_2$ injection well test at a well in West Texas (*Tang* and *Ambastha*, 1988). This well was a water injector for a long time. After having converted the well into a $CO_2$ injector, 31.4 MMSCF $CO_2$ was injected, and the last $CO_2$ injection rate was 1.576 MMSCF/Day. Additional well and reservoir data used in analysis are provided in Table 7.1.

**Table 7.1 - Reservoir and well data for Example 10**

| | |
|---|---|
| Porosity | 0.185 |
| Thickness | 30 ft |
| Oil compressibility | $7 \times 10^{-6}$ psi$^{-1}$ |
| Water compressibility | $3 \times 10^{-6}$ psi$^{-1}$ |
| Formation compressibility | $13 \times 10^{-6}$ psi$^{-1}$ |
| Average $CO_2$ compressibility at 80°F, 1400-1800 psi | $128 \times 10^{-6}$ psi$^{-1}$ |
| $CO_2$ formation volume factor | 0.438 RB/MSCF |
| $CO_2$ viscosity at bottomhole conditions | 0.067 cp |
| Wellbore radius | 0.33 ft |
| Total $CO_2$ injected | 31.4 MMSCF |
| Last $CO_2$ injection rate | 1.576 MMSCF/Day |
| After water injection and before $CO_2$ injection: | |
| Estimated water saturation | 0.75 |
| Estimated oil saturation | 0.25 |

Table 7.2 presents pressure falloff data for this example. Pressure data were recorded using a Hewlett-Packard quartz crystal gauge and thus, pressure data should be accurate. Figure 7.4 presents a log-log graph of pressure drop as a function of shut-in time for the test. Figure 7.4 shows minimal wellbore storage effects because of a lack of a

**Table 7.2 - Pressure falloff data for Example 10**

| Time, minutes | Pressure, psi | Time, minutes | Pressure, psi | Time, minutes | Pressure, psi |
|---|---|---|---|---|---|
| 0. | 1770.46 | 9.80 | 1610.40 | 109.22 | 1509.18 |
| 0.10 | 1751.37 | 10.74 | 1606.25 | 114.22 | 1507.06 |
| 0.20 | 1739.84 | 11.64 | 1602.31 | 119.22 | 1504.64 |
| 0.30 | 1731.12 | 12.69 | 1598.07 | 124.22 | 1502.52 |
| 0.40 | 1724.41 | 13.74 | 1594.11 | 129.22 | 1500.81 |
| 0.50 | 1718.77 | 14.79 | 1590.47 | 134.22 | 1498.99 |
| 0.60 | 1713.91 | 15.84 | 1587.53 | 139.22 | 1496.61 |
| 0.70 | 1709.61 | 16.74 | 1587.52 | 144.22 | 1494.50 |
| 0.80 | 1705.75 | 17.79 | 1586.75 | 154.22 | 1490.62 |
| 0.90 | 1702.21 | 18.84 | 1585.74 | 164.22 | 1488.03 |
| 1.00 | 1699.96 | 19.89 | 1584.37 | 174.22 | 1485.56 |
| 1.10 | 1695.93 | 21.84 | 1581.57 | 184.22 | 1484.06 |
| 1.20 | 1693.12 | 23.79 | 1578.86 | 194.22 | 1482.75 |
| 1.40 | 1687.83 | 25.89 | 1575.93 | 204.22 | 1480.84 |
| 1.50 | 1685.70 | 27.84 | 1573.21 | 214.22 | 1478.91 |
| 1.60 | 1683.49 | 29.94 | 1570.45 | 224.22 | 1476.38 |
| 1.70 | 1681.40 | 31.89 | 1568.10 | 234.22 | 1474.46 |
| 1.80 | 1679.40 | 33.84 | 1565.84 | 244.22 | 1472.03 |
| 1.90 | 1677.51 | 35.84 | 1563.53 | 264.22 | 1468.06 |
| 2.00 | 1675.70 | 37.84 | 1561.24 | 284.22 | 1464.29 |
| 2.10 | 1673.96 | 39.84 | 1559.23 | 304.22 | 1460.57 |
| 2.20 | 1672.28 | 41.84 | 1557.09 | 324.22 | 1456.56 |
| 2.40 | 1669.15 | 43.84 | 1554.83 | 344.22 | 1452.62 |
| 2.60 | 1666.22 | 45.84 | 1552.73 | 364.22 | 1449.28 |
| 2.80 | 1663.47 | 48.14 | 1550.46 | 384.22 | 1445.61 |
| 3.33 | 1657.27 | 49.91 | 1548.72 | 404.22 | 1442.09 |
| 3.80 | 1651.82 | 52.01 | 1546.72 | 424.22 | 1439.01 |
| 4.30 | 1646.03 | 54.11 | 1544.69 | 444.22 | 1436.14 |
| 4.80 | 1642.46 | 58.91 | 1540.28 | 464.22 | 1432.74 |
| 5.30 | 1638.29 | 64.22 | 1535.76 | 484.22 | 1430.03 |
| 5.80 | 1634.38 | 69.22 | 1532.60 | 534.22 | 1424.39 |
| 6.30 | 1630.73 | 74.22 | 1528.82 | 584.22 | 1418.46 |
| 6.80 | 1627.32 | 79.22 | 1525.32 | 634.22 | 1413.32 |
| 7.30 | 1624.11 | 84.22 | 1522.68 | 684.22 | 1411.03 |
| 7.80 | 1621.08 | 89.22 | 1519.74 | 709.22 | 1408.89 |
| 8.30 | 1618.23 | 94.22 | 1516.95 | 734.22 | 1406.94 |
| 8.80 | 1615.50 | 99.22 | 1514.13 | 784.22 | 1402.71 |
| 9.30 | 1612.91 | 105.22 | 1511.24 | 792.22 | 1402.03 |

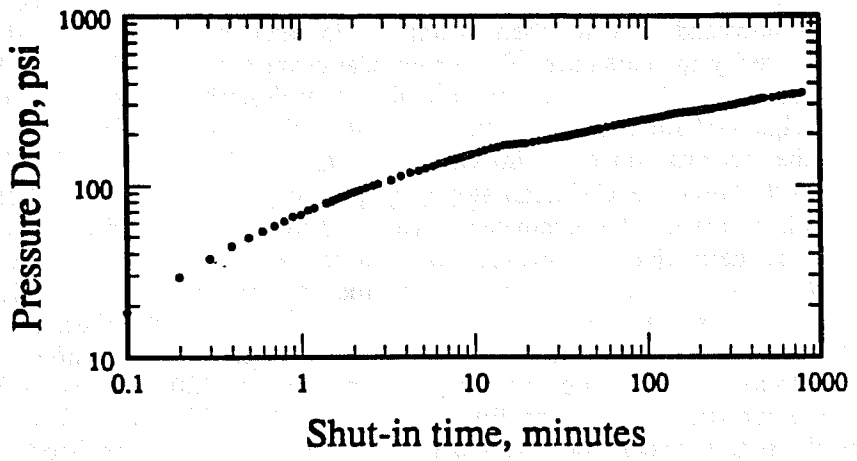


Figure 7.4: Log-log graph for Example 10.

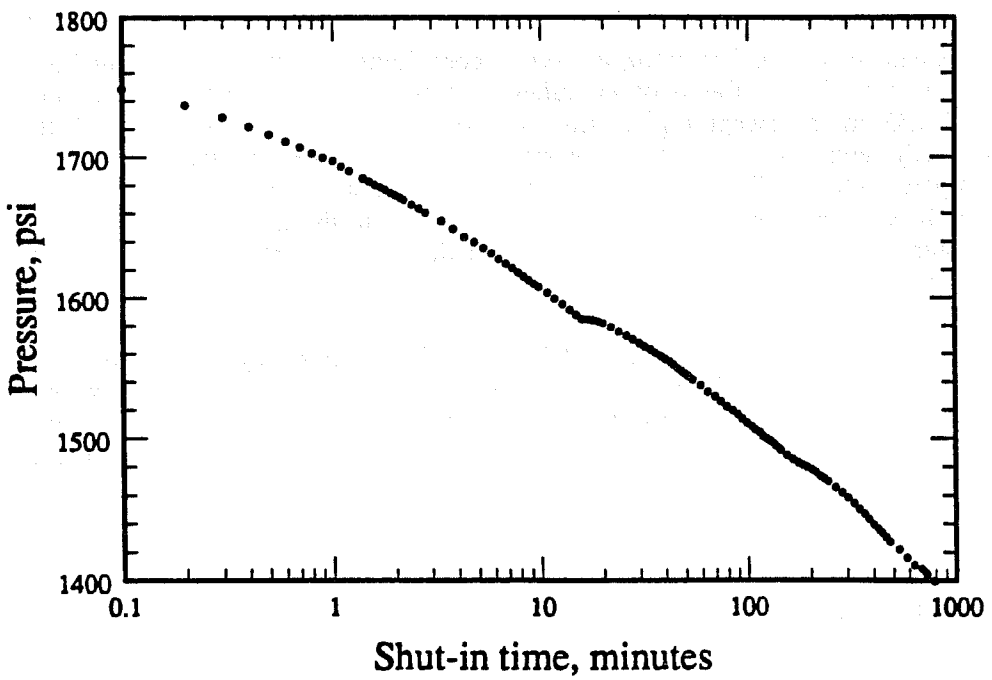


Figure 7.5: Semi-log graph for Example 10.

unit slope line through the initial data points. Figure 7.5 presents a semilog graph of pressure as a function of shut-in time for the test. Figure 7.5 does not exhibit an unambiguous semilog line. Figure 7.6 shows a Cartesian graph of pressure as a function of shut-in time for the test. Figure 7.6 shows a Cartesian line of slope 0.2 psi/min from 200 minutes to about 400 minutes. However, as *Barua* and *Horne* (1987) show for an in-situ combustion falloff test, selecting a correct Cartesian pseudosteady line can be difficult. They used an automated type-curve matching method to locate the correct Cartesian pseudosteady line for their example. For Example 10, semilog slope graphs were used to verify the existence of a correct Cartesian pseudosteady line. The pressure transient data was differentiated using the algorithm described in App. E. Figure 7.7 shows the *Agarwal* slope as a function of shut-in time for $L$ = 0.1, 0.2, and 0.5. To compute the *Agarwal* slope, an injection time, $t_p$, of 31.4/1.576 = 19.9 days was used. Figure 7.8 shows the Cartesian slope, $dp_{ws}/d\,\Delta t$, as a function of shut-in time for $L$ = 0.1, 0.2, and 0.5. The parameter $L$ was used to reduce the effect of noise on calculated pressure derivatives. However, for a large value of $L$, oversmoothing may result (*Bourdet et al.*, 1984), as appears to be the case in Figs. 7.7c and 7.8c. Figure 7.7a indicates the existence of a semilog line corresponding to the inner region mobility from 50 minutes to 150 minutes. The semilog slope decreases after 150 minutes, and then follows a unit slope line from approximately 200 minutes to 360 minutes. Thus, a pseudosteady Cartesian line should exist from 200 minutes to 360 minutes. During the time between 200 and 360 minutes, the existence of pseudosteady state is observed on Fig. 7.8a as a flat Cartesian slope of 0.2 psi/min.

Using a semilog slope of 50 psi/ natural log cycle from Fig. 7.7a, $(k/\mu)_1$ is estimated to be 32.5 md/cp. Assuming a zero residual oil saturation after $CO_2$ injection and a $CO_2$ saturation, $S_g$, of 0.35 in the swept inner region, the total compressibility in the swept inner region is:

$$c_t = c_f + S_w c_w + S_g c_g = (13 + 0.65 \times 3 + 0.35 \times 128) \times 10^{-6} = 59.75 \times 10^{-6}\ \text{psi}^{-1} \quad (7.1)$$

Using a Cartesian slope of 0.2 psi/min, the swept pore volume is 40,114 reservoir bbls or a front radius of 114 ft. Based on cumulative volume of $CO_2$ injected and a $CO_2$ saturation of 0.35 in the swept region, the front radius is estimated to be 112.5 ft. Thus, front radii estimates from the material balance, and the pseudosteady state method compare well. If $CO_2$ saturation in the swept inner region is different from 0.35, there will be a discrepancy in front radii estimates from the material balance, and the pseudosteady state method. Using a deviation time of 150 minutes in Eq. (6.7) yields a front radius of 104 ft.

A decrease in semilog slope on Fig. 7.7a after 150 minutes may be explained as either a short injection time effect for a falloff test in a two-region reservoir, or the effect of an intermediate region with a larger storativity than the inner region storativity for a three-region reservoir. For an injection time, $t_p$, of 31.4/1.576 = 19.9 days, and a front radius, $R$, of 114 ft, the parameter, $t_{pD}/R_D^2$, is:

$$\frac{t_{pD}}{R_D^2} = \frac{0.0002637\ k_1\ t}{(\phi\mu c_t)_1\ R^2} = \frac{0.0002637 \times 32.5 \times (19.9 \times 24)}{(0.185)\ (59.75 \times 10^{-6})\ (114)^2} = 28.5 \quad . \quad (7.2)$$

From a water injection falloff test prior to $CO_2$ injection, $k/\mu$ of 15.2 md/cp was calculated (*Tang* and *Ambastha*, 1988). This $k/\mu$ of 15.2 md/cp was assumed to be

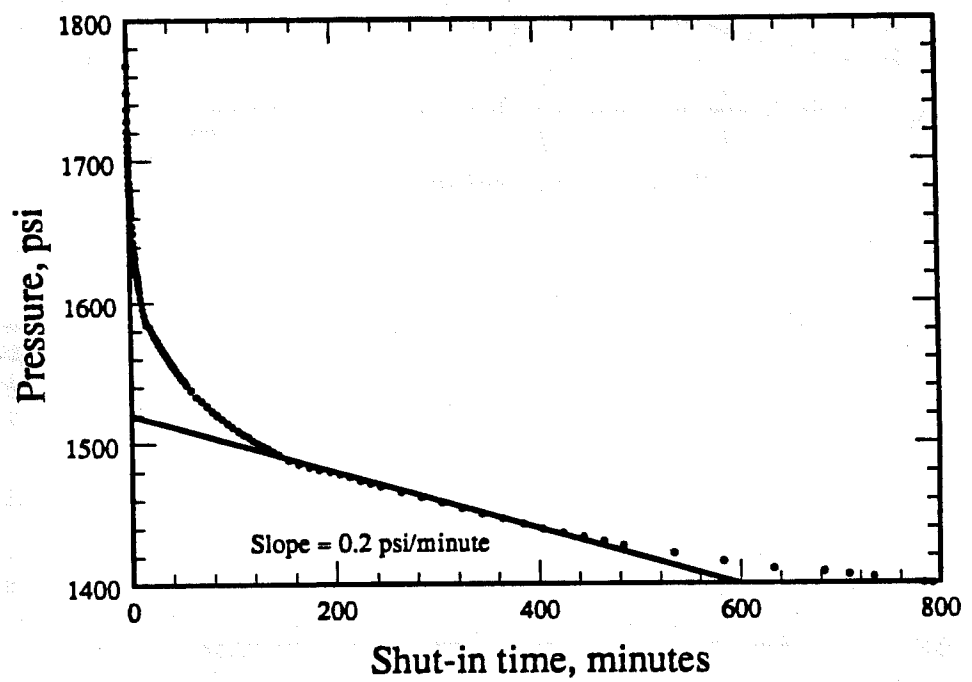


Figure 7.6: Cartesian graph for Example 10.

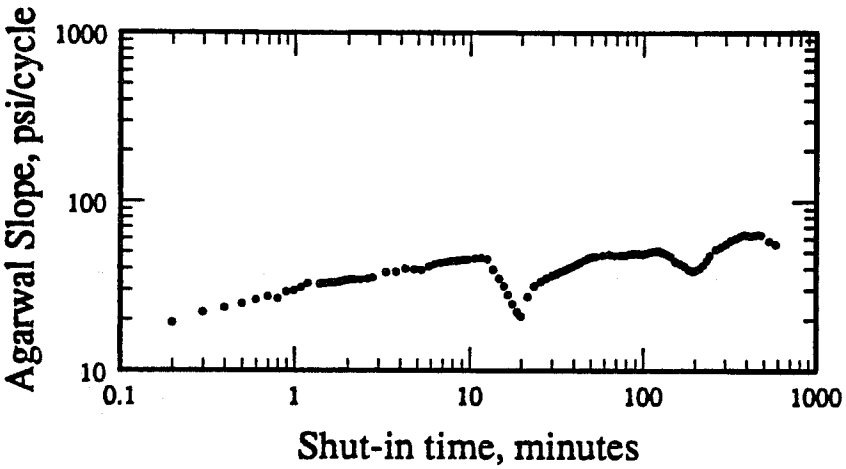


Figure 7.7a: $L = 0.1$

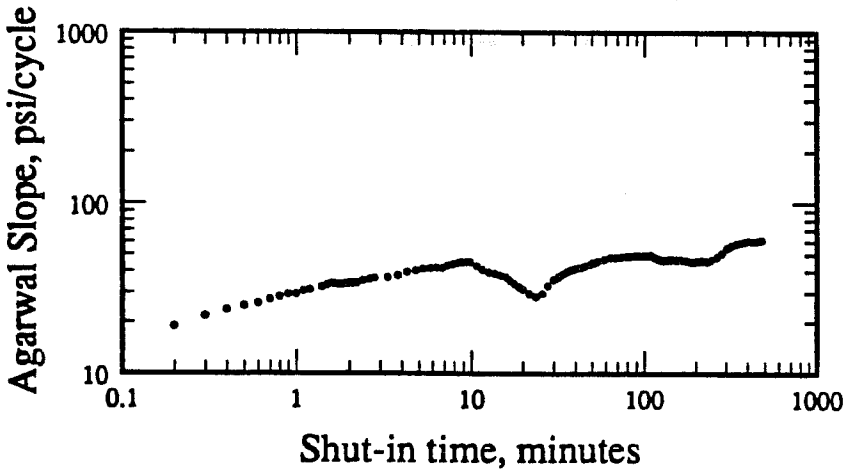


Figure 7.7b: $L = 0.2$

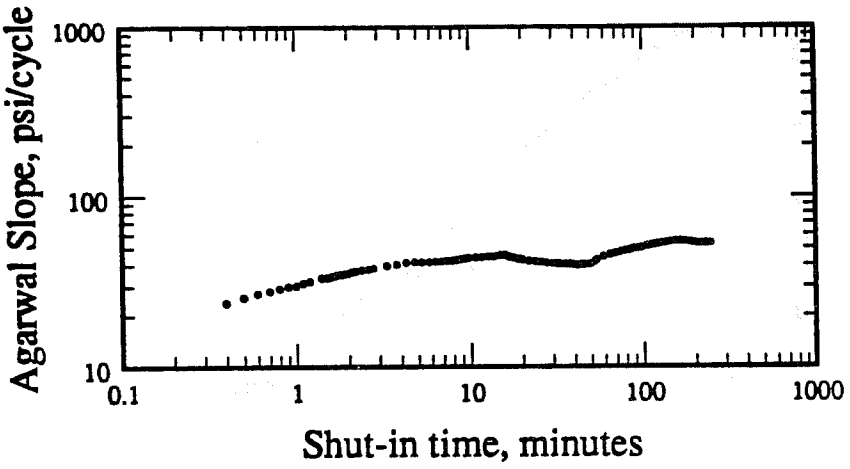


Figure 7.7c: $L = 0.5$

Figure 7.7: Agarwal slope graph for Example 10 (a. $L = 0.1$, b. $L = 0.2$, and c. $L = 0.5$).

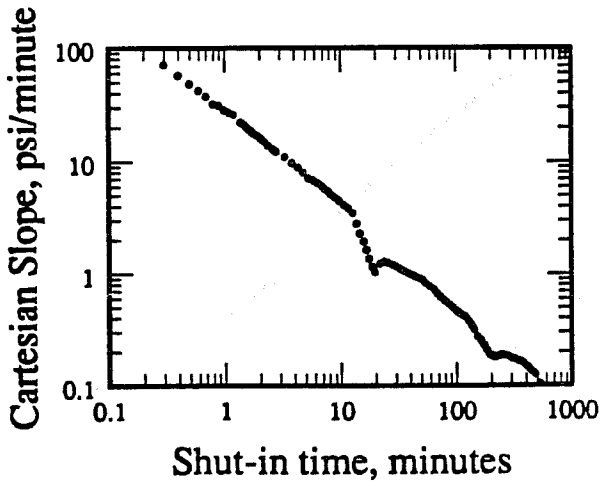


Figure 7.8a: $L = 0.1$

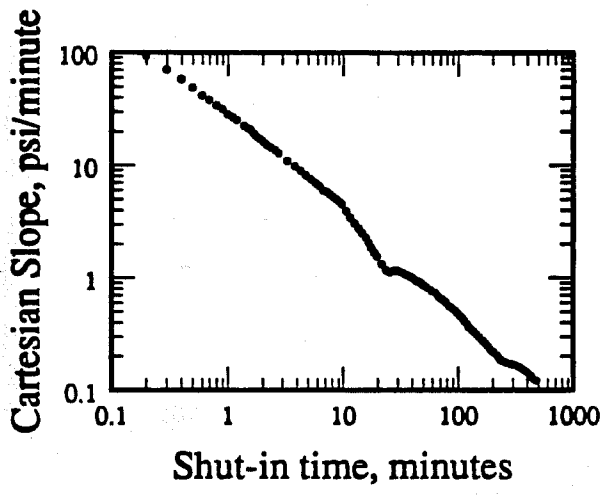


Figure 7.8b: $L = 0.2$

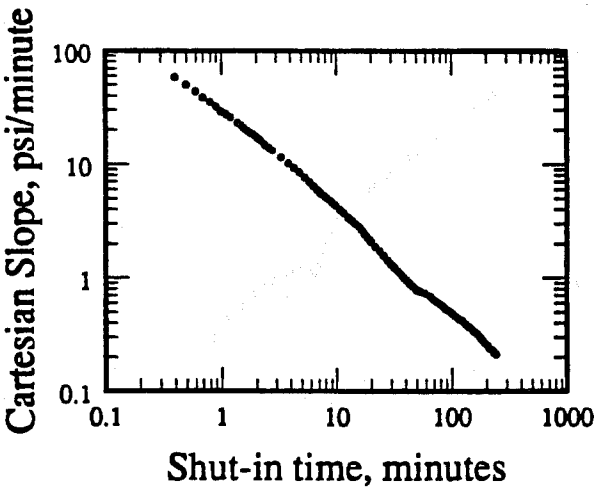


Figure 7.8c: $L = 0.5$

Figure 7.8: Cartesian slope graph for Example 10 (a. $L = 0.1$, b. $L = 0.2$, and c. $L = 0.5$).

$(k/\mu)_2$ for a two-region, composite reservoir configuration resulting after $CO_2$ injection. Thus, $M$ = 32.5/15.2 = 2.14. Since water injection continued for a long time before $CO_2$ injection in this well, an approximation for the total compressibility in the unswept region after $CO_2$ injection is:

$$c_t = c_f + S_w c_w + S_o c_o = (13 + 0.65 \times 3 + 0.35 \times 7) \times 10^{-6} = 17.4 \times 10^{-6} \text{ psi}^{-1} \quad . \quad (7.3)$$

Thus, for a two-region composite reservoir configuration resulting after $CO_2$ injection, $F_S$ = 59.75/17.4 = 3.4. For $M$ = 2.14, and $F_S$ = 3.4, the *Agarwal* falloff pressure derivative is within 4% of a drawdown pressure derivative, if $t_{pD}/R_D^2 \geq 10$, and does not exhibit a decrease in semilog slope after the end of infinite-acting radial flow corresponding to the inner region mobility. Thus, a decrease in semilog slope on Fig. 7.7a may be due to the effect of an intermediate region with a larger storativity than the inner region storativity for a three-region reservoir. However, if a three-region reservoir model is appropriate, then $M_{13}$ = 2.14, $F_{S13}$ = 3.4, and $F_{S12} < 1$ probably can not explain the development of a pseudosteady state Cartesian line corresponding to the volume of $R_2$ unless $F_{S12}$ is quite small. Figures 7.9 through 7.11 show the effect of $F_{S12}$ on semilog slope, Cartesian slope, and effective Cartesian slope. Figures 7.9 through 7.11 are for $R_{D2}$ = 114/0.33 = 345.5, assuming that pseudosteady state develops corresponding to a swept volume of $R_2$. Assuming a 10 ft radial extent of the intermediate region, $R_{D1}$ = 104/0.33 = 315.15 was used to generate the responses. Also, the deviation time method yields a front radius of 104 ft corresponding to $R_1$. Figures 7.9 through 7.11 use $M_{12}$ = 1. Figure 7.9 shows that the deviation time method should yield a front radius corresponding to $R_1$ as the dimensionless deviation time is 0.18 for all values of $F_{S12}$. The semilog slope decreases after the end of infinite-acting radial flow corresponding to the inner region mobility for $F_{S12}$ = 0.1 and 0.01. As the outer region effects are felt, the semilog slope starts to increase, and at late time, the semilog slope becomes $M_{13}/2$ after exhibiting a maximum semilog slope. The transition time between the minimum and the maximum semilog slopes is about 1 log cycle for $F_{S12}$ = 0.1, and about 2 log cycles for $F_{S12}$ = 0.01.

Figure 7.10 shows that the Cartesian slope shows an approximately constant value for a short time for $F_{S12}$ = 0.01 only. The effective Cartesian slope graph of Fig. 7.11 shows that for $F_{S12}$ = 0.01, an effective Cartesian slope of approximately constant value slightly less than $2\pi$ develops for a short time. Thus, using an effective total compressibility, a slightly overestimated value for the swept volume of $R_2$ may be obtained, if $F_{S12}$ is of the order of 0.01. If $F_{S12}$ is of the order of 0.01, then a much larger effective compressibility than $c_t$ given by Eq. (7.1) should be used for the pseudosteady state method, resulting in a smaller swept pore volume, and a smaller front radius than 114 ft obtained using $c_t$ given by Eq. (7.1). A smaller front radius than 114 ft would not be compatible with the material balance estimate for front radius. Also, Fig. 7.7a shows a much smaller transition time between the minimum and the maximum semilog slopes than the transition time on Fig. 7.9 for $F_{S12}$ = 0.01. Therefore, it appears that for this example, a decrease in semilog slope after the end of infinite-acting radial flow corresponding to the inner region mobility may be due to $L$ = 0.1 used in the differentiation algorithm, and is not due to three-region reservoir behavior. However, the applicability of a three-region reservoir model for $CO_2$ injection well tests should be addressed in future research projects through an analysis of simulated $CO_2$ falloff tests.

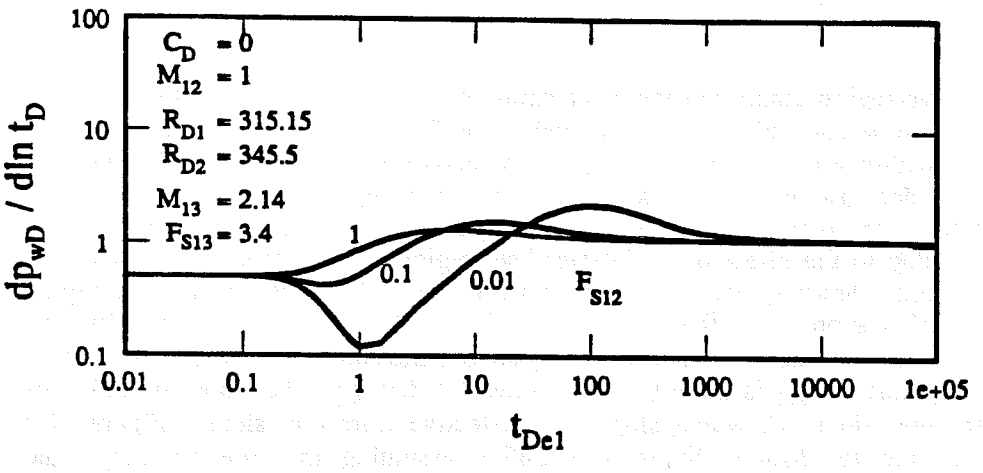


Figure 7.9: Effect of $F_{S12}$ on semi-log slope for an infinitely-large three-region reservoir with $C_D = 0$, $M_{12} = 1$, $M_{13} = 2.14$, $R_{D1} = 315.15$, $R_{D2} = 345.5$, and $F_{S13} = 3.4$.

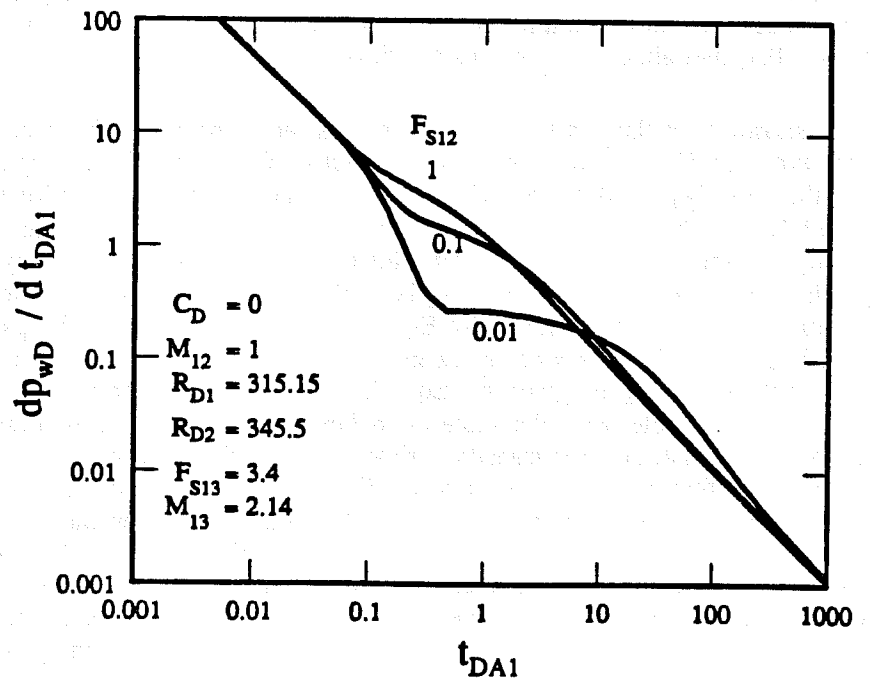


Figure 7.10: Effect of $F_{S12}$ on Cartesian slope for an infinitely-large three-region reservoir with $C_D = 0$, $M_{12} = 1$, $M_{13} = 2.14$, $R_{D1} = 315.15$, $R_{D2} = 345.5$, and $F_{S13} = 3.4$.

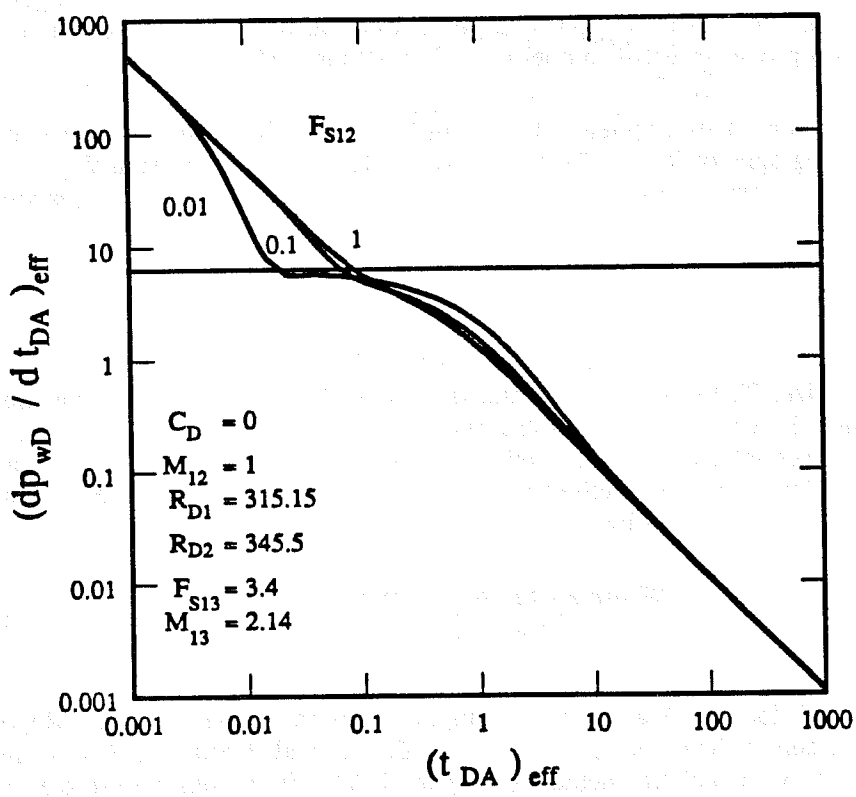


Figure 7.11: Effect of $F_{S12}$ on effective Cartesian slope for an infinitely-large three-region reservoir with $C_D = 0$, $M_{12} = 1$, $M_{13} = 2.14$, $R_{D1} = 315.15$, $R_{D2} = 345.5$, and $F_{S13} = 3.4$.

Figure 7.7b indicates the existence of a semilog line corresponding to the inner region mobility from 50 minutes to 230 minutes, with a slope of 52 psi/ natural log cycle resulting in a $(k/\mu)_1$ of 31.24 md/cp. The semilog slope on Fig. 7.7b follows a unit slope line after 230 minutes to about 360 minutes. Figure 7.8b shows a Cartesian slope of 0.2 psi/min from 230 minutes to 360 minutes, yielding a swept pore volume of 40,114 reservoir bbls, or a front radius of 114 ft. Using a deviation time of 230 minutes in Eq. (6.7) yields a front radius of 126 ft. Thus, the results for $(k/\mu)_1$ and swept pore volume from slope graphs of Fig. 7.7a and 7.7b are comparable. However, Fig. 7.7b suggests a two-region reservoir model with a skin at the discontinuity for this well test, as $M = 2.14$ and $F_S = 3.4$ are too small to produce a pseudosteady state Cartesian line if $s_f = 0$ (see Fig. 6.10). The difference in conceptual models for this well test resulted because of the values of $L$ used in the differentiation algorithm. The parameter $L$ in differentiation algorithm may also cause confusion in the identification of a proper reservoir model in other well-test scenarios.

Selecting a correct pseudosteady Cartesian line is facilitated by a unit slope line on semilog slope graphs of Figs. 7.7a and b for Ex. 10. If only Cartesian slope graphs of Figs. 7.8a and b were available, selecting a correct pseudosteady line corresponding to the swept volume would have been difficult.

## 7.2 SUMMARY

To summarize, Table 7.3 presents the input data for the deviation time method for all examples. Examples 10a and 10b refer to the results for Example 10 with $L$ = 0.1 and 0.2, respectively, in the differentiation algorithm. Table 7.4 presents analysis results from the deviation time method in the column labelled "estimated $R$". Percent difference in Table 7.4 is given by:

$$\% \text{ difference} = \frac{(\text{Estimated } R - \text{Reported } R)}{\text{Reported } R} \times 100 \tag{7.4}$$

"Reported $R$" for Exs. 1 and 8 are the input values in simulated tests. "Reported $R$" for Exs. 4 and 5 have been obtained by *Barua* and *Horne* (1987) using an automated type-curve matching method. "Reported $R$" for all other examples were obtained using the pseudosteady state method. A significantly smaller front radius estimate from the deviation time method than the front radius estimate from an automated type-curve matching method or the pseudosteady state method suggests gravity override, channeling, and/or viscous fingering effects. A large positive percent difference for Exs. 3 and 9 in Table 7.4 suggests gravity, channeling, and/or viscous fingering effects. A large positive percent difference for Ex. 1 may be explained by the difference between the burning front radius and the front radius corresponding to a sharp mobility change.

An alternative indicator for recognizing gravity override, channeling, and/or viscous fingering effects from the pressure transient data is:

$$G = \left[\frac{R_{pss}}{R_{dev}}\right]^2 , \tag{7.5}$$

**Table 7.3 - Input data for the deviation time method**

| Example Number | $(k/\mu)_1$, md/cp | $(\phi c_t)_1$, $10^4$ psi$^{-1}$ | $t_{end}$ hours |
|---|---|---|---|
| 1 | 21251 | 3.3915 | 0.0694 |
| 2 | 5685.5 | 35.343 | 0.1667 |
| 3 | 4907.5 | 1.0262 | 0.5 |
| 4 | 12647 | 1.19 | 0.3 |
| 5 | 28839 | 6.258 | 1 |
| 6 | 11200 | 940.8 | 10 |
| 7 | 64.5 | 3.651 | 0.5 |
| 8 | 100 | 0.895 | 0.1 |
| 9 | 102.6 | 0.0684 | 1.5 |
| 10a | 32.5 | 0.5975 | 2.5 |
| 10b | 31.24 | 0.5975 | 3.83 |

**Table 7.4 - Analysis results from the deviation time method**

| Example Number | Reported $R$, ft | Estimated $R$, ft | % difference |
|---|---|---|---|
| 1 | 84.5 | 53.6 | -36.6 |
| 2 | 12.8 | 13.3 | 3.9 |
| 3 | 166 | 126 | -24.1 |
| 4 | 144 | 144.8 | 0.55 |
| 5 | 173.7 | 174.4 | 0.004 |
| 6 | 31.8 | 28 | -11.9 |
| 7 | 8.3 | 7.6 | -8.4 |
| 8 | 80 | 86 | 7.5 |
| 9 | 386 | 122 | -68.4 |
| 10a | 114 | 104 | -8.8 |
| 10b | 114 | 126 | 10.5 |

if the pressure transient data is analyzed using the pseudosteady state and the deviation time methods. The pseudosteady state method yields a front radius estimate, $R_{pss}$. The deviation time method yields a front radius estimate, $R_{dev}$. Thus, $G$ is a geometric factor proportional to the ratio of the swept volume estimates from the pseudosteady state and the deviation time methods. An expression for $G$ in terms of the parameters obtained from semilog and Cartesian graphs of the pressure transient data is:

$$G = \frac{m_s\ (t_{De})_{end}}{0.024\ m_c\ t_{end}}\ , \tag{7.6}$$

where $m_s$ is the slope of the semilog graph of pressure vs. time in psi/cycle, $m_c$ is the slope of a Cartesian graph of pressure vs. time in psi/day, and $t_{end}$ is the real deviation time in hours. If a pressure derivative graph is used to obtain the real deviation time, $(t_{De})_{end} = 0.18$ should be used in Eq. (7.6). If a semilog graph of pressure vs. time is used to obtain the real deviation time, $(t_{De})_{end} = 0.4$ should be used in Eq. (7.6).

A value of $G$ larger than unity suggests gravity override, channeling, and/or viscous fingering effects. Table 7.5 presents the calculated $G$ values for all examples, except Ex. 8, because Ex. 8 was not analyzed using the pseudosteady state method. The Cartesian line slope for Ex. 4 is the slope obtained by *Barua* and *Horne* (1987) using an automated type-curve matching method. For Ex. 9, slopes $m_s$ and $m_c$ are in psi$^2$-cp/cycle and psi$^2$-cp/day, respectively. Examples 3 and 9 suggest significant gravity override, channeling, and/or viscous fingering effects. A large value of $G$ for Ex. 1 may be explained by the difference between the burning front radius and the front radius corresponding to a sharp mobility change.

**Table 7.5 - Calculation of G Values**

| Example Number | $m_s$, psi/cycle | $m_c$, psi/day | $t_{end}$, hours | $(t_{De})_{end}$, Dimensionless | $G$, Dimensionless |
|---|---|---|---|---|---|
| 1 | 0.16 | 15.05 | 0.0694 | 0.4 | 2.553 |
| 2 | 4.65 | 504 | 0.1667 | 0.4 | 0.922 |
| 3 | 6 | 114.8 | 0.5 | 0.4 | 1.742 |
| 4 | 5.5 | 309.6 | 0.3 | 0.4 | 0.99 |
| 5 | 0.8 | 13.75 | 1 | 0.4 | 0.97 |
| 6 | 7.05 | 9.12 | 10 | 0.4 | 1.29 |
| 7 | 9.2 | 264 | 0.5 | 0.4 | 1.16 |
| 9 | $3.83 \times 10^6$ | $41.28 \times 10^5$ | 1.5 | 0.4 | 10.3 |
| 10a | 115.15 | 288 | 2.5 | 0.18 | 1.2 |
| 10b | 119.8 | 288 | 3.83 | 0.18 | 0.81 |

# 8. SUMMARY OF RESULTS

Radial composite reservoir models have been used to analyze well-tests from a variety of enhanced oil recovery projects, geothermal reservoirs, and acidization projects for a number of years. However, transient pressure responses for a well in a composite reservoir have not been well understood. This study presents transient pressure derivative responses for a well in a variety of two- and three- region composite reservoir situations. Both drawdown and buildup responses have been considered. This study presents new correlating parameters, and design equations for composite reservoirs. The applicability and the limitations of different methods proposed in the literature to estimate a front radius, or swept volume have been discussed. Guidelines are provided for sufficient test data collection to ensure reliable type-curve matching. Non-uniqueness problems in type-curve matching well-test data from composite reservoirs have been studied.

An analytical solution for the pressure transient response for a well in a two-region composite reservoir with a thin skin at the discontinuity was developed. Such a model may be a practical approach to model well-tests from enhanced oil recovery projects such as steam injection, in-situ combustion, and $CO_2$ flooding, and possibly geothermal reservoirs. This study shows that neglecting a thin skin at the discontinuity may cause significant errors in parameter estimation. Also, a thin skin at the discontinuity increases the likelihood of observing a short duration pseudosteady state behavior corresponding to the swept volume.

New drawdown and buildup derivative type-curves for a well with storage and skin, and located in the center of a finite, homogeneous reservoir have been presented. Design equations for the time to the beginning and the end of the semi-log straight line have been developed. The drawdown and the buildup responses for a well in a closed reservoir were compared with the responses for a well in a reservoir with a constant-pressure outer boundary. Producing time effects and outer boundary condition should be considered for a proper type-curve matching analysis of buildup derivative data obtained from a well in a finite, homogeneous reservoir.

# 9. CONCLUSIONS AND RECOMMENDATIONS

This study considers transient pressure derivative responses for a well in either a homogeneous, a two-region, or a three-region reservoir. Correlating parameters identified for transient pressure derivative responses in several situations are summarized in the following:

1. The correlating parameters for drawdown response for a well in a finite, homogeneous reservoir are $C_D e^{2s}$ and $r_{eD}^2/C_D$. A drawdown type-curve is presented in Fig. 5.2.
2. The parameters, $C_D e^{2s}$ and $r_{eD}^2/C_D$, describe buildup response after long producing times for a well in a finite, homogeneous reservoir with a constant-pressure or a closed outer boundary. A buildup pressure derivative type-curve for a well in the center of a circular, homogeneous reservoir with a constant-pressure outer boundary is presented in Fig. 5.4. A buildup pressure derivative type-curve for a closed outer boundary has been presented previously by *Mishra* and *Ramey* (1987). For buildup response after short producing time, the parameter $t_{pDA}$ is the third parameter. The *Agarwal* slope does not correlate buildup responses for a well in a finite, homogeneous reservoir for all producing times.
3. The parameters, mobility ratio ($M$) and storativity ratio ($F_S$), describe drawdown response for a well in an infinitely large, two-region composite reservoir in the absence of wellbore storage, and with no skin at the discontinuity. A drawdown type-curve is presented in Fig. 6.4.
4. The correlating parameters for drawdown response for a well in a finite, two-region composite reservoir in the absence of wellbore storage and with no skin at the discontinuity are $M$, $F_S$, and $r_{eD}/R_D$. The parameter $r_{eD}/R_D$ is applicable for both a closed, or a constant-pressure outer boundary.
5. The drawdown pressure derivative response or buildup response after long producing time for a well in an infinitely large, two-region composite reservoir with a skin at the discontinuity is described by the parameters - $C_D e^{2s}$, $R_D^2/C_D$, $M$, $F_S$, and $s_f$. For a finite outer boundary, $r_{eD}/R_D$ is an additional parameter. For buildup after short producing time, $t_{pD}/R_D^2$ is an additional parameter.
6. The drawdown pressure derivative response for a well in an infinitely large, three-region composite reservoir is described by the parameters, $M_{12}$, $M_{13}$, $F_{S12}$, $F_{S13}$, and $R_2/R_1$, in the absence of wellbore storage and skin.

## 9.1 CONCLUSIONS

Based on this work and the publications resulting from this study (*Ambastha* and *Ramey*, 1987, 1988 a and b; *Tang* and *Ambastha*, 1988), the following is concluded regarding different methods proposed in the literature to estimate swept volume, or a front radius:

### Deviation Time Method

1. Ten well tests reported in the literature exhibiting composite reservoir behavior have been analyzed using the deviation time method. These well tests cover simulated and field test data from in-situ combustion, steam injection, $CO_2$ flooding, water flooding, and acidizing projects.

2. The limitations on the deviation time method due to wellbore storage effects have been quantified. Wellbore storage effects should be minimized in a composite reservoir well test to observe a semi-log line corresponding to the inner region mobility.
3. The estimate of discontinuity radius from the deviation time method is sensitive to the real and the dimensionless deviation times used. Thus, the identification of a proper semi-log line, and an accurate deviation time that corresponds to the accuracy for $(t_{De})_{end}$ are important considerations in the application of the deviation time method. A pressure derivative graph may be useful in identifying a proper semi-log line, and in obtaining an accurate deviation time.
4. If a semi-log graph of pressure as a function of time is being analyzed, $(t_{De})_{end} = 0.4$ is appropriate. If a graph of semi-log pressure derivative as a function of time is being analyzed, $(t_{De})_{end} = 0.18$ is appropriate. The use of $(t_{De})_{end} = 0.18$ or 0.4, depending on how deviation time is obtained, maintains the consistency between real data and the system response in dimensionless terms.
5. The estimated discontinuity radius from the deviation time method may represent a lower bound for discontinuity radius, if the swept inner region is not cylindrical. A comparison of the estimates of discontinuity radii from the deviation time and other methods may provide information about gravity override and viscous fingering effects.
6. The deviation time method results in an estimate for inner region radius for a three-region composite reservoir. But the deviation time method may yield a meaningless front radius if the effects of mobility and storativity contrasts between the inner and the intermediate region produce an apparently longer semi-log line corresponding to the inner region mobility.
7. Obtaining an accurate deviation time for small mobility contrasts may be difficult.

## Intersection Time Method

1. The intersection time method is not suitable for composite reservoir well test analysis for three reasons. Either, a well test will not be run long enough in most cases to see a second semi-log line, or outer boundary effects will mask the second semi-log line. This conclusion is in agreement with qualitative observations of previous investigators. Also, wellbore storage may mask the first semi-log line rendering the intersection time method inapplicable.

## Pseudosteady State Method

1. Correlations have been developed for the time to the end of pseudosteady state behavior corresponding to the swept inner region for large mobility and storativity ratio cases, and with or without a thin skin at the discontinuity. These correlations should be of help in choosing a correct pseudosteady Cartesian line. If a pseudosteady Cartesian line develops, the pseudosteady state method should yield a correct swept volume and "average" front radius for irregular swept region shapes.
2. The effect of a thin skin at the discontinuity is similar to the effect of storativity ratio on the pressure transient response. The pseudosteady state behavior corresponding to the volume of the inner region may be observed even for moderate values of skin at the discontinuity.

3. The presence of a thin skin at the discontinuity can explain the development of pseudosteady state corresponding to the swept volume for small mobility and storativity contrasts.
4. A falloff test after short injection time may produce an apparent Cartesian slope which remains approximately constant for a short duration. Such a Cartesian slope may not be related to pseudosteady state corresponding to the swept volume.
5. For a three-region composite reservoir, the pseudosteady state method results in a swept volume for the intermediate region radius, $R_2$, if an effective total compressibility corresponding to the inner and the intermediate regions is used to analyze the pseudosteady state data. However, at times, the development of an apparent pseudosteady state may yield an overestimated value for the volume corresponding to $R_2$. The development of an apparent pseudosteady state may be ascertained by computing $(t_{DA})_{eff}$ corresponding to the time to start of an approximately constant Cartesian slope.

### Type-Curve Matching

1. Conditions have been established for the applicability of a derivative type-curve matching method. Guidelines have been provided for sufficient test data collection to ensure reliable type-curve matching.
2. A relation for $t_{pD}/R_D^2$ required for a maximum *Agarwal* slope to be within 5% of the maximum drawdown semi-log pressure derivative has been developed. This relation should be helpful in well-test design and interpretation to estimate whether $t_{pD}/R_D^2$ is large enough for well-test data to be type-curve matched on a drawdown type-curve such as Fig. 6.4.
3. Non-uniqueness problems in type-curve matching well-test data from a composite reservoir have been studied. Knowledge of the expected range of parameter values may assist in making reasonable estimates of the parameters by type-curve matching.

## 9.2 RECOMMENDATIONS

Future studies in composite reservoir well testing should address:

1. Analysis of simulated $CO_2$ falloff tests, and
2. Analysis of simulated steam injection falloff tests.

Such simulation studies should be performed using one-dimensional radial model to investigate the effects of a thin skin at the discontinuity, and to develop correlations for effective properties to be used in well-test analysis. Simulation studies using two- and three-dimensional models should be performed to investigate the effects of gravity override/ underride, viscous fingering, and channeling on well-test data.

## NOMENCLATURE

$A$ = Area, $\pi R^2$ or $\pi r_e^2$
$B$ = Formation volume factor, bbl/STB
$c_t$ = Total system compressibility, psi $^{-1}$
$C$ = Wellbore storage coefficient, bbl/psi
$C_A$ = Shape factor
$C_j$ = Arbitrary constants
$Ei$ = Exponential Integral
$F_S$ = Storativity ratio for a two-region reservoir, $(\phi\ c_t\ )_1/(\phi\ c_t\ )_2$
$F_{S12}$ = Storativity ratio between regions 1 and 2 for a three-region reservoir, $(\phi\ c_t\ )_1/(\phi\ c_t\ )_2$
$F_{S13}$ = Storativity ratio between regions 1 and 3 for a three-region reservoir, $(\phi\ c_t\ )_1/(\phi\ c_t\ )_3$
$G$ = Geometric factor defined by Eq. (7.5)
$h$ = Formation thickness, ft
$I_j$ = Modified Bessel function of first kind of order $j$
$k$ = Permeability, md
$K_j$ = Modified Bessel function of second kind of order $j$
$l$ = Laplace parameter
$L$ = Parameter for the differentiation algorithm of App. E
$L^{-1}$ = Inverse Laplace transform
$m_c$ = Cartesian line slope, psi/day
$m_s$ = Semi-log line slope, psi/cycle
$M$ = Mobility ratio for a two-region reservoir, $(k\ /\ \mu\ )_1/(k\ /\ \mu\ )_2$
$M_{12}$ = Mobility ratio between regions 1 and 2 for a three-region reservoir, $(k\ /\ \mu\ )_1/(k\ /\ \mu\ )_2$
$M_{13}$ = Mobility ratio between regions 1 and 3 for a three-region reservoir, $(k\ /\ \mu\ )_1/(k\ /\ \mu\ )_3$
$p$ = Pressure, psi
$p_D$ = Dimensionless pressure drop
$\bar{p}$ = Average reservoir pressure, psi
$\bar{p}_D$ = Dimensionless pressure drop in Laplace space
$q$ = Flow rate, STB/Day
$r$ = Radius, ft
$R$ = Discontinuity radius for a two-region reservoir, ft
$R_{D1}$ = Dimensionless discontinuity radius for region 1 for a three-region reservoir, $R_1/r_w$
$R_{D2}$ = Dimensionless discontinuity radius for region 2 for a three-region reservoir, $R_2/r_w$
$s$ = Skin effect at the wellbore, $k_1 h\ (\Delta p)_{skin}\ /\ 141.2\ qB\ \mu_1$
$s_f$ = Skin effect at the front (or discontinuity)
$S_{or}$ = Residual oil saturation, fraction
$t$ = Time, hour
$t_{DA}$ = Dimensionless time based on area $A$, $0.000264(k\ /\ \phi\ \mu\ c_t)_1 t/A$
$t_{De}$ = Dimensionless time based on $R$, $0.000264(k\ /\ \phi\ \mu\ c_t)_1 t/R^2$
$(t_{De})_{end}$ = Dimensionless deviation time, $0.000264(k\ /\ \phi\ \mu\ c_t)_1 t_{end}/R^2$
$(t_{De})_{II}$ = Dimensionless time of the start of second semi-log line
$(t_{De})_{\max}$ = Dimensionless time for maximum semi-log slope
$(t_{De})_{depart}$ = Dimensionless time for slope response to deviate from infinitely large composite reservoir behavior
$t_{end}$ = Deviation time, hours
$V_s$ = Swept volume, ft$^3$

## Greek Symbols

$\alpha$ = Tolerance in Eq. (5.11), fraction
$\alpha_{ij}$ = Coefficients in Eqs. (4.27) through (4.30)
$\beta$ = Parameter in Eq. (B.11)
$\partial$ = Partial
$\Delta p_s$ = Pressure drop across skin, psi
$\Delta p_{s_f}$ = Pressure drop across skin at the discontinuity, psi
$\Delta t$ = Shut-in time, hours
$\eta$ = Diffusivity ratio, $(k / \phi \mu c_t)_1/(k / \phi \mu c_t)_2$
$\mu$ = Viscosity, cp
$\phi$ = Porosity, fraction
$\chi$ = Parameter defined by Eq. (6.31)

## Subscripts

$a$ = Time point $a$ in App. E
$b$ = Time point $b$ in App. E
$c$ = Cartesian
$D$ = Dimensionless
$e$ = Exterior or equivalent
$eff$ = Effective
$f$ = Front or flowing
$i$ = Initial, or time point $i$ in App. E
$p$ = Producing (or injection)
$pss$ = Pseudosteady state
$s$ = Swept or shut-in
$ss$ = Steady state
$t$ = Total
$X$ = Intersection
$w$ = Wellbore
1 = Inner region
2 = Outer region for a two-region composite reservoir or intermediate region for a three-region composite reservoir
3 = Outer region for a three-region composite reservoir

## REFERENCES


1. Aarstad, K: "*Criteria for Determining Times for End of Transient Flow and Start of Pseudosteady State Flow*," Engineer Thesis, Stanford University, Stanford, CA (Aug. 1987) 162 pp.

2. Abbaszadeh-Dehghani, M. and Kamal, M.M.: "Pressure Transient Testing of Water Injection Wells," paper SPE 16744 presented at the Annual Mtg. of SPE of AIME in Dallas, TX (Sept. 27-30, 1987).

3. Abramowitz, M. and Stegun, I.A. (ed.): "*Handbook of Mathematical Functions with Formulas, Graphs and Mathematical Tables*," National Bureau of Standards Applied Mathematics Series-55 (June 1964) 227-53.

4. Adams, A.R., Ramey, H.J., Jr., and Burgess, R.J.: "Gas Well Testing in a Fractured Carbonate Reservoir," *J. Pet. Tech.* (Oct. 1968) 1187-94.

5. Agarwal, R.G.: "A New Method to Account for Producing Time Effects when Drawdown Type Curves are Used to Analyze Pressure Buildup and Other Test Data," paper SPE 9289 presented at the 55th Annual Meeting of SPE of AIME in Dallas, TX (Sept. 21-24, 1980).

6. Agarwal, R.G., Al-Hussainy, R., and Ramey, H.J., Jr.: "An Investigation of Wellbore Storage and Skin Effect in Unsteady Liquid Flow: I. Analytical Treatment," *Soc. Pet. Eng. J.* (Sept. 1970) 279-90.

7. Ambastha, A.K. and Ramey, H.J.,Jr.: "A Critical Evaluation of the Deviation Time Method to Calculate Discontinuity Radius from Well Tests in Composite Reservoirs," paper OSEA 88187 presented at the 7th Offshore South East Asia Conf. in Singapore (Feb. 2-5, 1988b).

8. Ambastha, A.K. and Ramey, H.J., Jr.: "Thermal Recovery Well Test Design and Interpretation," paper SPE 16746 presented at the 62nd Annual Mtg. of SPE of AIME in Dallas, TX (Sept. 27-30, 1987).

9. Ambastha, A.K. and Ramey, H.J., Jr.: "Well-Test Analysis for a Well in a Finite, Circular Reservoir," prepared for Geothermal Reservoir Engineering Workshop at Stanford University, Stanford, CA (Jan. 1988a).

10. Aziz, K. and Flock, D.L.: "Unsteady State Gas Flow - Use of Drawdown Data in the Prediction of Gas Well Behavior," *J. Can. Pet. Tech.*, 2 (1), (1963) 9-15.

11. Barua, J. and Horne, R.N.: "*Computer Analysis of Thermal Recovery Well Test Data*," SUPRI-A Tech. Report 45, DOE Report No. DOE/SF/11564-10 (March 1985).

12. Barua, J. and Horne, R.N.: "Computerized Analysis of Thermal Recovery Well Test Data," *SPE Form. Eval.* (Dec. 1987) 560-66 (see also SPE 12745 presented at the California Regional Mtg. of SPE of AIME in Long Beach, CA, April 11-13, 1984).

13. Benson, S.M. and Bodvarsson, G.S.: "Nonisothermal Effects During Injection and Falloff Tests," *SPE Form. Eval.* (Feb. 1986) 53-63.

14. Bixel, H.C., and van Poollen, H.K.: "Pressure Drawdown and Buildup in the Presence of Radial Discontinuities," *Soc. Pet. Eng. J.* (Sept. 1967) 301-09.

15. Bixel, H.C., Larkin, B.K., and van Poollen, H.K.: "Effect of Linear Discontinuities on Pressure Buildup and Drawdown Behavior," *J. Pet. Tech.* (Aug. 1963) 885.

16. Bourdet, D., Ayoub, J.A., and Pirard, Y.M.: "Use of Pressure Derivative in Well Test Interpretation," paper SPE 12777 presented at the California Reg. Mtg. of SPE of AIME, Long Beach, CA (April 11-13, 1984).

17. Bourdet, D., Ayoub, J.A., Whittle, T.M., Pirard, Y.M., and Kniazeff, V.: "Interpreting Well Tests in Fractured Reservoirs," *World Oil* (Oct. 1983b) 77-87.

18. Bourdet, D., Whittle, T.M., Douglas, A.A., and Pirard, Y.M.: "A New Set of Type-curves Simplifies Well Test Analysis," *World Oil* (May 1983a) 95-106.

19. Brown, L.P.: "Pressure Transient Behavior of the Composite Reservoir," paper SPE 14316 presented at the 60th Annual Mtg. of SPE of AIME, Las Vegas, NV (Sept. 22-25, 1985).

20. Carter, R.D.: "Pressure Behavior of a Limited Circular Composite Reservoir," *Soc. Pet. Eng. J.* (Dec. 1966) 328-34.

21. Chen, H.K. and Brigham, W.E.: "Pressure Buildup for a Well with Storage and Skin in a Closed Square," *J. Pet. Tech.* (Jan. 1978) 141-146.

22. Closmann, P.J. and Ratliff, N.W.: "Calculation of Transient Oil Production in a Radial Composite Reservoir," *Soc. Pet. Eng. J.* (Dec. 1967) 355-58.

23. Cobb, W.M. and Smith, J.T.: "An Investigation of Pressure Buildup Tests in Bounded Reservoirs," *J. Pet. Tech.* (Aug. 1975) 991-996; *Trans.*, AIME, **259**.

24. Craft, B.C. and Hawkins, M.H.: *Applied Petroleum Reservoir Engineering*, Prentice Hall Inc., Englewood Cliffs, N. J. (1959) p. 295.

25. Da Prat, G., Bockh, A., and Prado, L.: "Use of Pressure Falloff Tests to Locate the Burning Front in the Miga Field, Eastern Venezuela," paper SPE 13667 presented at the California Reg. Mtg. of SPE of AIME, Bakersfield, CA (March 27-29, 1985).

26. Earlougher, R.C., Jr.: "*Advances in Well Test Analysis*," Monograph Volume 5, Society of Petroleum Engineers of AIME, Dallas (1977) Ch. 2.

27. Earlougher, R.C., Jr. and Kersch, K.M.: "Analysis of Short-Time Transient Test Data by Type-Curve Matching," *J. Pet. Tech.* (July 1974) 793-800; *Trans.*, AIME, **257**.

28. Earlougher, R.C., Jr., Ramey, H.J., Jr., Miller, F.G., and Mueller, T.D.: "Pressure Distributions in Rectangular Reservoirs," *J. Pet. Tech.* (Feb. 1968) 199-208.

29. Eggenschwiler, M., Ramey, H.J., Jr., Satman, A., and Cinco-Ley, H.: "Interpretation of Injection Well Pressure Transient Data in Thermal Oil Recovery," paper presented at VI Journadas Tecnicas de Petroleo Meeting, Maracaibo, Venezuela, Oct. 30- Nov. 3, 1979 (see also paper SPE 8908 presented at the California Reg. Mtg. of SPE of AIME, Los Angeles, CA, April 9-11, 1980).

30. Fair, W.B., Jr.: "Pressure Buildup Analysis with Wellbore Phase Redistribution Effects," *Soc. Pet. Eng. J.* (April 1981) 259-70.

31. Fassihi, M.R.: "Evaluation of an Analytical Technique for Estimating Swept Volume in Thermal Recovery Projects from Falloff Tests," paper SPE/DOE 12657 presented at the SPE/DOE Fourth Symposium on Enhanced Oil Recovery, Tulsa, OK (April 15-18, 1984).

32. Grant, M.A. and Sorey, M.L.: "The Compressibility and Hydraulic Diffusivity of a Water-Steam Mixture," *Water Resources Research* (June 1979) 684-86.

33. Gringarten, A.C., Bourdet, D., Landel, P-A., and Kniazeff, V.: "A Comparison Between Different Skin and Wellbore Storage Type Curves for Early-Time Transient Analysis," paper SPE 8205 presented at the 54th Annual Mtg. of SPE of AIME, Las Vegas (Sept. 23-26, 1979).

34. Hatzignatiou, D.G., Ogbe, D.O., Dehgani, K., and Economides, M.J.: "Interference Pressure Behavior in Multi-Layered Composite Reservoirs," paper SPE 16766 presented at the Annual Mtg. of SPE of AIME in Dallas, TX (Sept. 27-30, 1987).

35. Hazebroek, P., Rainbow, H., and Matthews, C.S.: "Pressure Fall-off in Water Injection Wells," *Trans.*, AIME (1951) **213**, 250-60.

36. Hopkinson, J.L., Natanson, S.G., and Temple, A.P.: "Effects of Reservoir Heterogeneity on Performance," paper SPE 1581-G presented at the Annual Mtg. of SPE of AIME in Denver, CO (Oct. 2-5, 1960).

37. Horne, R.N., Satman, A., and Grant, M.A.: "Pressure Transient Analysis of Geothermal Wells with Phase Boundaries," paper SPE 9274 presented at the 55th Annual Meeting of SPE of AIME, Dallas, TX (Sept. 21-24, 1980).

38. Horner, D.R.: "Pressure Buildup in Wells," *Proc.*, Third World Pet. Cong., The Hague (1951) Sec. II, 503-23.

39. Hurst, W.: "Interference Between Oil Fields," *Trans.*, AIME (1960) **219**, 175-92.

40. Jaeger, J.C.: "Some Problems Involving Line Sources in Conduction of Heat," *Phil. Mag.* (1944) Vol. 35, 169.

41. Jones, P.: "Reservoir Limit Test on Gas Wells," *J. Pet. Tech.* (June 1962) 613-19.

42. Kazemi, H.: "Locating a Burning Front by Pressure Transient Measurements," *J. Pet. Tech.* (Feb. 1966) 227-32.

43. Kazemi, H., Merrill, L.S., and Jargon, J.R.: "Problems in Interpretation of Pressure Falloff Tests in Reservoirs With and Without Fluid Banks," *J. Pet. Tech.* (Sept. 1972) 1147-56.

44. Kumar, A. and Ramey, H.J., Jr.: "Well-Test Analysis for a Well in a Constant-Pressure Square," *Soc. Pet. Eng. J.* (April 1974) 107-116.

45. Larkin, B.K.: "Solutions to the Diffusion Equation for a Region Bounded by a Circular Discontinuity," *Soc. Pet. Eng. J.* (June 1963) 113-15.

46. Larsen, L.: "Limitations on the Use of Single and Multiple-Rate Horner, Miller-Dyes-Hutchinson, and Matthews-Brons-Hazebroek Analysis," paper SPE 12135 presented at the 1983 SPE Annual Mtg. in San Francisco, CA (Oct. 5-8, 1983).

47. Loucks, T.L. and Guerrero, E.T.: "Pressure Drop in a Composite Reservoir," *Soc. Pet. Eng. J.* (Sept. 1961) 170-76.

48. MacAllister, D.J.: "Pressure Transient Analysis of $CO_2$ and Enriched-Gas Injection and Production Wells," paper SPE 16225 presented at the Production Operations Symposium of SPE of AIME in Oklahoma City, OK (March 8-10, 1987).

49. Mangold, D.C., Tsang, C.F., Lippmann, M.J., and Witherspoon, P.A.: "A Study of a Thermal Discontinuity in Well Test Analysis," *J. Pet. Tech.* (June 1981) 1095-1105.

50. Matthews, C.S. and Russell, D.G.: "*Pressure Buildup and Flow Tests in Wells*," Monograph Series, Society of Petroleum Engineers of AIME, Dallas (1967) **1**, Ch. 2.

51. Matthews, C.S., Brons, F., and Hazebroek, P.: "A Method for Determination of Average Pressure in a Bounded Reservoir," *Trans.*, AIME (1954) **201**, 182-191.

52. Merrill, L.S., Kazemi, H., and Gogarty, W.B.: "Pressure Falloff Analysis in Reservoirs with Fluid Banks," *J. Pet. Tech.* (July 1974) 809-18.

53. Messner, G.L. and Williams, R.L.: "Application of Pressure Transient Analysis in Steam Injection Wells," paper SPE 10781 presented at California Reg. Mtg. of SPE of AIME, San Francisco, CA (March 24-26, 1982a).

54. Messner, G.L. and Williams, R.L.: "Further Investigation of Pressure Transient Testing in Steamflood Projects," paper SPE 11087 presented at the 57th Annual Mtg. of SPE of AIME, New Orleans, LA (Sept. 26-29, 1982b).

55. Miller, C.C., Dyes, A.B., and Hutchinson, C.A., Jr.: "The Estimation of Permeability and Reservoir Pressure From Bottom-Hole Pressure Build-Up Characteristics," *Trans.*, AIME (1950) **189**, 91-104.

56. Mishra, S. and Ramey, H.J., Jr.: "A New Derivative Type-Curve for Pressure Buildup Analysis with Boundary Effects," *Proc.*, 12th Workshop on Geothermal Reservoir Engineering at Stanford Univ., Stanford, CA (Jan. 20-22, 1987) 45-47.

57. Mortada, M.: "Oilfield Interference in Aquifers of Non-Uniform Properties," *Trans.*, AIME (1960) **219**, 412-14.

58. Mueller, T.D. and Witherspoon, P.A.: "Pressure Interference Effects Within Reservoirs and Aquifers," *J. Pet. Tech.* (April 1965) 471-74.

59. Obut, S.T.: "*Determination of the Front Position with the Pressure Transient Analysis in the Presence of an Infinite Conductivity Vertical Fracture,*" M.S. Thesis, The Pennsylvania State Univ., University Park, PA (1983).

60. Obut, S.T. and Ertekin, T.: "A Composite System Solution in Elliptical Flow Geometry," paper SPE 13078 presented at the Annual Mtg. of SPE of AIME in Houston, TX (Sept. 16-19, 1984).

61. Odeh, A.S.: "Flow Test Analysis for a Well with Radial Discontinuity," *J. Pet. Tech.* (Feb. 1969) 207-10.

62. Olarewaju, J.S. and Lee, W.J.: "A Comprehensive Application of a Composite Reservoir Model to Pressure Transient Analysis," paper SPE 16345 presented at the California Reg. Mtg. of SPE of AIME in Ventura, CA (April 8-10, 1987a).

63. Olarewaju, J.S. and Lee, W.J.: "An Analytical Model for Composite Reservoirs Produced at Either Constant Bottomhole Pressure or Constant Rate," paper SPE 16763 presented at the Annual Mtg. of SPE of AIME in Dallas, TX (Sept. 27-30, 1987b).

64. Onyekonwu, M.O.: "*Interpretation of In-situ Combustion Thermal Recovery Falloff Tests,*" Ph.D. Thesis, Stanford University, Stanford, California (1985).

65. Onyekonwu, M.O. and Horne, R.N.: "Pressure Response of a Reservoir with Spherically Discontinuous Properties," *J. Pet. Tech.* (Nov. 1983) 2127-34.

66. Onyekonwu, M.O., Ramey, H.J., Jr., and Brigham, W.E.: "Application of Superposition and Pseudosteady State Concepts to Thermal Recovery Well Tests," paper SPE 15536 presented at the 61st Annual Mtg. of SPE of AIME, New Orleans, LA (Oct. 5-8, 1986b).

67. Onyekonwu, M.O., Ramey, H.J., Jr., Brigham, W.E., and Jenkins, R.: "Interpretation of Simulated Falloff Tests," paper SPE 12746 presented at the California Reg. Mtg. of SPE of AIME, Long Beach, CA (April 11-13, 1984a).

68. Ramey, H.J., Jr.: "Approximate Solutions for Unsteady Liquid Flow in Composite Reservoirs," *J. Can. Pet. Tech.* (Jan-March 1970) 32-37.

69. Ramey, H.J., Jr.: *Personal Communication* (April 1987).

70. Ramey, H.J., Jr. and Cobb, W.M.: "A General Pressure Buildup Theory for a Well in a Closed Drainage Area," *J. Pet. Tech.* (Dec. 1971) 1493-1505.

71. Ramey, H.J., Jr., Kumar, A., and Gulati, M.S.: "*Gas Well Test Analysis under Waterdrive Conditions*," Monograph prepared for American Gas Association at Stanford University, Stanford, CA (1973).

72. Rowan, G. and Clegg, M.W.: "An Approximate Method for Transient Radial Flow," *Soc. Pet. Eng. J.* (Sept. 1962) 225-56.

73. Satman, A.: "An Analytical Study of Interference in Composite Reservoirs," *Soc. Pet. Eng. J.* (April 1985) 281-90.

74. Satman, A.: "An Analytical Study of Transient Flow in Stratified Systems With Fluid Banks," paper SPE 10264 presented at the Annual Mtg. of SPE of AIME in San Antonio, TX (Oct. 5-7, 1981).

75. Satman, A. and Oskay, M.M.: "Effect of a Tilted Front on Well Test Analysis," paper SPE 14701 submitted to SPE, Richardson, TX (1985).

76. Satman, A., Eggenschwiler, M., Tang, R. W., and Ramey, H.J., Jr.: "An Analytical Study of Transient Flow in Systems with Radial Discontinuities," paper SPE 9399 presented at the 55th Annual Mtg. of SPE of AIME, Dallas, TX (Sept. 21-24, 1980).

77. Sosa, A., Raghavan, R., and Limon, T.J.: "Effect of Relative Permeability and Mobility Ratio on Pressure Falloff Behavior," *J. Pet. Tech.* (June 1981) 1125-35.

78. Stanislav, J.F., Easwaran, C.V., and Kokal, S.L.: "Analytical Solutions for Vertical Fractures in a Composite System," paper no. 86-37-39 presented at the 37th Annual Tech. Mtg. of the Petroleum Society of CIM at Calgary, Alberta, Canada (June 8-11, 1986).

79. Stanislav, J.F., Easwaran, C.V., and Kokal, S.L.: "Interpretation of Thermal Well Testing," paper SPE 16747 presented at the Annual Mtg. of SPE of AIME in Dallas, TX (Sept. 27-30, 1987).

80. Stehfest, H.: "Algorithm 368, Numerical Inversion of Laplace Transforms," D-5, *Communications of ACM* (Jan. 1970) vol. 13, No. 1, 49.

81. Tang, R.W.: "*Transient Pressure Analysis in a Composite Reservoir*," SUPRI-A Tech. Report 31, DOE Report No. DOE/ET/ 12056-31 (Aug. 1982).

82. Tang, R.W. and Ambastha, A.K.:"Analysis of $CO_2$ Pressure Transient Data with Two- and Three-Region Radial Composite Models," paper SPE 18275 to be presented at the 1988 Annual SPE of AIME Meeting in Houston, TX (Oct. 1988).

83. Tek, M.R., Grove, M.L., and Poettmann, F.H.: "Methods for Predicting the Back-Pressure Behavior of Low-Permeability Natural-Gas Wells," *Trans.*, AIME (1957) **210**, 302.

84. Teng, E.: "*Transient Pressure Analysis in Composite Reservoirs with Rectangular Discontinuities*," M.S. Report, Stanford Univ., Stanford, CA (Sept. 1984) 153 pp.

85. Theis, C.V.: "The Relation Between the Lowering of the Piezometric Surface and the Rate and Duration of Discharge of a Well Using Ground-water Storage," *Trans.*, AGU (1935) 519-24.

86. Tiab, D. and Kumar, A.: "Application of the $p'_D$ Function to Interference Analysis," *J. Pet. Tech.* (Aug. 1980) 1465-70.

87. Turki, L: "*Decline Curve Analysis in Composite Reservoirs*," Engineer Thesis, Stanford University, Stanford, CA (Dec. 1986) 118 pp.

88. Van Everdingen, A.F. and Hurst, W.: "The Application of the Laplace Transformation to Flow Problems in Reservoirs," *Trans.*, AIME (1949) Vol. 186, 305-324.

89. Van Poollen, H.K.: "Radius of Drainage and Stabilization Time Equations," *Oil and Gas Journal* (Sept. 14, 1964) 138-43.

90. Van Poollen, H.K.: "Transient Tests Find Fire Front in an In-situ Combustion Project," *Oil and Gas Journal* (Feb. 1, 1965) 78-80.

91. Vongvuthipornchai, S. and Raghavan, R.: "A Note on the Duration of the Transitional Period of Responses Influenced by Wellbore Storage and Skin," *SPE Form. Eval.* (March 1988) 207-214.

92. Walsh, J.W., Jr., Ramey, H.J., Jr., and Brigham, W.E.: "Thermal Injection Well Falloff Testing," paper SPE 10227 presented at the 56th Annual Mtg. of SPE of AIME, San Antonio, TX (Oct. 5-7, 1981).

93. Wattenbarger, R.A. and Ramey, H.J., Jr.: "An Investigation of Wellbore Storage and Skin Effects in Unsteady Liquid Flow: II. Finite Difference Treatment," *Soc. Pet. Eng. J.* (Sept. 1970) 291-97.

# APPENDIX A

## Beginning of Infinite-acting Radial Flow for a Line-source and a Finite-radius Well

In this appendix, the time to the beginning of a semilog straight line for a line-source well and for a finite-radius well is considered. Simple examples of line-source and finite-radius wells considered here illustrate that drawdown wellbore pressure behavior approaches a semilog straight line at a later time on a derivative graph than on a pressure graph at the same specified accuracy for pressure and pressure derivative.

### Case I. Line-source Well

For a line-source well producing at a constant rate in an infinitely large homogeneous reservoir, the pressure response at any location is given by (*Theis*, 1935):

$$p_D\ (r_D, t_D) = -\frac{1}{2}\, Ei\left[-\frac{r_D^2}{4t_D}\right] \quad . \tag{A.1}$$

Equation (A.1) is also called the exponential-integral solution (*Matthews* and *Russell*, 1967; *Horner*, 1951), the line-source solution or the *Theis* (1935) solution. The definition and approximations for the exponential-integral are presented in *Abramowitz* and *Stegun* (1964). *Earlougher* (1977) discusses the exponential-integral solution, and states that the exponential-integral solution can be approximated by:

$$p_D\ (r_D, t_D) \approx \frac{1}{2}\left[\ln\left(\frac{t_D}{r_D^2}\right) + 0.80907\right] \quad , \tag{A.2}$$

when:

$$t_D\ /\ r_D^2 > 100 \quad . \tag{A.3}$$

However, *Earlougher* (1977) also points out that the difference between Eqs. (A.1) and (A.2) is only about 2% when $t_D/r_D^2 > 5$. The semilog derivative for the well pressure, $r_D = 1$, from Eq. (A.1) is:

$$\frac{dp_{wD}}{d\ \ln t_D} = 0.5\ e^{-1/4\ t_D} \quad . \tag{A.4}$$

The semilog pressure derivative from Eq. (A.2) is:

$$\frac{dp_{wD}}{d\ \ln t_D} = 0.5 \quad . \tag{A.5}$$

From Eqs. (A.4) and (A.5), the semilog derivative from the exponential-integral solution is within 2% and 5% of 0.5 when $t_D$ = 12.4 and 4.9, respectively. Thus, even though the pressures at the wellbore from the exponential-integral solution and log-approximation are within 2% when $t_D > 5$, the semilog slopes are within 2% when $t_D > 12$. Though $t_D$ of 5 and 12 are not dramatically different, the following is observed:

1. About one-half more log cycle of time is required to get within 2% of 0.5 on a semilog derivative graph. Thus, it may appear that a semilog line has been reached on a pressure-log time graph, although the slope may change until a later time on a derivative graph before reaching a constant slope.
2. The line-source well is a simple case. In more complicated cases, larger differences in design criteria may be observed by analyzing pressure and pressure derivative responses.

## Case II. Finite-radius Well

*Mueller* and *Witherspoon* (1965) presented $p_D$ as a function of $r_D$ and $t_D$ for an infinitely large reservoir with a finite-radius well producing at a constant rate. Their work shows that the pressure transient response at a finite-radius well with no wellbore storage or skin develops a semilog line for $t_D \geq 25$. *Bourdet et al.* (1983a) presented a drawdown pressure derivative type-curve for a finite-radius well producing at a constant rate with wellbore storage and skin in an infinite reservoir. Their type curve is reproduced in Fig. A.1. The beginning of a semilog line corresponding to infinite-acting radial flow is characterized by an approach of $(t_D / C_D)\, p'_D$ to a value of 0.5, where:

$$(t_D/C_D)\, p'_D = (t_D/C_D)\, \frac{dp_D}{d\,(t_D / C_D)} = t_D\, \frac{dp_D}{dt_D} = \frac{dp_D}{d \ln t_D} \quad . \tag{A.6}$$

The group $C_D\, e^{2s}$ is a correlating parameter in Fig. A.1. The curve for $C_D\, e^{2s} = 0.1$ approximates the case of zero wellbore storage and skin. Figure A.1 shows that the curve for $C_D\, e^{2s} = 0.1$ approaches $(t_D / C_D)\, p'_D$ of 0.5 at $t_D / C_D \approx 1000$. Considering $s = 0$, $t_D / C_D \approx 1000$ is equivalent to $t_D \approx 100$ for $C_D\, e^{2s} = 0.1$.

On Fig. A.1, two design criteria for the beginning of a semilog line available in the literature are shown. Criterion (1) is (*Ramey et al.*, 1973):

$$t_D > (60 + 3.5\, s)\, C_D \quad , \tag{A.7}$$

marked for $s = 0$ on Fig. A.1. Criterion (2) is (*Chen* and *Brigham*, 1978):

$$t_D > 50\, C_D\, e^{0.14\, s} \quad , \tag{A.8}$$

marked for $s = 5$ on Fig. A.1. Equations (A.7) and (A.8) were both developed by analyzing pressure responses. Both criteria appear to underestimate the time to the beginning of the semilog line on a derivative graph.

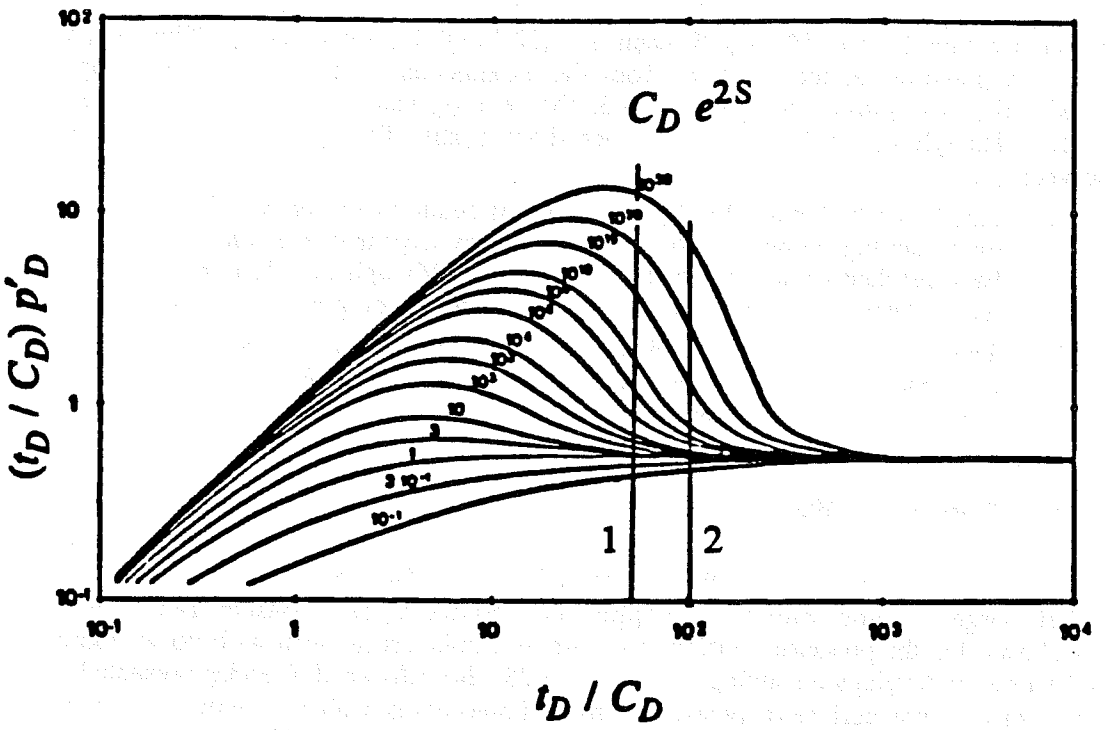


Figure A.1: Pressure derivative type-curve for an infinite, homogeneous reservoir (after *Bourdet et al.*, 1983a).

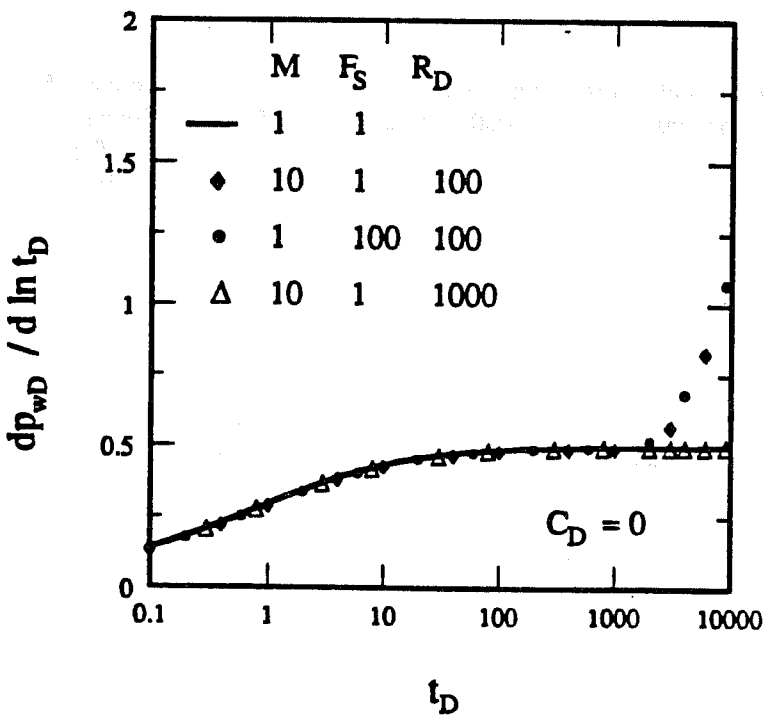


Figure A.2: Beginning of semi-log line.

Figure A.2 shows semilog derivative behavior for a finite-radius well with no wellbore storage in an infinitely large homogeneous or composite reservoir. The semilog derivative is within 5% and 2% of 0.5 at $t_D = 43$, and 142, respectively, for homogeneous and composite reservoirs both. *Tiab* and *Kumar* (1980) stated that the semilog derivative is within 5% of 0.5 at $t_D \geq 100$. The cases shown for a composite reservoir suggest that the time to the beginning of the first semilog line corresponding to the inner region mobility is independent of $M$, $F$ and $R_D$. Comparing $t_D \geq 142$ for semilog derivative to be within 2% of 0.5 with $t_D \geq 25$ for pressure response to be within 2% of the log approximation of the exponential-integral solution, we observe that about one-half more log cycle of time is required to reach the beginning of a semilog line on a derivative graph.

Based on the analysis of these two examples, the following is observed:

1. If a pressure derivative approach is to be used for well test analysis, well test design should be based on design equations develped from the analysis of derivative responses, as the derivative approach results in different design equations.
2. Pressure derivative behavior for a reservoir model may yield design equations showing the need for longer tests than presently available design equations based on the analysis of pressure behavior, if a specialized method, dependent on the presence of a certain flow regime in test data, is to be used.

The second remark was shown to be true in this appendix for a line-source well, and a finite-radius well producing at a constant rate with no wellbore storage in an infinitely large homogeneous or composite reservoir. The time to the beginning of a semilog line was considered.

# APPENDIX B

## Development of Design Equations

This appendix presents the development of design equations reported in this study. The data used to develop the design equations are presented. Accuracy of design equations has also been investigated.

### 1. Time to the End of Storage-Dominated Period

During the storage-dominated period, the slope of a log-log graph of $p_{wD}$ vs. $t_D$ is:

$$\frac{d \ln (p_{wD})}{d \ln (t_D)} = 1 \ . \tag{B.1}$$

Table B.1 presents the $t_D/C_D$ values by which the slope $d \ln (p_{wD})/d \ln (t_D)$ has decreased by 2% from the initial value of unity.

**Table B.1 - The $t_D/C_D$ values for the end of storage-dominated period (Log-log slope within 2% of 1)**

| $C_D e^{2s}$ | $t_D/C_D$ for slope = 0.98 | $t_D/C_D$ from Eq. (B.2) |
|---|---|---|
| 10 | 0.018 | 0.018 |
| 100 | 0.058 | 0.066 |
| $10^3$ | 0.11 | 0.114 |
| $10^4$ | 0.16 | 0.162 |
| $10^5$ | 0.21 | 0.21 |
| $10^6$ | 0.264 | 0.258 |
| $10^7$ | 0.31 | 0.306 |
| $10^{10}$ | 0.46 | 0.45 |
| $10^{20}$ | 0.93 | 0.93 |
| $10^{30}$ | 1.4 | 1.41 |

Based on the $t_D/C_D$ values from Table B.1, a design equation for the time to the end of storage-dominated period as a function of $C_D e^{2s}$ is:

$$\frac{t_D}{C_D} \approx 0.048 \log (C_D e^{2s}) - 0.03 \ . \tag{B.2}$$

The $t_D/C_D$ values from Eq. (B.2) are presented in column 3 of Table B.1 for comparison with the $t_D/C_D$ values in column 2 of Table B.1. Equation (B.2) applies for a well producing at a constant rate from an infinitely large or finite, and homogeneous or composite reservoir.

## 2. Time to the Beginning of Infinite-acting Radial Flow

During the infinite-acting radial flow period, the dimensionless semilog pressure derivative is:

$$\frac{dp_{wD}}{d \ln t_D} = 1/2 \ . \tag{B.3}$$

Columns 2 and 3 of Table B.2 present the $t_D/C_D$ values for the semilog slope to be within 2% and 5% of 0.5 for several values of $C_D e^{2s}$ shown in column 1 of Table B.2.

**Table B.2 - The $t_D/C_D$ values for the beginning of infinite-acting radial flow (Semi-log slope within 2% and 5% of 0.5)**

| $C_D e^{2s}$ | $t_D/C_D$ for Slope = 0.51 | $t_D/C_D$ for Slope = 0.525 | $t_D/C_D$ from Eq. (B.4) | $t_D/C_D$ from Eq. (B.5) |
|---|---|---|---|---|
| 10 | 435 | 149 | 460 | 140 |
| 100 | 641 | 245 | 640 | 250 |
| $10^3$ | 813 | 341 | 820 | 360 |
| $10^4$ | 985 | 445 | 1000 | 470 |
| $10^5$ | 1208 | 559 | 1180 | 580 |
| $10^6$ | 1313 | 666 | 1360 | 690 |
| $10^7$ | 1494 | 790 | 1540 | 800 |
| $10^{10}$ | 2019 | 1219 | 2080 | 1130 |
| $10^{20}$ | 3801 | 2595 | 3880 | 2230 |
| $10^{30}$ | 5619 | 4121 | 5680 | 3330 |

Based on the data in Table B.2, the semilog slope is within 2% of 0.5 at the time:

$$\frac{t_D}{C_D} \approx 280 + 180 \log (C_D e^{2s}) \ , \tag{B.4}$$

and the semilog slope is within 5% of 0.5 at the time:

$$\frac{t_D}{C_D} \approx 30 + 110 \log (C_D e^{2s}) \ . \tag{B.5}$$

The $t_D/C_D$ values from Eqs. (B.4) and (B.5) are presented in columns 4 and 5 of Table B.2. A good comparison between the $t_D/C_D$ values in columns 2 and 4, and the $t_D/C_D$ values in columns 3 and 5 demonstrates the validity of Eqs. (B.4) and (B.5).

Equations (B.4) and (B.5) are valid for a well producing at a constant rate from an infinitely large or finite, homogeneous reservoir provided the outer boundary effects are not felt before the establishment of infinite-acting radial flow. Also, Eqs. (B.4) and (B.5) describe the time to the beginning of infinite-acting radial flow corresponding to the inner region mobility for a well in an infinitely large or finite, radial composite reservoir provided the outer region effects are not felt before the establishment of infinite-acting radial flow corresponding to the inner region mobility.

### 3. Time to the End of Infinite-acting Radial Flow for a Well in a Finite, Circular Homogeneous Reservoir

From Fig. 5.2, the drawdown semilog slope for a constant-pressure outer boundary drops faster than the drawdown slope for a closed outer boundary rises. However, the data presented in Table B.3 approximately applies for the drawdown response of a well in a finite homogeneous reservoir with either a closed or a constant-pressure outer boundary.

**Table B.3 - The $t_D/C_D$ values for the end of infinite-acting radial flow (Semi-log slope within 2% of 0.5)**

| $r_{eD}^2/C_D$ | $t_D/C_D$ for slope = 0.51 or 0.49 | $t_D/C_D$ from Eq. (B.6) |
|---|---|---|
| $10^3$ | 175 | 175 |
| $10^4$ | 1750 | 1750 |
| $10^5$ | 17500 | 17500 |
| $10^6$ | 175000 | 175000 |
| $10^7$ | 1750000 | 1750000 |

For selected values of $r_{eD}^2/C_D$, Table B.3 presents the $t_D/C_D$ values by which the semilog pressure derivative has changed by 2% of 0.5. The data of Table B.3 suggests:

$$\frac{t_D}{C_D} \approx \frac{0.175\, r_{eD}^2}{C_D} \quad . \tag{B.6}$$

As observed from Fig. 5.4, Eq. (B.6) is also applicable for the buildup response of a well in a finite homogeneous reservoir with a constant-pressure outer boundary provided $t_D$ of Eq. (B.6) is modified to $\Delta t_D$. The calculated $t_D/C_D$ values from Eq. (B.6) are presented in column 3 of Table B.3 for comparison with the $t_D/C_D$ values in column 2 of Table B.3.

The data presented in Table B.4 applies for the buildup response of a well in a closed reservoir.

**Table B.4 - The $\Delta t_D/C_D$ values for the end of infinite-acting radial flow (Semi-log slope within 2% of 0.5)**

| $r_{eD}^2/C_D$ | $\Delta t_D/C_D$ for slope = 0.49 | $\Delta t_D/C_D$ from Eq. (B.7) |
|---|---|---|
| $10^3$ | 15 | 10 |
| $10^4$ | 95 | 100 |
| $10^5$ | 600 | 500 |
| $10^6$ | 5000 | 5000 |
| $10^7$ | 50000 | 50000 |

For selected values of $r_{eD}^2/C_D$, Table B.4 presents the $\Delta t_D/C_D$ values by which the semilog pressure derivative has decreased by 2% of 0.5. The data of Table B.4 suggests:

$$\frac{\Delta t_D}{C_D} \approx \frac{0.01\, r_{eD}^2}{C_D} \quad \text{for} \quad \frac{r_{eD}^2}{C_D} < 10^5 \quad , \text{ and}$$

$$\approx \frac{0.005\, r_{eD}^2}{C_D} \quad \text{for} \quad \frac{r_{eD}^2}{C_D} \geq 10^5 \quad . \tag{B.7}$$

The calculated $\Delta t_D/C_D$ values from Eq. (B.7) are presented in column 3 of Table B.4 for comparison with the $\Delta t_D/C_D$ values in column 2 of Table B.4.

## 4. Maximum Semi-log Slope and the Time to the Maximum Derivative for a Two-Region Composite Reservoir

Table B.5 presents the drawdown maximum semilog pressure derivative, $(dp_{wD}/d \ln t_D)_{max}$, and the time to the maximum pressure derivative, $(t_{De})_{max}$, for a well in an infinitely large composite reservoir. The data of Table B.5 suggests:

$$\left[\frac{dp_{wD}}{d \log t_D}\right]_{max} \approx (1.1 + \log F_S) \quad , \text{ for } M = 1$$

$$\approx (0.7 + \log F_S)\, M \quad , \text{ for } M \geq 10 \ , \tag{B.8}$$

and

$$(t_{De})_{max} \approx (1.8 + 0.4 \log F_S)\, M \quad . \tag{B.9}$$

Equations (B.8) and (B.9) apply only if $M \geq 1$, and $F_S \geq 10$. Figures B.1 and B.2 show the accuracy of Eqs. (B.8) and (B.9) compared to actual values for maximum semilog slope and the time to maximum pressure derivative. Equations (B.8) and (B.9) apply for the drawdown response of a well in a finite composite reservoir provided the outer boundary effects do not mask the development of the maximum semilog slope. Equations (B.8) and (B.9) also apply for the buildup response of a well in a composite reservoir provided the limit on $t_{pD}/R_D^2$ presented in Fig. 6.28 is satisfied.

## 5. Time to the Beginning of Infinite-acting Radial Flow Corresponding to the Outer Region Mobility for a Two-Region Composite Reservoir

Table B.6 presents the dimensionless time, $(t_{De})_{II}$, values by which the drawdown semilog slope, $dp_{wD}/d \ln t_D$, is within 2% of $M/2$. Based on the data in Table B.6, $(t_{De})_{II}$ is:

$$(t_{De})_{II} \approx 90\, (1 + \log F_S)\, M \quad . \tag{B.10}$$

Equation (B.10) applies if $M \geq 10$, and $F_S \geq 1$. The accuracy of Eq. (B.10) in forecasting the time to the beginning of infinite-acting radial flow corresponding to the outer region mobility is shown in Fig. B.3.

**Table B.5 - The $t_D/C_D$ values for the beginning of inifinite-acting radial flow (Semi-log slope within 2% and 5% of 0.5)**

| $C_D e^{2s}$ | $t_D/C_D$ for Slope = 0.51 | $t_D/C_D$ for Slope = 0.525 | $t_D/C_D$ from Eq. (B.8) | $t_D/C_D$ from Eq. (B.9) |
|---|---|---|---|---|
| 10 | 435 | 149 | 350 | 144 |
| 100 | 641 | 245 | 550 | 244 |
| $10^3$ | 813 | 341 | 750 | 344 |
| $10^4$ | 985 | 445 | 950 | 444 |
| $10^5$ | 1208 | 559 | 1150 | 544 |
| $10^6$ | 1313 | 666 | 1350 | 644 |
| $10^7$ | 1494 | 790 | 1550 | 744 |
| $10^{10}$ | 2019 | 1219 | 2150 | 1044 |
| $10^{20}$ | 3801 | 2595 | 4150 | 2044 |
| $10^{30}$ | 5619 | 4121 | 6150 | 3044 |

**Table B.6 - The $t_D/C_D$ values for the end of infinite-acting radial flow (Semi-log slope within 2% of 0.5)**

| $r_{eD}^2/C_D$ | $t_D/C_D$ for slope = 0.51 | $t_D/C_D$ from Eq. (B.10) |
|---|---|---|
| $10^3$ | 175 | 175 |
| $10^4$ | 1750 | 1750 |
| $10^5$ | 17500 | 17500 |
| $10^6$ | 175000 | 175000 |
| $10^7$ | 1750000 | 1750000 |

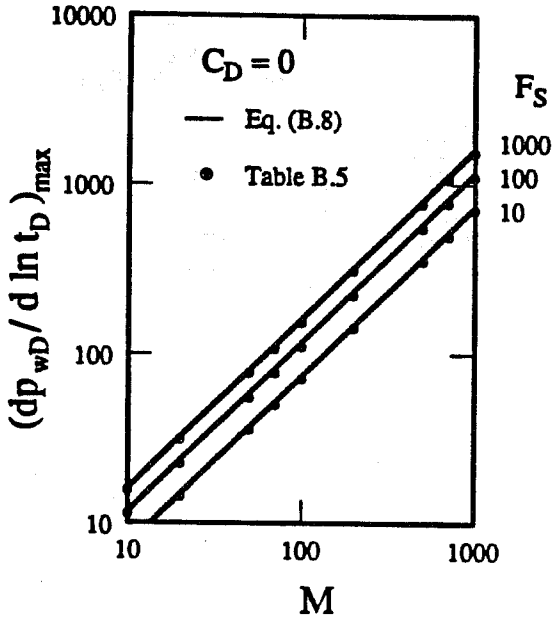


Figure B.1: Verification of the accuracy of Eq. (B.8).

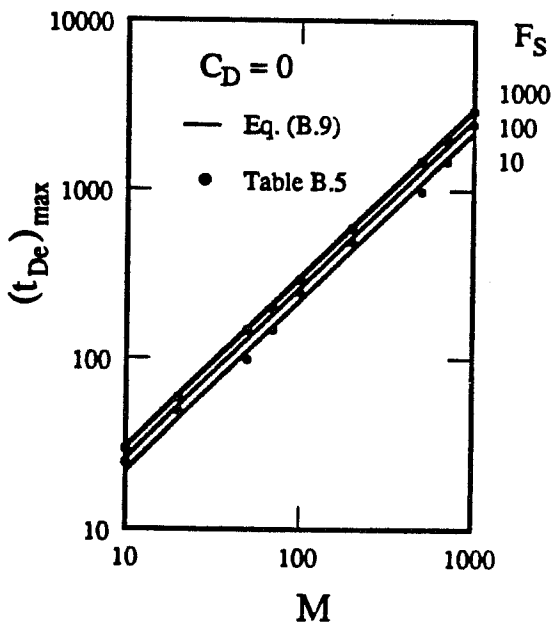


Figure B.2: Verification of the accuracy of Eq. (B.9).

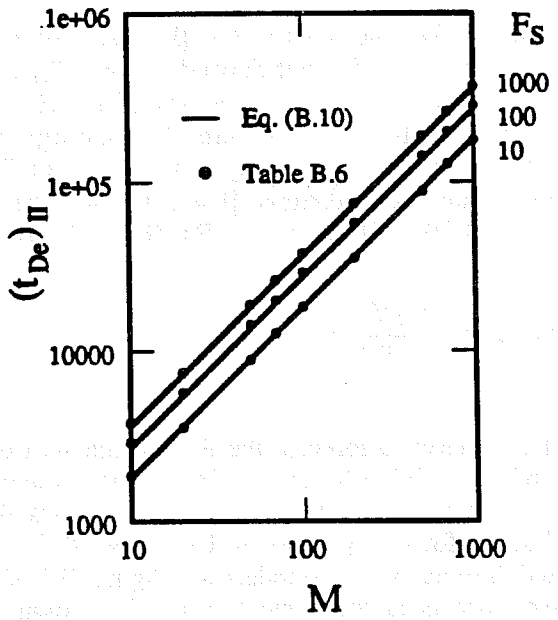


Figure B.3: Verification of the accuracy of Eq. (B.10).

## 6. Time to the Beginning of Outer Boundary Effects for a Finite Two-Region Composite Reservoir

The time to the start of outer boundary effects for a finite two-region composite reservoir is obtained as the time when the semilog slope for the finite outer boundary case is different from the semilog slope for the infinite outer boundary case by 2%. Table B.7 presents the dimensionless time, $(t_{De})_{depart}$, values for the start of outer boundary effects on drawdown behavior for a two-region composite reservoir with a closed outer boundary. The data of Table B.7 suggests:

$$(t_{De})_{depart} \approx \frac{(r_{eD}/R_D)^2 M}{\beta F_S} \quad , \tag{B.11}$$

where $1 < \beta < 2\pi$. For small values of $r_{eD}/R_D$ and a large $F_S$, $\beta \rightarrow 1$. For large values of $r_{eD}/R_D$, $\beta \rightarrow 2\pi$. The parameter $\beta$ is insensitive to $M$, but depends on $r_{eD}/R_D$ and $F_S$. Table B.8 presents $\beta$ values obtained empirically for several combinations of $r_{eD}/R_D$ and $F_S$. The data of Table B.8 is presented graphically on Fig. B.4. Figures B.5 through B.7 present a comparison of the results from Eq. (B.11) with the $(t_{De})_{depart}$ values from Table B.7 for $r_{eD}/R_D$ = 10, 100, and 1000. For approximate calculations, $\beta$ = 5 would forecast $(t_{De})_{depart}$ reasonably well for $r_{eD}/R_D \geq 100$, and $F_S \leq 200$. Using $\beta$ = 5, Eq. (B.11) becomes:

$$(t_{De})_{depart} \approx \frac{(r_{eD}/R_D)^2 M}{5 F_S} \quad . \tag{B.12}$$

Equation (B.11) or (B.12) can also be used to forecast the time to the start of outer boundary effects for drawdown behavior, and the buildup behavior after a long producing time with a constant-pressure outer boundary, as shown in Fig. B.8. Figure B.8 shows the drawdown semilog slope, and the buildup $MDH$ slope for $C_D$ = 0, $M$ = 10, $F_S$ = 1000, and $r_{eD}/R_D$ = 1000 for closed, constant-pressure, and infinite outer boundaries. Figure B.8 shows that the time to the start of the outer boundary effects is the same for the drawdown responses for closed and constant-pressure outer boundaries, and the buildup response for a constant-pressure outer boundary. However, the outer boundary effects start earlier for the buildup response for a closed outer boundary.

**Table B.7 - The time to the start of outer boundary effects on drawdown behavior for a two-region composite reservoir with a closed outer boundary**

| $M$ | $F_S$ | $(t_{De})_{depart}$ for $r_{eD}/R_D = 10$ | $(t_{De})_{depart}$ for $r_{eD}/R_D = 100$ | $(t_{De})_{depart}$ for $r_{eD}/R_D = 1000$ |
|---|---|---|---|---|
| 10 | 10 | 22 | 1585 | $1.56 \times 10^5$ |
| 20 | | 45 | 3217 | $3.17 \times 10^5$ |
| 50 | | 107 | 8106 | $8 \times 10^5$ |
| 100 | | 220 | 15850 | $1.57 \times 10^6$ |
| 200 | | 448 | 32157 | $3.17 \times 10^6$ |
| 500 | | 1071 | 81053 | $7.94 \times 10^6$ |
| 1000 | | 2195 | $1.58 \times 10^5$ | $1.56 \times 10^7$ |
| 10 | 100 | 4.8 | 182 | 15684 |
| 20 | | 9.4 | 373 | 31744 |
| 50 | | 22.8 | 935 | 80101 |
| 100 | | 45.7 | 1820 | $1.57 \times 10^5$ |
| 200 | | 91.2 | 3724 | $3.17 \times 10^5$ |
| 500 | | 225 | 11699 | $8.01 \times 10^5$ |
| 1000 | | 455 | 18187 | $1.57 \times 10^6$ |
| 10 | 1000 | 1.35 | 35.4 | 1605 |
| 20 | | 2.5 | 70.6 | 3269 |
| 50 | | 5.8 | 170.4 | 8218 |
| 100 | | 11.3 | 351.7 | 16041 |
| 200 | | 22.5 | 703.2 | 32681 |
| 500 | | 55.9 | 1700 | 82179 |
| 1000 | | 110.6 | 3515 | $1.6 \times 10^5$ |

**Table B.8 - β values for Eq. (B.11)**

| $F_S$ | β for $r_{eD}/R_D = 10$ | β for $r_{eD}/R_D = 100$ | β for $r_{eD}/R_D = 1000$ |
|---|---|---|---|
| 10 | 5 | 6.25 | 6.25 |
| 20 | 3.66 | 6.22 | 6.26 |
| 50 | 2.7 | 5.75 | 6.27 |
| 100 | 2 | 5.56 | 6.25 |
| 200 | 1.58 | 4.8 | 6.25 |
| 500 | 1.2 | 3.65 | 6.24 |
| 1000 | 0.8 | 2.86 | 6.25 |

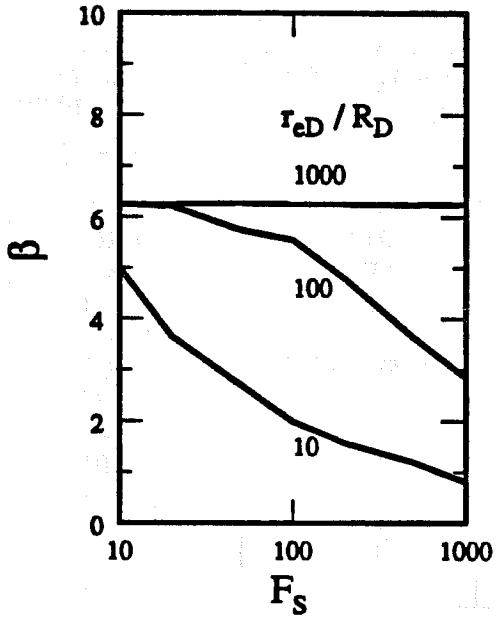


Figure B.4: Parameter β as a function of $F_S$ and $r_{eD}/R_D$.

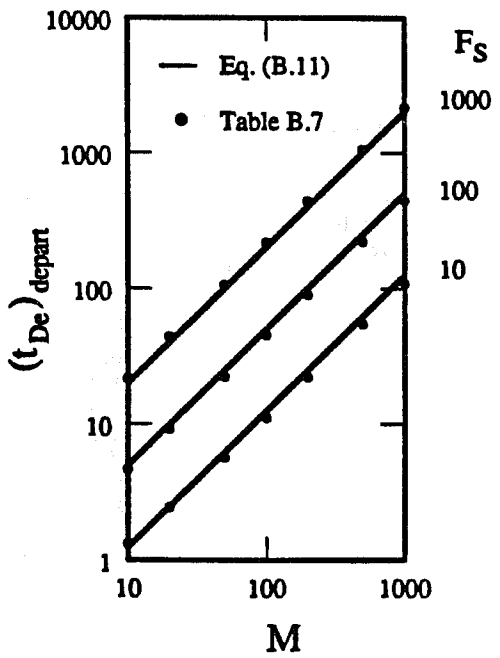


Figure B.5: Verification of the accuracy of Eq. (B.11) for $r_{eD}/R_D$ = 10.

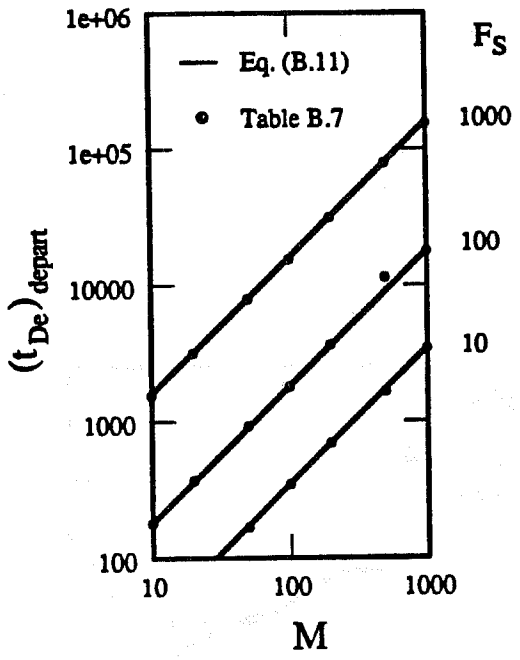


Figure B.6: Verification of the accuracy of Eq. (B.11) for $r_{eD}/R_D$ = 100.

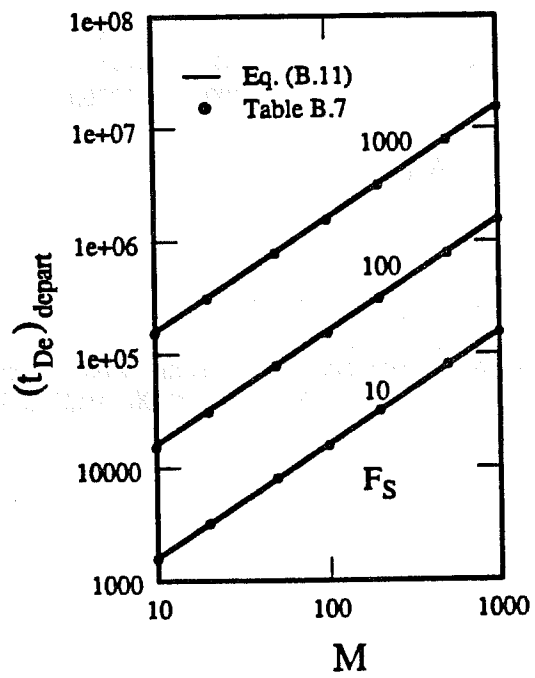


Figure B.7: Verification of the accuracy of Eq. (B.11) for $r_{eD}/R_D$ = 1000.

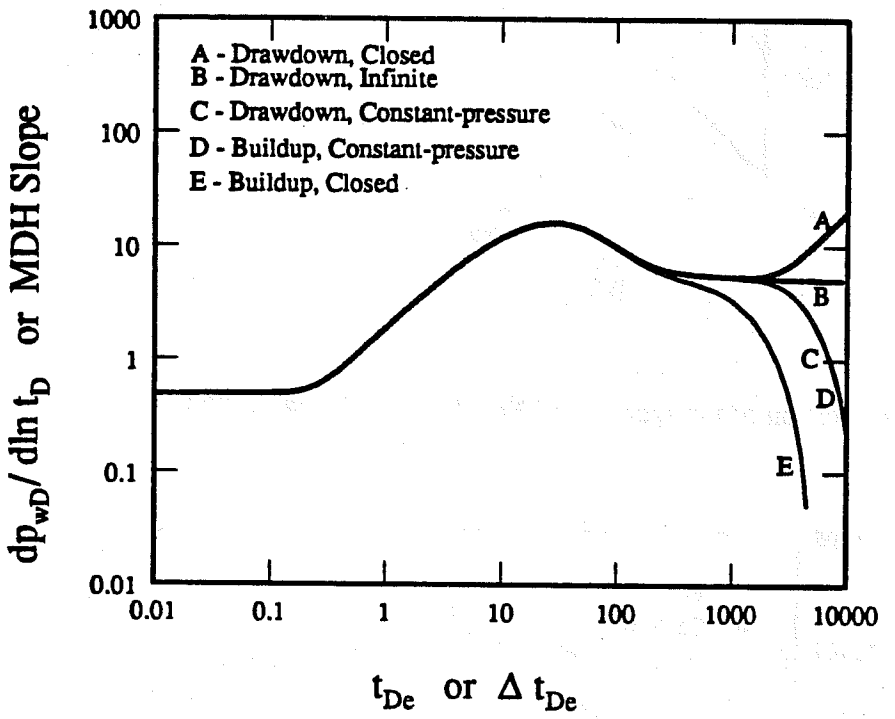


Figure B.8: Drawdown semi-log slope, and the buildup *MDH* slope for a two-region composite reservoir with $C_D = 0$, $M = 10$, $F_S = 1000$, and $r_{eD}/R_D = 1000$ for several outer boundary conditions.

# APPENDIX C

## Late Time Drawdown Solution for a Well in a Two-Region Composite Reservoir

### 1. Infinitely Large Reservoir

Dimensionless wellbore pressure drop using *Ramey's* (1970) approximate solution is:

$$p_{wD}\,(t_D) = -\frac{1}{2}\left[Ei\left(-\frac{1}{4t_D}\right) - Ei\left(-\frac{R_D{}^2}{4t_D}\right) + M\; e^{\frac{(\eta-1)R_D{}^2}{4t_D}} \cdot Ei\left(-\frac{\eta R_D{}^2}{4t_D}\right)\right] + s \quad . \tag{C.1}$$

All $Ei$ terms can be replaced by their log approximations and the exponential term will be within 1% of 1.00, if:

$$t_{De} \geq \frac{100\,M}{F_S} \quad , \text{ for } M/F_S \geq 1$$

$$\geq 100 \quad , \quad \text{for } M/F_S \leq 1 \quad . \tag{C.2}$$

The simplification of Eq. (C.1) under the conditions of Eq. (C.2) results in:

$$p_{wD}\,(t_D) = \frac{1}{2}\left[M\,\ln\left(\frac{2.2458\,t_D}{\eta\,R_D{}^2}\right) + \ln\left[R_D{}^2\right]\right] + s \quad . \tag{C.3}$$

Equation (C.3) represents a late time drawdown solution for dimensionless wellbore pressure-drop.

### 2. Finite Reservoir with a Constant-Pressure Outer Boundary

The reservoir approaches steady-state at late time for a constant-pressure outer boundary. At late time, total pressure drop in the system is:

$$(p_i - p_{wf}) = \frac{141.2\,qB\,\mu_1}{k_1 h}\,\ln\,(R/r_w) + \frac{141.2\,qB\,\mu_2}{k_2 h}\,\ln\,(r_e/R) + \Delta p_s \quad . \tag{C.4}$$

Multiplying both sides of Eq. (C.4) by $k_1 h/141.2\ qB\mu_1$ and using the definitions for dimensionless terms given in Sec. 4, an expression for dimensionless wellbore pressure drop in a finite composite reservoir with a constant-pressure outer boundary results as:

$$p_{wD} = \ln (R_D) + M \ln \left[\frac{r_{eD}}{R_D}\right] + s \quad . \tag{C.5}$$

### 3. Finite Reservoir with a Closed Outer Boundary

A reservoir approaches pseudosteady state behavior at late time for a closed outer boundary. In the following derivation, $\phi_1 = \phi_2$, and Darcy units have been used for convenience. At late time, flow rate at any $r$ can be written as:

$$q(r) = \pi\phi h \frac{dp}{dt}\left[(c_t)_1 (R^2 - r^2) + (c_t)_2 (r_e^2 - R^2)\right] \quad \text{for } r \le R, \text{ and}$$

$$= \pi\phi h \frac{dp}{dt} (c_t)_2 (r_e^2 - r^2) \qquad \text{for } r \ge R \quad . \tag{C.6}$$

Also, the production rate at the well is:

$$q_w = q(r_w) = \pi\phi h \frac{dp}{dt}\left[(c_t)_1 (R^2 - r_w^2) + (c_t)_2 (r_e^2 - R^2)\right] \quad . \tag{C.7}$$

Using Eqs. (C.6) and (C.7), assuming $R \gg r_w$, and letting $\kappa = (c_t)_1 R^2 + (c_t)_2 (r_e^2 - R^2)$ yields:

$$\frac{q(r)}{q_w} = \frac{(c_t)_1 (R^2 - r^2) + (c_t)_2 (r_e^2 - R^2)}{\kappa} \quad \text{for } r \le R \text{ , and}$$

$$= \frac{(c_t)_2 (r_e^2 - r^2)}{\kappa} \qquad \text{for } r \ge R \quad . \tag{C.8}$$

From Darcy's law:

$$q(r) = \frac{2\pi rhk}{\mu} \frac{dp}{dr} \quad . \tag{C.9}$$

Integrating Eq. (C.9) from $r$ to $r_w$, and using Eq. (C.8) yields:

$$\frac{2\,\pi k_1 h\,(p_r - p_{wf})}{q_w \mu_1} = \int_{r_w}^{R} \left[1 - \frac{(c_t)_1\, r^2}{\kappa}\right] \frac{dr}{r} + M \int_{R}^{r} \frac{(c_t)_2\,(r_e^2 - r^2)}{\kappa} \frac{dr}{r} \quad \text{for } r \geq R \quad \text{,and}$$

$$= \int_{r_w}^{r} \left[1 - \frac{(c_t)_1\, r^2}{\kappa}\right] \frac{dr}{r} \qquad \text{for } r \leq R \quad , \tag{C.10}$$

where $M = (k/\mu)_1/(k/\mu_2)$. Simplifying the right-hand-side of Eq. (C.10) assuming $R \gg r_w$ yields:

$$\frac{2\,\pi k_1 h\,(p_r - p_{wf})}{q_w \mu_1} = \ln(R/r_w) - \frac{(c_t)_1\, R^2}{2\,\kappa} + \frac{M\,(c_t)_2}{\kappa}\left[r_e^2 \ln(r/R) - \frac{r^2 - R^2}{2}\right] \quad \text{for } r \geq R \text{ d}$$

$$= \ln(r/r_w) - \frac{(c_t)_1\,(r^2 - r_w^2)}{2\,\kappa} \quad \text{for } r \leq R \quad . \tag{C.11}$$

The volumetric average reservoir pressure is:

$$\bar{p} = \frac{\int_{r_w}^{r_e} 2\,\pi rh\; p_r\; dr}{\int_{r_w}^{r_e} 2\,\pi rh\; dr} = \frac{NUM}{\pi\, hr_e^2} \quad , \tag{C.12}$$

assuming $r_e \gg r_w$. The expression for $NUM$ can be written as:

$$NUM = I_1 + I_2 = \int_{r_w}^{R} 2\,\pi rhp_r\; dr + \int_{R}^{r_e} 2\,\pi\, rhp_r\; dr \quad . \tag{C.13}$$

Using Eq. (C.11), the integral $I_1$ becomes:

$$I_1 = 2\,\pi h \int_{r_w}^{R} r \left[p_{wf} + \frac{q_w \mu_1}{2\,\pi k_1 h}\left\{\ln(r/r_w) - \frac{(c_t)_1}{2\,\kappa}(r^2 - r_w^2)\right\}\right] dr \quad . \tag{C.14}$$

Assuming $R \gg r_w$, and neglecting terms like $R^2 r_w^2$ and $r_w^2$, integration of the right-hand-side of Eq. (C.14) yields:

$$I_1 = \pi h R^2 \left[p_{wf} + \frac{q_w \mu_1}{2\,\pi k_1 h}\left\{\ln(R/r_w) - \frac{1}{2} - \frac{(c_t)_1\, R^2}{4\,\kappa}\right\}\right] \quad . \tag{C.15}$$

Similarly, using Eq. (C.11), the integral $I_2$ becomes:

$$I_2 = 2\,\pi h \int_R^{r_e} r \left[ p_{wf} + \frac{q_w \mu_1}{2\,\pi k_1 h} \left\{ \ln\,(R/r_w) - \frac{(c_t)_1\, R^2}{2\,\kappa} + \frac{M\,(c_t)_2}{\kappa} \left[ r_e^2 \ln\,(r/R) - \frac{r^2 - R^2}{2} \right] \right\} \right] dr \tag{C.16}$$

Integrating the right-hand-side of Eq. (C.16), and simplifying yields:

$$I_2 = \pi h (r_e^2 - R^2) \left[ p_{wf} + \frac{q_w \mu_1}{2\,\pi k_1 h} \left\{ \ln\,(R/r_w) - \frac{(c_t)_1\, R^2}{2\,\kappa} - \frac{M\,(c_t)_2}{4\,\kappa} \left[ 3\,r_e^2 - R^2 \right] \right\} \right]$$

$$+ \pi\, h r_e^2\, \frac{M\,(c_t)_2}{\kappa} \left[ r_e^2 \ln\,(r_e/R) \right] \frac{q_w \mu_1}{2\,\pi k_1 h} \quad . \tag{C.17}$$

Using Eqs. (C.15) and (C.17) in Eq. (C.13), substituting the result in Eq. (C.12), and simplifying, we obtain:

$$\overline{p} = p_{wf} + \frac{q_w \mu_1}{2\,\pi k_1 h} \left\{ \ln\,(R/r_w) - \frac{R^2}{2\,r_e^2} - \frac{(c_t)_1\, R^2}{2\,\kappa} \left[ 1 - \frac{R^2}{2\,r_e^2} \right] \right.$$

$$\left. + \frac{M\,(c_t)_2\, R^2}{4\,\kappa} \left[ 1 - \frac{R^2}{r_e^2} \right] - \frac{3\,M(c_t)_2\, R^2}{4\,\kappa} \left[ \frac{r_e^2}{R^2} - 1 \right] + \frac{M(c_t)_2\, r_e^2}{\kappa} \ln\,(r_e/R) \right\} \tag{C.18}$$

Rearranging Eq. (C.18) yields:

$$q_w = \frac{2\,\pi k_1 h\,(\overline{p} - p_{wf})}{\mu_1\, \chi} \quad , \tag{C.19}$$

where using the expression for $\kappa = (c_t)_1\, R^2 + (c_t)_2\,(r_e^2 - R^2)$ and $F_S = (c_t)_1/(c_t)_2$, the

parameter $\chi$ becomes:

$$\chi = \ln (R/r_w) - \frac{R^2}{2\,r_e^2} - \frac{\left[1 - \frac{R^2}{2\,r_e^2}\right]}{2\left[1 + \frac{1}{F_S}\left[\frac{r_e^2}{R^2} - 1\right]\right]} + \frac{M\left[1 - \frac{R^2}{r_e^2}\right]}{4\left[F_S + \frac{r_e^2}{R^2} - 1\right]}$$

$$- \frac{3\,M\left[\frac{r_e^2}{R^2} - 1\right]}{4\left[F_S + \frac{r_e^2}{R^2} - 1\right]} + \frac{M\,\ln (r_e/R)}{1 + \frac{R^2}{r_e^2}(F_S - 1)} \quad . \tag{C.20}$$

If $R = r_w$, $M = 1 = F_S$, and $r_e \gg r_w$ then Eq. (C.20) yields:

$$\chi = \ln (r_e/r_w) - 3/4 \quad . \tag{C.21}$$

Equation (C.21) is the limiting form of $\chi$ for a homogeneous reservoir.

At late time for a closed reservoir, equating production to expansion yields:

$$q_w = - c_t\,V\,\frac{d\bar{p}}{dt} \quad . \tag{C.22}$$

Integrating Eq. (C.22) from 0 to $t$ yields:

$$q_w t = - c_t\,V \int_{p_i}^{\bar{p}} d\bar{p} = \pi\,\phi h\,(p_i - \bar{p})\left[(c_t)_1\,R^2 + (c_t)_2\,(r_e^2 - R^2)\right] \quad . \tag{C.23}$$

Multiplying both sides by of Eq. (C.23) by $2\,k_1/\mu_1$, and rearranging yields:

$$\frac{2\,\pi k_1 h\,(p_i - \bar{p})}{q_w \mu_1} = \frac{2\,k_1 t}{\phi\mu_1\left[(c_t)_1\,R^2 + (c_t)_2\,(r_e^2 - R^2)\right]}$$

$$= \frac{2\,t_D}{R_D^2 + \frac{1}{F_S}(r_{eD}^2 - R_D^2)} = \frac{2\,t_{De}}{1 + \frac{1}{F_S}\left[\frac{r_e^2}{R^2} - 1\right]} \quad . \tag{C.24}$$

Using Eqs. (C.19) and (C.24) results in an expression for dimensionless wellbore pressure drop as:

$$p_{wD} = \frac{2\,\pi k_1 h\,(p_i - p_{wf})}{q_w \mu_1} = \frac{2\,t_{De}}{1 + \frac{1}{F_S}\left[\frac{r_e^2}{R^2} - 1\right]} + \chi + s \qquad \text{(C.25)}$$

Equation (C.25) includes wellbore skin as an additive term.

# APPENDIX D

## Late Time Buildup Solution for a Well in an Infinitely Large, Two-Region Composite Reservoir

The dimensionless buildup pressure is:

$$p_{wDs}\ (\Delta t_D) = p_{wD}\ (t_{pD}) + p_{wD}\ (\Delta t_D) - p_{wD}\ (t_{pD} + \Delta t_D) \quad . \tag{D.1}$$

Using individual expressions similar to Eq. (C.3) for the $p_{wD}$ terms on the right-hand-side of Eq. (D.1) yields:

$$p_{wDs}\ (\Delta t_D) = \frac{1}{2}\left[M\ \ln\left[\frac{2.2458\ t_{pD}\ \Delta t_D}{\eta R_D^2\ (t_{pD} + \Delta t_D)}\right] + \ln\ (R_D^2)\right] + s \quad , \tag{D.2}$$

if:

$$\frac{t_{pD}}{R_D^2} \geq 100\ \eta \quad , \text{ for } \eta \geq 1$$

$$\geq 100 \quad , \text{ for } \eta \leq 1 \quad . \tag{D.3}$$

and:

$$\Delta t_{De} \geq 100\ \eta \quad , \text{ for } \eta \geq 1$$

$$\geq 100 \quad , \text{ for } \eta \leq 1 \quad . \tag{D.4}$$

The pressure derivative, $dp_{wDs}\ (\Delta t_D)\ /\ d\ (\Delta t_D)$, is:

$$\frac{dp_{wDs}\ (\Delta t_D)}{d\ (\Delta t_D)} = \frac{d}{d\ (\Delta t_D)}\left[p_{wD}\ (\Delta t_D) - p_{wD}\ (t_{pD} + \Delta t_D)\right] \quad , \tag{D.5}$$

where:

$$p_{wD}\ (\Delta t_D) - p_{wD}\ (t_{pD} + \Delta t_D) = \frac{1}{2}\left[M\ \ln\left[\frac{\Delta t_D}{t_{pD} + \Delta t_D}\right]\right] \quad , \tag{D.6}$$

if the condition represented by Eq. (D.4) is satisfied.

# APPENDIX E

## Differentiation Algorithm

The differentiation algorithm described in this appendix is similar to the differentiation algorithm found most satisfactory by *Bourdet et al.* (1984). As per *Bourdet et al.* (1984), the differentiation algorithm uses one point before ("left") and one after ("right") the point of interest, calculates the two corresponding derivatives, and places their weighted mean at the point considered.

Let the time point of interest be $t_i$. Time point, $t_a$, to the right and time point, $t_b$, to the left are:

$$\log (t_a) = \log (t_i) + L \quad , \text{ and} \tag{E.1}$$

$$\log (t_b) = \log (t_i) - L \quad . \tag{E.2}$$

A Cartesian pressure derivative is then calculated as:

$$\left[\frac{dp}{dt}\right]_i = \frac{1}{2}\left[\frac{p_a - p_i}{t_a - t_i} + \frac{p_i - p_b}{t_i - t_b}\right] \quad . \tag{E.3}$$

If measured pressure data is not available at time point $t_a$ or $t_b$, then a linear interpolation scheme based on sequential search is used to calculate $p_a$ or $p_b$. Also, the derivative is not calculated, if $t_b$ is less than the time corresponding to the first measured time-pressure data, or if $t_a$ is larger than the time corresponding to the last measured time-pressure data.

*Bourdet et al.* (1984) suggest common values for L to be between 0 and 0.5, excluding zero. The noise effect is reduced by choosing a value of $L$ large enough. However, if $L$ is large, more of the true signal is also lost, and the shape of the original type-curve may be affected. Thus, an analyst has to be careful in choosing a proper value of $L$. Figures E.1 and E.2 present semi-log and Cartesian pressure derivatives calculated using the differentiation algorithm of this appendix for two values of $L$ = 0.1 and 0.5. Solid lines on Figs. E.1 and E.2 show the derivatives calculated for a two-region composite reservoir response with $C_D$ = 0, $M$ = 10, and $F_S$ = 10 using the *Stehfest* (1970) algorithm. Circles and diamonds show the results of numerical differentiation of dimensionless pressure values using $L$ = 0.1 and 0.5, respectively. Thirteen pressure values per cycle were used for the numerical differentiation. A random noise in the pressure data was not introduced for this example. A good agreement between the derivatives calculated from the *Stehfest* (1970) algorithm and the numerical differentiation suggests that the differentiation algorithm of this appendix may be a useful algorithm to differentiate well-test data from composite reservoirs.

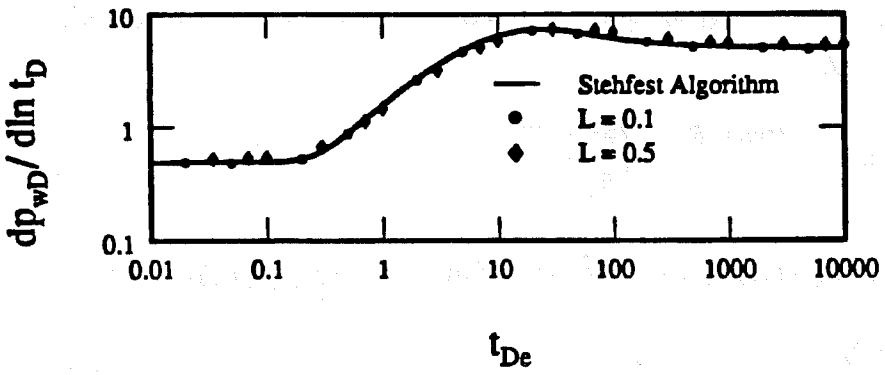


Figure E.1: Checking the differentiation algorithm for the calculation of semi-log slope for a two-region composite reservoir with $C_D = 0$, $M = 10$, $F_S = 10$.

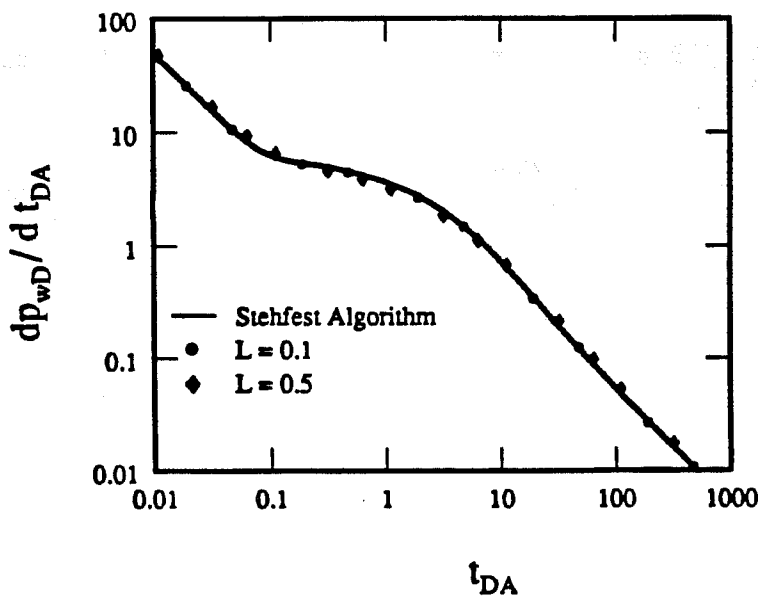


Figure E.2: Checking the differentiation algorithm for the calculation of Cartesian slope for a two-region composite reservoir with $C_D = 0$, $M = 10$, $F_S = 10$.

# APPENDIX F

# Effective Properties for a Three-Region Composite Reservoir

## 1. Derivation of $(\phi c_t)_{eff}$

If the inner and the intermediate regions are considered to form one region, then an expression for $(\phi c_t)_{eff}$ is:

$$(\phi c_t)_{eff} = \frac{(\phi c_t)_1 R_1^2 + (\phi c_t)_2 (R_2^2 - R_1^2)}{R_2^2} \quad . \tag{F.1}$$

Dividing both sides of Eq. (F.1) by $(\phi c_t)_1 R_1^2$, and using $F_{S12} = (\phi c_t)_1/(\phi c_t)_2$ yields:

$$\frac{(\phi c_t)_{eff} R_2^2}{(\phi c_t)_1 R_1^2} = 1 + \frac{1}{F_{S12}} \left[(R_2/R_1)^2 - 1\right] \quad . \tag{F.2}$$

## 2. Derivation of $(k/\mu)_{eff}$

If the inner and the intermediate regions are considered to form one region, then for radial flow in beds in series, $(k/\mu)_{eff}$ is (*Craft* and *Hawkins*, 1959):

$$\left[\frac{k}{\mu}\right]_{eff} = \frac{\ln (R_2/r_w)}{(\mu/k)_1 \ln (R_1/r_w) + (\mu/k)_2 \ln (R_2/R_1)} \tag{F.3}$$

Dividing both sides of Eq. (F.3) by $(k/\mu)_1$, and using $R_{D2} = R_2/r_w$, $R_{D1} = R_1/r_w$, and $M_{12} = (k/\mu)_1/(k/\mu)_2$ yields:

$$\frac{(k/\mu)_{eff}}{(k/\mu)_1} = \frac{\ln (R_{D2})}{\ln (R_{D1}) + M_{12} \ln (R_2/R_1)} \tag{F.4}$$

Program # 1 --- Two-region composite reservoir with $s_f$
Program # 2 --- Program for differentiation algorithm of App. E.
Program # 3 --- Three-region composite reservoir

```
*     ***************************************************
*     *  Program # 1
*     *  ***********
*     *  Name : Anil Kumar Ambastha
*     *  Date : May    11, 1988
*     *
*     *  Purpose of this program is to generate the
*     *  pressure transient response for a well
*     *  in a two-region composite reservoir.
*     *
*     *  Wellbore storage and skin at the well are
*     *  allowed.  Well produces at a constant rate.
*     *
*     *  The outer boundary condition can be either
*     *  infinite, constant-pressure or closed.
*     *
*     *  There is a thin skin at the discontinuity.
*     *
*     *  Both buildup and drawdown responses
*     *  can be generated.
*     ***************************************************
*     VARIABLE IDENTIFICATION LIST
*     ****************************

*     CD --- WELLBORE STORAGE AT THE ACTIVE WELL
*     SKIN --- SKIN AT THE ACTIVE WELL
*     SKIN2 --- SKIN AT THE DISCONTINUITY
*     AMOB --- MOBILITY RATIO (K1*MU2)/(K2*MU1)
*     DIF --- DIFFUSIVITY RATIO (K1* PHICTMU2)/(K2* PHICTMU1)
*     STO --- STORATIVITY RATIO (PHICT1/PHICT2)
*     RD --- DIMENSIONLESS DISCONTINUITY RADIUS
*     RED --- DIMENSIONLESS OUTER BOUNDARY RADIUS

      IMPLICIT REAL*8 (A-H,O-Z)
      DIMENSION TD(20)
      COMMON M,JCODE,CD,SKIN,AMOB,DIF,RD,RED,SKIN2

*     OPENING OUTPUT FILES
*     ********************

*     FOR DRAWDOWN:
*     *************

*     pd --- contains pwd as a function of tde data
*     pdp --- contains semi-log slope as a function of tde data
*     pdc --- contains Cartesian slope as a function of tdA data

*     FOR BUILDUP:
*     ************

*     pd --- contains pwds as a function of DELTA tde data
*     pdp --- contains MDH slope as a function of DELTA tde data
*     pdc --- contains Cartesian slope as a function of DELTA tdA data
*     pdh --- contains Agarwal slope as a function of DELTA tde data
```

```
      OPEN(UNIT=7,FILE="pd")
       OPEN(UNIT=8,FILE="pdp")
      OPEN(UNIT=9,FILE="pdc")
      OPEN(UNIT=10,FILE="pdh")
*     ****************************************

C     === Unformatted input section ===
*     ---------------------------------

      PRINT *,'READ THE VALUE OF CD AND SKIN > '
      READ(5,*)CD,SKIN
      PRINT *,'SKIN AT THE DISCONTINUITY > '
      READ(5,*)SKIN2
      PRINT *,'MOBILITY RATIO (ZONE 1 BY ZONE 2) > '
      READ(5,*)AMOB
      PRINT *,'STORATIVITY RATIO (ZONE 1 BY ZONE 2) > '
      READ(5,*)STO
      PRINT *,'DIMENSIONLESS DISCONTINUITY RADIUS > '
      READ(5,*)RD
      PRINT *,'# OF CYCLES OF DATA REQUIRED > '
      READ(5,*)NC
      PRINT *,'GIVE FIRST VALUE OF TD (BASED ON RW) > '
      READ(5,*)TD1
      PRINT *,'NUMBER OF TERMS TO BE USED IN STEHFEST > '
      READ(5,*)NTERM
*     ------------------------------------------------

C     READ CODES FOR BOUNDARY CONDITIONS

      PRINT *,'SUPPLY RESPONSE FUNCTION CODE: '
      PRINT *,'1 ---- DRAWDOWN '
      PRINT *,'2 ---- BUILDUP  > '
      READ(5,*)ICODE

      PRINT *,'SUPPLY OUTER BOUNDARY CONDITION CODE: '
      PRINT *,'1 --- INFINITE'
      PRINT *,'2 ---- CLOSED'
      PRINT *,'3 ---- CONSTANT-PRESSURE > '
      READ(5,*)JCODE

      IF(ICODE.EQ.2)THEN
        PRINT *,'DIMENSIONLESS PRODUCING TIME (BASED ON RW) > '
        READ(5,*)TPD
      ENDIF

      IF(JCODE.NE.1)THEN
        PRINT *,'DIMENSIONLESS OUTER RADIUS > '
        READ(5,*)RED
      ELSE
*     For infinite reservoir, a fictitious red is supplied
        RED=1.e30
      ENDIF
C     **** input section ends ***
*     ************************************************
```

```
      M=777
      PI=2.*ASIN(1.)
C     COMPUTE DIFFUSIVITY RATIO
      DIF=AMOB/STO

C     GENERATE THE FIRST SET OF TD VECTOR

      TD(1)=TD1
      TD(2)=1.5*TD1
      TD(3)=2.*TD1
      TD(4)=2.5*TD1
      TD(5)=3.*TD1
      TD(6)=3.5*TD1
      TD(7)=4.*TD1
      TD(8)=4.5*TD1
      TD(9)=5.*TD1
      TD(10)=6.*TD1
      TD(11)=7.*TD1
      TD(12)=8.*TD1
      TD(13)=9.*TD1
*     ----------------------------------------------

C     WRITE THE NUMBER OF DATA POINTS GENERATED
C     The program generates 13 data points per cycle.

      WRITE(7,*)13*NC
      WRITE(8,*)13*NC
      WRITE(9,*)13*NC
      IF(ICODE.EQ.2)WRITE(10,*)13*NC
*     ----------------------------------------------

C     GENERATE AND PRINT THE PRESSURE TRANSIENT RESPONSE

      IF(ICODE.EQ.2)THEN
        CALL INVERT(TPD,NTERM,PD1,PDP1)
      ENDIF

      DO 1 I=1,NC
      DO 2 J=1,13
      SPC=TD(J)
      IF(ICODE.EQ.2)THEN
         SPC1=SPC+TPD
        CALL INVERT(SPC1,NTERM,PD2,PDP2)
      ENDIF
      CALL INVERT(SPC,NTERM,PD,PDP)
      IF(ICODE.EQ.1)PDC=PDP
      IF(ICODE.EQ.2)THEN
        PD=PD1+PD-PD2
         PDC=PDP-PDP2
        PDH=SPC1/TPD*SPC*PDC
      ENDIF
      PDP=SPC*PDC

C     CONVERT THE BASE OF 'SPC' FROM RW TO DISCONTINUITY RADIUS
```

```
      SPC=SPC/RD/RD

C     REPORT THE RESULTS:
*     ------------------

      WRITE(7,9)SPC,PD
       WRITE(8,9)SPC,PDP
       WRITE(9,9)SPC/PI,PDC*PI*RD*RD
      IF(ICODE.EQ.2) WRITE(10,9)SPC,PDH
    2 TD(J)=10.*TD(J)
    1 CONTINUE
    9 FORMAT(2X,F20.6,2X,F20.6)
      STOP
      END

**********************************************************************

      SUBROUTINE LAP(S,PWDL,PDPL)
      IMPLICIT REAL*8 (A-H,O-Z)
      DOUBLE PRECISION MMBSI0,MMBSI1,MMBSK0,MMBSK1
      COMMON M,JCODE,CD,SKIN,AMOB,DIF,RD,RED,SKIN2

C     COMPUTE THE ARGUMENTS OF BESSEL FUNCTIONS

      ARG1=DSQRT(S)
      ARG2=RD*ARG1
      ARG3=DSQRT(DIF)*ARG2
      IF (JCODE.NE.1) ARG4=DSQRT(S*DIF)*RED


C     COMPUTE NEEDED BESSEL FUNCTIONS (THESE ARE SCALED BY EXPONENTIALS)

      A1=MMBSI0(2,ARG1,IER)
      A2=MMBSI0(2,ARG2,IER)

      B1=MMBSI1(2,ARG1,IER)
      B2=MMBSI1(2,ARG2,IER)

      D1=MMBSK0(2,ARG1,IER)
      D2=MMBSK0(2,ARG2,IER)
      D3=MMBSK0(2,ARG3,IER)

      E1=MMBSK1(2,ARG1,IER)
      E2=MMBSK1(2,ARG2,IER)
      E3=MMBSK1(2,ARG3,IER)

      IF(JCODE.EQ.2)THEN
        C11=-MMBSK1(2,ARG4,IER)
        C22=MMBSI1(2,ARG4,IER)
      ENDIF
      IF(JCODE.EQ.3)THEN
        C11=MMBSK0(2,ARG4,IER)
        C22=MMBSI0(2,ARG4,IER)
      ENDIF
```

```
      IF(JCODE.NE.1)THEN
        A3=MMBSI0(2,ARG3,IER)
        B3=MMBSI1(2,ARG3,IER)
      ENDIF
C     CALCULATION OF MULTIPLYING FACTORS
       F1=DEXP(ARG1)
       F2=DEXP(ARG2)
       F3=DEXP(ARG3)
      IF(JCODE.NE.1)THEN
       IF(ARG4.LE.88.)THEN
         F4=DEXP(ARG4)
       ELSE
         F4=DEXP(88.00D00)
       ENDIF
      ENDIF

C     COMPUTATION OF THE COEFFICIENTS OF EQNS. FOR C1,C2 AND C3.
C     FOR FINITE RESERVOIRS, WE HAVE C4 ALSO.

        AL11=(CD*S*(A1-SKIN*ARG1*B1)-ARG1*B1)*F1
        AL12=(CD*S*(D1+SKIN*ARG1*E1)+ARG1*E1)/F1
        AL21=(SKIN2*RD*ARG1*B2+A2)*F2
        AL22=(D2-SKIN2*RD*ARG1*E2)/F2
        AL23=-D3/F3
        AL31=AMOB*ARG1*B2*F2
        AL32=-AMOB*ARG1*E2/F2
        AL33=DSQRT(S*DIF)*E3/F3

      IF(JCODE.NE.1)THEN
        AL24=-A3*F3
        AL34=-DSQRT(S*DIF)*B3*F3
        AL43=C11/F4
        AL44=C22*F4
      ENDIF
C     CALCULATION OF C1, C2 AND C3
C     C4 IS ALSO CALCULATED FOR FINITE RESERVOIRS

        S1=AL21*AL33-AL23*AL31
       S2=AL22*AL33-AL32*AL23

      IF(JCODE.EQ.1)THEN
       C2=S1/(S*(AL12*S1-AL11*S2))
       C1=(1.-S*AL12*C2)/S/AL11
       C3=-(AL31*C1+AL32*C2)/AL33
      ENDIF
      IF(JCODE.NE.1)THEN
        S3=AL43/AL44
        S4=AL24*AL31-AL21*AL34
        S5=S1+S3*S4
        S6=AL22*AL34-AL24*AL32
        S7=-AL11*S2+AL12*S1+S3*(AL12*S4+AL11*S6)
         C2=S5/S/S7
        C1=(1.-S*AL12*C2)/S/AL11
C       C4=S3*(AL31*C1+AL32*C2)/(AL33-AL34*S3)
```

```
C      C3=-C4/S3
       ENDIF
C      CALCULATION OF TRANSFORMED SOLUTION


C      PWDL REPRESENTS LAPLACE TRANSFORM OF PWD

       PWDL=C1*(A1-SKIN*ARG1*B1)*F1+C2*(D1+SKIN*ARG1*E1)/F1
       PDPL=PWDL*S
       RETURN
       END

*************************************************************************

C              THE STEHFEST ALGORITHM
C             ******************************
C
       SUBROUTINE INVERT(TD,N,PD,PDP)
C          THIS FUNTION COMPUTES NUMERICALLY THE LAPLACE TRNSFORM
C          INVERSE OF F(S).
       IMPLICIT  REAL*8 (A-H,O-Z)
       COMMON M,JCODE,CD,SKIN,AMOB,DIF,RD,RED,SKIN2
       DIMENSION G(50),V(50),H(25)
C
C          NOW IF THE ARRAY V(I) WAS COMPUTED BEFORE THE PROGRAM
C          GOES DIRECTLY TO THE END OF THE SUBRUTINE TO CALCULATE
C          F(S).
       IF (N.EQ.M) GO TO 17
       M=N
       DLOGTW=0.6931471805599
       NH=N/2
C
C          THE FACTORIALS OF 1 TO N ARE CALCULATED INTO ARRAY G.
       G(1)=1
       DO 1 I=2,N
       G(I)=G(I-1)*I
1      CONTINUE
C
C          TERMS WITH K ONLY ARE CALCULATED INTO ARRAY H.
       H(1)=2./G(NH-1)
       DO 6 I=2,NH
       FI=I
       IF(I-NH) 4,5,6
4      H(I)=FI**NH*G(2*I)/(G(NH-I)*G(I)*G(I-1))
       GO TO 6
5      H(I)=FI**NH*G(2*I)/(G(I)*G(I-1))
6      CONTINUE
C
C          THE TERMS (-1)**NH+1 ARE CALCULATED.
C          FIRST THE TERM FOR I=1
       SN=2*(NH-NH/2*2)-1
C
C          THE REST OF THE SN'S ARECALCULATED IN THE MAIN RUTINE.
```

```
C
C
C       THE ARRAY V(I) IS CALCULATED.
      DO 7 I=1,N
C
C       FIRST SET V(I)=0
      V(I)=0.
C
C       THE LIMITS FOR K ARE ESTABLISHED.
C       THE LOWER LIMIT IS K1=INTEG((I+1/2))
      K1=(I+1)/2
C
C       THE UPPER LIMIT IS K2=MIN(I,N/2)
      K2=I
      IF (K2-NH) 8,8,9
9     K2=NH
C
C       THE SUMMATION TERM IN V(I) IS CALCULATED.
8     DO 10 K=K1,K2
      IF (2*K-I) 12,13,12
12    IF (I-K) 11,14,11
11    V(I)=V(I)+H(K)/(G(I-K)*G(2*K-I))
      GO TO 10
13    V(I)=V(I)+H(K)/G(I-K)
      GO TO 10
14    V(I)=V(I)+H(K)/G(2*K-I)
10    CONTINUE
C
C       THE V(I) ARRAY IS FINALLY CALCULATED BY WEIGHTING
C       ACCORDING TO SN.
      V(I)=SN*V(I)
C
C       THE TERM SN CHANGES ITS SIGN EACH ITERATION.
      SN=-SN
7     CONTINUE
C
C       THE NUMERICAL APPROXIMATION IS CALCULATED.
17    PD=0.
      PDP=0.
      A=DLOGTW/TD
      DO 15 I=1,N
      ARG=A*I
      CALL LAP(ARG,PWDL,PDPL)
      PD=PD+V(I)*PWDL
      PDP=PDP+V(I)*PDPL
15    CONTINUE
      PD=PD*A
      PDP=PDP*A
18    RETURN
      END
```

```
C     ******************************************************
*     *       Program # 2
*     *       ************
C     *       NAME: ANIL K. AMBASTHA
C     *       DATE: MAY 11, 1988
C     *       THIS PROGRAM COMPUTES THE SLOPE OF A
C     *       GIVEN T VS. P ARRAY.
C     *       SLOPE = dP / dT or dP/dln T or dln P/dln T
c     *     Uses linear interpolation to get pressure
c     *     values at time where there is no measured data
C     ******************************************************

C     VARIABLE IDENTIFICATION LIST
*     ****************************

C     D --- INCREMENTAL TIME
C     NDATA --- NUMBER OF DATA POINTS ON A T VS. P ARRAY
C     T --- TIME POINTS (THIS IS INDEPENDENT VARIABLE)
C     P --- PRESSURE POINTS (THIS IS DEPENDENT VARIABLE)
C     ICODE --- CODE FOR THE TYPE OF SLOPE DESIRED
C             =1 --- CARTESIAN SLOPE
C             =2 --- SEMI-LOG SLOPE (MDH SLOPE FOR BUILDUP)
C             =3 --- LOG-LOG SLOPE
C             =4 --- AGARWAL SLOPE  (HORNER SLOPE IS NEGATIVE
C                    OF AGARWAL SLOPE)
C
      IMPLICIT REAL*8(A-H,O-Z)
      DIMENSION T(200),P(200)
      OPEN(UNIT=7,FILE="data")
      OPEN(UNIT=8,FILE="output")
      WRITE(6,*)'TIME INCREMENT TO SELECT '
      WRITE(6,*)'POINTS FOR SLOPE CALCULATION > '
      WRITE(6,*)'USE VALUE BETWEEN 0 AND 0.5 (RECOMMENDED = 0.2) > '
      READ(5,*)D
C     ENTER THE CODE FOR TYPE OF SLOPE DESIRED
      WRITE(6,*)'1 -- CARTESIAN, 2 -- SEMI-LOG, '
      WRITE(6,*)'3 -- LOG-LOG, 4 -- AGARWAL SLOPE.'
      WRITE(6,*)'ENTER THE CODE FOR TYPE OF SLOPE DESIRED > '
      READ(5,*)ICODE
      IF(ICODE.EQ.4)THEN
        WRITE(6,*)'ENTER PRODUCING TIME > '
        READ(5,*)TP
      ENDIF
C     READ THE DATA
C     *************
      READ(7,*)NDATA
      DO 1 I=1,NDATA
    1 READ(7,*)T(I),P(I)
C     CALCULATE THE SLOPES
C     ********************
      DO 2 I=1,NDATA
      TA=10.0D00**(DLOG10(T(I))+D)
      TB=10.0D00**(DLOG10(T(I))-D)
      IF(TB.LT.T(1))THEN
```

```
        GO TO 2
      ENDIF
      IF(TA.GT.T(NDATA))THEN
        GO TO 2
      ELSE
C     TAKE THE CENTERED DERIVATIVE
        CALL TABSEQ(T,P,NDATA,TA,PA)
        CALL TABSEQ(T,P,NDATA,TB,PB)
        S1=(PA-P(I))/(TA-T(I))
        S2=(P(I)-PB)/(T(I)-TB)
        SLOPE=0.5*DABS(S1+S2)
      ENDIF
    8 IF(ICODE.EQ.1)WRITE(8,110)T(I),SLOPE
      IF(ICODE.EQ.2)WRITE(8,110)T(I),SLOPE*T(I)
      IF(ICODE.EQ.3)WRITE(8,110)T(I),SLOPE*T(I)/P(I)
      IF(ICODE.EQ.4)WRITE(8,110)T(I),SLOPE*T(I)*(TP+T(I))/TP
    2 CONTINUE
  110 FORMAT(2X,F15.6,2X,F15.6)
      STOP
      END

C     ******************************************************

      SUBROUTINE TABSEQ(X,Y,N,XX,YY)
      IMPLICIT REAL*8(A-H,O-Z)
      DIMENSION X(N),Y(N)
C.....TABLE LOOK-UP USING SEQUENTIAL SEARCH
C     LINEAR INTERPOLATION BETWEEN TABLE VALUES USED.
C
C     X-VECTOR OF INDEPENDENT VALUES (ARGUMENTS)
C     Y-VECTOR OF DEPENDENT VARIABLES(FUNCTION VALUES)
C     N-NUMBER OF TABLE ENTRIES
C     XX-ARGUMENT
C     YY-INTERPOLATED FUNCTION OF ARUGUMENT XX
      IF(XX.LT.X(1)) GO TO 99
      I=1
  100 I=I+1
      IF(I.GT.N) GO TO 98
      IF(XX.GT.X(I)) GO TO 100
      YY=Y(I-1)+(Y(I)-Y(I-1))*(XX-X(I-1))/(X(I)-X(I-1))
      RETURN
   99 YY=Y(1)
      WRITE(6,89)XX
   89 FORMAT(1H ,'WARNING - ARGUMENT OUT OF TABLE,XX = ',F12.5)
      RETURN
   98 YY=Y(N)
      WRITE(6,89)XX
      RETURN
      END
```

```
*     ****************************************************
*     *  Program # 3
*     *  ************
*     *  Name : Anil Kumar Ambastha
*     *  Date : May    11, 1988
*     *
*     *  Purpose of this program is to generate
*     *  pressure transient response for a well
*     *  in a three-region composite reservoir.

*     *  Wellbore storage and skin at the well are
*     *  allowed.  Well produces at a constant rate.

*     *  The outer boundary is assumed to be infinite.
*     ****************************************************
*     VARIABLE IDENTIFICATION LIST
*     ****************************

*     CD --- WELLBORE STORAGE AT THE ACTIVE WELL
*     SKIN --- SKIN AT THE ACTIVE WELL
*     AMOB12 --- MOBILITY RATIO (K1*MU2)/(K2*MU1)
*     AMOB23 --- MOBILITY RATIO (K2*MU3)/(K3*MU2)
*     STO12 --- STORATIVITY RATIO (PHICT1/PHICT2)
*     STO13 --- STORATIVITY RATIO (PHICT1/PHICT3)
*     DIF12 --- DIFFUSIVITY RATIO (K1* PHICTMU2)/(K2* PHICTMU1)
*     DIF13 --- DIFFUSIVITY RATIO (K1* PHICTMU3)/(K3* PHICTMU1)
*     RD1 --- DIMENSIONLESS DISCONTINUITY DISTANCE (R1/rw)
*     RD2 --- DIMENSIONLESS DISCONTINUITY DISTANCE (R2/rw)
*     RED --- DIMENSIONLESS OUTER RADIUS

      IMPLICIT REAL*8 (A-H,O-Z)
      DIMENSION TD(20)
      COMMON M,JCODE,CD,SKIN,AMOB12,AMOB23,DIF12,DIF13,RD1,RD2,RED
      OPEN(UNIT=7,FILE="pd")
       OPEN(UNIT=8,FILE="pdp")
      OPEN(UNIT=9,FILE="pdc")

      PI=2.0D00*ASIN(1.0)
C     === Unformatted input section ===

      PRINT *,'READ THE VALUE OF CD AND SKIN >  '
      READ(5,*)CD,SKIN
      PRINT *,'MOBILITY RATIO (1 by 2 and 2 by 3) > '
      READ(5,*)AMOB12,AMOB23
      PRINT *,'STORATIVITY RATIO (1 BY 2 and 1 by 3) > '
      READ(5,*)STO12,STO13
      PRINT *,'DIMENSIONLESS DISCONTINUITY DISTANCE (RD1 and RD2) > '
      READ(5,*)RD1,RD2
      PRINT *,'# OF CYCLES OF DATA REQUIRED > '
      READ(5,*)NC
      PRINT *,'GIVE FIRST VALUE OF TD > '
      READ(5,*)TD1
      PRINT *,'NUMBER OF TERMS TO BE USED IN STEHFEST > '
      READ(5,*)NTERM
```

```
      PRINT *,'SUPPLY OUTER BOUNDARY CONDITION CODE: '
      PRINT *,'1 --- INFINITE'
      PRINT *,'2 ---- CLOSED'
      PRINT *,'3 ---- CONSTANT-PRESSURE > '
      READ(5,*)JCODE

      IF(JCODE.NE.1)THEN
        PRINT *,'DIMENSIONLESS OUTER RADIUS'
        READ(5,*)RED
      ELSE
        RED=1.e30
      ENDIF
C     **** input section ends ***

      M=777
C     CALCULATE DIFFUSIVITY RATIOS (DIF12 AND DIF13)
      AMOB13=AMOB12*AMOB23
      DIF12=AMOB12/STO12
      DIF13=AMOB13/STO13

C     GENERATE THE FIRST SET OF TD VECTOR

      TD(1)=TD1
      TD(2)=1.5*TD1
      TD(3)=2.*TD1
      TD(4)=2.5*TD1
      TD(5)=3.*TD1
      TD(6)=3.5*TD1
      TD(7)=4.*TD1
      TD(8)=4.5*TD1
      TD(9)=5.*TD1
      TD(10)=6.*TD1
      TD(11)=7.*TD1
      TD(12)=8.*TD1
      TD(13)=9.*TD1

C     WRITE THE NUMBER OF DATA POINTS GENERATED

      WRITE(7,*)13*NC
      WRITE(8,*)13*NC
      WRITE(9,*)13*NC

C     GENERATE AND PRINT THE PRESSURE TRANSIENT RESPONSE

      DO 1 I=1,NC
      DO 2 J=1,13
      SPC=TD(J)
      CALL INVERT(SPC,NTERM,PD,PDP)
C     CALCULATE CARTESIAN SLOPE
      PDC=PDP*PI*RD1*RD1
C     CALCULATE SEMI-LOG GRAPH SLOPE (BASE e)
      PDP=SPC*PDP
C     CONVERT BASE OF 'SPC' FROM RW TO DISCONTINUITY DISTANCE
      SPC=SPC/RD1/RD1
```

```
C     REPORT THE RESULTS
*     ******************

      WRITE(7,9)SPC,PD
       WRITE(8,9)SPC,PDP
       WRITE(9,9)SPC/PI,PDC
  2   TD(J)=10.*TD(J)
  1   CONTINUE
  9   FORMAT(2X,F15.5,2X,F15.7)
      STOP
      END
*************************************************************************

      SUBROUTINE LAP(S,PWDL,PDPL)
      IMPLICIT REAL*8 (A-H,O-Z)
      DOUBLE PRECISION MMBSI0,MMBSI1,MMBSK0,MMBSK1
      COMMON M,JCODE,CD,SKIN,AMOB12,AMOB23,DIF12,DIF13,RD1,RD2,RED

C     COMPUTE THE ARGUMENTS OF BESSEL FUNCTIONS

      ARG1=DSQRT(S)
      ARG2=RD1*ARG1
      ARG3=DSQRT(DIF12)*ARG2
      ARG4=RD2*DSQRT(S*DIF12)
      ARG5=RD2*DSQRT(S*DIF13)


C     COMPUTE BESSEL FUNCTIONS SCALED BY EXPONENTIALS

      A1=MMBSI0(2,ARG1,IER)
      A2=MMBSI0(2,ARG2,IER)
      A3=MMBSI0(2,ARG3,IER)
      A4=MMBSI0(2,ARG4,IER)

      B1=MMBSI1(2,ARG1,IER)
      B2=MMBSI1(2,ARG2,IER)
      B3=MMBSI1(2,ARG3,IER)
      B4=MMBSI1(2,ARG4,IER)

      D1=MMBSK0(2,ARG1,IER)
      D2=MMBSK0(2,ARG2,IER)
      D3=MMBSK0(2,ARG3,IER)
      D4=MMBSK0(2,ARG4,IER)
      D5=MMBSK0(2,ARG5,IER)

      E1=MMBSK1(2,ARG1,IER)
      E2=MMBSK1(2,ARG2,IER)
      E3=MMBSK1(2,ARG3,IER)
      E4=MMBSK1(2,ARG4,IER)
      E5=MMBSK1(2,ARG5,IER)

C     CALCULATION OF MULTIPLYING FACTORS
       F1=DEXP(ARG1)
```

```
      F2=DEXP(ARG2)
      F3=DEXP(ARG3)
    IF(ARG4.LE.88.)THEN
      F4=DEXP(ARG4)
    ELSE
      F4=DEXP(88.d00)
    ENDIF
    IF(ARG5.LE.88.)THEN
      F5=DEXP(ARG5)
    ELSE
      F5=DEXP(88.d00)
    ENDIF

C   COMPUTATION OF THE COEFFICIENTS OF EQNS. FOR C1 THROUGH C5.

      AL11=(CD*S*(A1-SKIN*ARG1*B1)-ARG1*B1)*F1
      AL12=(CD*S*(D1+SKIN*ARG1*E1)+ARG1*E1)/F1
      AL21=A2*F2
      AL22=D2/F2
      AL23=-A3*F3
      AL24=-D3/F3
      AL31=AMOB12*ARG1*B2*F2
      AL32=-AMOB12*ARG1*E2/F2
      AL33=-DSQRT(S*DIF12)*B3*F3
      AL34=DSQRT(S*DIF12)*E3/F3
      AL43=A4*F4
      AL44=D4/F4
      AL45=-D5/F5
      AL53=AMOB23*DSQRT(S*DIF12)*B4*F4
      AL54=-AMOB23*DSQRT(S*DIF12)*E4/F4
      AL55=DSQRT(S*DIF13)*E5/F5

C   CALCULATION OF C1 THROUGH C5

      X1=AL43*AL55-AL45*AL53
      X2=AL45*AL54-AL44*AL55
      X3=AL33*X2+AL34*X1
       S1=AL31*AL12-AL32*AL11
      S2=AL22*AL11-AL21*AL12
      S3=AL23*X2+AL24*X1

    IF(JCODE.EQ.1)THEN
      C2=(S3*AL31-AL21*X3)/(S*(X3*S2+S1*S3))
      C1=(1.-S*AL12*C2)/S/AL11
      C3=-(AL31*C1+AL32*C2)*X2/(AL33*X2+AL34*X1)
      C4=(-X1*(AL31*C1+AL32*C2))/(AL33*X2+AL34*X1)
      C5=-(AL53*C3+AL54*C4)/AL55
    ENDIF

C   CALCULATION OF TRANSFORMED SOLUTION

C   PWDL REPRESENTS LAPLACE TRANSFORM OF PWD

    PWDL=C1*(A1-SKIN*ARG1*B1)*F1+C2*(D1+SKIN*ARG1*E1)/F1
```

```
      PDPL=PWDL*S
      RETURN
      END
*************************************************************************
C
C              THE STEHFEST ALGORITHM
C             ********************************
C
      SUBROUTINE INVERT(TD,N,PD,PDP)
C          THIS FUNTION COMPUTES NUMERICALLY THE LAPLACE TRNSFORM
C          INVERSE OF F(S).
      IMPLICIT REAL*8 (A-H,O-Z)
      COMMON M,JCODE,CD,SKIN,AMOB12,AMOB23,DIF12,DIF13,RD1,RD2,RED
      DIMENSION G(50),V(50),H(25)
C
C          NOW IF THE ARRAY V(I) WAS COMPUTED BEFORE THE PROGRAM
C          GOES DIRECTLY TO THE END OF THE SUBRUTINE TO CALCULATE
C          F(S).
      IF (N.EQ.M) GO TO 17
      M=N
      DLOGTW=0.6931471805599
      NH=N/2
C
C          THE FACTORIALS OF 1 TO N ARE CALCULATED INTO ARRAY G.
      G(1)=1
      DO 1 I=2,N
      G(I)=G(I-1)*I
1     CONTINUE
C
C          TERMS WITH K ONLY ARE CALCULATED INTO ARRAY H.
      H(1)=2./G(NH-1)
      DO 6 I=2,NH
      FI=I
      IF(I-NH) 4,5,6
4     H(I)=FI**NH*G(2*I)/(G(NH-I)*G(I)*G(I-1))
      GO TO 6
5     H(I)=FI**NH*G(2*I)/(G(I)*G(I-1))
6     CONTINUE
C
C          THE TERMS (-1)**NH+1 ARE CALCULATED.
C          FIRST THE TERM FOR I=1
      SN=2*(NH-NH/2*2)-1
C
C          THE REST OF THE SN'S ARECALCULATED IN THE MAIN RUTINE.
C
C
C          THE ARRAY V(I) IS CALCULATED.
      DO 7 I=1,N
C
C          FIRST SET V(I)=0
      V(I)=0.
C
C          THE LIMITS FOR K ARE ESTABLISHED.
```

```
C       THE LOWER LIMIT IS K1=INTEG((I+1/2))
      K1=(I+1)/2
C
C       THE UPPER LIMIT IS K2=MIN(I,N/2)
      K2=I
      IF (K2-NH) 8,8,9
9     K2=NH
C
C       THE SUMMATION TERM IN V(I) IS CALCULATED.
8     DO 10 K=K1,K2
      IF (2*K-I) 12,13,12
12    IF (I-K) 11,14,11
11    V(I)=V(I)+H(K)/(G(I-K)*G(2*K-I))
      GO TO 10
13    V(I)=V(I)+H(K)/G(I-K)
      GO TO 10
14    V(I)=V(I)+H(K)/G(2*K-I)
10    CONTINUE
C
C       THE V(I) ARRAY IS FINALLY CALCULATED BY WEIGHTING
C       ACCORDING TO SN.
      V(I)=SN*V(I)
C
C       THE TERM SN CHANGES ITS SIGN EACH ITERATION.
      SN=-SN
7     CONTINUE
C
C       THE NUMERICAL APPROXIMATION IS CALCULATED.
17    PD=0.
      PDP=0.
      A=DLOGTW/TD
      DO 15 I=1,N
      ARG=A*I
      CALL LAP(ARG,PWDL,PDPL)
      PD=PD+V(I)*PWDL
      PDP=PDP+V(I)*PDPL
15    CONTINUE
      PD=PD*A
      PDP=PDP*A
18    RETURN
      END
```

☆ U.S. GOVERNMENT PRINTING OFFICE: 1989-661-023/00046